Short term effects of c-MYC activation on β-cell physiology and glucose homeostasis in the *pIns-c-MycER*^{TAM} transgenic mouse

by

Yi-Fang Wang BSc MSc

A thesis submitted in partial fulfilment of the requirements for the degree of Doctor of Philosophy in Life Sciences

Life Sciences, University of Warwick

January 2012

Table of Contents

Figures

Tables

Abbreviations

4-OHT	4-Hydroxytamoxifen
5-HT	5-hydroxytryptamine
AD	average difference
ADP	adenosine diphosphate
ATP	adenosine triphosphate
βIRKO	β-cell-specific insulin receptor knockout
b	basic
cAMP	cyclic adenosine monophosphate
CD	cervical dislocation
CDK	cyclin-dependent kinase
cDNA	complementary DNA
ChIP	chromatin immunoprecipitation
cRNA	complementary RNA
CTD	carboxy-terminal domain
DAB	3,3'-diaminobenzidine
DAPI	4',6-diamidino-2-phenylindole
DDR	DNA damage response
DETs	differentially expressed transcripts
DSBs	double-strand breaks
EDTA	Ethylenediaminetetra acetic acid
ER	endoplasmic reticulum

ER^{TAM}	estrogen receptor
EW	*plns-c-MycER^{TAM}* WT littermates treated with exenatide
FITC	fluorescein isothiocyanate
GC-RMA	GeneChip robust multi-array analysis
GO	gene ontology
GSIS	glucose stimulated insulin secretion
H	Haematoxylin
H2O2	Hydrogen peroxide
HAT	histone acetyltransferase
HDACs	histone deacetylases
HH	hyperinsulinaemic hypoglycaemia
HIP	human islet amyloid polypeptide
HLH	helix-loop-helix
HSP	Heat shock protein
IHC	Immunohistochemistry
IAPP	islet amyloid polypeptide
IP	Intraperitoneal
LZ	leucine zipper
MAS	Microarray Suite
MB	Myc boxes
MM	mismatch
MOMP	mitochondrial-outer-membrane permeabilization
MYC-OFF	*plns-c-MycER^{TAM}* mice treated with peanut oil
MYC-ON	*plns-c-MycER^{TAM}* mice treated with 4-OHT

NEFAs	non-esterified fatty acids
NLP	natural language processing
NOD	non-obese diabetic
NSF	soluble N-ethylmaleimide-sensitive fusion
NTD	amino‑terminal domain
ODEs	ordinary differential equations
OGTT	Glucose tolerance test
PBS	Phosphate Buffered Saline
pIns	insulin promoter
PM	perfect match
PP	pancreatic peptide
RIN	RNA integrity numbers
RMA	robust multi-array analysis
ROS	reactive oxygen species
RRP	readily releasable pool
RT	Room Temperature
SAGE	Serial analysis of gene expression
SC	subcutaneous
SD	standard deviation
SNARE	soluble N-ethylmaleimide-sensitive fusion attachment protein receptor
SSBs	single-strand breaks
STZ	streptozotocin
T1DM	Type 1 diabetes mellitus

T2DM	Type 2 diabetes mellitus
TAGs	triacylglycerides
TBE	Tris/borate/EDTA buffer
TdT	deoxynucleotidyl
TL	Time Line
TUNEL	terminal deoxynucleotidyl-mediated dUTP nick-end labeling
VDCCs	voltage-dependent calcium channels
WT	Wild Type
WT-4-OHT	*plns-c-MycER*^{TAM} WT littermates treated with 4-OHT
WW	*plns-c-MycER*^{TAM} WT littermates treated with water vehicle

Conventions

The following conventions have been used throughout this thesis to ensure consistency throughout:

1. Protein symbols are written in standard font, with all letters in uppercase: e.g. MYC, MAX and MDM2.

2. Gene symbols for human genes are written in *italics*, with all letters uppercase: e.g. *MYC*, *MAX* and *MDM2*; gene symbols for mouse and rat genes are written in *italics*, with the first letter uppercase, followed by all lowercase letters: e.g. *Myc*, *Max* and *Mdm2*; gene symbols for other organisms are written in *italics*, with all letters lowercase: e.g. *myc*, *max*, and *mdm2*.

3. The term ‘exenatide’ also refers to exendin-4 when no ambiguity exists.

4. Glucose levels presented in the result section refer to fed glucose levels when no ambiguity exists.

Acknowledgements

I would first like to thank my supervisors and my colleagues in the Life Sciences at Warwick University. Thank you for your advice and help throughout my PhD study in both my academic and personal life. I am extremely grateful! Many thanks go to Dr. Samuel Robson for providing his microarray data sets. A special thank you goes to Owen and my family. Without your support I would never have finished this thesis. I would also like to thank Wallis, Tom, and Ofelia. Thank you very much for your putting up with me and encouraging me throughout the difficult times I had.

Declaration

The author declares that, to the best of her knowledge, the work contained within this thesis is original and her own work under the supervision of her supervisors, Dr. Michael Khan and Prof. David Epstein.

The material in this thesis is submitted for the degree of PhD to the University of Warwick only and has not been submitted to any other university. All sources of information have been specifically acknowledged in the form of references.

Abstract

Injection of 4-hydroxytamoxifen (4-OHT) activates the oncogene c-*myc* in transgenic *pIns-c-MycER*^{TAM} mice, triggering β-cell proliferation in the short term as well as apoptosis and reduced insulin secretion, leading to hyperglycaemia. This hyperglycaemia is preceded by a short period of hypoglycaemia, which may be caused by: (i) increased insulin secretion or release from dying cells; (ii) rapid β-cell proliferation; and (iii) increased insulin sensitivity. This thesis characterizes the initial stages of the expression of c-MYC in the *pIns-c-MycER*^{TAM} mouse model and attempts to identify the causes of the transient hypoglycaemia using mathematical models. Furthermore, microarray data were analysed to investigate the early hypoglycaemia from the point of view of transcriptomics. The size and mass of β-cells were quantified during the transient period of hypoglycaemia by means of immunohistochemistry. These data were incorporated in a detailed mathematical model of β-cell dynamics.

Chapter 1. Introduction

The vertebrate pancreas has two functions. One is the secretion of digestive enzymes (exocrine function), and the other is glucose homeostasis (endocrine function). Pancreatic islets are composed of α, β, δ, and pancreatic peptide (PP) endocrine cells. The α-cells secrete glucagon, which stimulates gluconeogenesis and glycogenolysis, whereas the β-cells secrete insulin, which promotes glucose disposal in the periphery and inhibits gluconeogenesis and glycogenolysis. Insulin plays a critical role in reducing plasma glucose levels following feeding. The balance between glucagon and insulin is important in maintaining glucose concentration, energy homeostasis, and energy balance, as reviewed in Gromada *et al*. (2007). In response to the stimuli that would result in rising plasma glucose, normal β-cells will secrete insulin at appropriate levels to maintain normal blood glucose levels. Conversely, when the blood glucose levels tend to drop, such as during prolonged fasting or extended exercise, insulin secretion is inhibited (Cryer, 1993). Diabetes is characterised by hyperglycaemia and β-cell failure or destruction. Type 1 diabetes mellitus (T1DM) is ascribed to an autoimmune assault against β-cells causing extrinsic apoptosis, whereas Type 2 diabetes mellitus (T2DM) is associated with metabolic disorders, such as insulin resistance and dysfunction of glucose stimulated insulin secretion (GSIS) in β-cells. Both T1DM and T2DM possess an absolute or relative deficiency of β-cells triggered by apoptosis (Bouwens and Rooman, 2005; Butler *et al*., 2003). Current treatments for diabetes include injection of exogenous insulin or oral glucose-lowering drugs but incur the side effects of iatrogenic hypoglycaemia and destruction of β-cells. Although the islet transplantation is a

potential treatment for T1DM, the number of patients who can receive the treatment is limited. While most of the current treatments do not significantly arrest the decreasing β-cell number or β-cell dysfunction, the study of β-cell regeneration and proliferation endogenous has become an important field.

1.1. The c-*Myc* oncogene

The proto-oncogene c-*myc*, a cellular homolog oncogene of v-*myc* (Alitalo *et al*., 1983; Crews *et al*., 1982; Sheiness *et al*., 1978), is a member of the *myc* family (c-*myc*, N-*myc*, and L-*myc*; Kohl *et al*., 1983; Nau *et al*., 1985; Schwab *et al*., 1984), which encodes a basic (b) helix-loop-helix (HLH) leucine zipper (LZ) transcriptional factor, c-MYC. It was the first studied oncogene in Burkitt's lymphoma (Spencer and Groudine, 1991). In up to 70% of human tumours, c-*MYC* is implicated (Nilsson and Cleveland, 2003), including bladder, breast, cervix, colon, gastric, hepatocellular, small-cell lung, ovarian carcinomas, lymphoma, leukaemia, osteosarcomas, and glioblastomas. MYC protein has also been reported as an important regulator in metazoan growth, proliferation, and apoptosis (Green and Evan, 2002; Henriksson and Luscher, 1996; Oster *et al*., 2002). This section will describe the role of c-MYC in proliferation, apoptosis, and glucose homeostasis.

1.1.1 MYC protein

The transcriptional factor, c-MYC, plays an important role in cell proliferation, cell growth, differentiation, and apoptosis (Amati and Land, 1994), as reviewed in Pelengaris *et al*. (2002a), Dang *et al*. (2006) and Vita and Henriksson (2006).

There are several distinct functional domains in c-MYC; they are shown in Figure 1.1.1. The carboxy-terminal domain (CTD) of c-MYC contains a bHLHLZ motif, which can dimerize another nuclear protein, MAX. The MYC-MAX hereodimers initiate transcriptional activities by binding to specific DNA sequences such as the E-box sequence (CACGTG; Blackwood and Eisenman, 1991). MIZ1 (Myc-interacting zinc-finger protein 1), as MAX, binds to the CTD. The amino-terminal domain (NTD) contains conserved domains known as Myc boxes (MB). Myc Boxes I and II (MBI and MBII) are important for the transactivation of MYC's target genes, and MBII is required for all known c-MYC biological functions and is also involved in most of c-MYC target genes' activation or deactivation (Bahram *et al*., 2000; Stone *et al*., 1987). After c-MYC has bound to the target gene's promoter region, the MBII domain recruits co-activating proteins, such as TIP48/49 and TRRAP (transformation/transcription domain-associated protein), which constitute a common unit of numerous complexes. One example is the TIP60 and GCN5 complex, possessing histone acetyltransferase (HAT) activity (McMahon *et al*., 1998) which acetylates the K residue of the chromosomal histone and results in a more open chromosome structure (Bouchard *et al*., 2001; Davie and Hendzel, 1994; Frank *et al*., 2001). Another example that contains TRRAP is the complex containing the p400 and E1A binding protein (Fuchs *et al*., 2001). This complex possesses ATPase and helicase activities and suppresses HAT activity.

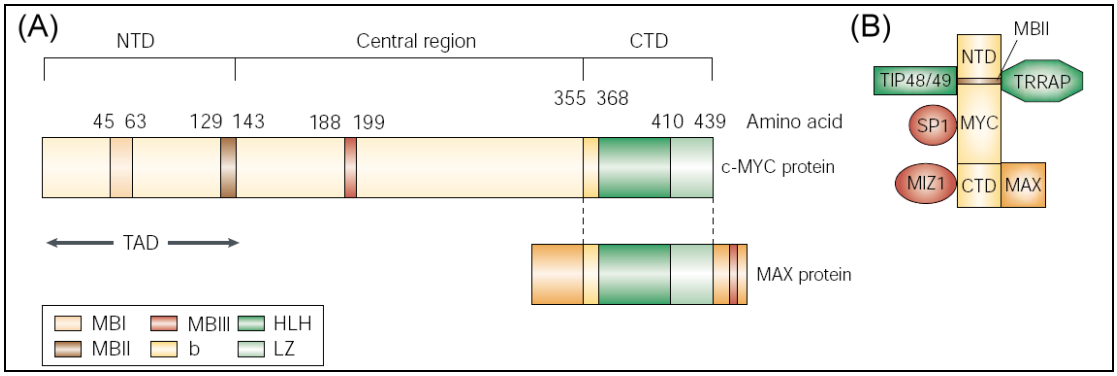

Figure 1.1.1. Functional domains of c-MYC. Image was adapted from Pelengaris *et al*. (2002a), figure 1.

(A) functional domains of c-MYC, and (B) MYC interacting proteins. The carboxy-terminal domain (CTD) contains the basic (b) helix-loop-helix (HLH) leucine zipper (LZ) motif, which can form a heterodimer with MYC's partner protein, MAX. MIZ1, as MAX, binds to the CTD. The amino-terminal domain (NTD) contains conserved components, MBI and MBII, which are important for the c-MYC target genes transactivation. MYC-MAX heterodimer binds to the promoter region of target genes, and recruits other cofactors, i.e. TRRAP (transformation/transcription domain-associated protein), TIP48/49, and SP1 (Sp1 transcription factor), to these conserved domains. TRRAP is able to activate the histone acetyltransferase (HAT) activity to remodel the chromatin whereas TIP48 and TIP49 are hexameric ATPases and contribute to the chromatin remodelling by their ATP-hydrolyzing and helicase activities. SP1 interacts with c-MYC by binding to the central region.

1.1.2 MYC and proliferation

The transcriptional regulation of c-MYC target genes relies on its partner protein, MAX. MYC and MAX are dimerized through the bHLHLZ motif. After the complex binds to the E-box sequence of target DNA, the transcriptional process is initiated. MYC-MAX heterodimers recruit TRRAP, which is a complex with HAT activity, as a co-activator, so that MYC-MAX heterodimers are able to enter the chromosome to activate transcription (Amati *et al*., 1993a; Amati *et al*., 1993b). MAX also binds with MAD, which replaces the original MYC after it degrades

rapidly after activating transcription (Hurlin *et al*., 1996; Zervos *et al*., 1993). MAD family members (MAD1, MXI1, MAD3 and MAD4), MNT (also known as ROX) and MGA, which act as antagonists to MYC, dimerize with MAX through bHLHz motifs and bind at E-box sequences (Ayer *et al*., 1993; Hurlin *et al*., 1997). The MYC/MAX/MAD network has been recognised as a standard model to describe the competition of MAX between MYC and MAD (Ayer *et al*., 1995; Grandori *et al*., 2000; Schreiber-Agus *et al*., 1995). Whereas the MYC-MAX heterodimer activates transcription, the MAD-MAX or MNT-MAX heterodimer acts as a suppressor. The MAD-MAX dimer binds to the E-box and recruits histone deacetylases (HDACs), which result in histone deacetylation, through the adaptor protein SIN3 (Ayer *et al*., 1995; Schreiber-Agus *et al*., 1995). Therefore, the MAD-MAX dimer represses the transcription of genes. This dimerization has also been confirmed as necessary for oncogenic MYC's dual functions (Amati *et al*., 1993b).

One of the main functions of c-MYC is the regulation of cell proliferation, in particular progressing the cell cycle from the G_0 phase into G_1 and S phase (Amati *et al*., 1998; Freytag, 1988). After the MYC-MAX heterodimer binds directly to the E-box sequence, it subsequently activates the transcription of *CCND2*, which encodes cyclin D2, and *CDK4*, which encodes cyclin-dependent kinase 4 (Bouchard *et al*., 1999; Hermeking *et al*., 2000). KIP1 (also known as p27), which is a cyclin-dependent kinase (CDK) inhibitor (Kiyokawa *et al*., 1996), is sequestrated from the cyclin D2-CDK4 complex by the expression of *CCND2* and *CDK4* (Bouchard *et al*., 1999); after which $p27^{KIP1}$ is degraded by two other c-MYC target genes, i.e. *CUL-1* (cullin 1) and *CKS* (CDC28 protein kinase regulatory subunit; Coller *et al*., 2000; O'Hagan *et al*., 2000a). c-MYC also phosphorylates the cyclin E-CDK2 complex by cyclin-activating kinase to prevent the binding of $p27^{KIP1}$

(Perez-Roger *et al*., 1999). c-MYC regulates the increase of CDK4 and CDK2 and hyperphosphorylates the retinoblastoma protein (RB); as a consequence, the release of E2F from RB induces cell proliferation (Weintraub *et al*., 1995; Weintraub *et al*., 1992). Furthermore, the tumour suppressor $p21^{CIP1}$, which is a CDK inhibitor, is also suppressed by MYC after DNA damage, which renders $p21^{CIP1}$ unable to activate cell cycle arrest in the G_1 phase (Herold *et al*., 2002; Seoane *et al*., 2002).

The ability to induce cell proliferation and hence to hamper cell terminal differentiation is another characteristic of c-MYC (La Rocca *et al*., 1994; Ryan and Birnie, 1997). The protein MYC and apoptosis will be discussed in more detail Section 1.1.3.

1.1.3 MYC and apoptosis

MYC-induced apoptosis demonstrates the dual function of this oncogene, as reviewed in Prendergast (1999). Apoptosis is programmed cell death, which is an intrinsic mechanism in metazoan organisms (Kerr *et al*., 1972). There are typical characteristics of apoptosis with morphological changes. It begins with condensation of the nuclear materials, followed by cell shrinkage. Cytoplasmic blebbing is the next event, and eventually the apoptotic cell detaches from other cells (Kerr *et al*., 1972). Adhikary and Eilers (2005) concluded that MYC triggers apoptosis through two distinct pathways and both of them trigger *cytochrome c* release from mitochondria; one is MYC-ARF/p53 independent signalling, and another is the MYC-ARF/p53 dependent pathway. Figure 1.1.2 summarises the key known and hypothesised pathways involving c-MYC.

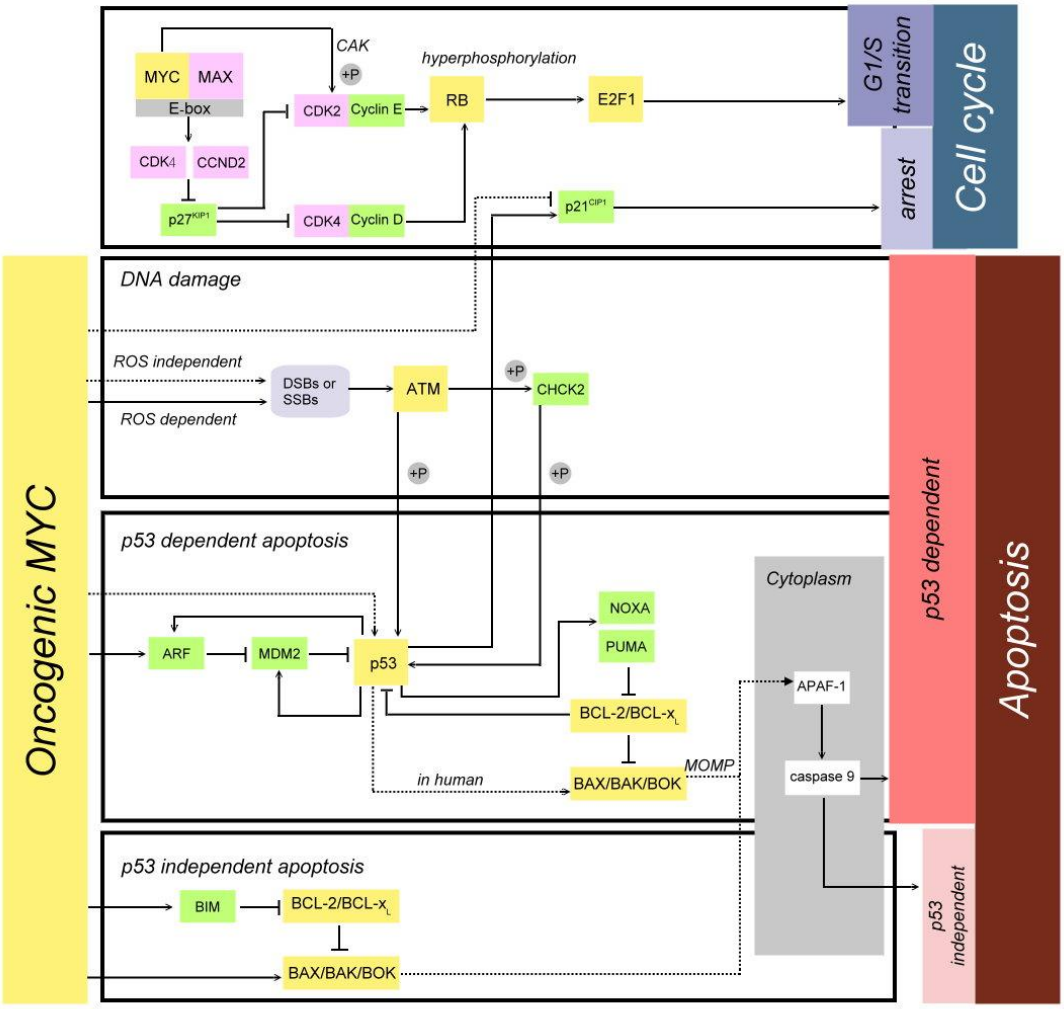

Figure 1.1.2. c-MYC regulated cell proliferation and apoptosis network.

One of the most well-known functions of MYC is its ability to transit cell cycle into the S phase. MYC binds to its partner protein, MAX, on the c-terminal basic-helix-loop-helix-zipper (bHLHZ) domain; after which they are able to bind a specific DNA sequence, E-box (CAGTG). MYC activates CCNDK2 and CDK4, and thus suppresses $p27^{KIP1}$. The sequestration of $p27^{KIP1}$ from cyclin D/CDK4 and cyclin E/CDK2 complexes consequently results in the increase of CDK4 and CDK2, which enables hyperphosphorylation of retinoblastoma protein (RB) and causes cell proliferation. However, MYC-induced apoptosis or cell cycle arrest is another pivotal event in anti-carcinogenesis. MYC-induced apoptosis is mediated by ARF/p53-dependent and ARF/p53-independent signalling pathways, both of which release *cytochrome c* from mitochondria into cytosol during apoptosis. In the MYC-ARF/p53-independent pathway, MYC activates BAX and BH3 (BCL-2 homology

domain 3)-only protein, i.e. BIM1, to sequester the anti-apoptotic protein BCL-2/BCL-x_L, which suppresses mitochondrial-outer-membrane permeabilization (MOMP). On the other hand, in the MYC-ARF/p53-dependent pathway, MYC activates $p19^{ARF}$, which inhibits MDM2 (murine double minute 2) and thus stabilises and activates p53. The activation of p53 induces pro-apoptotic genes, such as *BAX*, *PUMA* and *FAS* receptor; thus, they inhibit anti-apoptotic genes, such as *BCL-2* and *BCL-x_L*, finally resulting in apoptosis. Moreover, MYC-induced DNA damage, DNA double-strand breaks (DSBs) or single-strand breaks (SSBs), through reactive oxygen species (ROS)-dependent or ROS-independent system also play an important role in evoking apoptosis through ATM-dependent pathway. It is also believed that p53 at low levels of DSBs is able to activate $p21^{CIP1}$ and trigger cell cycle arrest before the S phase.

The *TP53* gene (also called p53, which is the protein product of *TP53*) has been studied for more than 20 years. It was first described as a tumour suppressor gene in 1979 (Lane and Crawford, 1979; Linzer and Levine, 1979). Only when cells are stressed, for example by DNA damage, hypoxia, nucleotide depletion, viral infection, heat shock, or oncogenic stimuli, will this tumour suppressor be activated to repair the damage of DNA, to induce apoptosis, and to arrest cell cycle, as reviewed in Vogelstein *et al*. (2000). This is why TP53 has been called "the guardian of the genome" (Lane, 1992; Macdonald, 2004). The connectivity of p53 in its cellular regulatory network has the properties of a 'scale-free network': a small group of proteins, i.e. p53, MDM2 (murine double minute 2), $p14^{ARF}$ /$p19^{ARF}$ (p14 in human and p19 in mouse), and E2F-4 are highly connected and control most proteins in this system (Vogelstein *et al*., 2000).

MDM2, a negative regulator limiting the tumour suppressor function of p53 (Chen *et al*., 1996; Momand *et al*., 1992), is a key regulator of p53 stability and activity. When the level of MDM2 rises, MDM2 serves as an E3 ubiquitin ligase for

p53 and binds to p53 directly and ubiquitinates p53, thus causing p53 proteolysis (Haupt *et al*., 1997; Honda *et al*., 1997; Kubbutat *et al*., 1997). Liberating p53 from MDM2 is a critical step in the activation of p53, and there are different ways to achieve this purpose by blocking MDM2 expression (Chen *et al*., 1998; Tortora *et al*., 2000), inhibiting MDM2-p53 binding (Kussie *et al*., 1996), or limiting MDM2 ubiquitin ligase activity (Sun, 2003). When p53 is activated, it activates pro-apoptotic genes, i.e. *BAX*, *PUMA* (p53-upregulated modulator of apoptosis) and *FAS* receptor (Lane, 1992).

One of the events that triggers the activation of p53 is ATM (ataxia-telangiectasia mutated)-dependent DNA damage, which is detected by checkpoints. This involves certain DNA damage-inducible kinases, i.e. ATM, CHK1, and CHK2. ATM is pivotal in DNA damage response (DDR), which directly phosphorylates p53 to weaken the MDM2-p53 complex, hence activates p53 (Banin *et al*., 1998; Canman *et al*., 1998; Khanna *et al*., 1998). In addition, ATM activates CHK2, which phosphorylates MDM2, and subsequently enhances the degradation of p53 (Khosravi *et al*., 1999). c-MYC also causes DNA damage, DNA double-strand breaks (DSBs) or single-strand breaks (SSBs), through the reactive oxygen species (ROS)-dependent (Vafa *et al*., 2002) or the ROS-independent pathway (Ray *et al*., 2006) before S phase. Oncogene-induced DDR triggers the activation of ATM, CHK2, ATR (ataxia telangiectasia and Rad3 related)-H2AX/CHK1, and p53 (Bartkova *et al*., 2005; Gorgoulis *et al*., 2005; Ismail *et al*., 2005), and has been suggested as a defence system against carcinogenesis in early stage cancer (Venkitaraman, 2005). Some studies found that p53 is able to activate $p21^{CIP1}$ at a low level of DBSs, resulting in cell cycle arrest (Sherr and Roberts, 1995).

Another mechanism that activates p53 is oncogenic stress, such as E1A (de Stanchina *et al*., 1998) and MYC (Zindy *et al*., 1998). MYC stimulates ARF protein to inactivate MDM2; in this manner, it inhibits MDM2-p53 interaction, which stabilizes and activates p53 (Kamijo *et al*., 1998; Stott *et al*., 1998). $p19^{ARF}$ is one of the protein products of the alternate reading frame of the mouse INK4a/ARF locus (Quelle *et al*., 1995). It is well known that $p19^{ARF}$ regulates apoptosis by inhibiting MDM2 to induce a p53-dependent pathway under oncogenic stress elicited from c-MYC deregulation (Kamijo *et al*., 1998; Zhang *et al*., 1998; Zindy *et al*., 1998; Zindy *et al*., 2003). MYC-ARF/p53 axis-induced apoptosis has been well studied (Sherr *et al*., 2005).

Adhikary and Eilers (2005) conclude that MYC triggers apoptosis through two distinct pathways, both of which trigger *cytochrome c* release from mitochondria; one is MYC-ARF/p53 dependent signalling, the other is the MYC-ARF/p53-independent pathway. In the latter one, c-MYC regulates BAX (Juin *et al*., 2002; Soucie *et al*., 2001). The BCL-2 family proteins suppress mitochondrial-outer-membrane permeabilization (MOMP) to prevent apoptosis (Martinou and Green, 2001). BIM is a BH3-only protein (where BH3 stands for BCL-2 homology domain 3), which is indirectly induced by MYC (Egle *et al*., 2004). It works together with BAX and promotes apoptosis by suppressing the protective action of BCL2/BCL-x_L (O'Connor *et al*., 1998; Soucie *et al*., 2001) which results in MOMP and release of *cytochrome c* from mitochondria into cytosol (Soucie *et al*., 2001); after which *cytochrome c* reacts with apoptotic protease-activating factor 1 (APAF1) triggering apoptosis (Juin *et al*., 1999).

1.1.4 MYC and glycaemic regulation

Glycolysis is one of the major pathways producing ATP (adenosine triphosphate), which stores energy for various molecular functions. Insulin secretion is pulsatile and occurs in response to a raised plasma glucose level (Goodner *et al*., 1977; Lang *et al*., 1979). The regulation of glucose stimulated-insulin secretion (GSIS) depends on glucose metabolism and the activity of β-cell plasma membrane ion channels (Ashcroft and Rorsman, 1989).

In the GSIS model, insulin is secreted by the following events. Glucose moves from the blood plasma into the β-cells through the glucose transporter II (GLUT2; Orci *et al*., 1989; Thorens *et al*., 1988). In the β-cell, high-K_m glucokinase (GK) acts as a glucose sensor, which phosphorylates glucose to glucose-6-phospate and is a rate-limiting step in glycolysis (Matschinsky, 1996). Furthermore, studies indicate that mutation of GK results in hypoglycaemia or hyperglycaemia as gain-of-function or loss-of-function, respectively (Christesen *et al*., 2002; Glaser *et al*., 1998; Gloyn, 2003). ATP is produced by glycolysis; an increasing ATP/ADP (adenosine diphosphate) ratio closes the ATP-sensitive K^+ (K_{ATP}) channels (Ashcroft *et al*., 1984; Cook and Hales, 1984; Misler *et al*., 1986). In β-cells, this potassium channel is composed of four inward-rectifier K^+ channel subunits, KIR6.2, and four outward sulphonylurea receptor subunits (SUR1), as reviewed in Aguilar-Bryan and Bryan (1999) and Ashcroft and Gribble (1999). The closed potassium channels gradually depolarize the cell membrane from the resting potential, which is -70 mV (Matthews and Sakamoto, 1975; Meissner and Schmelz, 1974), and trigger an action potential that activates the voltage-dependent calcium channels (VDCCs), resulting in a flux of extracellular Ca^{2+} into the β-cell (Misler *et al*., 1986). The entrance of calcium

triggers exocytosis of insulin-secreting granules and releases insulin into the plasma, as reviewed in Ashcroft *et al*. (1994). Exocytosis is regulated by soluble N-ethylmaleimide-sensitive fusion (NSF) attachment protein receptor (SNARE) proteins, which fuse the exocytotic vesicles to the plasma membrane. These SNARE proteins interact with VDCCs, which regulate Ca^{2+} entry and exocytosis of insulin secretion (Barg *et al*., 2002b). Some studies suggest that depolarization of membrane potential will open the voltage-dependent potassium (K_v) channel to repolarize the action potentials. In this way calcium influx and insulin secretion are restricted, as reviewed in MacDonald and Wheeler (2003). Figure 1.1.3 depicts the scheme of GSIS.

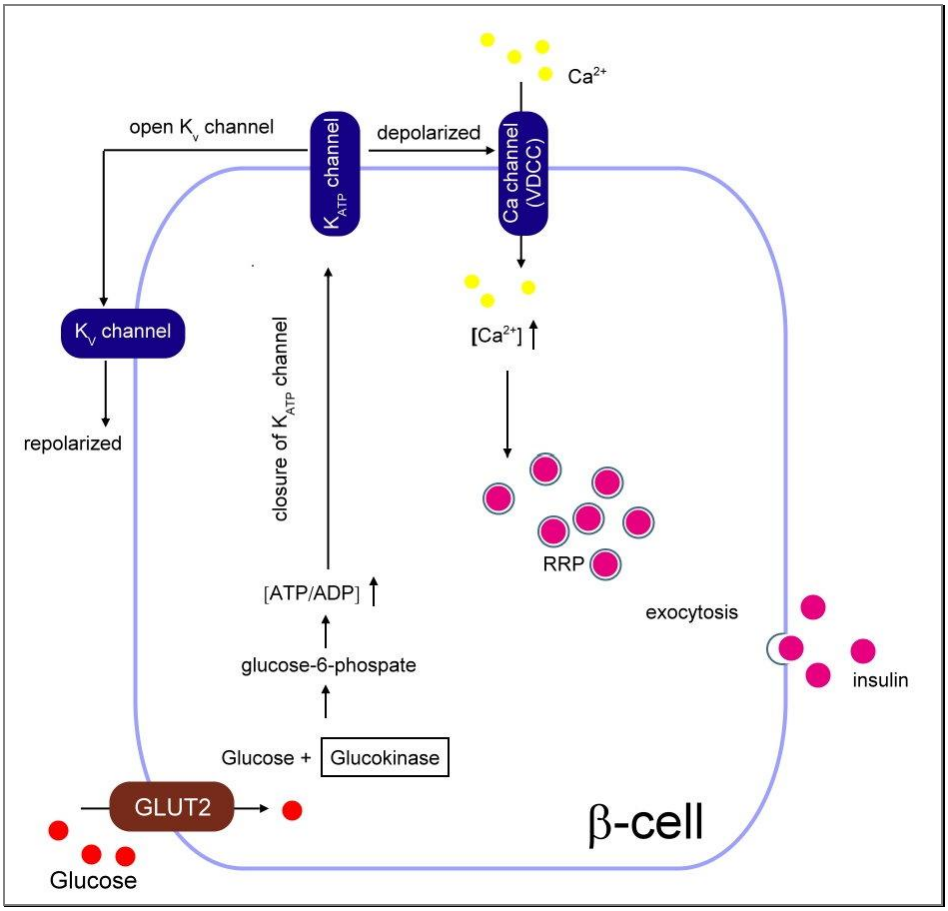

Figure 1.1.3. Scheme of GSIS.

Glucose is transported into the β-cell through the glucose transporter II (GLUT2), and is subsequently phosphorylated by the high-K_m glucokinase (GK) into glucose-6-phospate. As a result of glycolysis, the concentration of ATP/ADP is increased, which triggers the closure of K_{ATP} channels. The closed potassium channels gradually depolarise cell membrane from the resting potential and trigger an action potential that activates the voltage-dependent calcium channels (VDCCs) and causes the influx of extracellular calcium into the β-cell. The increased calcium concentration triggers the exocytosis of insulin-secreting granules from the 'readily releasable pool' (RRP) and releases insulin into the plasma.

About 1-5% of the granules in β-cells are able to release insulin immediately when required, a process completed in a few seconds (Barg *et al*., 2002a; Barg *et al*.,

2001; Barg *et al*., 2002b). More than 95% of the granules are in the reverse pool and require mobilization. After the consumption of this 'readily releasable pool' (RRP), the β-cells require some time to refill the pool (Barg *et al*., 2002a; Barg *et al*., 2002b; Gromada *et al*., 1999). The time difference of the insulin secretion from RRP (1^{st} phase) and refilling (2^{nd} phase) is responsible for the well-known biphasic secretion of insulin in the face of elevated extracellular glucose (Rorsman *et al*., 2000), as reviewed in Rorsman and Renström (2003). The 1^{st} phase insulin secretion is released by the Ca^{2+}-entry influx (Barg *et al*., 2002a) whereas the refilling of RRP in 2^{nd} phase needs a 'primer', namely ATP, Ca^{2+} and temperature, and only fuel secretagogues, i.e. glucose, are able to initiate the 2^{nd} phase secretion.

In addition to glucose, arginine and sulphonylurea may also act as insulin secretagogues. Insulin may itself play an important role in GSIS, through an autocrine or paracrine loop. Insulin activates insulin receptors on the surface of β-cells (Verspohl and Ammon, 1980). Insulin secreted from GSIS feedback loop activates insulin receptors in an autocrine fashion (Rothenberg *et al*., 1995; Xu *et al*., 1998) and this may contribute to increased insulin biosynthesis. Aspinwall *et al*. (1999) detected 5-hydroxytryptamine (5-HT) in a single mouse pancreatic β-cell *in vitro* system to observe the insulin secretion stimulated by exogenous insulin. They also found similar secretions in human, porcine, and canine β-cells and suggested that insulin activates the insulin receptor. In a β-cell-specific insulin receptor knockout (βIRKO) mice model, the loss of insulin receptors resulted in the loss of 1^{st} phase insulin secretion in GSIS (Kulkarni *et al*., 1999) but gradual 2^{nd} phase secretion was retained. However, in arginine-treated βIRKO mice (Srivastava and

Goren, 2003), the two phases of insulin secretion can still be detected. These results suggest the importance of insulin in GSIS.

Cell cycle entry or tumorigenesis consume a considerable amount energy which implies that the mitochondrial biogenesis and glycolysis signalling are important to these bioenergetic needs (Herzig *et al*., 2000; Sweet and Singh, 1995; Warburg, 1956; Warburg and Dickens, 1930). Although there is no direct evidence linking MYC to mitochondrial biogenesis, some studies have pointed out a relationship between MYC and glycolysis (Dang and Semenza, 1999; Li *et al*., 2005; Osthus *et al*., 2000; Zhang *et al*., 2007).

Osthus *et al*. (2000) suggested that MYC regulates glycolytic genes to increase glucose metabolism by using chromatin immunoprecipitation (ChIP) assays. Evidence shows that MYC regulates the activation of lactate dehydrogenase-A (LDH-A; Hu *et al*., 2011; Osthus *et al*., 2000; Shim *et al*., 1997), whose activity is important in tumour cells because it converts pyruvate to lactate in the final step of anaerobic glycolysis (Robey *et al*., 2005; Zhong *et al*., 1999); this is known as the Warburg effect (Warburg, 1956). However, recent studies demonstrate the link between MYC and mitochondrial biogenesis (Li *et al*., 2005; Osthus *et al*., 2000; Zhang *et al*., 2007). Further investigation of how MYC links the metabolic processes to the cell cycle entry is still pending (Morrish *et al*., 2008).

1.1.5 MYC and β-cell regulation

Interest in β-cell regeneration has increased recently as it has been proposed as a potential treatment for diabetes (Butler *et al*., 2007). The change of β-cell mass results from β-cell proliferation, size (hypertrophy or atrophy), and apoptotic deletion (Bouwens and Rooman, 2005) triggered by different physiological or pathological conditions, such as injury, pregnancy (Parsons *et al*., 1995; Parsons *et al*., 1992), obesity (Bruning *et al*., 1997; Cho *et al*., 2001a; Okada *et al*., 2007), insulin resistance (Bruning *et al*., 1997; Pick *et al*., 1998), or diabetes (Butler *et al*., 2003). It was reported that β-cell mass expands fast after birth, especially in infancy, in both humans and rodents mainly because of proliferation (Dor *et al*., 2004; Kassem *et al*., 2000; Meier *et al*., 2008; Teta *et al*., 2007) but β-cell replication rate is decreased in an age-dependent manner because of epigenetic modification of aging β-cells (Finegood *et al*., 1995; McEvoy, 1981; Meier *et al*., 2008). Several studies also pointed out β-cell mass gradually increases in adult rodents throughout their life time and is linearly correlated to its body weight after the first month of life (Bonner-Weir, 2000a; Finegood *et al*., 1995; Montanya *et al*., 2000). Montanya *et al*. (2000) showed that in male Lewis rats, the expansion of β-cell mass was mainly from the increased β-cell numbers (hyperplasia) before the age of 15 months, and an increase in β-cell size (hypertrophy) afterwards. Hypertrophy has also been recognised by many diabetic rodent models as a rapid and economical β-cell compensatory mechanism to maintain euglycaemia (Bonner-Weir *et al*., 1989; Jonas *et al*., 1999; Montanya *et al*., 2000; Pick *et al*., 1998).

Apart from the continuous growth of β-cells throughout the lifespan, direct or indirect β-cell turnover has been observed and widely studied in both humans and rodents (Bonner-Weir, 2000b). According to apoptopic and replication rate of β-cells *in vivo*, Finegood *et al*. (1995) used a mathematical model to estimate the lifespan of rat β-cell, which is about 58 days, and suggested the interplay of proliferation and apoptosis contributes to the maintenance of β-cell mass. Indirect evidence also showed the β-cell turnover in the human pancreas (Meier *et al*., 2005) but the replication rate of human β-cells is much lower than that in rodents (Bouwens *et al*., 1997; Bouwens and Pipeleers, 1998). An issue of great interest has been focused on the source of new β-cells in adults under different physiological demands. Two controversial hypotheses suggest that new β-cells are from self-replication (Dor *et al*., 2004; Nir *et al*., 2007; Teta *et al*., 2007) or neogenesis, such as from stem cells, progenitor cells from ductal epithelium (Bonner-Weir *et al*., 1993; Rooman *et al*., 2002), non-β-cell progenitors (Abouna *et al*., 2010), or transdifferentiation from pancreatic acinar cells (Lipsett and Finegood, 2002). However, some studies suggested that both β-cell proliferation and neogenesis contribute to β-cell regeneration (Rooman and Bouwens, 2004; Thyssen *et al*., 2006; Waguri *et al*., 1997).

c-MYC induced β-cell proliferation is similar to other cell types, and has been described in Section 1.1.2. Studies showed that different glucose concentrations stimulate β-cell proliferation or apoptosis (glucotoxicity; Efanova *et al*., 1998; Swenne, 1982; Yki-Jarvinen, 1992). Moreover, gene knockout studies, i.e. β-cell-specific insulin receptor knockout (βIRKO) mice, presented a deficiency of β-cell mass (Kulkarni *et al*., 1999; Otani *et al*., 2004). Thus the hypothesis of

insulin-induced β-cell proliferation has become widely studied (Beith *et al*., 2008; Okada *et al*., 2007).

1.2. MYC-regulated gene network

The targets of c-MYC are currently listed as 647 directly interacting genes (Zeller *et al*., 2003). If one expands the gene network by including indirect targets, c-MYC can be regarded as regulating 10-15% of cellular genes (Dang *et al*., 2006; Knoepfler, 2007) but with little overlap of the identified targets in different groups. In view of the complexity of the situation, it is necessary to use all available information and techniques to integrate the large amount of related information. Techniques such as microarray, chromatin immunoprecipitation (ChIP), and promoter microarrays (ChIP-on-chip) are used to study the gene expression levels and transcriptional promoters (Lee *et al*., 2002; Lockhart and Winzeler, 2000; Ren *et al*., 2000).

Studies based on using high-throughput analysis, such as serial analysis of gene expression (SAGE; Velculescu *et al*., 1995) and microarray, have pointed to genes that were up- or down-regulated by MYC *in vitro* (Coller *et al*., 2000; Guo *et al*., 2000; Hermeking *et al*., 2000; Menssen and Hermeking, 2002; O'Hagan *et al*., 2000b; Schuhmacher *et al*., 2001). Genes relating to cell cycle, signalling, growth, and cell adhesion were found regulated by MYC (Coller *et al*., 2000). Lawlor *et al*. (2006) applied microarray to study MYC-induced carcinogenesis in pancreas systematically *in vivo* using the *plns-c-MycER*^{TAM}*/RIP-Bclx*$_L$ transgenic mouse model. It is not surprising that the genes involved in gene ontological cell cycle and proliferation, e.g. cyclin D1 and cyclin D2, were found within 24 hours of MYC

activation. Furthermore, they also found the islet-specific genes, i.e. *Gad1*, *Ptprn*, *Slc2a2* (which encodes GLUT2) and *Ipf1* (which encodes PDX1; Schwitzgebel *et al*., 2003; Stoffers *et al*., 1997) were deregulated within 2-4 hours after switching MYC on. Robson *et al*. (2011) applied the *c-MycER*^{TAM} transgenic mouse model to study MYC activation in two different tissues *in vivo*, i.e. pancreas and skin, and showed that within 24 hours of MYC activation in β-cell, genes relating to DNA damage, intrinsic apoptosis, and the cell cycle were activated. These might provide clues about the linkage between MYC-induced proliferation and dedifferentiation in the early stage after MYC activation. However, the study of MYC-regulated genes *in vivo* has still been limited and the topic awaits further investigation.

1.3. Diabetes and treatment

Diabetes is characterised by a loss of β-cell function and hyperglycaemia, and carries an increased risk of cardiovascular disorder, adult blindness, stroke, limb amputation, and early death (Krolewski and Warram, 2005). There are two major types of diabetes, Type 1 (T1DM) and Type 2 (T2DM). The former one results from the autoimmune destruction of β-cells, whereas the latter is caused by peripheral insulin resistance and deregulated β-cell compensatory function.

Current treatment for T1DM is the injection of insulin or islet transplantation (Shapiro *et al*., 2000; Street *et al*., 2004). The treatment of T2DM includes maintaining a healthy life style and treatment with glucose-lowering agents, such as sulfonylureas, metformin, or thiazolidinediones, which are common oral antidiabetic drugs. Side effects of these drugs include increased β-cell death, weight gain, or

hypoglycaemia (Gerstein *et al*., 2008; Kahn *et al*., 2006). Hypoglycaemia is the most common and recognisable side effect of diabetes treatment (Cryer, 2002) and iatrogenic hypoglycaemia causes frequent morbidity. Symptoms are seizure and coma and sometimes hypoglycaemia is fatal (Feltbower *et al*., 2008; Gerich, 1989; Jacobson *et al*., 2007; Skrivarhaug *et al*., 2006). In a healthy, non-diabetic, adult, hypoglycaemia can be prevented or corrected by three physiological responses that defend against the progression of hypoglycaemia, namely reducing endogenous insulin secretion and increasing counterregulatory factors, such as glucagon, which stimulates hepatic glycogenolysis, and adrenaline, which also contributes to glycogenolysis and decreases the glucose clearance by tissues, to maintain the euglycaemia (Fanelli *et al*., 1994; Schwartz *et al*., 1987).

In comparison to intravenous glucose administration, oral glucose administration incurs the incretin effect, which has a different insulin secretion action, namely the gut-derived hormone enhances GSIS. Around 50-70% insulin is secreted after the oral glucose ingestion (Baggio and Drucker, 2007). Two gut-derived hormones have been defined and can result in the incretin effect: one is glucose-dependent insulinotropic polypeptide (GIP), which is secreted by K-cells mainly located in the upper small intestine (duodenum and jejunum, and some are presented in distal ileum). The other one is glucagon-like peptide (GLP)-1, which is produced by L-cells located in the small intestine and colon (Buchan *et al*., 1978; Buffa *et al*., 1975; Eissele *et al*., 1992; Kauth and Metz, 1987; Mortensen *et al*., 2003). Both are able to stimulate insulin secretion and thus reduce the glucose level after a meal (Ebert and Creutzfeldt, 1980; Orskov, 1992). Incretin-stimulated insulin secretion is the result of incretins binding to receptors on β-cells: GIP binds to glucose-dependent insulinotropic peptide receptor (GIPR; Maletti *et al*., 1984) and

GLP-1 binds to glucagon-like peptide-1 receptor (GLP-1R). This interaction triggers an increase of intracellular Ca^{2+} through voltage-dependent Ca^{2+} channels (Lu *et al*., 1993) and stimulation of exocytosis through the cAMP (cyclic adenosine monophosphate)/PKA (protein kinase A) signalling pathway (Ding and Gromada, 1997).

GLP-1 has been suggested as a possible treatment in T2DM (Holst, 1999), and recent studies suggest that GLP-1 is involved in β-cell regulation and increasing β-cell mass (Burcelin and Dejager, 2010). In T2DM patients it was observed that the incretin effect is reduced or absent (Nauck *et al*., 1986), but after administration of GLP-1, insulin secretion was restored (Hojberg *et al*., 2009). Furthermore, *in vitro* and *in vivo* data support that GLP-1 can prevent β-cell apoptosis in diabetic rodents, mouse insulinoma cell lines, and rat islets (Farilla *et al*., 2002; Hui *et al*., 2003; Li *et al*., 2003; Wang and Brubaker, 2002). New drugs based on GLP-1 have already been used clinically (Lovshin and Drucker, 2009). Exenatide, which is an analogue of GLP-1 and has been reported to stimulate β-cell proliferation *in vitro* and *in vivo*. It also enhances GSIS, induces satiety, and reduces the glucose level without causing hypoglycaemia (Baggio and Drucker, 2007; Drucker, 1998) whereas other drugs have to compromise with side effects, such as glucose counterregulation (Gerich, 1989), which is the mechanism preventing or correcting hypoglycaemia.

1.4. Transgenic mouse model

In several animal diabetes models, a deficiency of β-cell functions was hypothesised to result from β-cell dedifferentiation (Jonas *et al*., 1999; Laybutt *et al*., 2002), or from apoptosis (Pelengaris *et al*., 2002b; Pick *et al*., 1998). NOD

(non-obese diabetic) mouse (Atkinson and Leiter, 1999; Makino *et al*., 1980) or streptozotocin (STZ) induced β-cell deletion mouse model (Kolb, 1987; Like and Rossini, 1976) have been used to study T1DM. Apart from pancreatectomy or obese-induced diabetes mice, gene knockout mice, such as insulin receptor knockout mice, have also been widely applied to study the role of insulin resistance in T2DM (LeRoith and Gavrilova, 2006; Pattaranit *et al*., 2008).

A chimeric protein, *c-MycER*^{TAM}, in which human c-MYC has been fused to a mutated form of the estrogen receptor (ER; ER^{TAM}), can induce the activation of c-MYC by the injection of 4-hydroxytamoxifen (4-OHT; Littlewood *et al*., 1995; Pelengaris *et al*., 1999), and it has been set up as a transgenic animal model to turn MYC on or off. Pelengaris *et al*. (2002b) used *pIns-c-MycER*^{TAM} transgenic mice, in which the *c-MycER*^{TAM} is regulated by the insulin promoter (pIns) so that this fusion transcriptional factor is specifically targeted to insulin producing β-cells, to explore the role of c-MYC in apoptosis and proliferation in β-cells. Activation of c-MYC induces proliferation in a short transition but this proliferation is subsequently overwhelmed by apoptosis in β-cells. As a result, the transgenic mice become hyperglycaemic and unable to control the glucose homeostasis. However, deactivation of c-MYC by withdrawing 4-OHT leads to the regeneration of β-cells in this c-MYC activated transgenic mouse. Thus this animal model can be applied to the study of β-cells regeneration. Pelengaris *et al*. (2002b) also presented the doubly transgenic *pIns-c-MycER*^{TAM}*/RIP-Bclx*$_L$ mice by giving c-MYC activation with co-expression of *Bcl-x*$_L$ (which encodes an anti-apoptotic BCL-2 family protein). This triggers carcinogenesis without apoptosis but shows hyperglycaemia in the early stage (6-9 days). They also found indications that the *in vivo* effects of c-MYC

are reversible, i.e. deactivation of *c-MycER*^{TAM} elicits β-cell and islet regeneration and deactivation of *c-MycER*^{TAM} in *c-MycER*^{TAM}*/Bcl-x*$_L$ doubly transgenic model triggers regression of cancerous cells to normal cells with normal cell behaviour. Furthermore, using the *pIns-c-MycER*^{TAM} transgenic mice, Cano *et al*. (2008) confirmed β-cell regeneration after withdrawing tamoxifen in the transgenic animal system and suggested that retention of β-cells results from replication of surviving β-cells. However, Cano *et al*. (2008) also found early hypoglycaemia in this transgenic mouse and suggested that the low glucose level might be due to passive release of insulin because of on-going β-cell apoptosis. However, this appears not to be the case since hyperinsulinaemia precedes any significant decrease in β-cell mass in *pIns-c-MycER*^{TAM} mice. This view is supported by further functional studies in our group showing that hypoglycaemia is not prevented when MYC-induced apoptosis is fully prevented by co-expression of the anti-apoptotic protein BCL_{xL} in *pIns-c-MycER*^{TAM}*/RIP-Bcl*$_{xL}$ doubly transgenic mice (see Figure 1.4.1; Dr. Linda Cheung, unpublished data).

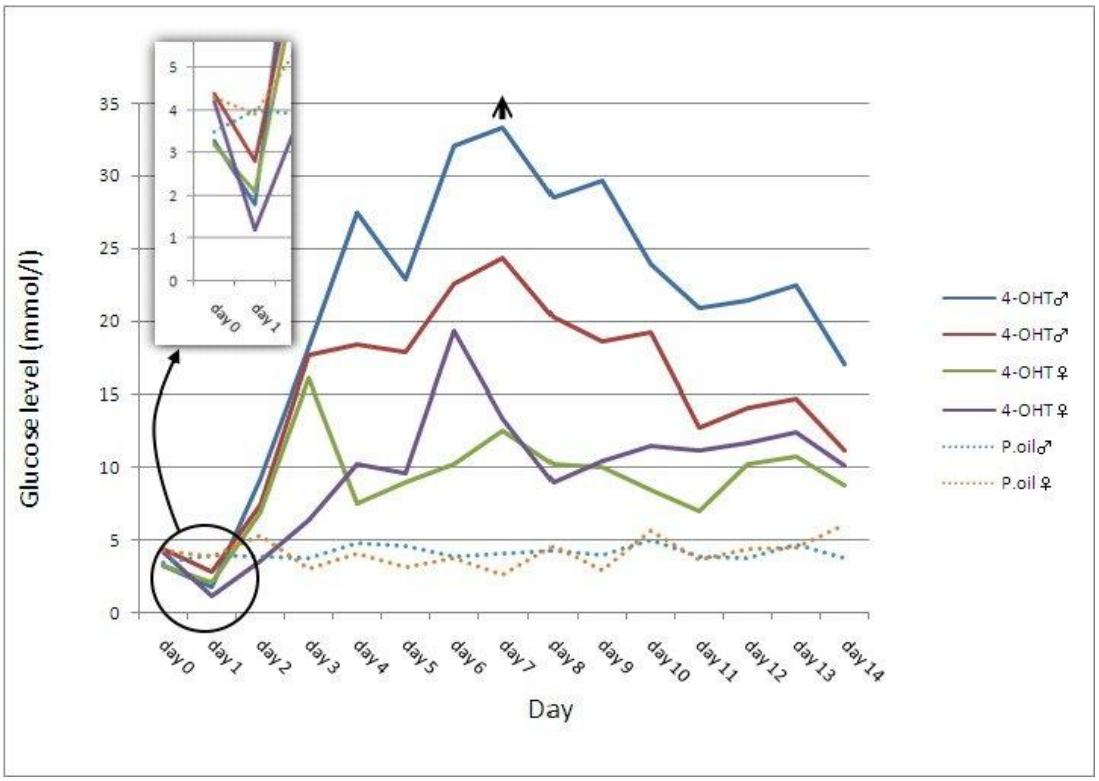

Figure 1.4.1. Glucose level in *plns-c-MycER*^{TAM}*/RIP-Bclx*$_L$ doubly transgenic mice. (Dr. Linda Cheung, unpublished data). Solid lines refer to the objects with treatment (4-OHT), whereas dash lines refer to the control group (WT littermates treated with peanut oil). 4-OHT, 4-hydroxytamoxifen; P.oil, a vehicle in which 4-OHT is made and acts as a control; ⇳, male; ♀, female; ↑, the glucose level is higher than the measurement range, which is 0.6-33.3 mmol/l.

Figure 1.4.1 shows the glucose level in the *plns-c-MycER*^{TAM}*/RIP-Bclx*$_L$ doubly transgenic mice after treating with 4-OHT (treatment, n=4) or the same amount of vehicle (control, n=2). The glucose level is different ($p<0.05$, paired t-test) between control and treatment mice in day 1. The difference ($p<0.01$, paired t-test) between day 0 and day 1 in the treatment group indicates a decrease of glucose level on day1, whereas there is no significant difference ($p=0.9126$, paired t-test) in the glucose level in the control group. Apart from hyperglycaemia, which is regarded as a

characteristic of diabetes, sudden hypoglycaemia was observed within 24 hours after c-MYC activation. This indicates that c-MYC-activated hypoglycaemia might not be directly linked to insulin released from apoptopic β-cells because apoptosis was blocked by the expression of BCL_{xL}.

MYC-activated diabetes animal models suggest that the activation of c-MYC reduces the expression of insulin, pancreatic duodenal homeobox factor-1 (PDX1), NKX6.1, GLUT2, and prepoinsulin I+II (PPI; Kaneto *et al*., 2002; Laybutt *et al*., 2002; Pascal *et al*., 2008; Pelengaris *et al*., 2002b). PDX1, also known as STF1, IDX1, IPF1, IUF1, which binds to A-box (Ohlsson *et al*., 1993), is an important transcriptional factor in pancreatic development and insulin transcription (Ahlgren *et al*., 1996; Ahlgren *et al*., 1998; Chakrabarti *et al*., 2002; Ohlsson *et al*., 1993). In PDX1-deficient animal models, impaired glucose tolerance and GSIS were found (Brissova *et al*., 2002; Johnson *et al*., 2003; Leibowitz *et al*., 2001; Seufert *et al*., 1998). Deficiency of PDX1 is further related to GLUT2, glucokinase (GK), MAFA, NKX6.1, and insulin, whose products are key factors in GSIS (reviewed in Babu *et al*., 2007). The *pIns-c-MycER*^{TAM} transgenic mouse can therefore be adopted for the study of β-cell regeneration or diabetes treatment without other confounding factors, such as obesity. There are many studies related to β-cell regeneration but a robust animal model is still necessary to demonstrate the process of β-cell regulations *in vivo*.

1.5. Mathematical model of physiological dynamics

The homeostasis between glucose, insulin, and β-cell mass plays an important role in the study of diabetes, which is characterized by hyperglycaemia, insulin resistance, and the persistence of β-cell dysfunction. Several mathematical models have been formulated to study glucose-insulin dynamics, in order to contribute to the understanding of the aetiology of diabetes. The main idea of formulating mathematical models is to preserve biologically relevance by referring to experimental data and subsequently testing the biological hypothesis by subjecting the predictive results from mathematical simulations to further experimentation. A mathematical model can also help the design of experiments by defining specific parameters which were ill-defined numerically by previous experiments. A simple mathematical model of the insulin-glucose feedback loop was proposed by Bolie (1961), describing the relationship between glucose and insulin by means of ordinary differential equations (ODEs). Based on this glucose-insulin fundamental feedback loop, the model can be extended. A three-ODE model of glucose-insulin dynamics, which is also known as the standard minimal model, was built by Bergman *et al*. (1981). It further extended the two-compartment glucose-insulin model into a three-compartment model, i.e. glucose, insulin, and remote insulin. Other physiological parameters relating to glycaemic homeostasis, such as glucagon, NEFAs (non-esterified fatty acids), TAGs (triacylglycerides), and leptin, can be also be incorporated into more extensive mathematical models (Pattaranit and van den Berg, 2008).

Absolute or relative deficiency of β-cell mass depicts the pathogenesis of T1DM

or T2DM. More details of β-cell mass regulation have been described in Section 1.1.5. Mathematical models of β-cell turnover have been introduced to simulate the phenomenon as well. Finegood *et al*. (1995) formulated a mathematical model to stimulate β-cell mass of adult rats between the ages of one and three month using the relationship between β-cell number, size, proliferation, neogenesis, and apoptosis. Using the human IAPP (islet amyloid polypeptide) transgenic (HIP) rat, Manesso *et al*. (2009) presented the dynamics of β-cell turnover, which was detected by immunostaining of Ki67, which is a marker for proliferation, and the terminal deoxynucleotidyl (TdT)-mediated dUTP nick-end labeling (TUNEL), which is a marker for apoptosis, and suggested that β-cell regeneration is contributed by neogenesis other than β-cell replication.

Apart from those physiological parameters, other perturbations of computational modelling can be implemented to suit the actual physiological situation, for example, introducing a time delay to describe insulin secretion in response to glucose stimulation or hepatic glycogenesis in response to insulin secretion (Bennett and Gourley, 2004; Giang *et al*., 2008; Li *et al*., 2006; Tolic *et al*., 2000).

As more experimental data were obtained, more sophisticated and robust mathematical models could be constructed to address biological questions. Several models were formulated to understand the relationship between glycaemic control and insulinemia within a limited time duration of the object's lifespan, i.e. the model is only representing a short-term simulation of the experimental period (Bergman *et al*., 1979; Bolie, 1961; Li *et al*., 2006; Panunzi *et al*., 2007). Thus, mathematical models combing long-term effect, such as β-cell regulation, with glycaemic controls, i.e. glucose level and insulin level, have been published as well to study the

aetiology of diabetes (Chen *et al*., 2010; de Winter *et al*., 2006; Hamren *et al*., 2008; Ribbing *et al*., 2010; Topp *et al*., 2000).

Neuroendocrine control systems, such as glucose homeostasis, respond rapidly to physiological challenges while concurrently undergoing adaptation on much slower time scales, such as β-cells adaption or decompensation during the progress of diabetes, e.g. Schmidt and Thews (1989) and Frayn (1996). Moreover, an interplay prevails between processes at disparate scales: the slow adaptation is dependent on the fast events. Such an interplay is a pervasive characteristic of many biological systems.

As is well known, the dynamics of such systems can be analysed by considering separate and distinct dynamical systems that correspond to the biological system as it operates on two or more "time scales". In such procedures, the approximation usually is exact if the slower component is "infinitely slower" than the faster component, see Keener and Sneyd (1998) for examples and applications. On a given time scale, the slower variables are "frozen" and appear as constant parameters, whereas the faster ones can often be treated using a quasi-steady state approximation (up to boundary or transition layers) in which the fast variable is essentially replaced by a function which relates its (fast-time system) equilibrium value to the prevailing values of the slower variables. Similarly, in those cases where the fast-time system does not equilibrate but tends to a periodic solution (e.g., a limit cycle or the stationary response to periodic forcing), intuition would suggest that the fast variables might be replaced by a long-term average. However, this intuition need not be correct. This thesis outlines a general method to tackle such problems on two time scales. The type of system describes the dynamics of an organism's physiology (or

the relevant part thereof) together with the dynamics of the (neuro)endocrine system that regulates this physiology. The method is applied to a well-established model of the regulation of glucose concentration in the blood plasma, which was extended with a slow component, viz. the dynamics of the mass of endocrine cells.

1.6. Aims and hypotheses

The thesis proposes to investigate the hypothesis that c-MYC regulates the expression of key genes required for regulation of insulin secretion, including those for differentiation and for glucose stimulation of insulin secretion (GSIS). This c-MYC-mediated regulation may have major implications, since c-MYC regulated insulin secretion is a potentially important mechanism coupling β-cell mass increases in pre-diabetic states to eventual depletion/reduction in insulin stores and aberrant GSIS. The aim of this thesis is to characterize the initial stage of the expression of c-MYC from the *pIns-c-MycER*^{TAM} mouse model. In particular, the objectives are to understand insulin secretion and glucose levels after c-MYC has been switched on in an *in vivo* experiment, and to analyse the experimental observations by means of an *in silico* analysis based on microarray analysis and a mathematical model.

Chapter 2. Material and Methods

2.1 Transgenic animal model

2.1.1. Genotyping of *pIns-c-MycER^{TAM}* mouse

Mouse ear snips were collected using the ear-punch technique for DNA extraction. Subsequently, 75 µl hotshot reagent (25 mM NaOH and 0.2 mM disodium ethylenediaminetetra acetic acid (EDTA), pH 12), the alkaline lysis reagent, was added to each sample for 30 minutes at 95 ℃. After the biopsy samples had been incubated with hotshot reagent, neutralizing reagent (40 mM Tris-HCl, pH 5) was added at the same volume to neutralize the reaction and the samples were subsequently kept at 4 ℃ overnight. These DNA samples were stored at 4 ℃, or -20 ℃ for longer storage. A master mix was prepared of 15.25 µl sterile H_2O, 2.5 µl ×10 PCR buffer (Invitrogen, Carlsbad, CA), 0.75 µl $MgCl_2$ (50mM; Invitrogen, Carlsbad, CA), 0.5 µl MYC5 3'-primer (10 pm/µl; sequence (5' to 3') AGG GTC AAG TTG GAC AGT GTC AGA GTC), 0.5 µl MERTM 5'-primer (10 pm/µl; sequence (5' to 3') CCA AAG GTT GGC AGC CCT CAT GTC), 0.25 µl Taq polymerase (500 U/µl; Invitrogen, Carlsbad, CA) and 0.25 µl dNTPs (10 mM; Invitrogen, Carlsbad, CA) for each DNA sample. An aliquot of 5 µl of each DNA sample was mixed with 20 µl master mix and subsequently processed using a PTC-100 Programmable Thermal Controller (MJ Research, Inc., Waltham, MA). The PCR programme procedure was as follows: step 1: 2 minutes at 94 ℃; step 2: 30 cycles of 1 minute at 94 ℃, 1 minute at 57 ℃, and 2 minutes at 72 ℃; and step 3: 10 minutes at 72 ℃. The positive control DNA sample was

plns-c-MycER^{TAM}-positive DNA, the false-positive control DNA sample was wild-type (WT) mouse DNA, and the negative control sample was water.

Agarose (Sigma-Aldrich, St. Louis, MO) was diluted into Tris/borate/EDTA buffer (TBE; 0.89 M Tris base, 0.02 M EDTA-Na_2-salt, 0.89 M boric acid) 1× at 10 mg/ml to make a 1% agarose gel by means of microwave irradiation. After the agarose had dissolved and the solution had cooled sufficiently, ethidium bromide (10 mg/l; Sigma-Aldrich, St. Louis, MO) was added at 0.04 µl/ml.

PCR products, positive, false-positive, and negative control samples were loaded on the 1% agarose gel with 6X loading buffer (0.25 % bromophenol blue, 0.25 % xylene cyanol FF and 30 % glycerol in water at 4 °C). A 1 kb DNA ladder (Invitrogen, Carlsbad, CA) was loaded alongside the samples. Gel electrophoresis was carried out at 100 Volts/cm for 1.5-2 hours. The gel was subsequently imaged by means of the Gene Genius Bio Imaging System with the GeneSnap Image Capture Suite (Syngene, Frederick, MD). The product size of a *plns-c-MycER*^{TAM} positive sample was expected to be 413 base pairs (Pelengaris *et al*., 2004) whereas there was no band at this a size in WT.

2.1.2. Administration of *pIns-c-MycER*^{TAM} mouse model

The switchable transgenic *plns-c-MycER*^{TAM} mouse model (Pelengaris *et al*., 2002b), in which c-MYC is switched on by means of daily intraperitoneal (IP) injection of 4-Hydroxytamoxifen (4-OHT; Sigma-Aldrich, St. Louis, MO), was employed in this study. 4-OHT was sonicated in peanut oil (Sigma-Aldrich, St. Louis, MO) at 1 mg/0.1 ml. Then 100 µl was applied to the positive control objects in both *plns-c-MycER*^{TAM} mice and their WT littermates every 24 hours through IP

injection. For negative controls, 100 μl vehicle was applied to both transgenic mice and their WT littermates. Male mice aged 2-3 months were used. All mice were housed and treated in accordance with protocols and regulations sanctioned by the Home Office under the Animals Act of 1986.

2.1.3. Experimental design

A. Dynamics of glucose and energy expenditure

Transgenic *pIns-c-MycER*^{TAM} mice were administered 4-OHT (MYC-ON) daily by intraperitoneal (IP) injection. Controls included vehicle (peanut oil) treatment of *pIns-c-MycER*^{TAM} mice (MYC-OFF) and their WT littermates (WT), as well as 4-OHT treatment of WT mice (WT-4-OHT). Whole-body plasma glucose was measured by means of the oxidase method (Accuchek® Advantage Plus Test Strips; Roche, Basel, Switzerland) at 0, 4, 8, 12, 16, 20, 24, 28, 32, and 36 hours after activation of c-MYC *in vivo*. Each experiment was performed in triplicate. Since ethical constraints limit blood sampling to no more than 0.01 ml per day (NC3Rs, 2011), the same individual cannot be measured at all time points. Therefore, it was found necessary to divide this experiment into three groups (it is assumed that the volume of blood needed to measure glucose level is about 5 μl), namely Time Line 1 (TL1), Time Line 2 (TL2), and Time Line 3 (TL3). In TL1, the blood glucose level was measured at 0, 12, 24, and 36 hours after the first IP injection of 4-OHT or vehicle; in TL2, the blood glucose level was measured before those objects were fasted (which is defined as -4 hours in this thesis), and 8, 20, and 32 hours after the first IP injection; and in TL3, the blood glucose level was tested at 4, 16, and 28 hours after the first IP injection. It was assumed that the glucose level at the start

point of each TL experiment is the same. A detailed experimental protocol is given in Figure 2.1.1.

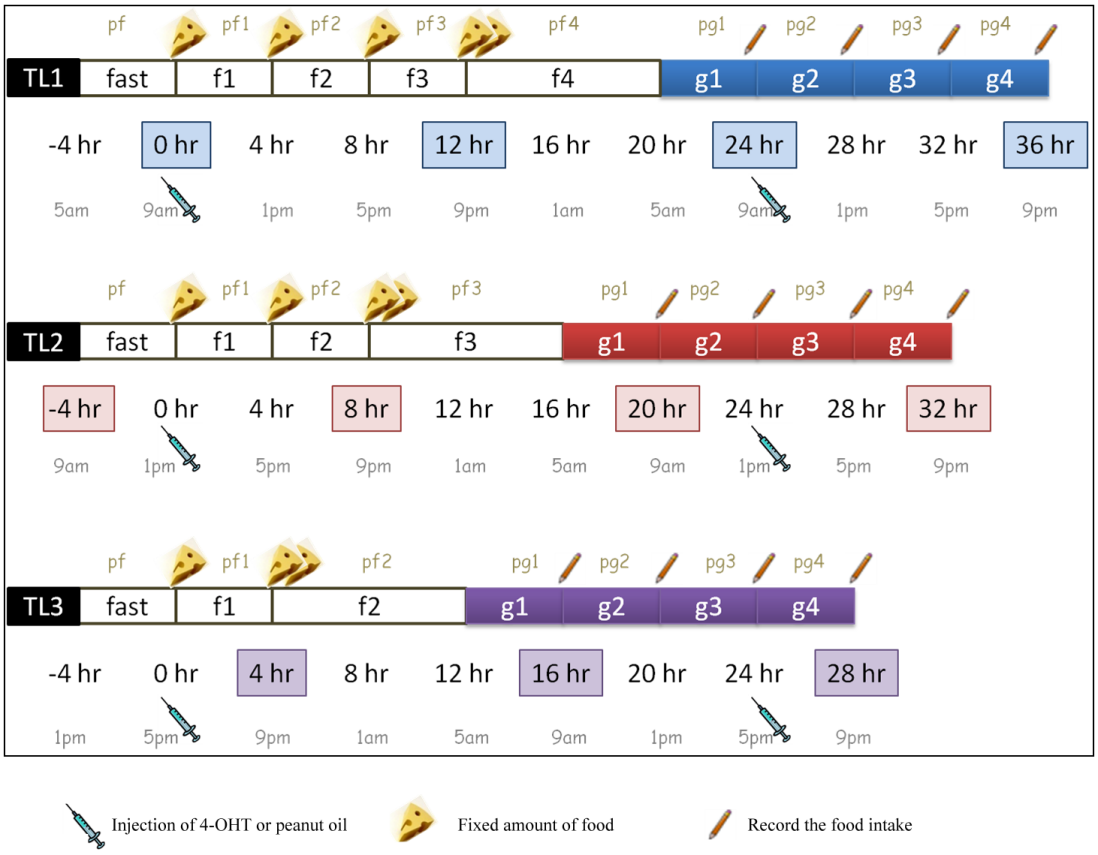

Figure 2.1.1. Experimental design for glucose and energy expenditure dynamics *in vivo*.

Glucose and energy expenditure dynamics within 36 hours of c-MYC activation of three different groups of mice were studied, i.e. *plns-c-MycER*^{TAM} mice treated with 4-OHT (MYC-ON), *plns-c-MycER*^{TAM} mice treated with peanut oil (MYC-OFF) and WT treated with peanut oil (WT). Each group contained three mice (n=3). The treatment of 4-OHT or peanut oil was given to the *plns-c-MycER*^{TAM} mice or their WT littermates every 24 hours through IP injection. In compliance with ethical prescriptions, a grid floor, which separates mice from the food debris and excreta and which enables the tracing of food intake (relevant to parameters *g1-g4* when mice were on a grid floor) and faeces production (relevant to parameters *pg1-pg4* when mice were on a grid floor), was applied to each cage for at most 16 hours. Since a grid floor could not be used for the entire experimental period, a limited amount of food (assumed 5 g/mouse/day) was provided from the start of each time line (TL) experiment until the last 16 hours so that food intake (relevant to parameters *f1-f4*) and faeces production (relevant to parameters *pf* and *pf1-pf4*) were still able to be traced during this period every 4 or 8 hours. Mice were fasted 4 hours prior to the initial time point zero in each TL group; this time point was labelled as -4 hour in this experiment. The body weight was recorded every 4 or

8 hours throughout the experimental period. Blood serum and pancreata were collected at the end of each TL experiment and final pancreatic weight was also recorded.

The energy balance is depicted diagrammatically Figure 2.1.2. Food intake (relevant to parameters *f1-f4* or *g1-g4* when mice were on a grid floor, see Figure 2.1.1) and faeces production (relevant to parameters *pf* and *pf1-pf4* or *pg1-pg4* when mice were on a grid floor, see Figure 2.1.1) were recorded during the TL experiments. Assimilation, which is the sum of body weight change (Δw) and energy usage, was evaluated as food intake less faeces production. Therefore, energy usage is defined as $\text{food intake} - \text{feces production} - \Delta w$. This thesis assumes the energy metabolism in rodents and man are similar.

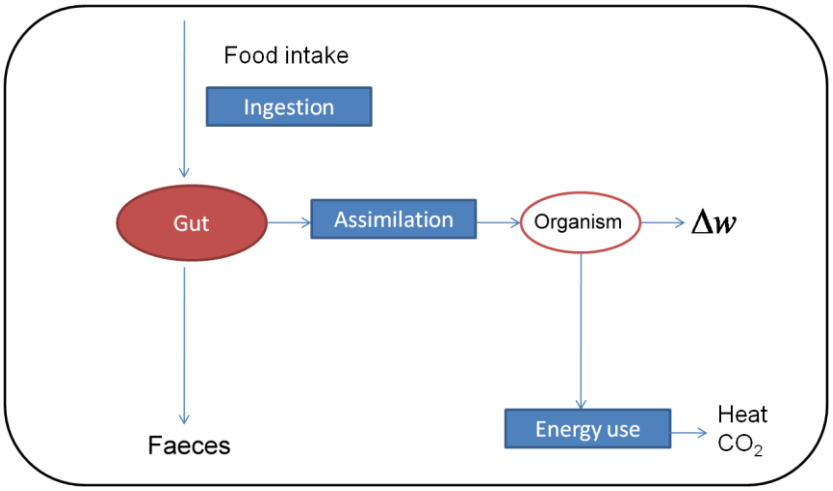

Figure 2.1.2. Energy usage scheme.

Food is ingested and subsequently transported into the gut. After the food is assimilated, energy is used for various biological activities, generation of heat, or CO_2. The net energy stored in the animal, Δw, is the difference of body weight before and after food utilization. If the energy used by the animal is bigger than this input, Δw is negative.

B. Insulin dynamics and morphological information

In the TLs experiment mentioned in Section 2.1.3. A, morphological data related to the pancreas, and physiological data, for example related to blood serum, were collected at 28, 32, and 36 hours after the first IP injection. In order to obtain more detailed information about the events that follow c-MYC activation, the following time points were further studied: before fasting (which is defined as -4 hours), and 8 and 16 hours after the first IP injection. In each group, the experiment was performed in triplicate on both *pIns-c-MycER^{TAM}* mice and their WT littermates, and each type of mouse was injected with either 4-OHT as treatment or the same volume of vehicle as control.

2.1.4. Treatment with exenatide

PIns-c-MycER^{TAM} male mice (n=3) were treated with exenatide at 50μg/kg by means of subcutaneous (SC) injection. Stock solution was prepared by dissolving 5 mg exenatide (Amylin, San Diego, CA) in 5 ml H_2O. When mice were given the injection, 50 μl stock solution was mixed with H_2O up to 5 ml. Because the degradation of GLP-1 is very fast (Hansen *et al*., 1999), and the half-life of GLP-1 is < 2 minutes (Baggio and Drucker, 2007), it is necessary to make sure the exentide has circulated in mice when the experiment starts, such as the treatment with 4-OHT. Two days pre-treatment was applied to acclimatize these mice and two injections were administered at 8am and 4pm daily (Samuel Robson, unpublished data). In the MYC-ON group, *pIns-c-MycER^{TAM}* mice treated with exenatide or vehicle were

defined as M^+/E^+ or M^+/E^-, whereas in the MYC-OFF group, mice treated with exenatide or vehicle were defined as M^-/E^+ or M^-/E^-.

The negative control consisted of *pIns-c-MycER*^{TAM} WT male littermates (n=3) treated with exenatide (EW) or the same volume of water vehicle (WW) by means of SC injection.

2.2 Morphological and physiological analysis

Mice were sacrificed by means of cervical dislocation (CD) after c-MYC activation according to the schedule outlined in Section 2.1.3. Blood and pancreata were collected. Blood was collected through cardiac puncture, put on ice for 30 minutes, and subsequently centrifuged (Centrifuge 5415R; Eppendorf, Hamburg, Germany) for 10 minutes at 4 ℃. The supernatant was collected for insulin analysis (Ultrasensitive Mouse Insulin ELISA, Mercodia, Uppsala, Sweden) following the protocol provided by the supplier.

Pancreata were dissected out as soon as the blood collection was finished, and were processed into frozen blocks for cryo-sectioning by the following steps:

1) Immersion in 4% formaldehyde (Formaldehyde-methanol free 16% w/v solution; TAAB, Berks, England; diluted in phosphate buffered saline (PBS)) for 2 hours at room temperature (RT);

2) Transferral to 30% sucrose (Sigma-Aldrich, St. Louis, MO; diluted in PBS) at 4 ℃ overnight;

3) Placing the pancreas into a small cubic mode, which was made of foil, to make sure the cryo-tissue is made into a cubic shape and ensuring the whole

organ is arranged in a crescent shape, then embedding in Tissue-Tek O.C.T. mounting medium (Sakura, Alphen a/d Rijn, The Netherlands), and placed on dry ice and ethanol;

4) Storage at -80 ℃.

Every 100 μm was defined as one level in a pancreas; accordingly the tissue was sectioned by a cryostat (OTF 5000 Cryostat; Bright, Huntingdon, England) at a thickness of 10 μm. Three continuous sections were collected on a single slide. After 3 slides were finished, the 10^{th} section was discarded to complete the section of one level because 3 slides were only able to support 9 sections, and sectioning of next level was continued in the same manner.

2.2.1. Immuno-staining

Immunohistochemistry (IHC), in which the basic concept is the identification of antigens in a biological tissue section by means of specific antibodies, has been applied to the diagnostic pathology for many years (Coons *et al*., 1941; Nakane and Pierce, 1966; Robinson and Dawson, 1975). It is a staining method that comprises tissue selection, fixation, sectioning, processing of staining, and interpretation of the staining result by microscopy. The use of IHC includes fluorophore-labelled (immunofluorescence) and enzyme-labelled (immunoperoxidase) antibodies to identify specific proteins or molecule of interest in cells or tissues. The staining results are studied under fluorescence-microscopy (for immunofluorescence) or light-microscopy (for immunoperoxidase). In this thesis, both methods were used to

identify β-cells (Section 2.2.1 A) and proliferating cells (Section 2.2.1 B) in mouse pancreatic islets.

A. Immunoperoxidase and haematoxylin staining

There were three sections on each slide, but only two sections were used for the DAB (3,3'-diaminobenzidine) and haematoxylin (H) staining; the first section was treated as control in staining and the third one was regarded as treatment. The second section was discarded so that more space was created between the first section and the third section to avoid cross-contamination during staining. A wax pen (Dako, Glostrup, Denmark) was used to draw a circle, which formed a hydrophobic barrier, around each section. Slides were post-fixed in 4 % formaldehyde for 10 minutes at 4 ℃, and were washed in PBS 2 times, 3 minutes for each wash on a shaker (at 50 rpm). Hydrogen peroxide (H_2O_2; Thermo Fisher Scientific, Pittsburgh, PA; diluted in sterile H_2O at 1/100) was applied to each section to bleach the samples for 30 minutes at RT, after which slides were washed in PBS for 5 minutes on a shaker (at 50 rpm). Goat serum solution was made of 150 µl goat serum (Sigma-Aldrich, St. Louis, MO) and 10 ml PBS. Triton (50 µl; Sigma-Aldrich, St. Louis, MO) was added into the goat serum solution to make the blocking solution, then applied to each tissue section for 30 minutes at RT to block tissues, after which the liquid covering the tissues was drained by means of gentle tapping. The primary antibody (Insulin-polyclonal guinea anti-swine; Dako, Glostrup, Denmark; diluted by goat serum solution at 1/200) was applied onto the treatment section, whereas the goat serum solution was applied onto the control section, and both were incubated for 1 hour at RT. The slides were subsequently washed in PBS+0.1% tween 3 times for

a duration of 5 minutes each time on a shaker (at 50 rpm). The secondary antibody (Guinea pig IgG (H and L) pre-absorbed antibody (HRP); Novus Biologicals, Littleton, CO; diluted by the goat serum solution at 1/500) was applied for 30 minutes onto the treatment section, and so was the goat serum solution to the control section, at RT. After slides were washed in PBS+0.1% tween 3 times, each time for a duration of 5 minutes on a shaker (50 rpm), DAB kit (DAB substrate kit for peroxidise; Vector Laboratories, Burlingame, CA) was applied onto each section for 2 minutes, as specified by the protocol supplied by the manufacturer. Slides were washed in sterile H_2O 2 times for 3 minutes on a shaker (50 rpm). The next step was the haematoxylin staining, which was carried out according to the following steps:

1) Bathe in haematoxylin (Carl Roth, Karlsruhe, Germany) for 1.5 minutes;
2) Wash under running water for 10 minutes;
3) Transfer into 70% ethanol for 1 minute;
4) Transfer into 80% ethanol for 1 minute;
5) Transfer into 90% ethanol for 1 minute;
6) Transfer into 100% ethanol for 2 minutes;
7) Immerse into xylene 2 times for 5 minutes under a fume hood;
8) Mount slides with mount medium (Leica, Wetzlar, Germany) and apply coverslips.

B. Immunofluorescence staining

Primary antibodies for Ki-67 and insulin were counterstained on the specimen, which was followed by the staining with fluorophore-labelled secondary antibodies, i.e. fluorescein isothiocyanate (FITC) and Alexa-633. Each slide contained three sections. The first specimen was the treatment, in which target antigens, i.e. insulin and Ki-67, could be recognised and the second section was treated to identify insulin only. In order to show that the fluorescent staining result was genuine, i.e. resulting from the specific antigen, a negative control was carried out in the third section, to which only the secondary antibody was applied. Immunofluorescence staining was carried out according to the following steps:

1) Circle each section by a wax pen, and post-fix slides in 4% formaldehyde for 10 minutes at 4 ℃, and sequentially rinse the slides in distilled water;

2) Prepare goat serum solution and blocking buffer, as described in Section 2.2.1 A;

3) Block tissue for 1 hour at RT, and after 30 minutes incubation under RT, remove the liquid by means of gentle tapping;

4) Apply primary antibody (Novocastra^{TM} Lyophilized Rabbit Polyclonal Antibody Ki-67 Antigen; Leica, Wetzlar, Germany) diluted by goat serum solution at 1/100 and incubate for 2 hours at RT;

5) Process the wash step, in which slides are washed in PBS+0.1% tween 3 times for a duration of 5 minutes on a shaker (at 50 rpm);

6) Apply secondary antibody, which is FITC goat anti-Rabbit IgG (H+L; 1/200 dilutions; Vector Laboratories, Burlingame, CA) and incubate for 30 minutes at RT;

7) Process the wash step;

8) Apply another primary antibody (Insulin-polyclonal guinea anti-swine; Dako, Glostrup, Denmark) diluted by goat serum solution at 1/100 and incubate for 1 hour at RT;

9) Process the wash step;

10) Apply another secondary antibody (Alexa 633 goat anti-Guinea pig; Invitrogen, Carlsbad, CA) diluted by the goat serum solution at 1/200 and incubate for 30 minutes at RT;

11) Process the wash step;

12) Mount slides with a drop of 4',6-diamidino-2-phenylindole (DAPI; Vector H-1200; Vector Laboratories, Burlingame, CA) onto each section to stain the nuclei as blue and apply coverslips;

13) Examine the fluorescent stained slides using confocal microscopy (Leica SP2).

The immunofluorescence staining of Caspase-3 (Cleaved Caspase-3 (Asp175) antibody; Cell Signaling, Danvers, MA) and insulin followed the same procedure.

2.2.2. β-cell mass analysis

The whole-slide image was captured by an automatic slide scanner (Mirax Midi; Carl Zeiss, Jena, Germany) located in the University Hospitals Coventry and Warwickshire with a ×20 objective. Mirax Viewer 1.12, developed by 3DHISTECH (Carl Zeiss, Jena, Germany), was used to view the scanning results at various digital magnifications.

At least five slides, which represented five different levels, from each individual mouse pancreas were studied. The following images were obtained to carry out β-cell mass analysis:

1) Whole cross-sectional area of a single pancreatic tissue with an optimal digital objective, which varied among different tissue sections;

2) Insulin-stained cross sectional area with a ×2 digital objective.

After images had been obtained with different magnifications, ImageJ 1.44p (Abramoff, 2004) was used to analyse the cross sectional area by measuring the pixels of the target area. The β-cell mass was then calculated as follows:

$$\beta\text{-cell mass} = \text{pancreas weight} \times \frac{\sum \text{cross-sectional area of insulin stained area}}{\sum \text{cross-sectional area of pancreatic tissue}}. \quad (1)$$

Because the cross-sectional area of the whole pancreatic area and the insulin-stained area were acquired at different digital magnifications, it was necessary to adjust them to a common scale. Therefore, the cross sectional area of the pancreatic tissue was adjusted by $\left(\frac{\text{magnification of insulin stained area}}{\text{magnification of whole pancreatic area}} \right)^2$.

2.2.3. β-cell number and β-cell size

β-cell number data were analysed under the digital objective of ×20 at Mirax Viewer 1.12. The insulin-stained cross sectional area was obtained as described in Section 2.2.2. Accordingly, β-cell size was calculated as $\frac{\sum \text{insulin - stained cross sectional area}}{\sum \beta \text{ - cell numbers}}$.

2.3 Microarray analysis

Two sets of microarray data were obtained from Dr. Samuel Robson. The first set of microarray data was designed to see the effects of c-MYC with time points of 4, 8, 16, and 32 hours after the first IP injection of 4-OHT, or the same volume of vehicle as control. Each time point and treatment was present in triplicate. Total RNA was extracted from islets, which were isolated by laser capture microdissection (Molecular Machines and Industries, Rockledge, FL) from pancreas sections. Total RNA was then processed using the two-cycle target labelling reaction and hybridized to Affymetrix MOE430 Plus 2.0 GeneChip microarrays (Robson, 2008). GeneSpring GX software (Agilent, Santa Clara, CA) was used for array analysis to study the MycER on/off mice system. These arrays were experiments of *plns-c-MycER*^{TAM} mice treated with vehicle (M^-/E^-) and *plns-c-MycER*^{TAM} mice treated with 4-OHT (M^+/E^-).

Another set of microarray data, kindly provided by Dr. Robson (unpublished), was used to study the effect of exenatide under the following conditions. Condition 1 (M^-/E^- vs M^-/E^+): transgenic mice were given peanut oil through IP

injection, then treated with exenatide (M^-/E^+) or the water vehicle (M^-/E^-) by SC injection to study the effect of exenatide only; condition 2 (M^+/E^+ vs M^+/E^-): c-MYC was switched on for 4, 8, 16, and 32 hours with the injection of 4-OHT, and mice were also given exenatide (M^+/E^+) or the same volumes of vehicle (M^+/E^-).

Details of the principles of microarray experiments and microarray data analysis are given in Appendix A.

2.3.1. Pre-processing of data

A number of quality-control measures were undertaken to ensure the arrays were sufficiently reliable for analysis. The first was the experimental quality, which ensured the RIN value of each array is above than 5 and the cRNA yields are more than 10 μg. After the cRNA generated from sample had been hybridized on the Affymetrix GeneChips, a 3'/5' ratio was detected to show the hybridization quality. After the quality control steps, the following samples were removed from the early effects of c-MYC analysis: $M^-/E^-8(2)$, $M^+/E^-16(3)$, and $M^+/E^-32(1)$; and the following samples were removed from the exenatide array analysis: $M^+/E^+16(2)$, $M^+/E^+32(3)$, $M^-/E^+4(2)$, and $M^+/E^+72(1)$.

2.3.2. Data normalisation and annotation

Data were normalized across all samples at the probe-level GC-RMA (GeneChip robust multiarray average summarization algorithm), as described in Section 1.2.3, and subsequently normalised by the median of all samples. Fold change ratios are used by this thesis by normalising the treatment arrays to their

control counterparts, for instance, 4-OHT treated mouse arrays (M^+/E^-) were normalized by their peanut oil treated experiment arrays (M^-/E^-) to ensure the expression of a gene presented in fold change, which was incurred by c-MYC activation.

2.3.3. Gene filtering and clustering

Affymetrix MOE430 Plus 2.0 GeneChip microarrays contains 45,101 transcripts, which are measured by different probe sets, from the mouse transcriptome. Microarray analysis aims to identify genes that exhibit different expression in response to the experimental treatment. This thesis focuses on genes that were differentially expressed in response to treatment with 4-OHT and exenatide.

Affymetrix GeneChips contain control probes, which are designed for the measurement of housekeeping genes and the spike-in control transcripts expression changes to ensure the quality of hybridisation. The first step was to remove these control probes because they are designed probes and the outcomes are predictable, which are used for quality control or error corrections (Gautier *et al*., 2004). The following step was identifying transcripts which were up- or down-regulated by 2 folds because of the treatment. All ratios, which are the expression levels of treatment divided by the expression levels of control, presented in this thesis have been transformed as by $log_2(ratio)$ because it generates a symmetric up- and down-regulated gene expression levels. For example, $log_2(1)=0$, means that the treatment did not change the gene expression level; $log_2(2)=1$, means that the specific transcript was up-regulated by 2 folds because of the treatment whereas $log_2(1/2)=-1$ indicates that the specific transcript was down-regulated by 2 folds in

response to the treatment. The last step was to apply a two-way (time and treatment) ANOVA analysis to filter out the statistically significant differentially expressed genes, and a *post-hoc* analysis (Benjamini Hochberg FDR) was carried out. This candidate gene list was used as the starting point for further analysis. Finally, k-means clustering (Tavazoie *et al.*, 1999) was applied to this candidate gene list, in order to categorise different gene expression patterns.

2.3.4. Functional analysis

Annotation of gene ontology (GO) and pathway analysis was carried out. GO classification defines the attributes of gene products in three non-overlapping domains of biological functions, namely biological processes, cellular components, and molecular function (Harris *et al*., 2004). Enrichment of GO terms was determined by using the GO browser in GeneSpring GX, using a standard hypergeometric distribution. A corrected p-value was computed according to the Benjamini-Hochberg correction (Benjamini and Hochberg, 1995) to compensate for the false positive rate. Pathway analysis provided by GeneSpring GX was applied for functional analysis. The pathway database constructed by GeneSpring GX is based on natural language processing (NLP; Joshi, 1991), and the majority of the pathway database is derived from Pubmed abstract by means of text-mining.

2.4 Mathematical model

A mathematical model was developed to describe the physiological mechanisms and various hypothetical scenarios to account for the observations. A method used to analyse the model is given in Appendix B. Section 2.4.1 outlines the

formulation of a model of glucose and insulin dynamics. Section 2.4.2 models the glucose input as a time-varying function. Apoptosis and proliferation rates of β-cells will be presented in Section 2.4.3 whereas neogenesis will be taken into account in Section 2.4.4. Finally, the procedure employed for parameter estimation for β-cell turnover will be outlined in Section 2.4.5.

2.4.1. Formulation of the model of glucose and insulin dynamics

Mathematical models have been applied to understand glycaemic feedback loops for many years (Bergman *et al.*, 1979; Bolie, 1961). The time-scale homogenization method was applied to glycaemic homeostasis to ensure that fast and slow responses interact in a physiologically realistic way. Sturis *et al.* (1991) described the oscillation between plasma insulin and plasma glucose with a time delay system and was subsequently developed by Tolic *et al*. (2000). In this thesis, the Sturis-Tolic system was used as the starting point. The model is described by ordinary differential equations.

The dynamics of plasma insulin ($I_p(t)$, mU) is presented as Eqn (2). This is related to glucose-stimulated insulin secretion (GSIS; $\psi_{IS}(G)$, see Eqn (8)), the intercellular exchange of insulin and insulin degradation. Interstitial insulin dynamics ($I_i(t)$, mU) is presented as Eqn (3). The state variable $G(t)$ denotes the blood plasma glucose content whereas $I_p(t)$ denotes the blood plasma insulin content and $I_i(t)$ denotes the remote insulin content (insulin in the interstitial spaces of the body tissues). Thus,

$$\frac{dI_p}{dt} = \psi_{\mathrm{IS}}(G) - \Phi(\frac{I_p}{V_p} - \frac{I_i}{V_i}) - \frac{I_p}{\tau_p}, \quad (2)$$

$$\frac{dI_i}{dt} = \Phi(\frac{I_p}{V_p} - \frac{I_i}{V_i}) - \frac{I_i}{\tau_i}, \quad (3)$$

where I_i denotes the remote insulin level (mU), Φ (l/hr) denotes the insulin transportation rate between two compartments, V_p denotes the insulin distribution volume in plasma (l), and V_i denotes the effective volume (l) in the intercellular space. τ_p and τ_i denote the mean life time (hr) of an insulin molecular in the blood plasma or in the interstitial space, respectively. Glucose dynamics is described by the following equation:

$$\frac{dG}{dt} = \psi_{in} - \psi_{\mathrm{II}}(G) - \psi_{\mathrm{ID}}(G, I_i) + \psi_{GR}(G, \omega_3) - \psi_{GX}(G). \quad (4)$$

The dynamics of glucose is determined by glucose influxes, i.e. glucose infusion rate (ψ_{in}, mg/hr) and hepatic glucose ($\psi_{GR}(G, \omega_3)$), which is secreted by the liver and dependent on both plasma glucose and plasma insulin, and glucose usage, i.e. insulin-independent ($\psi_{II}(G)$) and insulin-dependent ($\psi_{ID}(G, I_i)$) glucose consumptions. In addition to Sturis-Tolic's original definition, glucose excretion by kidneys ($\psi_{GX}(G)$) when the glucose level becomes very high was also taken into account in order to model hyperglycaemic excursions realistically.

This model describes the time delay caused by the fact that it takes time for insulin to transit to different compartments, being produced by GSIS, and inhibiting hepatic glucose production. A duration τ_d is defined. The delay is modelled as follows:

$$\frac{d\omega_1}{dt} = \frac{3}{\tau_d}(I_p - \omega_1), \tag{5}$$

$$\frac{d\omega_2}{dt} = \frac{3}{\tau_d}(\omega_1 - \omega_2), \tag{6}$$

$$\frac{d\omega_3}{dt} = \frac{3}{\tau_d}(\omega_2 - \omega_3), \tag{7}$$

where τ_d denotes a time constant, and $\omega_1(t)$ to $\omega_3(t)$ denote auxiliary parameters for the time delay (Pattaranit and van den Berg, 2008).

The dependencies in the Sturis-Tolic system are listed in Eqn (8) to Eqn (11). The ψ s are fluxes and rates modelled by empirical functions: ψ_{IS} denotes the insulin secretion from pancreatic β-cells:

$$\psi_{IS}(G) = \hat{\psi}_{IS}(1 + \exp\{\alpha_{IS}(1 - \frac{G/V_g}{\gamma_{IS}})\})^{-1}, \tag{8}$$

with positive parameters $\hat{\psi}_{IS}$, α_{IS}, γ_{IS} and V_g. The insulin-independent glucose uptake by cells is represented by ψ_{II}:

$$\psi_{II}(G) = \hat{\psi}_{II}[\delta(1 - \exp\{-\frac{G/V_g}{\gamma_{II,lo}}\}) + \frac{1-\delta}{1 + \exp\{\alpha_{II}(1 - \frac{G/V_g}{\gamma_{II,hi}})\}}], \tag{9}$$

with positive parameters $\hat{\psi}_{II}$, $\gamma_{II,lo}$, $\gamma_{II,hi}$, α_{II} and δ. The insulin-dependent glucose uptake is represented by ψ_{ID}:

$$\psi_{ID}(G) = \frac{G/V_g}{\gamma_{ID}}[\psi_0 + \frac{\hat{\psi}_{ID} - \psi_0}{1 + \exp\{-\alpha_{ID}\ln\{(I_i/\iota_{ID})(V_i^{-1} + (\Phi\tau_i)^{-1})\}\}}], \tag{10}$$

with positive parameters ψ_0, $\hat{\psi}_{ID}$, α_{ID}, γ_{ID} and ι_{ID}. The endogenous release of glucose is represented by ψ_{GR}:

$$\psi_{GR}(G,\omega_3)=\hat{\psi}_{GR}(1+\exp\{-\alpha_{GR,g}(1-\frac{G/V_g}{\gamma_{GR}})\})^{-1}(1+\exp\{-\alpha_{GR,i}(1-\frac{\omega_3/V_p}{\iota_{GR}})\})^{-1}, \quad (11)$$

with positive parameters $\hat{\psi}_{GR}$, $\alpha_{GR,g}$, $\alpha_{GR,i}$, γ_{GR} and ι_{GR}. Renal excretion of glucose, which becomes important at raised glucose levels, is represented by ψ_{GX}:

$$\psi_{GX}=\psi_{GX}^{*}\ln\{1+\alpha_{GX}\exp\{\frac{G/V_g}{\gamma_{GX}}\}\}, \quad (12)$$

with positive parameters ψ_{GX}^{*}, α_{GX} and γ_{GX}.

All the values of the above parameters listed in this section are given in Table 2.4.1 in Section 2.4.3.

2.4.2. Introducing of glucose input oscillation

In Sturis-Tolic's original model the glucose input (ψ_{in}) is a constant. To approximate the actual physiological situation better, this input is modelled here as a time-varying forcing function. In the top panel of Figure 2.4.1, ψ_{in} was changed from a constant into a periodic function of three supplements a day, and applied to the original model. Accordingly, Eqn (4) is rewritten as follows:

$$\frac{dG}{dt}=\psi_{\mathrm{in}}(t)-\psi_{\mathrm{II}}(G)-\psi_{\mathrm{ID}}(G,I_i)+\psi_{\mathrm{GR}}(G,w_3)-\psi_{\mathrm{GX}}(G). \quad (13)$$

The middle and bottom panels of Figure 2.4.1 represent the standard reference cycle of glucose and insulin dynamics of the Sturis-Tolic model after the glucose infusion rate was divided into three meals a day.

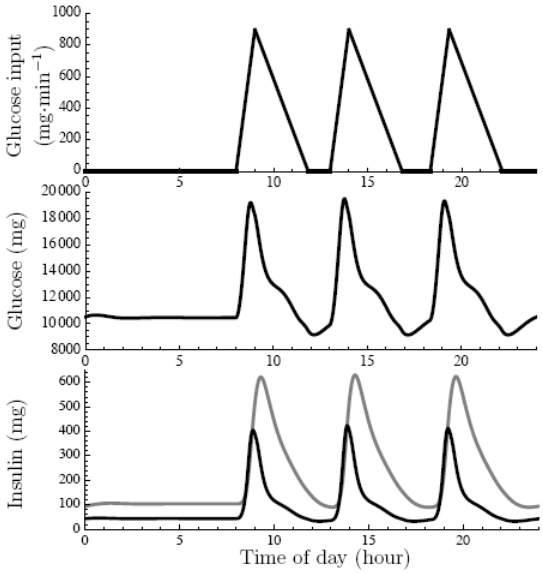

Figure 2.4.1. Reference cycle. Top: glucose infusion rate is split into three meals a day; middle: plasma glucose content; bottom: plasma (black line) and interstitial (grey line) insulin content.

2.4.3. Introducing of β-cell turnover

In this thesis, the β-cell turnover, which is a slow state variable, was considered. The dynamics of the β-cell mass is affected by β-cell proliferation, apoptosis, and neogenesis (Bonner-Weir, 2000b), which is represented here as follows:

$$\frac{dQ}{dt} = (\rho(I_p) - \mu(G, I_i))Q + \psi_{\mathrm{NG}}(G). \qquad (14)$$

Here ρ denotes the β-cell proliferation rate depending on the plasma insulin, μ denotes the β-cell apoptosis rate depending on the plasma glucose, and interstitial insulin. $\psi_{NG}(G)$ denotes the flux of neogenesis and depends on plasma glucose. $Q(t)$ expresses the ratio of β-cell mass to the standard β-cell mass:

$$Q(t) = \frac{\beta}{\beta_{ref}}, \qquad (15)$$

where β denotes the β-cell mass of a specific object, i.e. the experimental group, and β_{ref} denotes the β-cell mass of a reference object, i.e. the control group.

Johnson and Alejandro (2008) proposed the insulin 'sweet spot' hypothesis, which proposes that the relationship insulin between β-cell proliferation or apoptosis is not linear, and at both low and high insulin concentration stimulate β-cell proliferation (Beith *et al.*, 2008). Therefore, this thesis assumes that the proliferation rate of β-cells depends on plasma insulin according to the following equation:

$$\rho(I_p) = \rho_0(1 + \delta_0 \frac{I_p}{\iota_0 V_p + I_p}), \qquad (16)$$

with positive parameters ρ_0, δ_0, and ι_0, which represent the baseline of β-cell proliferation rate, the insulin-sensitive portion of β-cell proliferation, and the pivot point of β-cell proliferation rate (see Table 2.4.1). The death rate of the β-cells is assumed to be dependent on the glucose concentration (Efanova *et al.*, 1998) and the interstitial insulin level as follows:

$$\mu(G, I_i) = \hat{\mu}(1 + \frac{I_i / V_i}{\iota_{AI}})(1 + \exp\{\alpha_1 - \frac{G/V_g}{\gamma_1} - \alpha_2(1 - \frac{G/V_g}{\gamma_2})^4\})^{-1}, \qquad (17)$$

with positive parameters $\hat{\mu}$, α_1, α_2, γ_1, and γ_2, which represent the maximum β-cell death rate, the first sensitivity coefficient of β-cell death, the second sensitivity coefficient of β-cell death, the first pivot point of β-cell death rate, and the second pivot point of β-cell death rate.

As the evidence of neogenesis remains controversial, this thesis analyses the model first with the assumption that this term is absent. The GSIS is also affected by the β-cell dynamics. Accordingly, Eqn (2) is rewritten as follows:

$$\frac{dI_p}{dt} = Q\psi_{\mathrm{IS}}(G) - \Phi\left(\frac{I_p}{V_p} - \frac{I_i}{V_i}\right) - \frac{I_p}{\tau_p}. \qquad (18)$$

The Sturis-Tolic's extended model is depicted in the form of a diagram in Figure 2.4.2. The values of the parameters are given in Table 2.4.1.

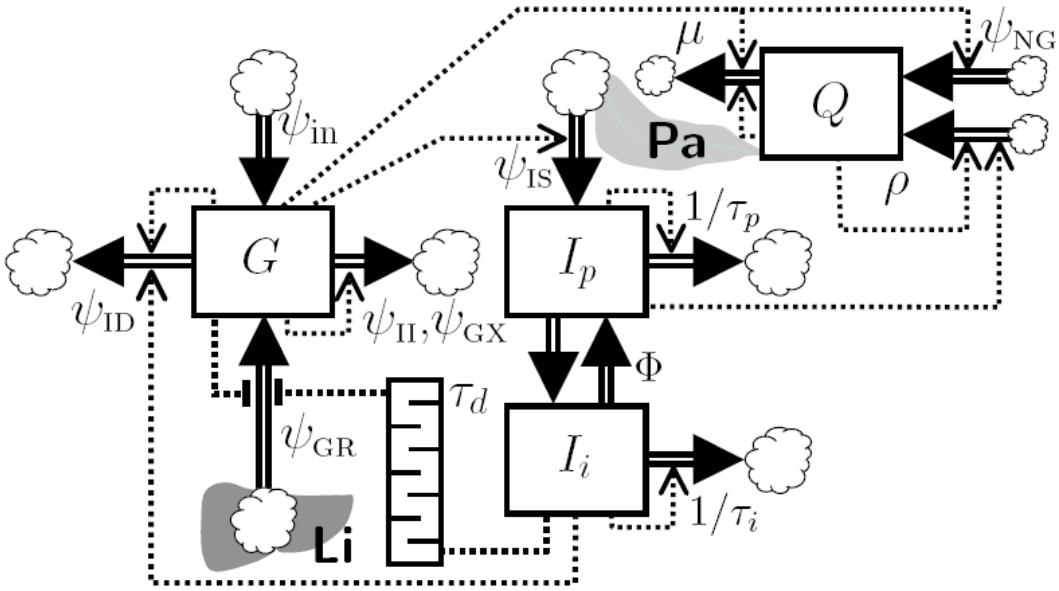

Figure 2.4.2. Diagram of Sturis-Tolic's extended model. Squares refer to variables, clouds denote to sources/sinks. Dotted lines refer to functional dependence (arrowheads: positive; blunt ends: negative). τ_d denotes a delay line interfering between I_i and ψ_{GR}. The state variable *Q* is the relative β-cell mass; with *Q* fixed at 1, the original Sturis-Tolic model is recovered. **Li**: liver, source of glucose derived from glycogen breakdown. **Pa**: pancreas, site of β-cells which are a source of insulin.

Table 2.4.1. Notation and parameter values.

Parameter	Value	Units	Interpretation
Φ	0.2	l min^{-1}	blood/interstitial space permeability
V_p	3	l	insulin distribution volume
V_i	11	l	interstitial space volume
V_g	10	l	glucose distribution volume
τ_a	6	min	mean lifetime of insulin in plasma
τ_i	100	min	mean lifetime of insulin in interstitial space
τ_d	36	min	response delay of glucose release
α_1	1.86	—	first sensitivity of β-cell death
α_2	14.5	—	second sensitivity of β-cell death
α_{II}	4.8	—	sensitivity of insulin-independent glucose uptake
α_{ID}	1.77	—	sensitivity of insulin-dependent glucose uptake
$\alpha_{GR,i}$	7.54	—	insulin sensitivity of hepatic glucose release
$\alpha_{GR,g}$	10	—	glucose sensitivity of hepatic glucose uptake
α_{IS}	6.67	—	sensitivity of insulin secretion
α_{GX}	0.00065	—	renal excretion parameter
$\alpha_{NG,i}$	0.5	—	sensitivity of neogenesis to insulin
$\alpha_{NG,g}$	0.5	—	sensitivity of neogenesis to glucose
γ_1	1.6	g l^{-1}	first pivot point of β-cell death rate
γ_2	2.6	g l^{-1}	second pivot point of β-cell death rate
$\gamma_{II,lo}$	144	mg l^{-1}	pivot point of non-splanchnic insulin-independent glucose uptake
$\gamma_{II,hi}$	2	g l^{-1}	pivot point of splanchnic insulin-independent glucose uptake
γ_{ID}	1	g l^{-1}	pivot point of insulin-dependent glucose uptake
γ_{GR}	2	g l^{-1}	pivot point of glucose release
γ_{IS}	2	g l^{-1}	pivot point of insulin secretion
γ_{GX}	0.3	g l^{-1}	renal excretion parameter
γ_{NG}	1.3	g l^{-1}	pivot point of neogenesis for glucose dependence
δ	0.34	—	contribution of non-splanchnic insulin-independent glucose uptake
δ_0	0.64	—	insulin-sensitive portion of β-cell proliferation
ι_0	115	mU l^{-1}	pivot point of β-cell proliferation rate
ι_{ID}	80	mU l^{-1}	pivot point of insulin-dependent glucose uptake
ι_{GR}	26	mU l^{-1}	pivot point of hepatic glucose release
ι_{AI}	0.3	U l^{-1}	Pivot point for apoptosis inhibition

ι_{NG}	30	mU l^{-1}	pivot point for neogenesis for insulin dependence
ψ_0	40	mg min^{-1}	baseline of insulin-dependent glucose uptake
$\hat{\psi}_{II}$	0.21	g min^{-1}	maximum flux: insulin-independent glucose uptake
$\hat{\psi}_{ID}$	0.94	g min^{-1}	maximum flux: insulin-dependent glucose uptake
$\hat{\psi}_{GR}$	0.18	g min^{-1}	maximum flux: hepatic glucose release
$\hat{\psi}_{IS}$	0.21	U min^{-1}	maximum flux: insulin secretion
$\hat{\psi}_{NG}$	0.001	min^{-1}	maximum flux: neogenesis of β-cell mass
ψ^*_{GX}	29	mg min^{-1}	renal excretion parameter
ρ_0	0.166	$year^{-1}$	baseline β-cell proliferation rate
$\hat{\mu}$	0.311	$year^{-1}$	maximum β-cell death rate

The term “pivot point” refers to midrange values, saturation constants etc. of saturating responses. Insulin units: $1\text{U} \cong 6.67$ nmol.

2.4.4. Model with neogenesis of β-cell turnover

There are several hypotheses concerning recovery of ablated β-cells, one of which states that the ablated β-cells are replenished by differentiation from the progenitor cells (De Leon *et al*., 2003), whereas some studies suggest that the β-cells replenish themselves from differentiation β-cells (Ackermann Misfeldt *et al*., 2008). A competing hypothesis is that β-cells themselves are capable of rapid proliferation (Dor *et al*., 2004; Lee *et al*., 2006; Nir *et al*., 2007). These hypotheses can be reconciled if the rapidly proliferating pool of cells is derived from proliferating adult β-cells that are triggered by activation of c-MYC. The neogenesis of β-cells from progenitor cells, which are referred to as the proliferator pool in this thesis, was represented by the following equation:

$$\psi_{\mathrm{NG}}(G) = \hat{\psi}_{\mathrm{NG}}(1+\exp\{\alpha_{\mathrm{NG,g}}(1-\frac{G/V_g}{\gamma_{NG}})\})^{-1}(1+\exp\{\alpha_{\mathrm{NG,i}}(1-\frac{I_i/V_g}{\iota_{NG}})\})^{-1}, \quad (19)$$

with positive parameters $\hat{\psi}_{NG}$, $\alpha_{NG,g}$, $\alpha_{NG,i}$, ι_{NG}, and γ_{NG}, which represent the maximum influx of neogenesis of β-cell mass, the sensitivity of neogenesis to glucose, the sensitivity of neogenesis to insulin, the pivot point for neogenesis for insulin dependence, and the pivot point of neogenesis for glucose dependence. The main assumption behind this equation is that the neogenesis is triggered by prolonged hyperglycaemia (Lipsett and Finegood, 2002) in association with raised insulin levels (Grossman *et al*., 2010). It can also be observed that the right-hand side of Eqn (19) behaves like a soft AND-gate, i.e. the flux ψ_{NG} is larger when both glucose and insulin levels are raised. The synchronicity of the prolonged high

glucose and insulin levels may be indicative of regulatory insufficiency. It would therefore make sense to control β-cell mass compensation as proposed by Eqn (19). From a mechanistic point of view, it is known that the pathway regulating β-cell proliferation can act like an AND-gate. Specifically, c-MYC activation induces proliferation in a short transition but is overwhelmed by apoptosis in β-cells, which leads to β-cell mass depletion, unless the system is suppressed by co-expression of an anti-apoptotic signal, i.e. BCL_{xL} (Pelengaris *et al*., 2002b). Jonas (2001) suggests that glucose induces the expression of c-MYC, whereas insulin induces an anti-apoptotic signal (Johnson *et al*., 2006). Thus, whereas glucose alone induces a net loss of β-cells (Van de Casteele *et al*., 2003), the simultaneous presence of glucose and insulin would stimulate rapid proliferation, possibly via rapid dedifferentiation of existing adult β-cells to the proliferative phenotype. It has been suggested that this dual proliferation/apoptosis pathway acting via c-MYC acts a fail-safe that defaults to β-cell loss unless both glucose and insulin are elevated (Pelengaris *et al*., 2002a).

The action of glucose is indirect and thought to be via GLP-1 (De Leon *et al*., 2003), and incretin and cytokine which is secreted by enteroendocrine L-cells. Since the half-life of GLP-1 is extremely short (Deacon *et al*., 1996; Hansen *et al*., 1999), an instantaneous functional dependence on G/V_p appears warranted. In principle, ψ_{NG} should also depend on, and be limited by, the amount of progenitor cells present in the pancreas; in the present model, this pool is assumed to be non-limiting and is thought of as an unlimited source.

2.4.5. Parameter estimation for β-cell turnover

Our system was based on the Sturis-Tolic model for glucose and insulin dynamics. The parameters that concern the fast time-scale system are adopted from Tolic *et al*. (2000). The model was further extended with β-cell dynamics, which is composed of the rate of proliferation, apoptosis and neogenesis of β-cells. Data taken from the experimental literature were used to estimate these parameters. Although this model describes the human system, the parameters values are taken from the rodent experimental data, which is a limitation. This thesis assumes that the physiological behaviour of rodent and human is approximately similar on the molecular level, so the parameters are assumed to be transferrable. To transform values that are not intrinsic, such as blood volume, a scaling factor can be applied to adjust the difference between body weight and the effective distribution volume of a specific content etc. However, an exception is the parameter $\hat{\psi}_{NG}$, but our method of estimating this parameter inherently contains the required scaling.

A. Death

Efanova *et al*. (1998) provided data on cell death rate under different glucose concentrations over 40 hours. If the average death rate during this period is λ, then $\text{alive cell}\,(\%) = \mathrm{N}_0 \times e^{-\lambda \times t}$, where N_0 denotes the initial percentage of living cells, which is here assumed to be 100%. Table 2.4.2 shows how the data obtained from the literature were converted into the death rate. The death rate can be plotted as a function of the ambient glucose concentration in Figure 2.4.3. Eqn (17) was fitted to these data by non-linear least-squares. However, the death rates shown here were

several orders of magnitude larger than the accepted β-cell turn-over rate that is obtained from literature (Dor *et al*., 2004; Topp *et al*., 2000). This can be attributed to the unfavourable *ex vivo* conditions under which these data were obtained.

Table 2.4.2. Glucose-related cell death data. This thesis plotted and transferred data from the original graph, Efanova *et al*. (1998) figure 1, manually, which is shown as below table. Given the 11mM glucose concentration as an example to estimate the death rate in this cell culture, the percentage of alive cells is 86.47(%). This thesis assumes death rate as λ, then Alive cell (%)=$N_0 \times e^{-\lambda t}$, 86.47(%)=100(%) × $e^{-\lambda \times 40}$, λ=0.0036 (1/hr). In this way the death rate for other concentrations can be estimated as well.

Glucose (mM)	Death cells(%) in 40 hrs	Alive cell (%) in 40 hrs	Death rate (1/hr)
0	36.18	63.82	0.0112
3	36.44	63.56	0.0113
5	32.00	68.00	0.0096
8	17.78	82.22	0.0049
11	13.53	86.47	0.0036
14	20.91	79.09	0.0059
17	22.33	77.67	0.0063
20	24.69	75.31	0.0071
23	35.38	64.62	0.0109
27	39.31	60.69	0.0125

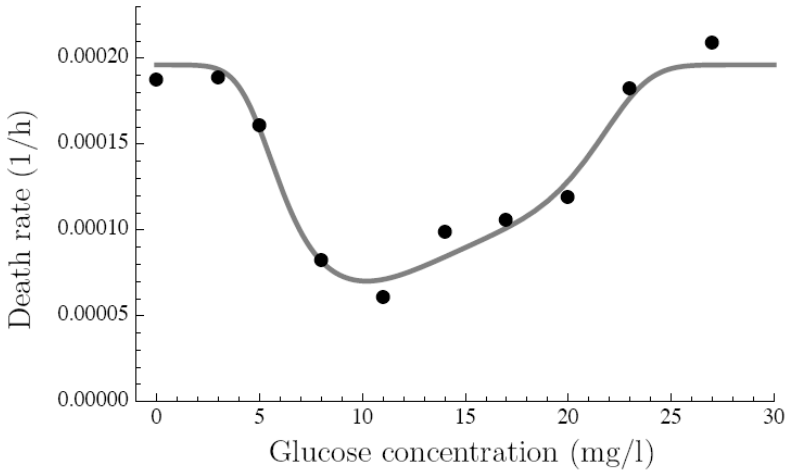

Figure 2.4.3. Pancreatic β-cell death rate data and least-squares fit of the formula used in the model.

Johnson *et al*. (2006) used different measurements to show a direct anti-apoptotic effect of insulin and demonstrated that the anti-apoptotic effects of insulin are related to the insulin concentration, i.e. in mouse islets cell culture, the effect is biphasic, in which the anti-apoptotic effect is strong at low insulin levels but is less strong when the insulin is increased, and it is strong again when insulin level is as high as hyper-physiological levels. Johnson and Alejandro (2008) analysed the trends and found that the relative potency of anti-apoptotic effect drops off more or less hyperbolically with insulin concentration *I*, which is shown as follows:

$$\text{relative effect} = \frac{1}{\iota_{\text{AI}} + I}, \qquad (20)$$

where ι_{AI} is approximately 0.3 U l^{-1}. The reciprocal of this protective effect appears as a prefactor of the death rate in Eqn (17).

B. Proliferation

β-cell proliferation is thought to be related to autocrine/paracrine secretion of insulin in recent studies (Beith *et al*., 2008; Okada *et al*., 2007). In this thesis, data from Beith *et al*. (2008) were used to derive the insulin-related proliferation rate. Data taken from the literature were used to fit a simple hyperbolic model, Eqn (16), shown in Figure 2.4.4. Table 2.4.3 shows the original data from Beith *et al*. (2008) and transfers the rates into the same time unit (hr^{-1}).

Table 2.4.3. Insulin-related cell proliferation data. This thesis further transfers the proliferation rate, obtained from Beith *et al*. (2008) figure 2, from (day^{-1}) to (hr^{-1}).

Insulin(nM)	**Proliferation rate(day^{-1})**	**Proliferation rate(hr^{-1})**
0.2	(130/24274)/3 = 0.0018	0.000075
2	(66/22206)/3 = 0.0010	0.000042
20	(58/20489)/3 = 0.0009	0.000038
200	(168/25585)/3 = 0.0022	0.000092

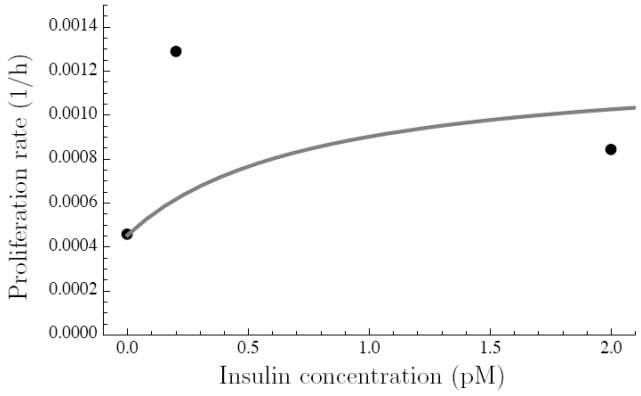

Figure 2.4.4. Pancreatic β-cell proliferation rate data and least-squares fit of the hyperbolic formula used in the model.

C. Neogenesis

Neogenesis of β-cells remains to be fully characterised in quantitative terms. The formula used in this thesis to represent the rate at which β-cells are replenished is therefore speculative. Steil *et al*. (2001) found an initially doubled plasma glucose level in rats that were given infusions of glucose. Figure 2.4.5 shows a simulation of this experiment. Within a day, euglycaemia was re-established and the β-cell mass had doubled.

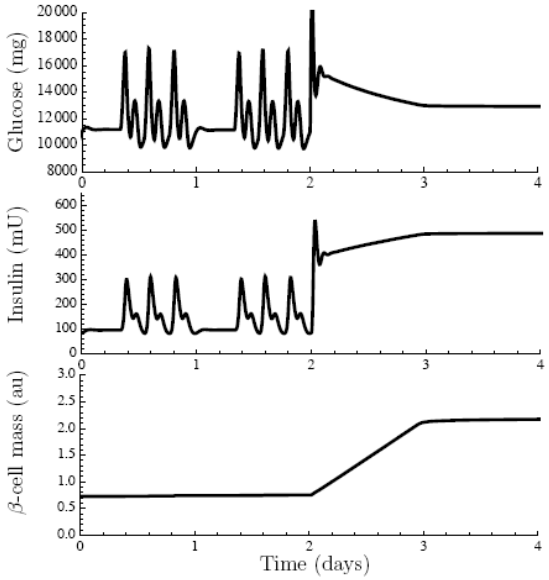

Figure 2.4.5. The Steil *et al*. (2001) experiment as simulated by the present model. After two control days, glucose is switched to an infusion. Top: plasma glucose content; middle: interstitial space insulin content; bottom: β-cell mass.

Chapter 3. Results

3.1 Microarray data

In this section, the results of two different sets of microarray data will be presented. Section 3.1.1 describes the early effect of c-MYC activation whereas in Section 3.1.2, the early effects of exenatide, which is one of the common drugs for treatment of diabetes, will be presented. To the best of the authors' knowledge, this is the first detailed investigation of the early effect of c-MYC.

3.1.1. Gene expression of c-MYC activation during hypoglycaemia

In the M^+/E^- vs M^-/E^- microarray experiment, 426 probe sets (~400 genes) were identified as statistically significant differentially expressed ($p<0.01$, 2-way ANOVA, Benjamini-Hochberg *post-hoc* analysis) in response to the activation of c-MYC. The k-means cluster method was applied to separate these differentially expressed transcripts (DETs) into two groups, which is shown in Figure 3.1.1. The majority of DETs were up-regulated after c-MYC activation. As shown in the left panel of Figure 3.1.1, cluster 1 was composed of 374 probe sets that were mainly up-regulated throughout the experiment, whereas most of the 52 probe sets in cluster 2, which is presented in the right panel of Figure 3.1.1, were down-regulated throughout the experiment. A detailed DETs list is show in Appendix C.

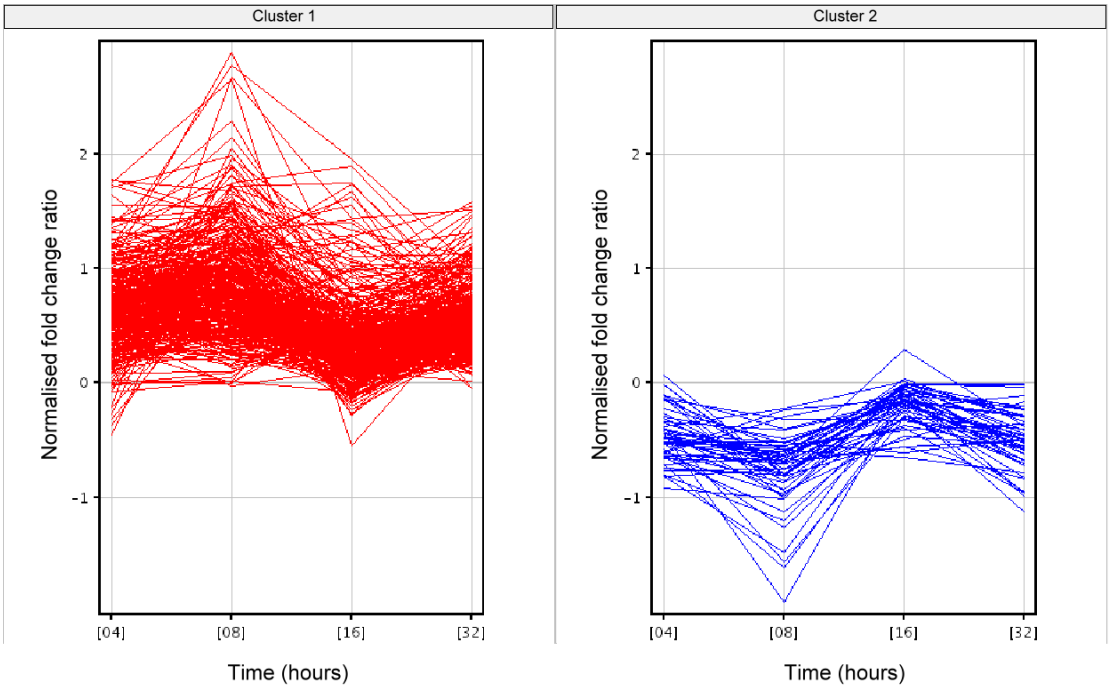

Figure 3.1.1. Differentially expressed transcripts in M^+/E^- vs M^-/E^- experiment.

Statistically significant differentially expressed transcripts (DETs) were defined ($p<0.01$, 2-way ANOVA, Benjamini-Hochberg *post-hoc* analysis), and clustered into 2 different groups by means of k-means clustering. Left panel: cluster 1, most of DETs were up-regulated after c-MYC activation and right panel: cluster 2, most of DETs were down-regulated after c-MYC activation. The fold change ratio referred to the expression level of treatment divided by the expression level of control, and then was transformed by $\log_2$. If the transcript was up-regulated, the normalised fold change ratio was positive, whereas the negative value was applied to indicate the transcript was down-regulated because of treatment.

Figure 3.1.2 shows biological processes GO terms of cluster 1. Significant biological process GO terms were defined by hypergeometric analysis (see Section 2.3.4), and 167 GO terms were deemed to be significant. These GO terms can be partitioned into three different categories according to their functions, in which were cellular process (such as RNA processing, ncRNA processing, and cellular metabolic process, DNA replication, cell cycle, and DNA duplex unwinding),

metabolic process (such as RNA metabolic process, amine metabolic process, DNA metabolic process, and mRNA metabolic process), and cellular component organization or biogenesis (such as ribonucleoprotein complex biogenesis, cellular component biogenesis at cellular level, and cellular component organization or biogenesis at cellular level). A detailed GO analysis result is listed in Appendix D.

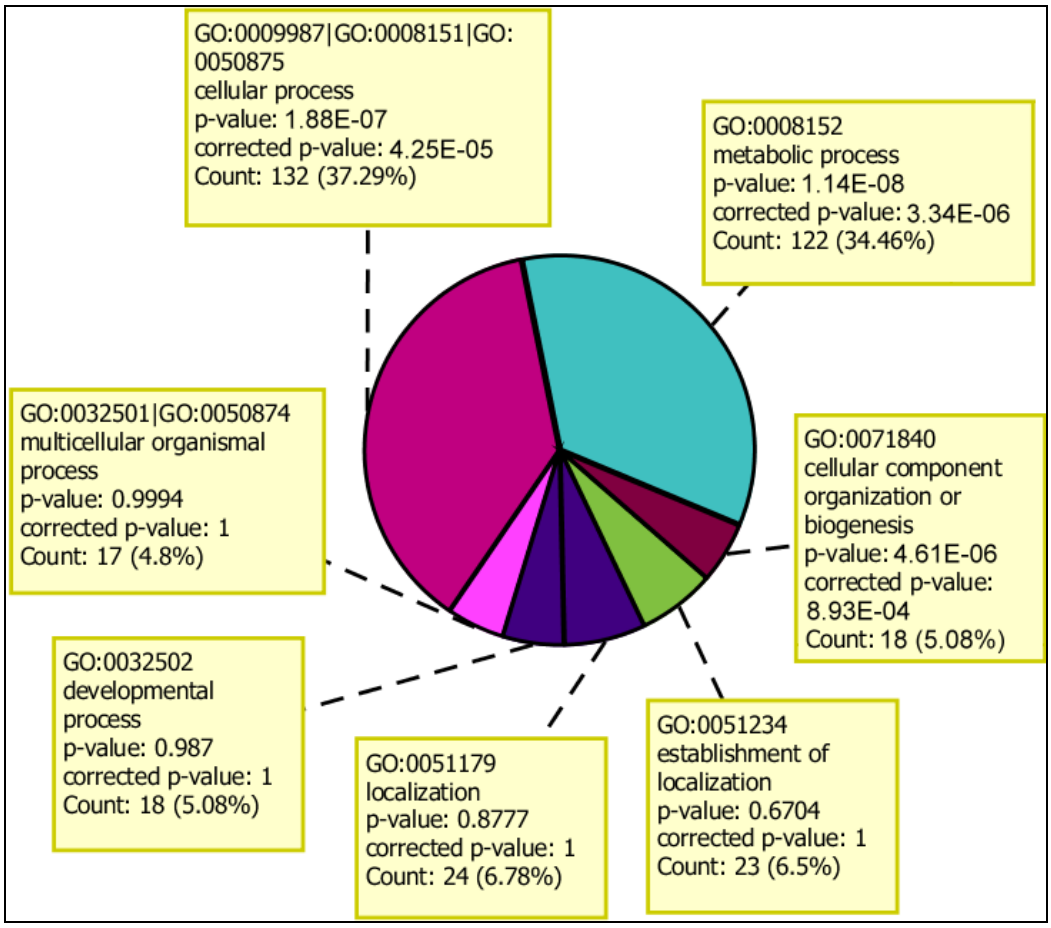

Figure 3.1.2. GO terms of cluster 1.

The biological process GO terms in cluster 1. The corrected p-value (see Section 2.3.4) is also shown to indicate the statistically significant GO terms in this cluster. Cellular process, metabolic process and cellular component organization or biogenesis were statistically significant GO terms. The number of transcripts mapping to a specific GO term is also presented, for example, in the cellular process term, the count was 132 (37.29%), which means 132 transcripts in cluster 1 were mapped to this GO term. These transcripts constituted 37.29% of whole transcripts in the mouse genome that were mapped to this term.

Genes relating to those significant GO terms are shown in Appendix E. Table 3.1.1 presents some selected genes from Appendix E. The majority of up-regulated genes were involved in the metabolic processes, i.e. catalytic activity,

nitrogen compound metabolic process, biosynthetic process, cellular metabolic process, primary metabolic process, and small molecule metabolic process, in the early c-MYC activation, whereas the cellular process (cell cycle activities, cell cycle process, cell division and DNA conformation change) and cellular component organization or biogenesis were also observed in this cluster.

Table 3.1.1. Significant biological processes and selected genes in cluster 1.

I. Cellular process

Genes relating to cell cycle, cell cycle process, cell division and DNA conformation change

Probe Set ID	Gene Symbol	Fold change ratio (Treatment/Control) at different time points				Ref_seq_id
		4	8	16	32	
1417910_at	*Ccna2*	-1.08	4.82	11.07	3.21	NM_009828
1448205_at	*Ccnb1*	1.09	3.82	9.56	3.63	NM_172301
1416492_at	*Ccne1*	2.10	4.16	5.80	1.28	NM_007633
1441910_x_at	*Ccne1*	1.93	8.88	1.74	1.6	NM_007633
1422535_at	*Ccne2*	2.17	8.20	6.32	5.7	NM_001037134 /// NM_009830
1417131_at	*Cdc25a*	2.55	2.19	1.49	3.07	NM_007658
1417132_at	*Cdc25a*	2.29	2.07	1.24	1.76	NM_007658
1452040_a_at	*Cdca3*	-1.08	1.05	5.51	1.1	NM_013538
1416802_a_at	*Cdca5*	-1.42	22.18	21.74	8.58	NM_026410
1424143_a_at	*Cdt1*	5.79	24.94	11.12	6.83	NM_026014
1449708_s_at	*Chek1*	2.69	6.39	4.48	4.69	NM_007691
1416698_a_at	*Cks1b*	1.52	3.58	3.15	2.45	NM_016904
1417457_at	*Cks2*	-1.24	3.77	8.09	6.65	NM_025415
1434079_s_at	*Mcm2*	1.84	4.18	2.56	3.05	NM_008564
1436708_x_at	*Mcm4*	2.10	8.25	1.43	2.69	NM_008565
1436808_x_at	*Mcm5*	4.34	28.35	2.00	9.02	NM_008566
1438320_s_at	*Mcm7*	2.81	5.93	3.11	3.61	NM_008568
1439269_x_at	*Mcm7*	2.40	7.40	2.73	3.72	NM_008568
1418281_at	*Rad51*	1.09	4.62	9.60	1.58	NM_011234

II. Metabolic process

Genes relating to cellular metabolic process

Probe Set ID	Gene Symbol	Fold change ratio (Treatment/Control) at different time points				Ref_seq_id
		4	8	16	32	
1427197_at	*Atr*	2.57	4.41	1.58	2.96	NM_019864
1448205_at	*Ccnb1*	1.09	3.82	9.56	3.63	NM_172301
1416492_at	*Ccne1*	2.10	4.16	5.80	1.28	NM_007633
1441910_x_at	*Ccne1*	1.93	8.88	1.74	1.60	NM_007633
1422535_at	*Ccne2*	2.17	8.20	6.32	5.70	NM_001037134 /// NM_009830
1424143_a_at	*Cdt1*	5.79	24.94	11.12	6.83	NM_026014
1449708_s_at	*Chek1*	2.69	6.39	4.48	4.69	NM_007691
1417457_at	*Cks2*	-1.24	3.77	8.09	6.65	NM_025415
1426351_at	*Hspd1*	1.31	1.84	2.45	2.63	NM_010477
1434079_s_at	*Mcm2*	1.84	4.18	2.56	3.05	NM_008564
1436708_x_at	*Mcm4*	2.10	8.25	1.43	2.69	NM_008565
1436808_x_at	*Mcm5*	4.34	28.35	2.00	9.02	NM_008566
1438320_s_at	*Mcm7*	2.81	5.93	3.11	3.61	NM_008568
1439269_x_at	*Mcm7*	2.40	7.40	2.73	3.72	NM_008568
1450376_at	*Mxi1*	2.36	1.42	2.52	4.78	NM_001008542 /// NM_001008543 /// NM_010847
1423747_a_at	*Pdk1*	4.74	4.40	2.45	5.13	NM_172665
1423748_at	*Pdk1*	5.64	6.35	4.16	6.23	NM_172665
1435836_at	*Pdk1*	3.28	2.66	1.76	3.01	NM_172665
1451845_a_at	*Ptrh2*	1.70	1.20	2.24	3.97	NM_001098810 /// NM_175004
1418281_at	*Rad51*	1.09	4.62	9.60	1.58	NM_011234

III. Cellular component organization or biogenesis

Genes relating to cellular component organization or biogenesis

Probe Set ID	Gene Symbol	Fold change ratio (Treatment/Control) at different time points				Ref_seq_id
		4	8	16	32	
1417910_at	*Ccna2*	-1.08	4.82	11.07	3.21	NM_009828
1448205_at	*Ccnb1*	1.09	3.82	9.56	3.63	NM_172301
1417131_at	*Cdc25a*	2.55	2.19	1.49	3.07	NM_007658
1417132_at	*Cdc25a*	2.29	2.07	1.24	1.76	NM_007658
1452040_a_at	*Cdca3*	-1.08	1.05	5.51	1.1	NM_013538
1416802_a_at	*Cdca5*	-1.42	22.18	21.74	8.58	NM_026410
1434079_s_at	*Mcm2*	1.84	4.18	2.56	3.05	NM_008564

The result of biological pathway analysis of cluster 1 is presented in Figure 3.1.3, which shows that c-MYC activation in early time point has already triggered complicated gene regulations and most of the regulated genes were located in cytoplasm or nucleus.

Mxi1 (MAX interactor 1), *Rad51* (RAD51 homolog (RecA homolog, E. coli; S. cerevisiae)), *Atr* (ataxia telangiectasia and Rad3 related) and *Ccne1* (cyclin E1) were up-regulated genes located in nucleus. *Mcm2* (minichromosome maintenance complex component 2), *Mcm4* (minichromosome maintenance complex component 4) and *Mcm7* (minichromosome maintenance complex component 7) were also up-regulated as a result of MYC activation.

Ccnb1 (cyclin B1), *Ccna2* (cyclin A2) and *Chek1* (CHK1 checkpoint homolog (S. pombe)), located in cytoplasm, are important cell cycle related genes and were up-regulated as well. Genes, i.e. *Pdk1* (pyruvate dehydrogenase kinase, isoenzyme 1), *Ptrh2* (peptidyl-tRNA hydrolase 2) and *Hspd1* (heat shock protein 1 (chaperonin)) located in mitochondrion were also up-regulated.

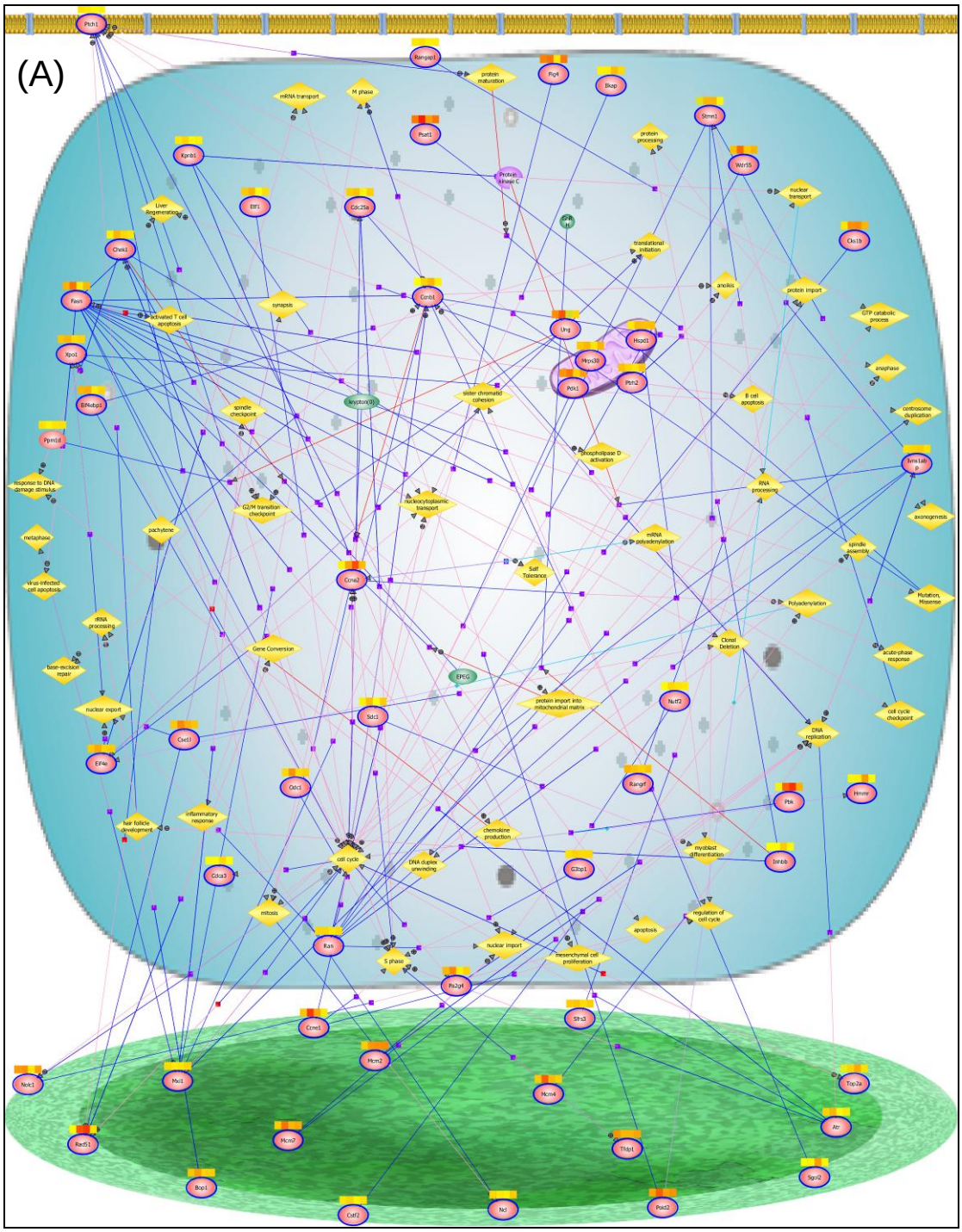
(A)
Ptch1
Rangap1
protein maturation
Pip4
Bicp
mRNA transport
M phase
Stmn1
Psat1
protein processing
Kpnb1
Wtr15
Protein kinase C
nuclear transport
Liver Regeneration
Eif1
Cdc25a
Sph1
Chek1
translational initiation
Cks1b
anoikis
protein import
Fas1
Ccnb1
synapse
activated T cell apoptosis
Ung
Hspd1
GTP catabolic process
Xpo1
Hsps30
anaphase
Pdk1
Pdhx2
B cell apoptosis
BRCtbp1
sister chromatid cohesion
spindle checkpoint
kinetochore (I)
centrosome duplication
Ppm1d
phospholipase D activation
Smc1a
response to DNA damage stimulus
RNA processing
nucleocytoplasmic transport
G2/M transition checkpoint
axonogenesis
pachytene
metaphase
mRNA polyadenylation
spindle assembly
Ccna2
Self Tolerance
virus-infected cell apoptosis
Mutation, Missense
Polyadenylation
rRNA processing
Clonal Deletion
Gene Conversion
acute-phase response
base-excision repair
EPEC
protein import into mitochondrial matrix
Nutf2
nuclear export
Sdc1
cell cycle checkpoint
DNA replication
Cxcl1
Eif4e
Cacr1
Rangrf
Hmmr
Ptk
inflammatory response
hair follicle development
chemokine production
cell cycle
myoblast differentiation
DNA duplex unwinding
C3bp1
Cdca3
Inf-bb
mitosis
regulation of cell cycle
apoptosis
Ran
nuclear import
S phase
mesenchymal cell proliferation
Ppp2r1
Stk3
Ccne1
Mcm2
Nolc1
Mcl1
Mcm4
Top2a
Atr
Rad51
Mcm7
Thip1
Bop1
Sgo2
Cstf2
Ncl
Psd2

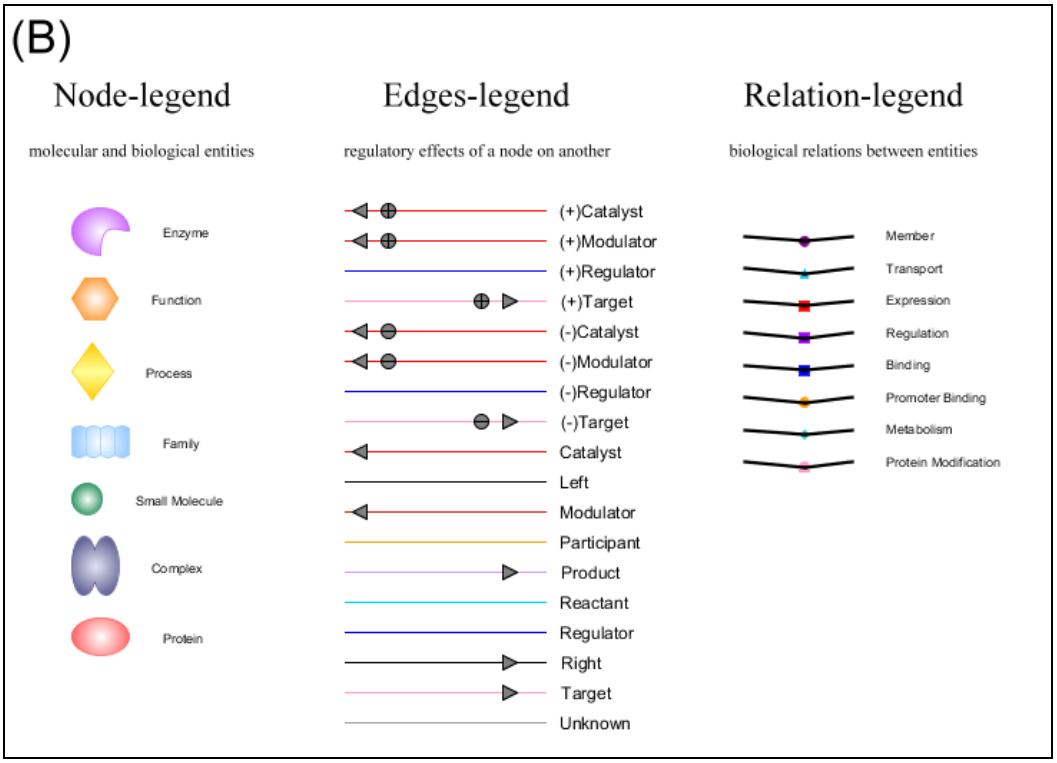

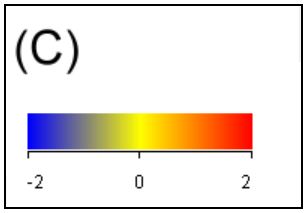

Figure 3.1.3. Biological pathways of up-regulated genes. (A) Biological pathways, (B) legends of pathway and (C) heatmap of expression level (of $\log_2$ normalisation).

A complicated gene regulatory network was triggered by c-MYC activation. Using a text-mining method (see Section 2.3.4), differentially expressed genes and their related functions are discovered. Because c-MYC activated a complicated gene network, a RAR compressed file, which contains the information in Figure 3.1.3, was generated and can be downloaded from https://files.warwick.ac.uk/yi-fangwang/files/thesis/pure_myc.rar. After the file is decompressed, a file named upregulated_gene_network.html, which is a navigable html page of Figure 3.1.3 (A) with hyperlink functions, can be found.

In the down-regulated cluster, cluster 2, no statistically significant biological process GO terms could be defined. The result of pathway analysis for cluster 2 is shown in Figure 3.1.4. *Cdkn2b* (cyclin-dependent kinase inhibitor 2B (p15, inhibits CDK4)), *Kdr* (kinase insert domain receptor, which is a type III receptor tyrosine kinase) and *Figf* (c-fos induced growth factor (vascular endothelial growth factor D)) were down-regulated through the experimental period after c-MYC activation.

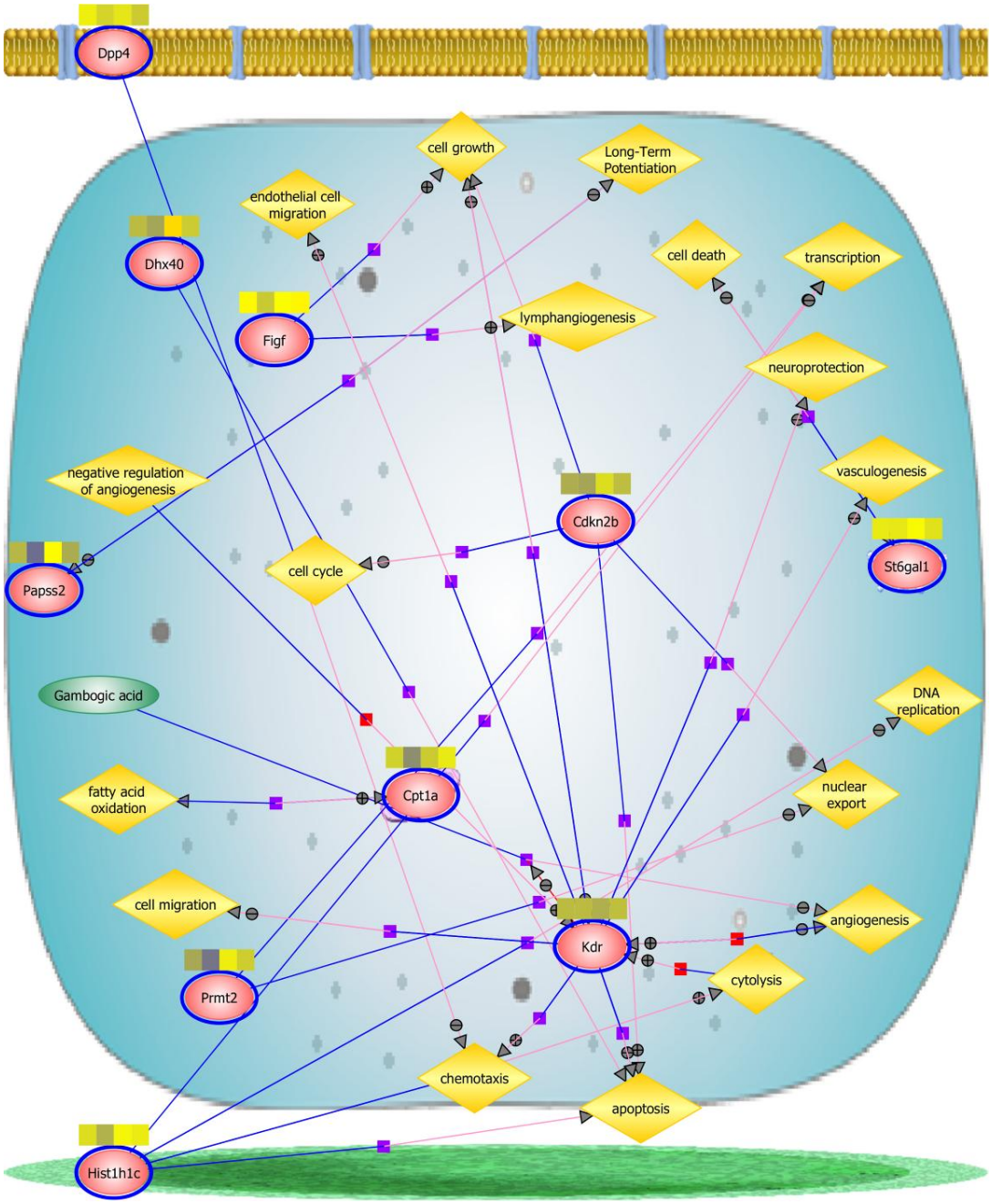

Figure 3.1.4. Biological pathways of down-regulated genes. Legends see Figure 3.1.3.

A full list of statistically significant differentially expressed transcripts is given in Appendix C.

3.1.2. Effect of exenatide and c-MYC during the early activation of c-MYC

In this section, the effects of two different conditions will be studied; condition 1 (M^+/E^+ vs M^+/E^-): the effect of exenatide under c-MYC activation, and condition 2 (M^-/E^+ vs M^-/E^-): the effects of exenatide without c-MYC activation. In condition 1, 43 transcripts in the MYC-activated transgenic mouse system exhibited significant changes in response to the exenatide treatment whereas 39 transcripts were significantly up- or down-regulated in condition 2. A full list of statistically significant differentially expressed transcripts under condition 1 and condition 2 is provided in Appendix F.

The statistically significant GO terms for condition 1 and condition 2 are presented in Table 3.1.2 and Table 3.1.3. Because of the stringency of the statistical analysis, only a few significant GO terms could be determined in condition 1 and condition 2. In condition 1, the significant GO terms were osteoblast fate commitment and embryonic pattern specification, whereas in condition 2, the significant GO terms were regulation of glycogen biosynthetic process, regulation of glucan biosynthetic process, positive regulation of glycogen biosynthetic process and regulation of polysaccharide biosynthetic process.

Table 3.1.2. GO terms of condition 1.

GO ACCESSION	GO Term	corrected p-value	Count in Selection	% Count in Selection	Count in Total	% Count in Total
GO:0002051	osteoblast fate commitment	9.44E-02	2	66.66	5	0.0290
GO:0009880	embryonic pattern specification	9.44E-02	3	100	28	0.1626

Table 3.1.3. GO terms of condition 2.

GO ACCESSION	GO Term	corrected p-value	Count in Selection	% Count in Selection	Count in Total	% Count in Total
GO:0005979	regulation of glycogen biosynthetic process	4.05E-02	2	100	5	0.0290
GO:0010962	regulation of glucan biosynthetic process	4.05E-02	2	100	5	0.0290
GO:0045725	positive regulation of glycogen biosynthetic process	4.05E-02	2	100	5	0.0290
GO:0032885	regulation of polysaccharide biosynthetic process	4.05E-02	2	100	5	0.0290

The pathway analysis results of condition 1 and condition 2 are shown in Figure 3.1.5 and Figure 3.1.6. In condition 1, *Vegfa* (vascular endothelial growth factor A), which was down-regulated, was shown as a hub gene to regulate several biological functions, such as endothelial cell migration, endothelial cell proliferation, ossification, apoptosis, endocytosys, positive regulation of mitosis, cell division, cell growth, neurogenesis, and transcription. *Smad5* (MAD homolog 5 (Drosophila)), *Hsph1* (heat shock 105kDa/110kDa protein 1) and *Hdac9* (histone deacetylase 9) were also down-regulated. *Fabp7* (fatty acid binding protein 7, brain), *Zbtb16* (zinc finger and BTB domain containing 16), *Nr1h4* (nuclear receptor subfamily 1, group H, member 4), *Ccrn4l* (CCR4 carbon catabolite repression 4-like (S. cerevisiae)) were up-regulated.

In condition 2, *Wnt4* (wingless-related MMTV integration site 4), *Vldlr* (very low density lipoprotein receptor), *Gna13* (guanine nucleotide binding protein, alpha 13), *Lyve1* (lymphatic vessel endothelial hyaluronan receptor 1), *Ccrn4l*, *Fkbp5* (FK506 binding protein 5) and *Btg3* (B-cell translocation gene 3) were up-regulated,

whereas *Hdac9*, *Terf2* (telomeric repeat binding factor 2), *Vdr* (vitamin D receptor) and *Cited2* (Cbp/p300-interacting transactivator, with Glu/Asp-rich carboxy-terminal domain, 2) were down-regulated.

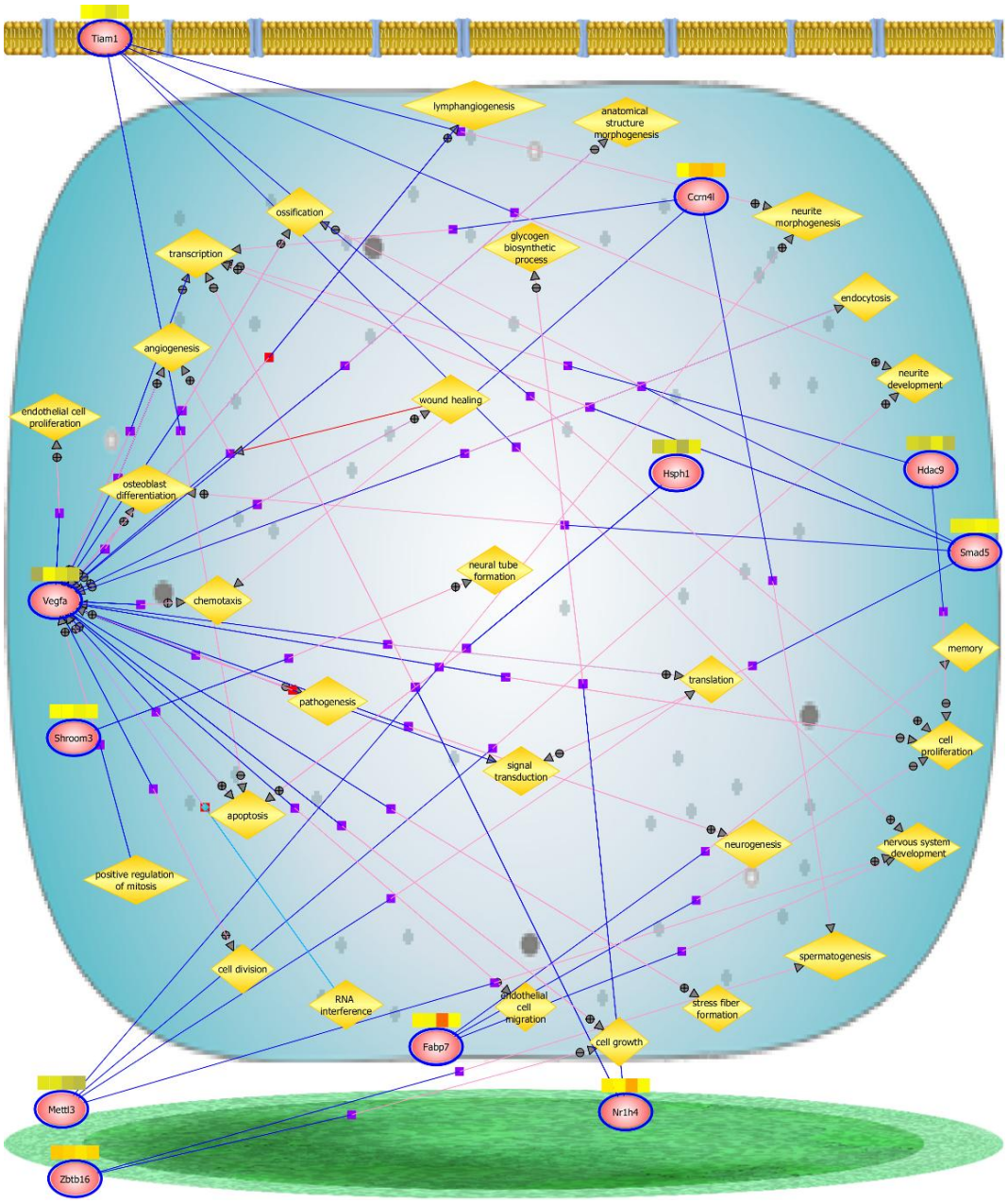

Figure 3.1.5. Biological pathways of condition 1.

Biological pathways of condition 1 (M^+/E^+ vs M^+/E^-): the effect of exenatide under c-MYC activation.

Legends see Figure 3.1.3.

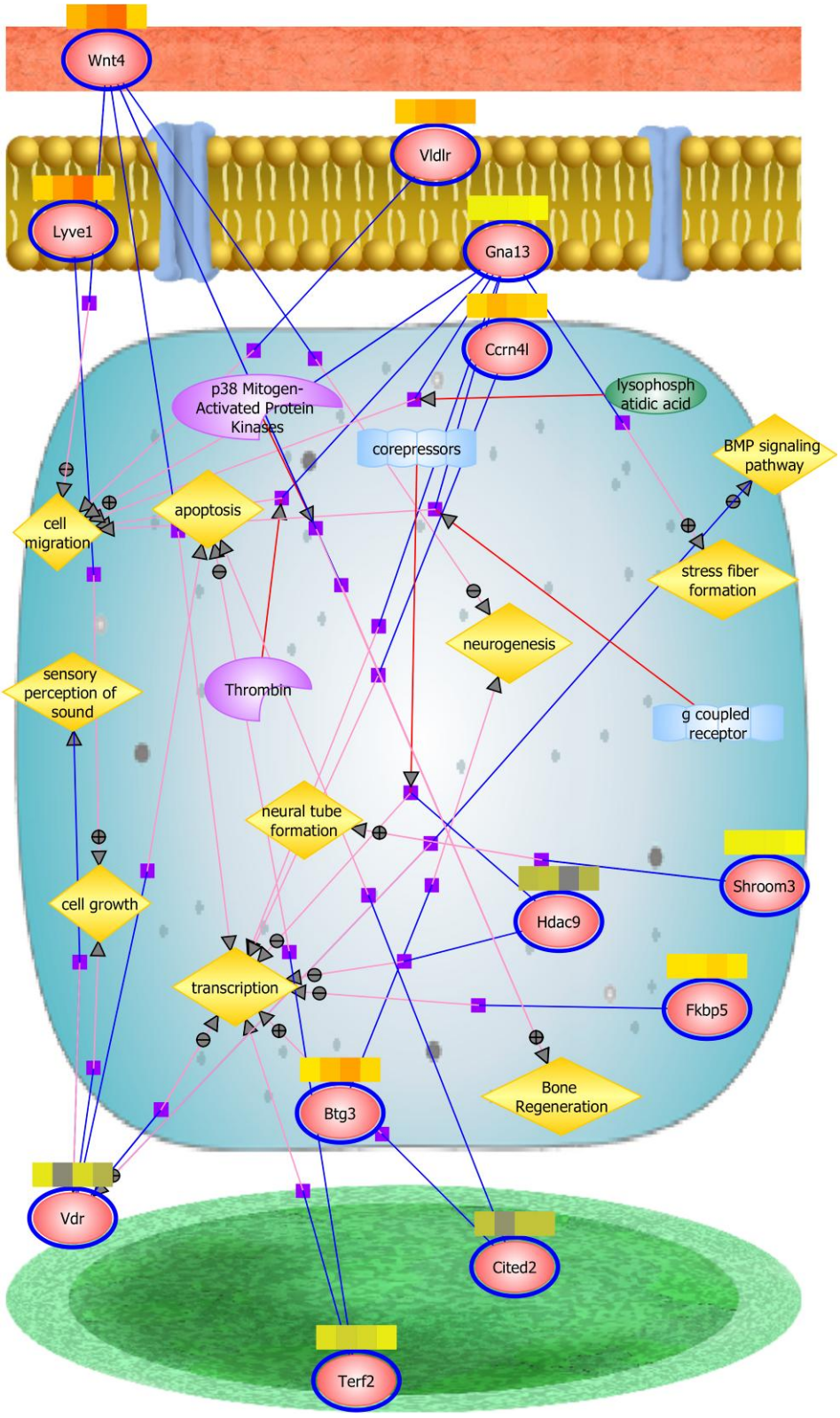

Figure 3.1.6. Biological pathways of condition 2.

Biological pathways of condition 2 (M^-/E^+ vs M^-/E^-): the effect of exenatide without c-MYC activation. Legends see Figure 3.1.3.

3.2 Hypoglycaemia in early c-MYC activation

In most *pIns-c-MycER*^{TAM} transgenic mouse studies, the main focus is on glucotoxicity (Cheung *et al*., 2010; Pascal *et al*., 2008), carcinogenesis (Pelengaris *et al*., 2004; Pelengaris and Khan, 2001; Pelengaris *et al*., 2002b), and the provenance of the new β-cells (Cano *et al*., 2008); invariably concentrating on the late stage of c-MYC activation in the *pIns-c-MycER*^{TAM} transgenic mouse. By contrast, this section presents *in vivo* data on the early effects of c-MYC in this transgenic animal system. The dynamics of glucose is presented in Section 3.2.1 and further results of the energy expenditure are shown in Section 3.2.2. In Section 3.2.3, the insulin levels of specific corresponding time points of glucose levels are presented. The application of exenatide in early c-MYC activation is presented in Section 3.2.4. Finally, β-cell mass quantification and β-cell numbers are presented in Section 3.2.5.

3.2.1. Hypoglycaemia starts within 16 hours of c-MYC activation

Glucose dynamics *in vivo* is presented in this section. The glucose dynamics of different TL experiments which record the blood glucose level every 4 or 8 hours continuously within 36 hours treatment of WT (wild-type littermates treated with peanut oil), MYC-OFF (*pIns-c-MycER*^{TAM} mice treated with peanut oil) and MYC-ON (*pIns-c-MycER*^{TAM} mice treated with 4-OHT) is shown in Figure 3.2.1. For more details of TL experiments, see Figure 2.1.1 in Section 2.1.3. Different TL experiments results were combined together in this figure according to different treatment groups to generate a continuous glucose profile, i.e. experimental results of WT from TL1, TL2 and TL3 were combined as Figure 3.2.1 (A); experimental results of MYC-OFF from TL1, TL2 and TL3 were combined as Figure 3.2.1 (B);

and experimental results of MYC-ON from TL1, TL2 and TL3 were combined as Figure 3.2.1 (C). The average glucose levels across all time points were stable for WT and MF, which were 7.8 ± 0.75 mmol/l (mean ± sample standard deviation (SD)) and 3.3 ± 0.53 mmol/l, respectively. In the MYC-ON group, the glucose level remained close to the average level, which was 3.6 ± 0.92 mmol/l, until 16 hours of c-MYC activation. A significant decline of the glucose level occurred and endured until 24 hours. Figure 3.2.1 (C) also shows that the decreased glucose level became hyperglycaemic at 32 hours but returned to euglycaemic at 36 hours.

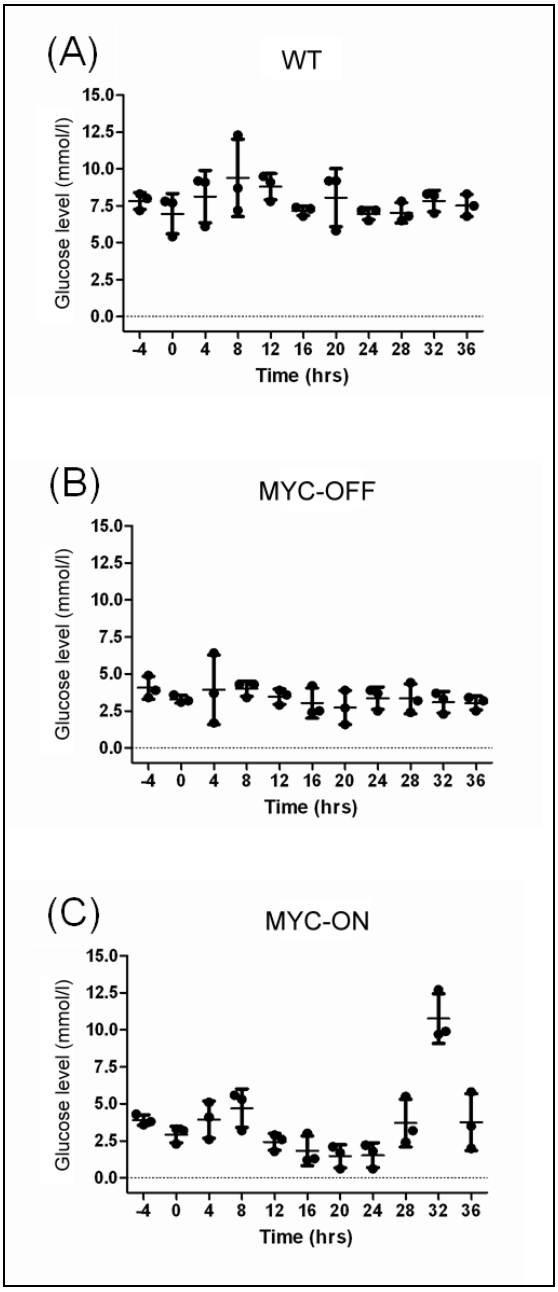

Figure 3.2.1. Glucose dynamics of c-MYC activation within 36 hours. Glucose level for (A) WT, (B) MYC-OFF, and (C) MYC-ON.

The experimental design is described in Figure 2.1.1 in Section 2.1.3. Different TL experiments were combined according to different treatment groups (n=3) to make a continuous blood glucose profile of c-MYC activation/control over 36 hours. (A) represents the blood glucose level of WT from TL1, TL2 and TL3, (B) is the glucose level of MYC-OFF from TL1, TL2 and TL3 and (C) represents the blood glucose level of MYC-ON from TL1, TL2 and TL3. The error bars represent the sample standard deviation (SD).

Apart from the possible c-MYC effect, glucose dynamics is coordinated through various metabolic and endocrine regulatory processes. Food intake contributes directly to glucose influx and will be discussed in Section 3.2.2, whereas insulin regulates blood glucose level via its endocrine actions, and will be considered in Section 3.2.3.

3.2.2. Altered energetic balance does not completely account for hypoglycaemia

Food intake and faeces production were evaluated throughout the TL experiments. Mice body weights were also recorded every 4 or 8 hours. The energy expenditure and food intake *in vivo* is presented in Figure 3.2.2. The energy usage throughout all TLs from 0 to 28 hours is presented in Figure 3.2.2 (A). There was no difference within MYC-ON and MYC-OFF groups but a statistical difference (paired t-test, p-value< 0.05) was detected between WT (0.0943 ± 0.0152 (g/hr); mean ± SD) and MYC-ON (0.0742 ± 0.0102 (g/hr)). The energy usage of WT (0.1235 ± 0.0220 (g/hr)), MYC-OFF (0.1014 ± 0.0463 (g/hr)) and MYC-ON (0.0773 ±0.0129 (g/hr)) during hypoglycaemia is shown in Figure 3.2.2 (B), which shows a statistically significant difference (paired t-test, p-value<0.01) in energy usage between WT and MYC-ON across the hypoglycaemic period, which was 8 to 20 hours. Food intake and faeces production during the experimental period and hypoglycaemic period are also presented in Figure 3.2.2 (C), (D), (G), and (H), which show a significant decrease of food intake in MYC-ON mice during experimental and hypoglycaemic periods compared to their WT and MYC-OFF littermates. A significant difference is observed in the change of body weight (Δw)

during the experimental period (Figure 3.2.2 (E)) between MYC-ON and MYC-OFF group whereas no significant difference is shown during hypoglycaemia (Figure 3.2.2 (F)).

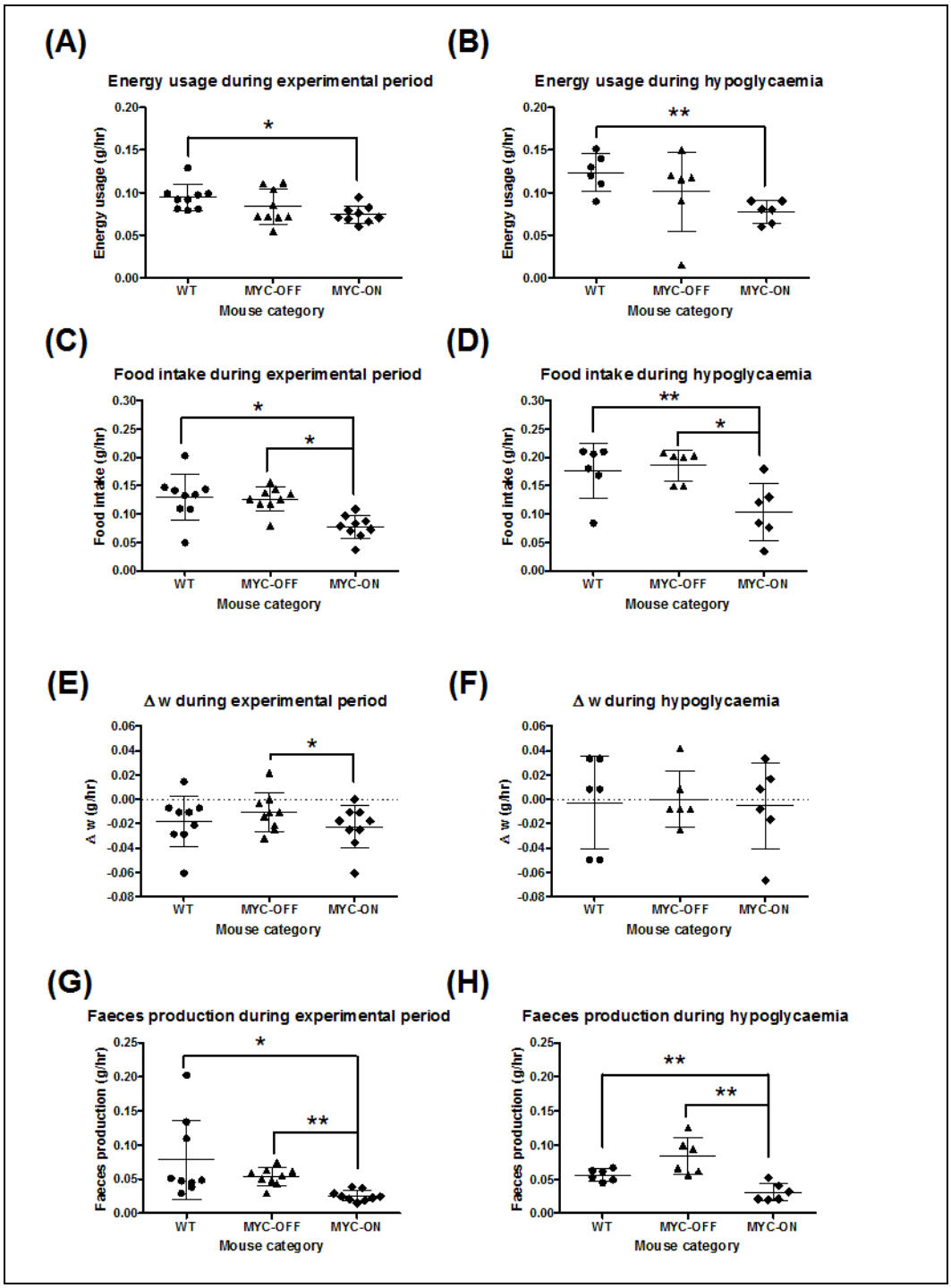

Figure 3.2.2. Energy expenditure dynamics.

Energy usage (A), food intake (C), change of body weight (Δw) (E), and faeces production (G) during the experimental period (n=9), and energy usage (B), food intake (D), Δw (F), and faeces production (H) during the hypoglycaemic period (n=6). The error bars represent the SD. * significant difference according to the paired t-test ($p<0.05$) and ** ($p<0.01$).

3.2.3. Hypoglycaemia results from hyperinsulinaemia

The analysis of the *in vivo* glucose dynamics in Section 3.2.1 confirms the existence of hyperglycaemia during 16-24 hours after c-MYC activation. Different scenarios can be hypothesised to explain this phenomenon: (i) increased insulin secretion or release from dying cells; (ii) rapid β-cell proliferation; and (iii) increased insulin sensitivity. The first two hypotheses can be addressed by testing the insulin levels and immuno-staining with specific antibodies (such as Ki-67 as a maker for proliferation and Caspase-3 as a marker for apoptosis). Figure 3.2.3 shows the fed blood glucose level and serum insulin level at -4, 8, 12, 16, 20, 28, 32, and 36 hours. The insulin level is similar in the WT and MYC-OFF treatments whereas MYC-OFF has a lower glucose level. Figure 3.2.3 (C) and Figure 3.2.3 (F) present the glucose level and its corresponding insulin level at different time points in MYC-ON mice. At 16 to 20 hours, MYC-ON mice were hypoglycaemic with an acute insulin release, which confirmed that hypoglycaemia occurred within 16 hours accompanied by a surge of insulin release in MYC-ON mice.

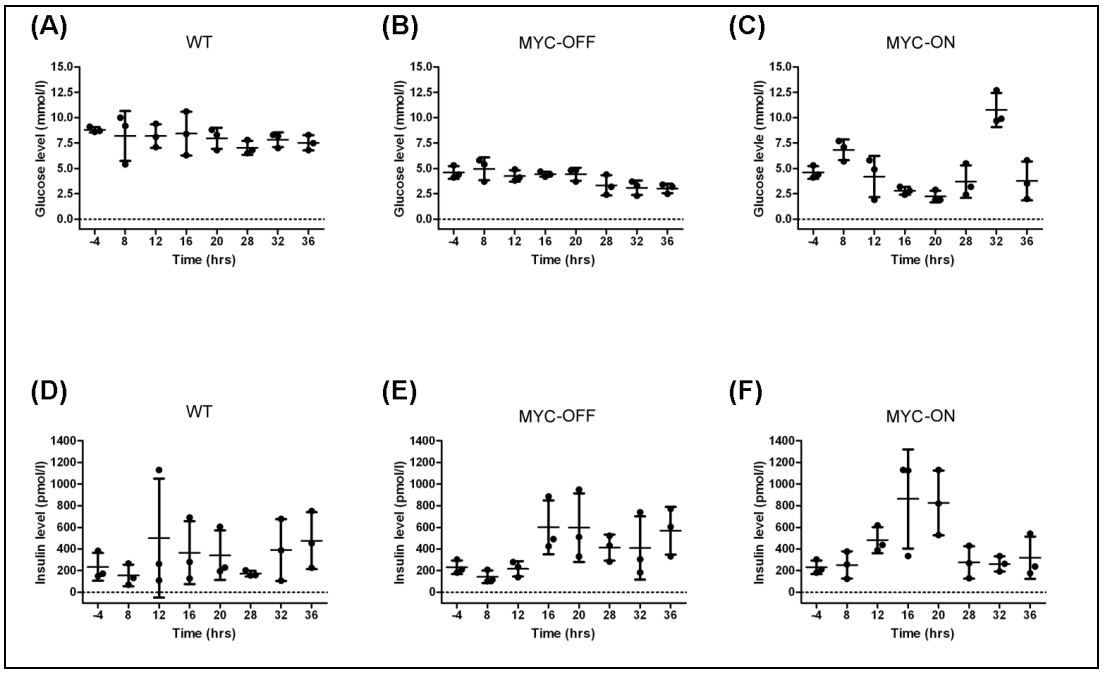

Figure 3.2.3. Early c-MYC activation causes hyperinsulinaemic hypoglycaemia (HH).

Glucose level for (A) WT, (B) MYC-OFF, and (C) MYC-ON mice and insulin level for (D) WT, (E) MYC-OFF, and (F) MYC-ON mice at initial time point and 8, 12, 16, 20, 28, 32, and 36 hours after the first injection of 4-OHT or the same volume of vehicle. n=3 and the error bars represent the SD.

In order to show that hypoglycaemia and hyperinsulinaemia at 16 hours were genuine, a further negative control group was presented in Figure 3.2.4. WT mice were treated with 4-OHT (WT-4-OHT) and the glucose and insulin levels were tested at 8 and 16 hours after the injection. Both glucose and insulin levels of WT-4-OHT (see Figure 3.2.4 (A) and Figure 3.2.4 (B)) were within the average levels comparing to the WT group (see Figure 3.2.3 (A) and Figure 3.2.3 (D)). Therefore, the administration of 4-OHT did not affect the whole blood glucose and serum insulin levels in the *pIns-c-MycER*^{TAM} transgenic mouse WT littermates.

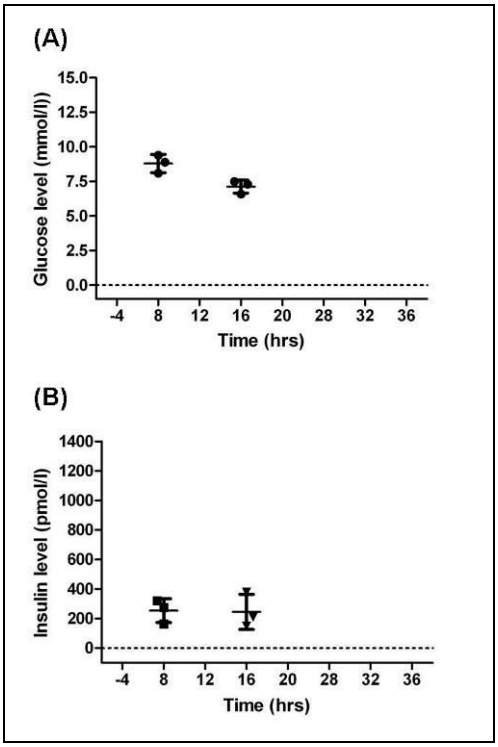

Figure 3.2.4. Administration of 4-OHT does not affect WT glucose and insulin levels.

WT type littermates of *pIns-c-MycER*^{TAM} mouse were treated with 4-OHT (WT-4-OHT). The glucose levels (A) and insulin levels (B) were tested at 8 and 16 hours after the treatment. n=3 and the error bars represent the SD.

3.2.4. Effects of exenatide

Exenatide is frequently employed in the treatment of T2DM, perhaps because it is well-known for having fewer side effects than other glucose-lowering agents, for example it will not cause hypoglycaemia. The *pIns-c-MycER*^{TAM} transgenic mouse system is a well-established conditional β-cell ablation animal model, which causes high glucose levels, without other confounding factors. This section presents the effect of exenatide on the glucose level of this transgenic model at early time points, in which *pIns-c-MycER*^{TAM} transgenic mice were experiencing hypoglycaemia.

Figure 3.2.5 shows the glucose level of exenatide treatment in *pIns-c-MycER*^{TAM} transgenic mice after 16 hours of c-MYC activation. It is clear that

glucose levels were significantly lower in the exenatide treated mice than in the untreated ones, which suggests that exenatide might further lower the glucose level in this transgenic mouse, even without c-MYC activation.

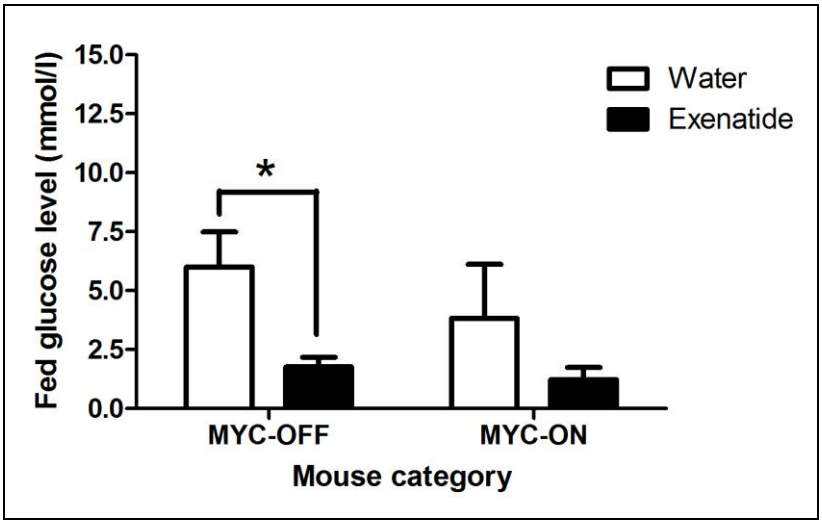

Figure 3.2.5. Exenatide treatment causes a decrease of glucose levels in MYC-OFF and does not correct c-MYC induced hypoglycaemia.

Glucose levels of MYC-OFF and MYC-ON at 16 hours treated with exenatide or water vehicle is presented. n=3 and the error bars represent the SD. *, significant difference according to the paired t-test ($p<0.05$).

A further negative control of WT littermates treated with exenatide (EW) or the same volume of vehicle (WW) is presented in Figure 3.2.6 and a decrease (paired t-test, p-value<0.05) of glucose levels was observed in the EW group whereas there was no statistically detectable change of glucose levels in the WW group.

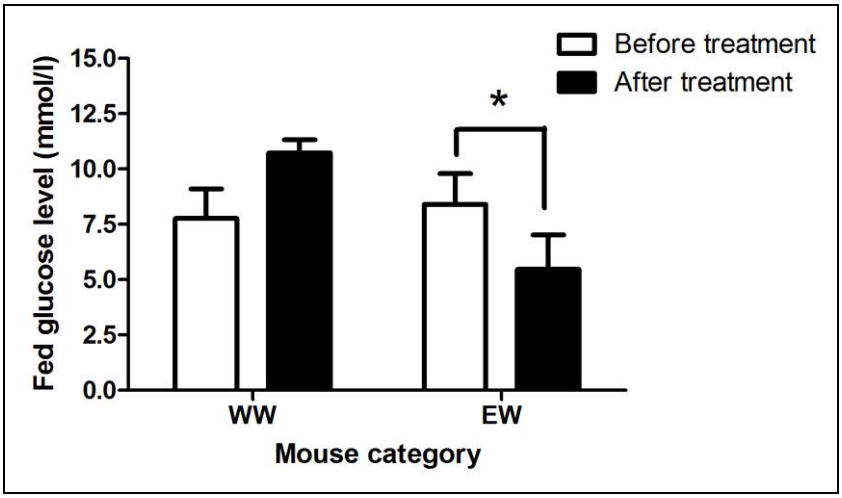

Figure 3.2.6. Treatment of exenatide lowers glucose levels in WT.

Glucose levels of WT treated with water vehicle (WW) or exenatide (EW). Fed glucose levels were measured before the SC injection (before treatment) and 2 hours after (after treatment). n=3 and the error bars represent the SD. *, significant difference according to the paired t-test ($p<0.05$).

3.2.5. Regulation of β-cells

Proliferation of β-cells after c-MYC activation is shown in Figure 3.2.7, in which representative figures of the experiment are presented, by means of immunofluorescence staining of Ki-67 and insulin in MYC-ON transgenic mice. The Ki-67 fluorescent staining was regarded as a marker for proliferation whereas the insulin fluorescent staining identified where the β-cells were. However, apoptosis was not observed from an early stage, such as 16 hours, of c-MYC activation because IHC staining of caspase-3 did not present any detectable fluorescent signals (data not shown).

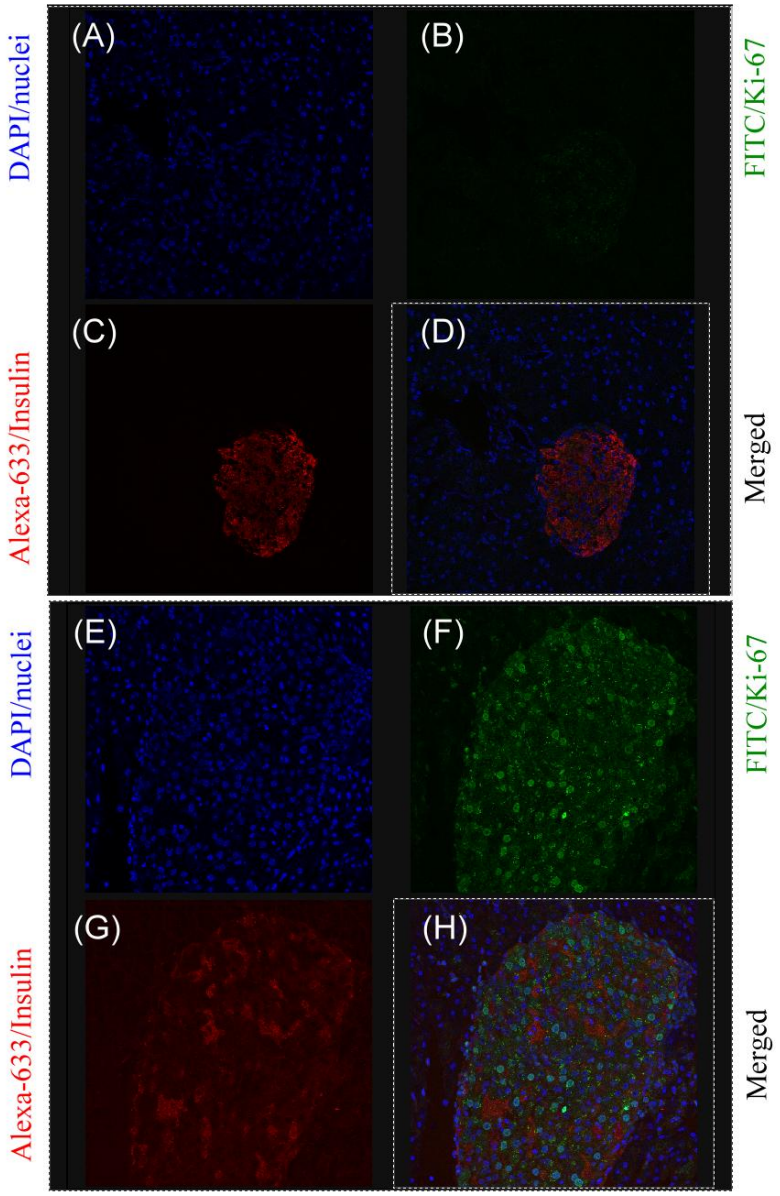

Figure 3.2.7. β-cell proliferation in early c-MYC activation.

After 16 hours of c-MYC activation, the proliferation of β-cells was detected by immunofluorescence staining of Ki-67 (green) and Insulin (red). (A)-(D) presents the staining result of WT and (E)-(H) presents the staining result of MYC-ON. The blue staining refers to DAPI, which stains the nuclei. Images were captured by confocal microscopy with x400.

As shown in Figure 3.2.3, the MYC-OFF (*plns-c-MycER*^{TAM} mice treated with peanut oil) and WT (WT littermates treated with peanut oil) groups had similar serum insulin levels but the blood glucose level in the MYC-OFF group was lower than the WT group, even without the activation of c-MYC. It might be inferred that the transgenic mouse system has a residual level of c-MYC activation at a small but steady level even without the administration of 4-OHT; this is called 'leakiness'. To investigate this possibility, β-cell mass quantification was carried out. The results are presented in Figure 3.2.8 at 8 and 16 hours after the first injection of 4-OHT or the same volume of vehicle. It is evident that *plns-c-MycER*^{TAM} mice had a bigger β-cell mass (3.45 ± 0.29 mg; mean ± SD) compared to their WT littermates (1.30 ± 0.14 mg), even when they had not received any 4-OHT treatment (see upper left panel of Figure 3.2.8). In the WT group, the β-cell masses for WT and WT-4-OHT were 1.93 ± 0.20 (mg) and 2.09 ± 0.80 (mg) at 8 hours, and 1.70 ± 0.17 (mg) and 1.56 ± 0.25 (mg) at 16 hours, and there was no significant change because of the 4-OHT treatment. In the MYC group, the treatment did change the β-cell mass at 8 hours which was 3.31 ± 0.63 (mg) for MYC-OFF and 4.55 ± 0.38 (mg) for MYC-ON, whereas no significant difference was observed at 16 hours between MYC-OFF (3.15 ± 0.60 mg) and MYC-ON (3.59 ±0.97 mg) groups.

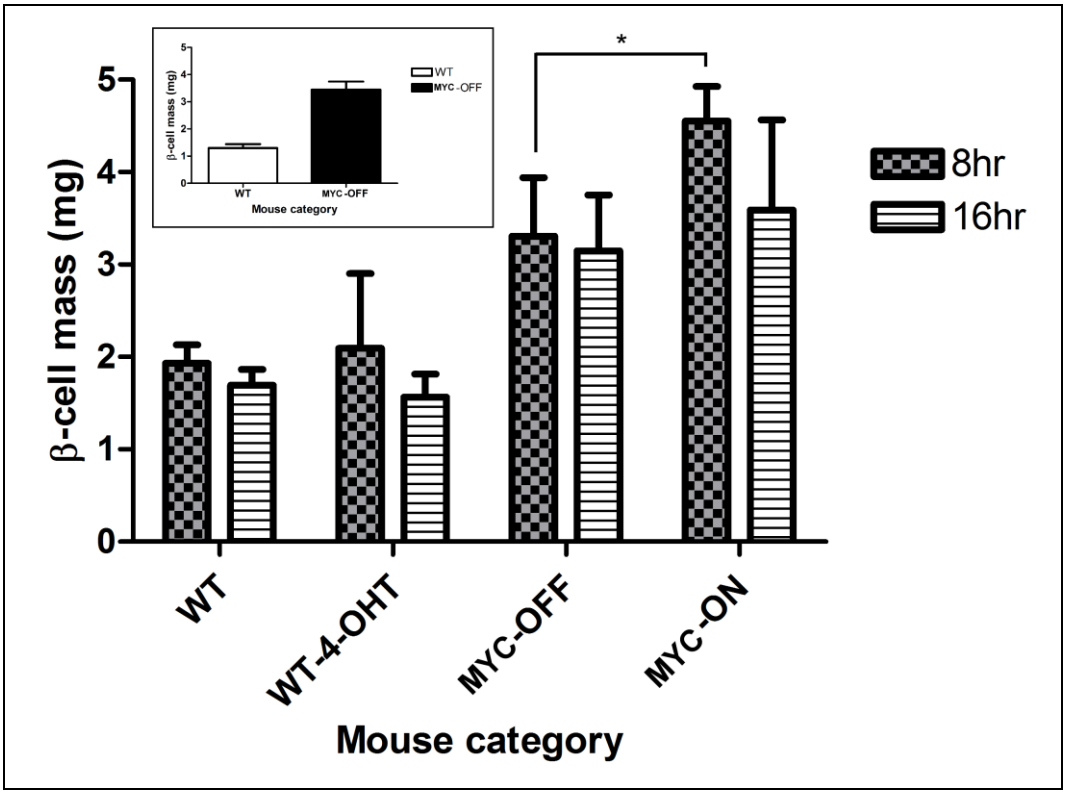

Figure 3.2.8. β-cell mass of *plns-c-MycER*^{TAM} mice or their WT littermates at 8 and 16 hours after the first injection of 4-OHT or peanut oil. Upper left panel, the β-cell mass of the control group of *plns-c-MycER*^{TAM} mice or WT. n=3 and the error bars represent the SD. *, ($p<0.05$).

Phenotype data, i.e., body weight and pancreas weight, on two experimental objects were lost, viz., WT-4-OHT2 at 8 hours (08WT-4-OHT2) and MYC-ON2 at 8 hours (08MYC-ON2). Apart from those two data points, the mean pancreas weights of the WT-4-OHT group and the MYC-ON group were calculated and used as 08WT-4-OHT2 and 08MYC-ON2's pancreas weights to compute their β-cell mass. The details of mouse body weight and pancreas weight of each treatment group at 8 and 16 hours is given in Table 3.2.1.

Table 3.2.1. Body weight and pancreas weight at 8 and 16 hours. n=3 in each group; all data represent a mean ± SD.

	8hr		16hr	
	body weight (g)	pancreas weight (mg)	body weight (g)	pancreas weight (mg)
WT	24.27±3.36	219.67±6.51	27.17±0.76	277.33±10.12
WT-4-OHT	27.85±1.85	220.50±19.50	27.90±0.70	266.67±22.94
MYC-OFF	23.73±1.36	234.67±24.85	23.80±1.06	232.33±16.77
MYC-ON	27.50±0.10	250.50±0.50	26.07±0.85	243.00±27.87

A surge of insulin secretion can be observed after 16 hours of c-MYC activation. In order to estimate the β-cell volume, the β-cell size at 16 hours was evaluated; results are presented in Figure 3.2.9. In the MYC-ON group, the β-cell size (1.48±0.21 (μm^2); mean ± SD) is statistically significantly larger than that in WT (0.90±0.05 (μm^2)) or WT-4-OHT (0.87±0.19 (μm^2)) group. Although the statistical analysis did not show the significant difference between WT and MYC-OFF (1.09±0.06 (μm^2)) groups, there was a trend for the transgenic mice to have larger β-cells even in the absence of activation of c-MYC. However, this thesis indicates that β-cell size was increased in the MYC-ON group.

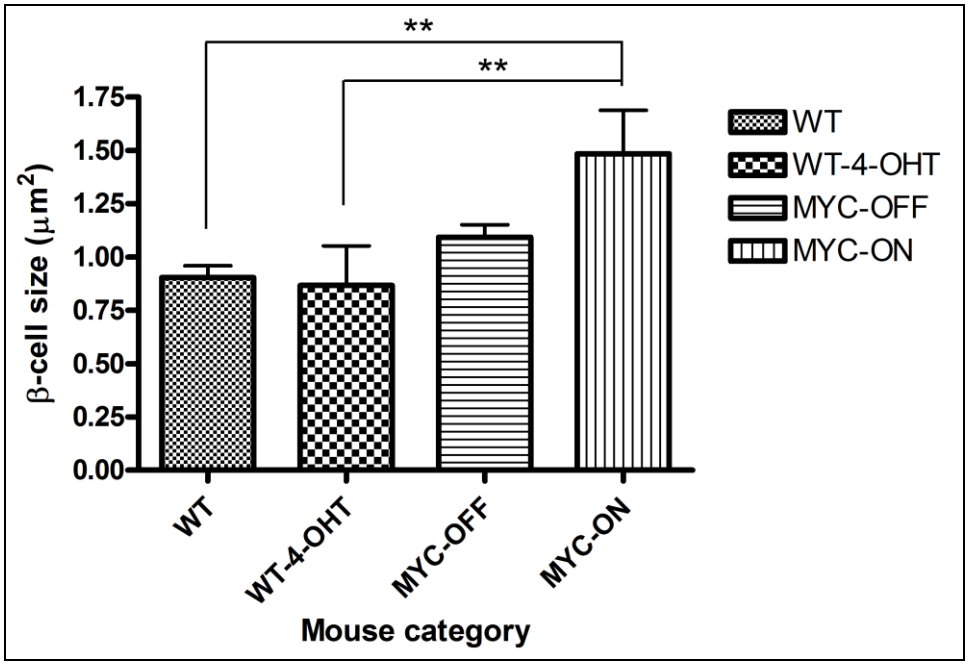

Figure 3.2.9. β-cell size of *pIns-c-MycER*^{TAM} mice or their WT littermates at 16 hours after the first injection of 4-OHT or peanut oil. n=3 and the error bars represent the sample standard deviation (SD). **, $p<0.01$.

3.3 Mathematical model

3.3.1. Analysis without neogenesis of β-cells

To analyse the dynamics without β-cells neogenesis, the parameter $\hat{\psi}_{NG}$ is set to zero. If the given parameter values obtained from the literature are accepted, the resulting β-cell dynamics is very slow, which can be considered as indirect evidence that neogenesis is an important factor in fast adaption, i.e. hours/days instead of months or years.

Using the method given in Appendix B, the system was rendered dimensionless, but retaining the dimension of time. The method also comprises the determination of the maximum absolute rates (the ξ s) and ranking of scaled variables according to these rates. For instance, if 10 g is chosen as the reference value for glucose and 44 mU as the reference value for insulin, then the rank is found as follows (ξ s all in min^{-1}; Q is already dimensionless):

$$x_1 = G/G_{ref} \quad x_2 = I_p/I_{ref} \quad x_3 = I_i/I_{ref} \quad x_4 = \omega_1/I_{ref} \quad x_5 = \omega_2/I_{ref} \quad x_6 = \omega_3/I_{ref}$$

$$x_7 = Q$$

$$\xi_1 = 4.8 \;\; \xi_2 = 0.11 \;\; \xi_3 = 0.066 \;\; \xi_4 = 0.028 \;\; \xi_5 = 0.028 \;\; \xi_6 = 0.028 \;\; \xi_7 = 8.7\times10^{-7}$$

A time-scale separation at $\nu = 7$ is apparent, with small parameter $\xi_\nu T = 8.7\times10^{-7}\ \text{min}^{-1}\times(24\times60\ \text{min}) = 0.00125$; a unit of slow time τ thus corresponding to 800 days.

In Appendix B, the dynamics in slow time for $x_7^{[1]}$ is derived by using Eqn (A 13), whereas the variables $x_1^{[1]}, \cdots, x_6^{[1]}$ are to be obtained as functions of $x_7^{[1]}$ on the basis of the slow-manifold condition, which corresponds to the stationary forced cycle in fast time when $x_7^{[1]}$ is held at a fixed value. These relations can be obtained numerically, and results are shown in Figure 3.3.1. In this system the reference cycle corresponds to a fairly high glycaemic load. At these high loads, the dynamics of the β-cell mass has two fixed points, i.e. a lower unstable one and a higher stable one. Topp *et al*. (2000) regards this kind of unstable fixed point as a "pathological fixed point," which means that if x_7 becomes lower than this equilibrium value, a destructive involution of β-cell mass will occur. The loss of β-cells leads to further hyperglycaemia and lower insulinaemia, which leads to further β-cell losses, so that this pathological fixed point will then decay to zero. This process may underlie non-autoimmune diabetes mellitus, as described by Imagawa *et al*. (2000).

When the glycaemic loads increase, these two points move together and collide. At a higher glycaemic loads, the globally attracting point is the trivial equilibrium Q=0, that is, zero β-cell mass. When β-cell death rate is increased at high glycaemic loads, the stable equilibrium value is decreased. It is due to the higher glucose toxicity (Efanova *et al*., 1998), and the increased susceptibility to apoptosis at higher insulin levels (Johnson and Alejandro, 2008); the latter authors describe this situation as a "sweet spot" for insulin in the high pico-molar range, and the high insulin level corresponds to order 1 levels in the scaled system.

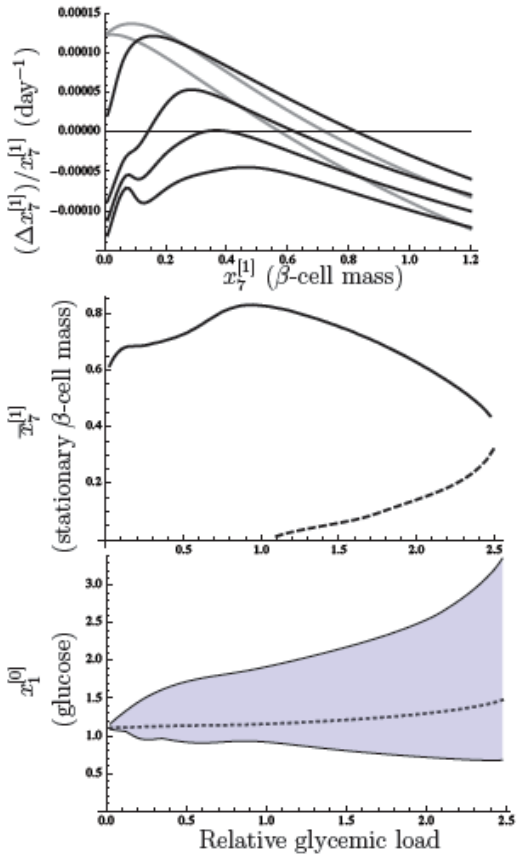

Figure 3.3.1. Dynamics of β-cell mass on the slow time scale. Top: relative daily change of β-cell mass, for various glycaemic loads (black curves, from top to bottom: 1, 2, 2.5 and 3 times the reference input; grey curves, from top to the bottom: 0.5 and 0 times the reference input). Middle: fixed point of the β-cell dynamics as a function of the relative glycaemic load (solid line: stable branch; dashed line: unstable branch). Bottom: fast-time scale glucose stationary cycle characteristics (dotted line: average value; bottom and top of filled region: minimum and maximum values).

Figure 3.3.2 shows a comparison of the dynamics under the situations of overfeeding and underfeeding. The dynamics was according to the approximation (which is simple and 1-dimensional) are shown, together with the solutions according to the dynamics of the original, 7-dimensional, system. The results are virtually indistinguishable. This means that the long-term dynamics is well-captured by the approximation. The full system was numerically integrated in fast time by using an explicit Runge-Kutta method of order 2(1), which is the *Mathematica* default method (Sofroniou and Spaletta, 2004). The slow system was evaluated using Euler-forward with a step size of one day, giving virtually the same result at less than a thousandth of the computational cost (run time; excluding the one-time cost of establishing the dynamics of x_7, which costs about 1% of the full-system's run time).

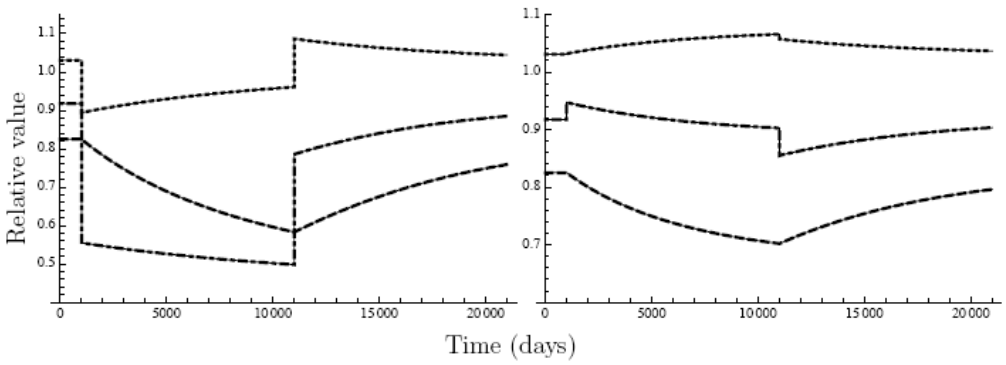

Figure 3.3.2. Simulations of overfeeding (left) and (underfeeding) right. On day 1,000, the glycaemic load is changed to 2.5 (left) or 0.1 (right) normal; on day 11,000 the load is restored to the normal value. Dotted line: $x_1^{[1]}$ (glucose); dot-dashed line: $x_2^{[1]}$ (plasma insulin); dashed line: $x_7^{[1]}$ (β-cell mass). Thin lines show the results of a direct simulation of the 7-dimensional system. ("Relative value" refers to scaling by G_{ref} and I_{ref}, as explained in the text; $Q=x_7=1$ corresponds to the stationary value of β-cell mass if the standard-cycle glycaemic load were administered at a constant rate; stationary values can be read off from Figure 3.3.1.)

It is tempting to treat the glycaemic load as a constant that represents the average of the daily cycle when a mathematical model for the long-term β-cell mass dynamics is formulated. Topp *et al*. (2000) and Winter *et al*. (2006) adopted this assumption. However, the dynamics of $x_7^{[1]}$ in slow time τ do in fact depend critically on the "temporal fine structure" of glucose uptake on the fast time scale t, through the integration in Eqn (A 13). If glucose uptake is replaced by its short-term average, such dependence is neglected. If one considers the case where the glycaemic load is taken up as a constant infusion (set to zero for the first 30 minutes after midnight, to execute a 24-hour cycle) instead of a daily 3-meal cycle, this neglect is apparent. Figure 3.3.3 shows the relative daily change of β-cell mass dynamics with various glucose inputs on a slow time scale. This long-term dynamics of the β-cell mass is notably different, i.e. the "pathological fixed point" remains very close to zero and the system achieves near-perfect regulation of the average glucose level even at a hyperglycaemic load that is 4 times higher than normal. Comparison with the case $\iota_{AI} \to \infty$ (data not shown) indicates that without compromising insulin's ability to regulate, the decrease of insulin's capability in inhibiting apoptosis is responsible for keeping the β-cell mass in check. If $\iota_{AI} \to \infty$, even with the normalisation of glucose levels is already reached at x_7-values, the fixed point of x_7 still increases quickly with the load.

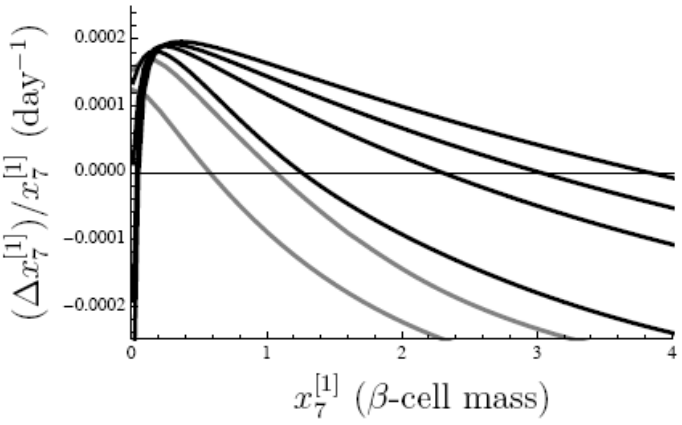

Figure 3.3.3. Dynamics of β-cell mass on the slow time scale: relative daily change of β-cell mass, for various glycaemic loads, given as a constant infusion (black curves, from left to right: 1, 2, 2.5, and 3 times the reference input; grey curves, from left to right: 0 and 0.5 times the reference input).

3.3.2. Extended model with neogenesis of β-cells

The dynamics shown in Figure 3.3.2 is very slow. An example of such slow dynamics is shown in Figure 3.3.4. When 80% of the β-cell mass is ablated, it takes 50 years to recover. It means that the subject will be suffering from the β-cell deficiency for life, and the baseline turn-over dynamics of β-cells is too sluggish to respond properly to such challenges. However, in reality, as shown in the literature, recovery from such damage is accomplished within a few weeks' time (Bouwens and Rooman, 2005). There are many different theories of the β-cell regeneration, as described in Section 2.4.4, including the idea that these the slowly proliferating β-cell pool may be supplied by a faster proliferating progenitor cell (De Leon *et al*., 2003) or the differentiated β-cells themselves (Ackermann Misfeldt *et al*., 2008) whereas it has also been suggested β-cells themselves are capable of rapid proliferation (Dor *et al*., 2004; Lee *et al*., 2006; Nir *et al*., 2007).

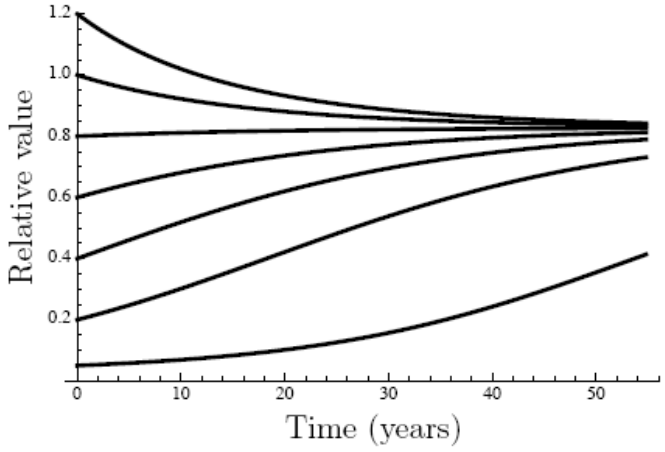

Figure 3.3.4. Dynamics of β-cell mass on the slow time scale: recovery to normal values after addition or destruction of β-cells at time t = 0. ("Relative value" has the meaning explained in the caption for Figure 3.3.2.)

Neogenesis of β-cells from the progenitor cells was introduced as described in Section 2.4.4 and the result is shown in Figure 3.3.5. When the model is extended with neogenesis, the recovery from ablated β-cell mass is faster and closer to the value that is quoted in the literature (Bouwens and Rooman, 2005). The slow-time approximation after combining the neogenesis is still working properly, apart from the fact that the time-scale separation is now up to two orders of magnitude worse because of the fast β-cell expansion that occurs when the β-cell mass ablation is too severe. The relationship between $\frac{d}{d\tau}x_7$ and x_7 still stays qualitatively equal, despite the fact that the lower, unstable fixed point is now very low and the positive rate of change that prevails when x_7 lies in between the fixed points is now several orders of magnitude larger.

As shown in the bottom panel of Figure 3.3.5, if the β-cell ablation is too critical, recovery will take disproportionally longer, i.e. when more than 80% of

β-cells are destroyed, recovery takes the best part of a year, which implies the subject is diabetic for a number of months until recovery occurs.

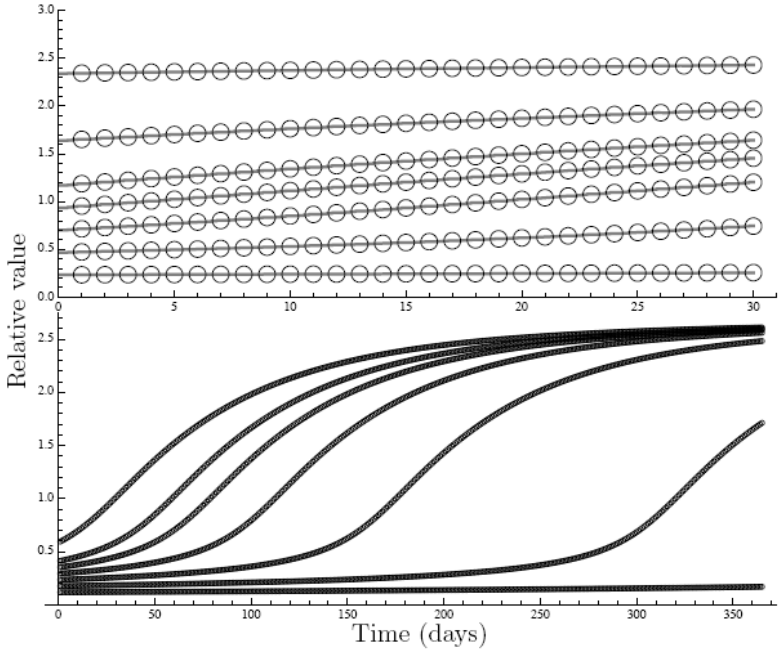

Figure 3.3.5. Model with neogenesis: recovery to normal values after addition or destruction of β-cells at time t = 0. Gray curves: direct simulation; circles: approximation according to slow-time approximation. Top panel: recovery over a month; bottom panel: recovery over a year. ("Relative value" has the meaning explained in the caption for Figure 3.3.2, but the normal stationary value is now different since the dynamics includes neogenesis.)

In T1DM, patients are suffering from an absolute β-cell mass losses because the autoimmune system destroys the pancreatic β-cells directly (Bach, 1994; Eisenbarth, 1986). The simulation in Figure 3.3.5 suggests that there is a critical level of depletion at which recovery becomes very slow. If the progenitor cells do not express the insulin-derived antigen, or do so in sufficiently low levels to escape immune attack, the progression to T1DM is a matter of the neogenic suppletion rate being unable to compensate for the losses, leading to a net regression of β-cell mass until the critical ablation level is reached. However, if progenitor cells are also

susceptible to immune attack, the rate of recovery will be further compromised and the rate at which the β-cell mass descends to the critical level may be accelerated.

Chapter 4. General Discussion

The oncogene c-Myc controls multiple cellular functions. In the switchable *pIns-c-MycER*^{TAM} transgenic mouse model, activation of c-MYC leads to acute cell proliferation in β-cells which is subsequently overwhelmed by apoptosis, results of which is hyperglycaemia, a main characteristic in diabetes. However, withdrawal of 4-OHT leads to restoration of β-cell mass in this transgenic animal model, which has been used to study β-cell regeneration and source of new β-cells. This thesis uses this transgenic animal model to study the early effects of c-MYC activation on β-cells, and the discussion will be presented in this chapter.

4.1 *In silico* analysis

The targets of c-MYC are about 600 genes which regulate more than 15% of the expression of the genome. In view of the complexity of the c-MYC regulatory network, this thesis employed Affymetrix GeneChips to study the effects of early c-MYC activation and the treatment of exenatide.

4.1.1. Early effects of c-MYC activation

In the M^+/E^- vs M^-/E^- study, significantly differentially expressed genes were separated into two different clusters by k-means. Cluster 1 contained most of the up-regulated genes whereas cluster 2 consisted of the down-regulated genes. With regards to cluster 1, it is perhaps not surprising that many of the genes were related to the cell cycle because the early c-MYC activation triggers proliferation in the

pIns-c-MycER^{TAM} transgenic mouse (Pelengaris *et al*., 2002b). As shown in Figure 3.1.3, c-MYC activation in early time point has already triggered complicated gene regulations and most of the regulated genes were located in the cytoplasm or nucleus.

Mxi-1, *Rad51*, *Atr* and *Ccne1* were up-regulated genes located in the nucleus. *Mxi-1* encodes MXI1 or MAD2 (also called MXD2), which is regarded as a tumour suppressor that competes with the bHLH protein, MAX, with MYC (Ayer *et al*., 1995; Grandori *et al*., 2000; Schreiber-Agus *et al*., 1995; Wechsler *et al*., 1996). *Ccne1* encodes an important regulator in the cell cycle of the G_1/S transition, cyclin E1, which activates with CDK2 and enables the hyperphosphorylation of RB (Geng *et al*., 1996; Lew *et al*., 1991; Zariwala *et al*., 1998). This pathway is also one of the well-known MYC-activated proliferation pathways. The *Rad51* gene encodes RAD51, which is expressed in proliferating cells, especially in the S or S/G_2 phase but the expression level is low in the G_0/G_1 (Chen *et al*., 1997; Xia *et al*., 1997; Yamamoto *et al*., 1996). RAD51 has also been reported in the DNA repair mechanisms by forming nucleoprotein filaments on single-stranded DNA (Baumann *et al*., 1996; Stark *et al*., 2002). Phosphoinositide 3-kinase related kinases (PIKKs), ATM, ATR, and DNA-PK are key factors involved in the DNA damage repair mechanism to maintain the genomic integrity by mediating cell cycle arrest in G_1, S, or G_2 phases (Bakkenist and Kastan, 2004; Bartek *et al*., 2004; Lukas *et al*., 2004; Shiloh, 2003). ATR kinase phosphorylates CHK1 in response to single strand DNA breaks (Abraham, 2001). Mini-chromosome maintenance (MCM) deficient genes *Mcm2*, *Mcm4*, and *Mcm7* were also up-regulated because of MYC activation. MCM proteins are important in DNA replication-licensing by binding to origins of DNA replication before the S phase and at early G1 phase to unwind the template DNA

ahead of the replication fork (Bailis and Forsburg, 2004; Labib and Diffley, 2001; Lei, 2005). An overexpression/deregulation of MCM proteins has been observed in premalignant lesions and cancers (Bailis and Forsburg, 2004; Blow and Gillespie, 2008).

Ccnb1, *Ccna2*, and *Chek1*, located in cytoplasm, are important cell cycle related genes and were up-regulated as well. Cyclin B1 is one of the key regulators of cell cycle: it binds to CDC2 and activates downstream transcripts, and subsequently progresses the cell cycle from the G_2 to the M phase (Jackman *et al*., 2003; Jin *et al*., 1998; Pines and Hunter, 1991). *Ccna2* encodes cyclin A2, which is another important protein in cell cycle in G1/S and G2/M transitions (Gong and Ferrell, 2010). The *Chek1* gene encodes CHEK1, which is one of the subtypes of checkpoint kinases (Chks) and is activated by phosphorylation (Sanchez *et al*., 1997) and subsequently arrests the cell cycle in late S or G_2 phases (Mailand *et al*., 2000; Peng *et al*., 1997). The genes *Pdk1* (pyruvate dehydrogenase kinase, isoenzyme 1), *Ptrh2* (peptidyl-tRNA hydrolase 2) and *Hspd1* (heat shock protein 1 (chaperonin)) located in mitochondrion were also up-regulated.

In cluster 2, as shown in Figure 1.3.4, *Cdkn2b*, *Kdr* and *Figf* were down-regulated through the experimental period after c-MYC activation. *Cdkn2b* is located on chromosome 9p21, next to *Cdkn2a* (encodes p16), and encodes a cyclin-dependent kinase inhibitor 2B (p15), which inhibits CDK4 (Sherr, 2004; Tycko, 2000). The cell proliferation after c-MYC activation can be confirmed by observing the inhibition of *Cdkn2b* in these array data. The suppression of this cell-cycle inhibitory gene by MYC through the interaction with MIZ1 has also been discussed (Seoane *et al*., 2001; Staller *et al*., 2001). *Kdr* encodes two receptors for

vascular endothelial growth factor (VEGF), which is a major growth factor for endothelial cells (Liu and Ellis, 1998). Genes relating to mitochondria biogenesis were also observed in this analysis. Other array studies have also suggested the implication of c-MYC in the metabolic regulatory network (Li *et al*., 2005; Robson *et al*., 2011).

4.1.2. Dynamic changes in islet-specific gene expression during exendatide treatment *in vivo*

Early effects of exanatide treatment on c-MYC activation in mice, i.e. condition 1 (M^+/E^+ vs M^+/E^-) have been examined. The dynamic effects of exanatide treatment on islet gene expression in non-diabetic mice *in vivo* without activation of c-MYC in β-cells have also been presented, i.e. condition 2 (M^-/E^+ vs M^-/E^-). In condition 1, genes related to development were suppressed, such as *Vegfa* and *Smad5*. Suppression of *Hsph1* and *Hdac9* was also observed. *Vegfa* was shown as a hub gene to regulate multi-biological functions, such as endothelial cell migration, endothelial cell proliferation, ossification, apoptosis, endocytosis, positive regulation of mitosis, cell division, cell growth, neurogenesis, and transcription (Ferrara, 1999). During endocrine pancreatic islet development, inductive signals are produced by the blood vessel endothelium, such as VEGF (Lammert *et al*., 2001). After the endocrine pancreatic cells have been formed, they start to generate a certain level of VEGFs. Lammert *et al*. (2003) used the VEGF-A deleted transgenic *pdx1-cre x VEGFloxP* mice to demonstrate the loss of capillary network formation inside islets, thus effecting the optimized blood glucose regulation. The down-regulated *Kdr* in M^+/E^- vs M^-/E^- group, also indicated a suppression of VEGF. *Smad5* protein product has

been identified as a key component in transforming growth factor-β (TGF-β) signalling, which regulates cell proliferation, differentiation, recognition, apoptosis, and specification of developmental fate by binding to and bringing together type I and type II receptor serine/threonine kinases (Attisano and Wrana, 2002; Shi and Massague, 2003). SMAD proteins can be divided into three subgroups according to their functions: SMAD5 is the receptor-specific to SMAD proteins (R-SMAD), which are direct targets for the activated type I serine/threonine kinase receptors (Lutz and Knaus, 2002; Moustakas *et al*., 2001). *In vitro* and *in vivo* studies pointed out that SMAD5 is essential in developmental processes (Chang *et al*., 1999; Chang *et al*., 2001). *Hsph1* encodes HSP (heat shock protein)105, which is one of the common HSPs in mammals (Ishihara *et al*., 1999). It enhances apoptosis in response to oxidative stress (Yamagishi *et al*., 2002) or endoplasmic reticulum (ER) stress through caspase-3-dependent signallings *in vitro* (Meares *et al*., 2008). *Hdac9* is required for HDACs, which represses transcriptional activities by catalyzing histone hypoacetylation, in the homologous recombination process (Kotian *et al*., 2011).

In condition 2 (M^-/E^+ vs M^-/E^-), genes involved in growth-regulatory and metabolic pathways, such as *Vdr* and *Vldlr*, were differentially expressed. *Wnt4* has been related to adipocyte differentiation (Nishizuka *et al*., 2008). *Gna13, Lyve1*, and *Ccrn4l* were up-regulated. *Fkbp5*, which is a co-chaperone of hsp90 and regulates glucocorticoid receptor (GR) sensitivity (Schiene-Fischer and Yu, 2001), was up-regulated. *Btg3* is a member of the antiproliferative BTG (B-cell translocation gene)/TOB (transducer of ErbB2 gene) family (Matsuda *et al*., 2001). It carries out its antiproliferactive action by inhibiting the transcriptional factor E2F1 (Ou *et al*., 2007).

Terf2, which encodes a telomere specific protein, TERF2, plays an important role in maintaining telomere length and structure (Chen *et al*., 2008; de Lange, 2002), was suppressed. Also, epigenetic genes, such as *Hdac9*, were found to be down-regulated. The protein encoded by *Cited2* is a CBP/p300-binding transcription co-activator without typical DNA binding domains (Dunwoodie *et al*., 1998; Shioda *et al*., 1997). *Cited2* has been suggested to have an important role in cell growth, malignant transformation, and hypoxia (Bhattacharya *et al*., 1999; Yin *et al*., 2002). In different cell types, apart from hypoxia, other biological stimuli can induce the expression of *Cited2*, such as IL-1a, -2, -4, -6, -9 and -11, granulocyte/macrophage colony-stimulating factor, interferon-g, platelet-derived growth factor, insulin, serum, and lipopolysaccharide (Bhattacharya *et al*., 1999; Sun *et al*., 1998). The analysis shows *Cited2* was down-regulated. Based on microarray experiments in different cell lines, *Cited2* was suppressed by TGF-β (Chen *et al*., 2001; Kang *et al*., 2003; Luo *et al*., 2005).

4.2 Effects of c-MYC activation *in vivo*

This thesis presents the early effects of c-MYC activation to investigate the relationship between β-cell proliferation and glucose homeostasis by manipulating the switchable *pIns-c-MycER*^{TAM} transgenic mouse model. A transient hypoglycaemia has been confirmed in early c-MYC activation, which is presented in Figure 3.2.1. Figure 3.2.1 (C) shows hypoglycaemia after c-MYC activation at 16 hours and it also exhibits a decrease in the glucose level back to euglycaemia at 36 hours. This is most likely due to glucose counterregulation. After transient hypoglycaemia, the MYC-ON (*pIns-c-MycER*^{TAM} mice treated with 4-OHT) group

became hyperglycaemic at 32 hours. This can be regarded as a rebound after hypoglycaemia because under stressful situations, the secretion of other hormones, for instance adrenaline, cortisol, and growth hormone, will be increased to maintain glucose concentration (Gerich, 1993). However, another explanation could be that the data were derived from a different group of mice, i.e. glucose levels at -4, 8, 20, and 32 hours were recorded in TL2 whereas glucose levels at 0, 12, 24, and 36 hours were recorded in TL1. Thus, there were two different groups of MYC-ON mice, and those in TL2 were experiencing hyperglycaemia at 32 hours whereas mice in TL1 were just at the onset of high glucose levels.

To further investigate the factors causing low glucose level in the early c-MYC activation, the energy expenditure and insulin level of objects were evaluated. The energy usage of WT (WT littermates treated with peanut oil), MYC-OFF (*pIns-c-MycER*^{TAM} mice treated with peanut oil) and MYC-ON groups is presented in Figure 3.2.2. A statistically detectable difference of energy usage was observed between WT and MYC-ON group throughout the whole experimental period, which was 28 hours. From the experiment shown in Section 3.2.1, the glucose levels of MYC-OFF and MYC-ON groups were lower than WT group (see Figure 3.2.1). If the energy usage during the experimental period accounts for the objects' glucose level, a difference of energy usage will be observed between the WT and MYC-OFF group as well because the glucose level of MYC-OFF was lower than WT. Furthermore, the energy usage of objects during the hypoglycaemic period, which was 8 to 20 hours, showed no significant difference within those three groups of mice. The results from Figure 3.2.2 (A) and Figure 3.2.2 (B) imply that the energy balance does not directly affect the glucose level although a trend of reducing energy usage was observed in MYC-ON group.

However, energy usage (by using food intake, faeces production and body weight) was simplified here: urine was not measured. Measurement of urine secretion is difficult because the urine will be absorbed by the litter quickly. If the litter has been removed and a grid floor is applied, the amount of urine production is still difficult to measure because it will have evaporated. Moreover, the measurement of urine might incur a systematic error because the polyuria in diabetic animals may lead to a decrease of body weight, which incurs errors in the energy expenditure. For future work, an indirect calorimetry system can be used so that energy expenditure and respiratory exchange can be obtained precisely (Arch *et al*., 2006).

A physiological parameter, insulin level, was also measured and is shown in Figure 3.2.3, which confirms that c-MYC-induced hypoglycaemia resulted from hyperinsulinaemia because insulin secretion is based on GSIS and is expected to be near zero when hypoglycaemia happens. However, in Figure 3.2.3 (C) and (F) at 16 and 20 hours, MYC-ON mice were hypoglycaemic with an acute insulin release, which points out an inappropriate insulin secretion because β-cells were not able to turn off the insulin secretion under low glucose level (Schwartz *et al*., 1987). This experiment also confirmed c-MYC activation causes hyperinsulinaemic hypoglycaemia (HH) within 16 hours in MYC-ON mice. In normal situation, hyperinsulinaemia results in hypoglycaemia, which incurs hyperphagia because hypoglycaemia *per se* triggers hunger and increase food ingestion (Lotter and Woods, 1977). However, this seems not to be the case because the MYC-ON mice did not have higher food ingestion during hypoglycaemia comparing to their WT or MYC-OFF littermates, as shown in Figure 3.2.2 (D). There are numerous factors that influence food intake, and one of the peripherally arising signals that is produced during the meal is the satiety signal from hormones, such as pancreatic islet

hormones (glucagon, amylin and insulin) and leptin from adipose tissue (Woods *et al*., 1998). However, insulin might reduce food intake after binding specific insulin receptor on hypothalamic neurons (Booth, 1968; Plum *et al.*, 2005; Woods *et al*., 1979).

Hypoglycaemia caused by c-MYC activation may be caused by: (i) increased insulin secretion or release from dying cells; (ii) rapid β-cell proliferation; and (iii) increased insulin sensitivity. This thesis further investigated the β-cells' regulation by means of immuno-staining. The immunofluorescence staining of Ki-67 (see Figure 3.2.7) indicates that β-cells were proliferating during the c-MYC-induced hypoglycaemia whereas no detectable fluorescent signals of Caspase-3 staining infer no apoptotic cells or a low number of apoptotic cells. Findings from the immnofluorescence staining suggest that the hypothesis of the passive release of insulin from apoptopic β-cells seems an unlikely explanation of c-MYC-induced transient hypoglycaemia.

In order to understand how c-MYC activation triggers hyperinsulinaemia, the β-cell mass and volume were further evaluated in this thesis. As shown in Figure 3.2.3, the MYC-OFF and WT groups had similar serum insulin levels but the blood glucose level in the MYC-OFF group was lower than the WT group, even without the activation of c-MYC. It might be inferred that the transgenic mouse system has a residual level of c-MYC activation at a small but steady level even without the administration of 4-OHT; this is called 'leakiness'. This thesis has shown that the β-cell mass of the MYC group was bigger than their WT littermates, which might explain why the MYC group had a lower glucose level to start with comparing to their WT littermates, although a bigger β-cell mass does not directly relate to

higher insulin levels, which cause lower glucose levels. However, the β-cell size result shows that after 16 hours of c-MYC activation, MYC-ON had a bigger β-cell size, whereas there was no difference between MYC-ON and MYC-OFF. Apart from the bigger β-cell size and mass, c-MYC activation might affect the insulin secretion signalling that caused dysfunction of insulin secretion. It should be noted that the increase of β-cell size or a bigger β-cell mass does not necessarily contribute to the increase of insulin level because normal β-cells should be able to control the release of insulin to maintain glucose homeostasis.

As regards to the insulin sensitivity measurement in this study, I did not have enough time to finish the quantifying of insulin action. A glucose tolerance test (OGTT) can be applied in future work to assess the insulin resistance in c-MYC-induced hypoglycaemic objects.

The effect of exenatide on glucose homeostasis during hypoglycaemia has also been studied in this thesis. As shown in Figure 3.2.5, the exenatide treatment decreased the glucose level in both MYC-ON and MYC-OFF groups. During the c-MYC-induced hypoglycaemia, exenatide treatment decreased the glucose levels in the MYC-ON group, although there was no statistically detectable difference. However, the exenatide treatment did not prevent the c-MYC-induced hypoglycaemia either. An additional experiment was carried out on a further control group to observe the effect of exenatide on WT, and the glucose levels are presented in Figure 3.2.6, which shows a decreased glucose level after exenatide treatment. This finding is in conflict with the observation from literature, which suggests that exenatide can lower glucose level without causing hypoglycaemia.

4.3 Mathematical model

The glycaemic homeostasis feedback loop operates on the ultradian time scale, whereas the adaptive changes in β-cell mass happen on a days-to-months time scale. Therefore, the interplay between the blood glucose homeostasis feedback loop and the adaptive changes in β-cell mass is a typical feature of endocrinological and neuroendocrinological regulation, where a slower adaptive feedback loop is superimposed on a faster feedback loop. The latter feedback loop is directly involved with a physiological system, whereas the former one regulates the level of activity in some manner, e.g. by controlling rates of transcription, translation, electrical activity (secretion), or number of endocrine cells (Brook and Marshall, 2001). Moreover, the dynamics of such systems usually exhibits a strongly non-linear character (Keener and Sneyd, 1998), which means that small variations in the precise time course of the fast processes (the temporal fine structure) can have a profound effect on the rates of change of the slow processes as was shown in Section 3.3.1. Time-scale separation can be a powerful tool to isolate a low-dimensional dynamical system modelling the slow adaptation process, which is relatively easy to analyse and visualise. A 7-dimensional model was reduced to 1-dimensional dynamics, which is straightforward to analyse; indeed, as Figure 3.3.1 shows, in qualitative terms the system is much like logistic growth with an Allee effect.

When Eqn (A 13) is evaluated, the causal relationships may be obscured. For example, in the present model, the rate of change of the β-cell mass is dependent, in the direct, mechanistic sense of the word, on glucose and insulin, as the model's equations make specific. However, the time courses of glucose and insulin depend on the prevailing β-cell mass, together with the input ψ_{in}, and as a result, in slow

time, the rate of change of the β-cell mass depends on the β-cell mass itself plus the input waveform, i.e., the rate of change in slow time is a *functional* of the input $\psi_{in}(t)$, as is clear from the integration over the fast-time scale cycle in Eqn (A13). In this way, the temporal fine structure is taken into account, in analogy to similar spatial homogenisation procedures (Holmes, 1995; Keener and Sneyd, 1998).

This thesis assumes that rapid β-cell mass compensation is driven by proliferation, based on the observation that β-cells can be driven into cell cycle by activation of c-MYC (Pelengaris *et al*., 2002b) and data on recovery from partial pancreatomy (De Leon *et al*., 2003; Leahy *et al*., 1988; Pearson *et al*., 1977) and hyperglycaemic challenge, reviewed by Bouwens and Rooman (2005). However, another possibility is that β-cells respond by adjusting the amount of hormone-producing machinery per cell (and thus, incidentally, cell volume) and that data concerning short-term changes in numbers of β-cells are distorted by the fact that temporarily depleted cells (degranulated cells) are spuriously not counted as β-cells. The relative importance of such non-proliferative adaptation, which possibly depends on the time scales and extend of challenge at hand, remains to be elucidated in detail; whereas hypertrophy was held to be the main mechanism for increases in β-cell mass in human until the last decade (Nielsen *et al*., 1999; Weir *et al*., 2001), recent years have been a change in emphasis towards proliferation and neogenesis (Bouwens and Rooman, 2005; Lingohr *et al*., 2002; Pelengaris *et al*., 2002b).

In the model considered here, all but one of the state variables was fast. The Sturis-Tolic model can be extended with further slow variables. One such variable might be the insulin sensitivity of the body's tissues, which plays a major role in the aetiology of T2DM (Salway, 1999). However, it seems obvious that a more precise

characterisation of neogenesis is essential to make progress: in particular, the maximum rate at which this pool can proliferate, as well as the rates at which it is restored (which may depend on the sources: β-cells are transdifferentiated pancreatic cells) are likely to be critical to the ability of neogenesis to furnish the amount of new β-cells required. The pathological fixed point, first noted and defined by Topp *et al*. (2000), becomes a prominent factor only when neogenesis is impaired, and, moreover, this pathological fixed point has a value that is dependent on the diet time course of the rate at which glucose is administered to the system. Whereas mathematical modelling can never replace the experiments that elucidate these processes, it can help to characterise the functional consequences of these findings along the lines outlined in this thesis.

A more robust model can be further built by combing experimental data obtaining from this thesis, such β-cell mass, β-cell number, and β-cell size. β-cell hypertrophy happens in the pre-diabetic stage of T2DM to compensate the demand of physiological changes. However, there is at present no mathematical model that considers the β-cell size, to simulate the β-cell regulation in diabetes.

Conclusion

β-cells are able to adapt to different physiological conditions dynamically by changing their mass or function to maintain blood glucose levels in a narrow range. This thesis applied the *pIns-c-MycER*^{TAM} transgenic mice to study the β-cell physiology and glucose homeostasis in short term c-MYC activation by means of *in vivo* experiments, *in silico* microarray analysis, and a mathematical model. This thesis confirmed that the transient hypoglycaemia in the *pIns-c-MycER*^{TAM} transgenic mice results from hyperinsulinaemia. Other factors, i.e. food intake and energy expenditure, which affect glucose levels were tested and discussed in this thesis.

This thesis investigated relationships between β-cell physiology and glucose homeostasis by evaluating the β-cell proliferation, apoptosis, mass and size. Proliferation and apoptosis in β-cells in short term c-MYC activation were examined by using immunofluorescence staining of Ki-67 and Caspase-3. This thesis confirmed that in the *pIns-c-MycER*^{TAM} transgenic mice, during the transient hypoglycaemia, β-cells were proliferating and there was no detectable apoptosis. This finding concludes that the hyperinsulinaemia was not the result of passive release of insulin from apoptopic β-cells. β-cell mass and β-cell size were evaluated by this thesis. Before the start of experiments, the transgenic mice had lower glucose levels compared to their WT littermates. Although the transgenic mice also had a higher β-cell mass to start with comparing to their WT littermates, this is not directly linked with the higher insulin levels in the transgenic mice, which caused lower glucose levels. This might be explained by the slight leakiness of c-MYC which means the transgenic mouse system has a residual level of c-MYC activation at a

small but steady level even without the administration of 4-OHT. The β-cell size evaluation result shows the transgenic mice had a larger β-cell size compared to their WT littermates 16 hours after 4-OHT injection, although a bigger β-cell size does not necessarily contribute to the increased insulin levels.

The GLP-1 analogue, exenatide, has been widely used in controlling the glucose levels of diabetic patients because it is reported to lower the glucose levels without causing hypoglycaemia. However, in this *in vivo* experiment, the exenatide treatment of *pIns-c-MycER*^{TAM} transgenic mice and their WT littermates incurs hypoglycaemia as well. Furthermore, the treatment of exenatide did not prevent the transient hypoglycaemia in 4-OHT administrated transgenic mice. This finding conflicts with the current studies and is worthy of further investigation of β-cell physiology.

In addition to *in vivo* experiments, this thesis applied *in silico* data to discuss the transient hypoglycaemia. Microarray analysis suggests that c-MYC activation triggers complicated gene regulatory networks, and most of these genes are up-regulated. The treatment of exenatide in the *pIns-c-MycER*^{TAM} transgenic mice during the early c-MYC activation was also presented in this thesis. The study of exenatide treatment array analysis was shown and revealed the metabolically related genes.

Finally, a theoretical mathematical model of glucose, insulin, and β-cell dynamics was built and separated into a fast and slow system. The interplay between blood glucose and insulin levels behaves as a fast feedback loop. β-cell mass changes in response to this endocinological regulation with a slower adaptive feedback loop, which is superimposed on a faster feedback loop. This thesis also

assumes that the rapid β-cell mass compensation is driven by proliferation because of the activation of c-MYC. However, other non-proliferative adaptation factors remain to be investigated.

It is proposed that further work should focus on:

1) Combining experimental data with mathematical models;

2) Using RT-PCR to confirm interested genes obtained from microarray analysis;

3) A more detailed monitoring of energy usage, over a longer timescale;

4) A glucose tolerance test to quantify the insulin sensitivity;

5) A detailed analysis of β-cell physiology of the exenatide treated mice.

Bibliography

Abouna, S., R.W. Old, S. Pelengaris, D. Epstein, V. Ifandi, I. Sweeney, and M. Khan. 2010. Non-beta-cell progenitors of beta-cells in pregnant mice. *Organogenesis*. 6:125-133.

Abraham, R.T. 2001. Cell cycle checkpoint signaling through the ATM and ATR kinases. *Genes Dev*. 15:2177-2196.

Abramoff, M.D., Magelhaes, P.J. and Ram, S.J. 2004. Image Processing with ImageJ. *Biophotonics International*. 11:7.

Ackermann Misfeldt, A., R.H. Costa, and M. Gannon. 2008. Beta-cell proliferation, but not neogenesis, following 60% partial pancreatectomy is impaired in the absence of FoxM1. *Diabetes*. 57:3069-3077.

Adhikary, S., and M. Eilers. 2005. Transcriptional regulation and transformation by Myc proteins. *Nature reviews. Molecular cell biology*. 6:635-645.

Affymetrix. 1999. Microarray Suite User Guide: Version 4. http://www.affymetrix.com/support/technical/manuals.affx.

Affymetrix. 2003. Microarray Suite User Guide: Version 5. http://www.affymetrix.com/support/technical/manuals.affx.

Aguilar-Bryan, L., and J. Bryan. 1999. Molecular biology of adenosine triphosphate-sensitive potassium channels. *Endocr Rev*. 20:101-135.

Ahlgren, U., J. Jonsson, and H. Edlund. 1996. The morphogenesis of the pancreatic mesenchyme is uncoupled from that of the pancreatic epithelium in IPF1/PDX1-deficient mice. *Development*. 122:1409-1416.

Ahlgren, U., J. Jonsson, L. Jonsson, K. Simu, and H. Edlund. 1998. beta-cell-specific inactivation of the mouse Ipf1/Pdx1 gene results in loss of the beta-cell phenotype and maturity onset diabetes. *Genes Dev*. 12:1763-1768.

Alitalo, K., J.M. Bishop, D.H. Smith, E.Y. Chen, W.W. Colby, and A.D. Levinson. 1983. Nucleotide sequence to the v-myc oncogene of avian retrovirus MC29. *Proceedings of the National Academy of Sciences of the United States of America*. 80:100-104.

Amati, B., K. Alevizopoulos, and J. Vlach. 1998. Myc and the cell cycle. *Frontiers in bioscience : a journal and virtual library*. 3:d250-268.

Amati, B., M.W. Brooks, N. Levy, T.D. Littlewood, G.I. Evan, and H. Land. 1993a. Oncogenic activity of the c-Myc protein requires dimerization with Max. *Cell*. 72:233-245.

Amati, B., and H. Land. 1994. Myc-Max-Mad: a transcription factor network controlling cell cycle progression, differentiation and death. *Current Opinion in Genetics & Development*. 4:102-108.

Amati, B., T.D. Littlewood, G.I. Evan, and H. Land. 1993b. The c-Myc protein induces cell cycle progression and apoptosis through dimerization with Max. *Embo J*. 12:5083-5087.

Arch, J.R., D. Hislop, S.J. Wang, and J.R. Speakman. 2006. Some mathematical and technical issues in the measurement and interpretation of open-circuit indirect calorimetry in small animals. *Int J Obes (Lond)*. 30:1322-1331.

Arteaga-Salas, J.M., H. Zuzan, W.B. Langdon, G.J. Upton, and A.P. Harrison. 2008. An overview of image-processing methods for Affymetrix GeneChips. *Brief Bioinform*. 9:25-33.

Ashcroft, F.M., and F.M. Gribble. 1999. ATP-sensitive K+ channels and insulin secretion: their role in health and disease. *Diabetologia*. 42:903-919.

Ashcroft, F.M., D.E. Harrison, and S.J. Ashcroft. 1984. Glucose induces closure of single potassium channels in isolated rat pancreatic beta-cells. *Nature*. 312:446-448.

Ashcroft, F.M., P. Proks, P.A. Smith, C. Ammala, K. Bokvist, and P. Rorsman. 1994. Stimulus-secretion coupling in pancreatic beta cells. *J Cell Biochem*. 55 Suppl:54-65.

Ashcroft, F.M., and P. Rorsman. 1989. Electrophysiology of the pancreatic beta-cell. *Prog Biophys Mol Biol*. 54:87-143.

Aspinwall, C.A., J.R. Lakey, and R.T. Kennedy. 1999. Insulin-stimulated insulin secretion in single pancreatic beta cells. *The Journal of biological chemistry*. 274:6360-6365.

Atkinson, M.A., and E.H. Leiter. 1999. The NOD mouse model of type 1 diabetes: as good as it gets? *Nature medicine*. 5:601-604.

Attisano, L., and J.L. Wrana. 2002. Signal transduction by the TGF-beta superfamily. *Science*. 296:1646-1647.

Ayer, D.E., L. Kretzner, and R.N. Eisenman. 1993. Mad: a heterodimeric partner for Max that antagonizes Myc transcriptional activity. *Cell*. 72:211-222.

Ayer, D.E., Q.A. Lawrence, and R.N. Eisenman. 1995. Mad-Max transcriptional repression is mediated by ternary complex formation with mammalian homologs of yeast repressor Sin3. *Cell*. 80:767-776.

Bach, J.F. 1994. Insulin-dependent diabetes mellitus as an autoimmune disease. *Endocr Rev*. 15:516-542.

Baggio, L.L., and D.J. Drucker. 2007. Biology of Incretins: GLP-1 and GIP. *Gastroenterology*. 132:2131-2157.

Bahram, F., N. von der Lehr, C. Cetinkaya, and L.G. Larsson. 2000. c-Myc hot spot mutations in lymphomas result in inefficient ubiquitination and decreased proteasome-mediated turnover. *Blood*. 95:2104-2110.

Bailis, J.M., and S.L. Forsburg. 2004. MCM proteins: DNA damage, mutagenesis and repair. *Current Opinion in Genetics & Development*. 14:17-21.

Bakkenist, C.J., and M.B. Kastan. 2004. Initiating cellular stress responses. *Cell*. 118:9-17.

Banin, S., L. Moyal, S. Shieh, Y. Taya, C.W. Anderson, L. Chessa, N.I. Smorodinsky, C. Prives, Y. Reiss, Y. Shiloh, and Y. Ziv. 1998. Enhanced phosphorylation of p53 by ATM in response to DNA damage. *Science*. 281:1674-1677.

Barg, S., L. Eliasson, E. Renstrom, and P. Rorsman. 2002a. A subset of 50 secretory granules in close contact with L-type Ca2+ channels accounts for first-phase insulin secretion in mouse beta-cells. *Diabetes*. 51 Suppl 1:S74-82.

Barg, S., X. Ma, L. Eliasson, J. Galvanovskis, S.O. Gopel, S. Obermuller, J. Platzer, E. Renstrom, M. Trus, D. Atlas, J. Striessnig, and P. Rorsman. 2001. Fast exocytosis with few Ca(2+) channels in insulin-secreting mouse pancreatic B cells. *Biophys J*. 81:3308-3323.

Barg, S., C.S. Olofsson, J. Schriever-Abeln, A. Wendt, S. Gebre-Medhin, E. Renstrom, and P. Rorsman. 2002b. Delay between fusion pore opening and peptide release from large dense-core vesicles in neuroendocrine cells. *Neuron*. 33:287-299.

Bartek, J., C. Lukas, and J. Lukas. 2004. Checking on DNA damage in S phase. *Nature reviews. Molecular cell biology*. 5:792-804.

Bartkova, J., Z. Horejsi, K. Koed, A. Kramer, F. Tort, K. Zieger, P. Guldberg, M. Sehested, J.M. Nesland, C. Lukas, T. Orntoft, J. Lukas, and J. Bartek. 2005. DNA damage response as a candidate anti-cancer barrier in early human tumorigenesis. *Nature*. 434:864-870.

Baumann, P., F.E. Benson, and S.C. West. 1996. Human Rad51 protein promotes ATP-dependent homologous pairing and strand transfer reactions in vitro. *Cell*. 87:757-766.

Beith, J.L., E.U. Alejandro, and J.D. Johnson. 2008. Insulin stimulates primary beta-cell proliferation via Raf-1 kinase. *Endocrinology*. 149:2251-2260.

Benjamini, Y., and Y. Hochberg. 1995. Controlling the False Discovery Rate: a Practical and Powerful Approach to Multiple Testing. *Journal of the Royal Statistical Society B*. 57.

Bennett, D.L., and S.A. Gourley. 2004. Global stability in a model of the glucose-insulin interaction with time delay. *European Journal of Applied Mathematics*. 15:203-221.

Bergman, R.N., Y.Z. Ider, C.R. Bowden, and C. Cobelli. 1979. Quantitative estimation of insulin sensitivity. *Am J Physiol*. 236:E667-677.

Bergman, R.N., L.S. Phillips, and C. Cobelli. 1981. Physiologic evaluation of factors controlling glucose tolerance in man: measurement of insulin sensitivity and beta-cell glucose sensitivity from the response to intravenous glucose. *The Journal of clinical investigation*. 68:1456-1467.

Bhattacharya, S., C.L. Michels, M.K. Leung, Z.P. Arany, A.L. Kung, and D.M. Livingston. 1999. Functional role of p35srj, a novel p300/CBP binding protein, during transactivation by HIF-1. *Genes Dev*. 13:64-75.

Blackwood, E.M., and R.N. Eisenman. 1991. Max: a helix-loop-helix zipper protein that forms a sequence-specific DNA-binding complex with Myc. *Science*. 251:1211-1217.

Blow, J.J., and P.J. Gillespie. 2008. Replication licensing and cancer--a fatal entanglement? *Nature reviews. Cancer*. 8:799-806.

Bolie, V.W. 1961. Coefficients of normal blood glucose regulation. *J Appl Physiol*. 16:783-788.

Bonner-Weir, S. 2000a. Islet growth and development in the adult. *J Mol Endocrinol*. 24:297-302.

Bonner-Weir, S. 2000b. Life and death of the pancreatic beta cells. *Trends Endocrinol Metab*. 11:375-378.

Bonner-Weir, S., L.A. Baxter, G.T. Schuppin, and F.E. Smith. 1993. A second pathway for regeneration of adult exocrine and endocrine pancreas. A possible recapitulation of embryonic development. *Diabetes*. 42:1715-1720.

Bonner-Weir, S., D. Deery, J.L. Leahy, and G.C. Weir. 1989. Compensatory growth of pancreatic beta-cells in adult rats after short-term glucose infusion. *Diabetes*. 38:49-53.

Booth, D.A. 1968. Effects of intrahypothalamic glucose injection on eating and drinking elicited by insulin. *J Comp Physiol Psychol*. 65:13-16.

Bouchard, C., O. Dittrich, A. Kiermaier, K. Dohmann, A. Menkel, M. Eilers, and B. Luscher. 2001. Regulation of cyclin D2 gene expression by the Myc/Max/Mad network: Myc-dependent TRRAP recruitment and histone acetylation at the cyclin D2 promoter. *Genes Dev*. 15:2042-2047.

Bouchard, C., K. Thieke, A. Maier, R. Saffrich, J. Hanley-Hyde, W. Ansorge, S. Reed, P. Sicinski, J. Bartek, and M. Eilers. 1999. Direct induction of cyclin D2 by Myc contributes to cell cycle progression and sequestration of p27. *Embo J*. 18:5321-5333.

Bouwens, L., W.G. Lu, and R. De Krijger. 1997. Proliferation and differentiation in the human fetal endocrine pancreas. *Diabetologia*. 40:398-404.

Bouwens, L., and D.G. Pipeleers. 1998. Extra-insular beta cells associated with ductules are frequent in adult human pancreas. *Diabetologia*. 41:629-633.

Bouwens, L., and I. Rooman. 2005. Regulation of pancreatic beta-cell mass. *Physiol Rev*. 85:1255-1270.

Brissova, M., M. Shiota, W.E. Nicholson, M. Gannon, S.M. Knobel, D.W. Piston, C.V. Wright, and A.C. Powers. 2002. Reduction in pancreatic transcription factor PDX-1 impairs glucose-stimulated insulin secretion. *The Journal of biological chemistry*. 277:11225-11232.

Brook, C.G.D., and N.J. Marshall. 2001. Essential endocrinology. Blackwell Science, Oxford; Malden, MA.

Bruning, J.C., J. Winnay, S. Bonner-Weir, S.I. Taylor, D. Accili, and C.R. Kahn. 1997. Development of a novel polygenic model of NIDDM in mice heterozygous for IR and IRS-1 null alleles. *Cell*. 88:561-572.

Buchan, A.M., J.M. Polak, C. Capella, E. Solcia, and A.G. Pearse. 1978. Electronimmunocytochemical evidence for the K cell localization of gastric inhibitory polypeptide (GIP) in man. *Histochemistry*. 56:37-44.

Buffa, R., J.M. Polak, A.G. Pearse, E. Solcia, L. Grimelius, and C. Capella. 1975. Identification of the intestinal cell storing gastric inhibitory peptide. *Histochemistry*. 43:249-255.

Burcelin, R., and S. Dejager. 2010. GLP-1: what is known, new and controversial in 2010? *Diabetes Metab*. 36:503-509.

Butler, A.E., J. Janson, S. Bonner-Weir, R. Ritzel, R.A. Rizza, and P.C. Butler. 2003. Beta-cell deficit and increased beta-cell apoptosis in humans with type 2 diabetes. *Diabetes*. 52:102-110.

Butler, P.C., J.J. Meier, A.E. Butler, and A. Bhushan. 2007. The replication of beta cells in normal physiology, in disease and for therapy. *Nat Clin Pract Endocrinol Metab*. 3:758-768.

Canman, C.E., D.S. Lim, K.A. Cimprich, Y. Taya, K. Tamai, K. Sakaguchi, E. Appella, M.B. Kastan, and J.D. Siliciano. 1998. Activation of the ATM kinase by ionizing radiation and phosphorylation of p53. *Science*. 281:1677-1679.

Cano, D.A., I.C. Rulifson, P.W. Heiser, L.B. Swigart, S. Pelengaris, M. German, G.I. Evan, J.A. Bluestone, and M. Hebrok. 2008. Regulated beta-cell regeneration in the adult mouse pancreas. *Diabetes*. 57:958-966.

Chakrabarti, S.K., J.C. James, and R.G. Mirmira. 2002. Quantitative assessment of gene targeting in vitro and in vivo by the pancreatic transcription factor, Pdx1. Importance of chromatin structure in directing promoter binding. *The Journal of biological chemistry*. 277:13286-13293.

Chang, H., D. Huylebroeck, K. Verschueren, Q. Guo, M.M. Matzuk, and A. Zwijsen. 1999. Smad5 knockout mice die at mid-gestation due to multiple embryonic and extraembryonic defects. *Development*. 126:1631-1642.

Chang, H., A.L. Lau, and M.M. Matzuk. 2001. Studying TGF-beta superfamily signaling by knockouts and knockins. *Mol Cell Endocrinol*. 180:39-46.

Chen, C.L., H.W. Tsai, and S.S. Wong. 2010. Modeling the physiological glucose-insulin dynamic system on diabetics. *J Theor Biol*. 265:314-322.

Chen, C.R., Y. Kang, and J. Massague. 2001. Defective repression of c-myc in breast cancer cells: A loss at the core of the transforming growth factor beta growth arrest program. *Proceedings of the National Academy of Sciences of the United States of America*. 98:992-999.

Chen, F., A. Nastasi, Z. Shen, M. Brenneman, H. Crissman, and D.J. Chen. 1997. Cell cycle-dependent protein expression of mammalian homologs of yeast DNA double-strand break repair genes Rad51 and Rad52. *Mutat Res*. 384:205-211.

Chen, J., X. Wu, J. Lin, and A.J. Levine. 1996. mdm-2 inhibits the G1 arrest and apoptosis functions of the p53 tumor suppressor protein. *Molecular and cellular biology*. 16:2445-2452.

Chen, L., S. Agrawal, W. Zhou, R. Zhang, and J. Chen. 1998. Synergistic activation of p53 by inhibition of MDM2 expression and DNA damage. *Proceedings of the National Academy of Sciences of the United States of America*. 95:195-200.

Chen, Y., Y. Yang, M. van Overbeek, J.R. Donigian, P. Baciu, T. de Lange, and M. Lei. 2008. A shared docking motif in TRF1 and TRF2 used for differential recruitment of telomeric proteins. *Science*. 319:1092-1096.

Cheung, L., S. Zervou, G. Mattsson, S. Abouna, L. Zhou, V. Ifandi, S. Pelengaris, and M. Khan. 2010. c-Myc directly induces both impaired insulin secretion and loss of beta-cell mass, independently of hyperglycemia in vivo. *Islets*. 2:37-45.

Cho, H., J. Mu, J.K. Kim, J.L. Thorvaldsen, Q. Chu, E.B. Crenshaw, 3rd, K.H. Kaestner, M.S. Bartolomei, G.I. Shulman, and M.J. Birnbaum. 2001a. Insulin resistance and a diabetes mellitus-like syndrome in mice lacking the protein kinase Akt2 (PKB beta). *Science*. 292:1728-1731.

Cho, R.J., M. Huang, M.J. Campbell, H. Dong, L. Steinmetz, L. Sapinoso, G. Hampton, S.J. Elledge, R.W. Davis, and D.J. Lockhart. 2001b. Transcriptional regulation and function during the human cell cycle. *Nat Genet*. 27:48-54.

Christesen, H.B., B.B. Jacobsen, S. Odili, C. Buettger, A. Cuesta-Munoz, T. Hansen, K. Brusgaard, O. Massa, M.A. Magnuson, C. Shiota, F.M. Matschinsky, and F. Barbetti. 2002. The second activating glucokinase mutation (A456V): implications for glucose homeostasis and diabetes therapy. *Diabetes*. 51:1240-1246.

Coller, H.A., C. Grandori, P. Tamayo, T. Colbert, E.S. Lander, R.N. Eisenman, and T.R. Golub. 2000. Expression analysis with oligonucleotide microarrays reveals that MYC regulates genes involved in growth, cell cycle, signaling, and adhesion. *Proceedings of the National Academy of Sciences of the United States of America*. 97:3260-3265.

Cook, D.L., and C.N. Hales. 1984. Intracellular ATP directly blocks K+ channels in pancreatic B-cells. *Nature*. 311:271-273.

Coons, A.H., H.J. Creech, and R.N. Jones. 1941. Immunological properties of an antibody containing a fluorescent group. *Proc Soc Exp Biol Med*. 47:200-202.

Crews, S., R. Barth, L. Hood, J. Prehn, and K. Calame. 1982. Mouse c-myc oncogene is located on chromosome 15 and translocated to chromosome 12 in plasmacytomas. *Science*. 218:1319-1321.

Cryer, P.E. 1993. Glucose counterregulation: prevention and correction of hypoglycemia in humans. *Am J Physiol*. 264:E149-155.
Cryer, P.E. 2002. Hypoglycaemia: the limiting factor in the glycaemic management of Type I and Type II diabetes. *Diabetologia*. 45:937-948.
Dang, C.V., K.A. O'Donnell, K.I. Zeller, T. Nguyen, R.C. Osthus, and F. Li. 2006. The c-Myc target gene network. *Semin Cancer Biol*. 16:253-264.
Dang, C.V., and G.L. Semenza. 1999. Oncogenic alterations of metabolism. *Trends Biochem Sci*. 24:68-72.
Davie, J.R., and M.J. Hendzel. 1994. Multiple functions of dynamic histone acetylation. *J Cell Biochem*. 55:98-105.
de Lange, T. 2002. Protection of mammalian telomeres. *Oncogene*. 21:532-540.
De Leon, D.D., S. Deng, R. Madani, R.S. Ahima, D.J. Drucker, and D.A. Stoffers. 2003. Role of endogenous glucagon-like peptide-1 in islet regeneration after partial pancreatectomy. *Diabetes*. 52:365-371.
de Stanchina, E., M.E. McCurrach, F. Zindy, S.Y. Shieh, G. Ferbeyre, A.V. Samuelson, C. Prives, M.F. Roussel, C.J. Sherr, and S.W. Lowe. 1998. E1A signaling to p53 involves the p19(ARF) tumor suppressor. *Genes Dev*. 12:2434-2442.
de Winter, W., J. DeJongh, T. Post, B. Ploeger, R. Urquhart, I. Moules, D. Eckland, and M. Danhof. 2006. A mechanism-based disease progression model for comparison of long-term effects of pioglitazone, metformin and gliclazide on disease processes underlying Type 2 Diabetes Mellitus. *Journal of Pharmacokinetics and Pharmacodynamics*. 33:313-343.
Deacon, C.F., L. Pridal, L. Klarskov, M. Olesen, and J.J. Holst. 1996. Glucagon-like peptide 1 undergoes differential tissue-specific metabolism in the anesthetized pig. *Am J Physiol*. 271:E458-464.
Ding, W.G., and J. Gromada. 1997. Protein kinase A-dependent stimulation of exocytosis in mouse pancreatic beta-cells by glucose-dependent insulinotropic polypeptide. *Diabetes*. 46:615-621.
Dor, Y., J. Brown, O.I. Martinez, and D.A. Melton. 2004. Adult pancreatic beta-cells are formed by self-duplication rather than stem-cell differentiation. *Nature*. 429:41-46.
Drucker, D.J. 1998. Glucagon-like peptides. *Diabetes*. 47:159-169.
Dudoit, S., J.P. Shaffer, and J.C. Boldrick. 2003. Multiple Hypothesis Testing in Microarray Experiments. *Statistical Science*. 18:71-103.
Duggan, D.J., M. Bittner, Y. Chen, P. Meltzer, and J.M. Trent. 1999. Expression profiling using cDNA microarrays. *Nat Genet*. 21:10-14.
Dunwoodie, S.L., T.A. Rodriguez, and R.S. Beddington. 1998. Msg1 and Mrg1, founding members of a gene family, show distinct patterns of gene expression during mouse embryogenesis. *Mech Dev*. 72:27-40.
Ebert, R., and W. Creutzfeldt. 1980. Gastric inhibitory polypeptide. *Clin Gastroenterol*. 9:679-698.
Efanova, I.B., S.V. Zaitsev, B. Zhivotovsky, M. Kohler, S. Efendic, S. Orrenius, and P.O. Berggren. 1998. Glucose and tolbutamide induce apoptosis in pancreatic beta-cells. A process dependent on intracellular Ca2+ concentration. *The Journal of biological chemistry*. 273:33501-33507.
Egle, A., A.W. Harris, P. Bouillet, and S. Cory. 2004. Bim is a suppressor of Myc-induced mouse B cell leukemia. *Proceedings of the National Academy of Sciences of the United States of America*. 101:6164-6169.

Eisenbarth, G.S. 1986. Type I diabetes mellitus. A chronic autoimmune disease. *N Engl J Med*. 314:1360-1368.
Eissele, R., R. Goke, S. Willemer, H.P. Harthus, H. Vermeer, R. Arnold, and B. Goke. 1992. Glucagon-like peptide-1 cells in the gastrointestinal tract and pancreas of rat, pig and man. *Eur J Clin Invest*. 22:283-291.
Fanelli, C., S. Pampanelli, L. Epifano, A.M. Rambotti, A. Di Vincenzo, F. Modarelli, M. Ciofetta, M. Lepore, B. Annibale, E. Torlone, and *et al*. 1994. Long-term recovery from unawareness, deficient counterregulation and lack of cognitive dysfunction during hypoglycaemia, following institution of rational, intensive insulin therapy in IDDM. *Diabetologia*. 37:1265-1276.
Farilla, L., H. Hui, C. Bertolotto, E. Kang, A. Bulotta, U. Di Mario, and R. Perfetti. 2002. Glucagon-like peptide-1 promotes islet cell growth and inhibits apoptosis in Zucker diabetic rats. *Endocrinology*. 143:4397-4408.
Feltbower, R.G., H.J. Bodansky, C.C. Patterson, R.C. Parslow, C.R. Stephenson, C. Reynolds, and P.A. McKinney. 2008. Acute complications and drug misuse are important causes of death for children and young adults with type 1 diabetes: results from the Yorkshire Register of diabetes in children and young adults. *Diabetes Care*. 31:922-926.
Ferrara, N. 1999. Molecular and biological properties of vascular endothelial growth factor. *J Mol Med (Berl)*. 77:527-543.
Finegood, D.T., L. Scaglia, and S. Bonner-Weir. 1995. Dynamics of beta-cell mass in the growing rat pancreas. Estimation with a simple mathematical model. *Diabetes*. 44:249-256.
Frank, S.R., M. Schroeder, P. Fernandez, S. Taubert, and B. Amati. 2001. Binding of c-Myc to chromatin mediates mitogen-induced acetylation of histone H4 and gene activation. *Genes Dev*. 15:2069-2082.
Frayn, K.N. 1996. Metabolic regulation : a human perspective. Blackwell Science, Oxford.
Freytag, S.O. 1988. Enforced expression of the c-myc oncogene inhibits cell differentiation by precluding entry into a distinct predifferentiation state in G0/G1. *Molecular and cellular biology*. 8:1614-1624.
Fuchs, M., J. Gerber, R. Drapkin, S. Sif, T. Ikura, V. Ogryzko, W.S. Lane, Y. Nakatani, and D.M. Livingston. 2001. The p400 complex is an essential E1A transformation target. *Cell*. 106:297-307.
Gautier, L., L. Cope, B.M. Bolstad, and R.A. Irizarry. 2004. affy--analysis of Affymetrix GeneChip data at the probe level. *Bioinformatics*. 20:307-315.
Geng, Y., E.N. Eaton, M. Picon, J.M. Roberts, A.S. Lundberg, A. Gifford, C. Sardet, and R.A. Weinberg. 1996. Regulation of cyclin E transcription by E2Fs and retinoblastoma protein. *Oncogene*. 12:1173-1180.
Gerich, J.E. 1989. Oral hypoglycemic agents. *N Engl J Med*. 321:1231-1245.
Gerich, J.E. 1993. Control of glycaemia. *Baillieres Clin Endocrinol Metab*. 7:551-586.
Gerstein, H.C., M.E. Miller, R.P. Byington, D.C. Goff, Jr., J.T. Bigger, J.B. Buse, W.C. Cushman, S. Genuth, F. Ismail-Beigi, R.H. Grimm, Jr., J.L. Probstfield, D.G. Simons-Morton, and W.T. Friedewald. 2008. Effects of intensive glucose lowering in type 2 diabetes. *N Engl J Med*. 358:2545-2559.
Giang, D.V., Y. Lenbury, A. De Gaetano, and P. Palumbo. 2008. Delay model of glucose–insulin systems: Global stability and oscillated solutions conditional on delays. *Journal of Mathematical Analysis and Applications*. 343:996-1006.

Glaser, B., P. Kesavan, M. Heyman, E. Davis, A. Cuesta, A. Buchs, C.A. Stanley, P.S. Thornton, M.A. Permutt, F.M. Matschinsky, and K.C. Herold. 1998. Familial hyperinsulinism caused by an activating glucokinase mutation. *N Engl J Med*. 338:226-230.

Gloyn, A.L. 2003. Glucokinase (GCK) mutations in hyper- and hypoglycemia: maturity-onset diabetes of the young, permanent neonatal diabetes, and hyperinsulinemia of infancy. *Hum Mutat*. 22:353-362.

Gong, D., and J.E. Ferrell, Jr. 2010. The roles of cyclin A2, B1, and B2 in early and late mitotic events. *Mol Biol Cell*. 21:3149-3161.

Goodner, C.J., B.C. Walike, D.J. Koerker, J.W. Ensinck, A.C. Brown, E.W. Chideckel, J. Palmer, and L. Kalnasy. 1977. Insulin, glucagon, and glucose exhibit synchronous, sustained oscillations in fasting monkeys. *Science*. 195:177-179.

Gorgoulis, V.G., L.V. Vassiliou, P. Karakaidos, P. Zacharatos, A. Kotsinas, T. Liloglou, M. Venere, R.A. Ditullio, Jr., N.G. Kastrinakis, B. Levy, D. Kletsas, A. Yoneta, M. Herlyn, C. Kittas, and T.D. Halazonetis. 2005. Activation of the DNA damage checkpoint and genomic instability in human precancerous lesions. *Nature*. 434:907-913.

Grandori, C., S.M. Cowley, L.P. James, and R.N. Eisenman. 2000. The Myc/Max/Mad network and the transcriptional control of cell behavior. *Annu Rev Cell Dev Biol*. 16:653-699.

Green, D.R., and G.I. Evan. 2002. A matter of life and death. *Cancer Cell*. 1:19-30.

Gromada, J., I. Franklin, and C.B. Wollheim. 2007. Alpha-cells of the endocrine pancreas: 35 years of research but the enigma remains. *Endocr Rev*. 28:84-116.

Gromada, J., M. Hoy, E. Renstrom, K. Bokvist, L. Eliasson, S. Gopel, and P. Rorsman. 1999. CaM kinase II-dependent mobilization of secretory granules underlies acetylcholine-induced stimulation of exocytosis in mouse pancreatic B-cells. *J Physiol*. 518 (Pt 3):745-759.

Grossman, E.J., D.D. Lee, J. Tao, R.A. Wilson, S.Y. Park, G.I. Bell, and A.S. Chong. 2010. Glycemic control promotes pancreatic beta-cell regeneration in streptozotocin-induced diabetic mice. *PLoS One*. 5:e8749.

Guo, Q.M., R.L. Malek, S. Kim, C. Chiao, M. He, M. Ruffy, K. Sanka, N.H. Lee, C.V. Dang, and E.T. Liu. 2000. Identification of c-myc responsive genes using rat cDNA microarray. *Cancer research*. 60:5922-5928.

Hamren, B., E. Bjork, M. Sunzel, and M. Karlsson. 2008. Models for plasma glucose, HbA1c, and hemoglobin interrelationships in patients with type 2 diabetes following tesaglitazar treatment. *Clin Pharmacol Ther*. 84:228-235.

Hansen, L., C.F. Deacon, C. Orskov, and J.J. Holst. 1999. Glucagon-like peptide-1-(7-36)amide is transformed to glucagon-like peptide-1-(9-36)amide by dipeptidyl peptidase IV in the capillaries supplying the L cells of the porcine intestine. *Endocrinology*. 140:5356-5363.

Harris, M.A., J. Clark, A. Ireland, J. Lomax, M. Ashburner, R. Foulger, K. Eilbeck, S. Lewis, B. Marshall, C. Mungall, J. Richter, G.M. Rubin, J.A. Blake, C. Bult, M. Dolan, H. Drabkin, J.T. Eppig, D.P. Hill, L. Ni, M. Ringwald, R. Balakrishnan, J.M. Cherry, K.R. Christie, M.C. Costanzo, S.S. Dwight, S. Engel, D.G. Fisk, J.E. Hirschman, E.L. Hong, R.S. Nash, A. Sethuraman, C.L. Theesfeld, D. Botstein, K. Dolinski, B. Feierbach, T. Berardini, S. Mundodi, S.Y. Rhee, R. Apweiler, D. Barrell, E. Camon, E. Dimmer, V. Lee, R.

Chisholm, P. Gaudet, W. Kibbe, R. Kishore, E.M. Schwarz, P. Sternberg, M. Gwinn, L. Hannick, J. Wortman, M. Berriman, V. Wood, N. de la Cruz, P. Tonellato, P. Jaiswal, T. Seigfried, and R. White. 2004. The Gene Ontology (GO) database and informatics resource. *Nucleic acids research*. 32:D258-261.

Haupt, Y., R. Maya, A. Kazaz, and M. Oren. 1997. Mdm2 promotes the rapid degradation of p53. *Nature*. 387:296-299.

Hayashizaki, Y., and J. Kawai. 2004. A new approach to the distribution and storage of genetic resources. *Nat Rev Genet*. 5:223-228.

Henriksson, M., and B. Luscher. 1996. Proteins of the Myc network: essential regulators of cell growth and differentiation. *Adv Cancer Res*. 68:109-182.

Hermeking, H., C. Rago, M. Schuhmacher, Q. Li, J.F. Barrett, A.J. Obaya, B.C. O'Connell, M.K. Mateyak, W. Tam, F. Kohlhuber, C.V. Dang, J.M. Sedivy, D. Eick, B. Vogelstein, and K.W. Kinzler. 2000. Identification of CDK4 as a target of c-MYC. *Proceedings of the National Academy of Sciences of the United States of America*. 97:2229-2234.

Herold, S., M. Wanzel, V. Beuger, C. Frohme, D. Beul, T. Hillukkala, J. Syvaoja, H.P. Saluz, F. Haenel, and M. Eilers. 2002. Negative regulation of the mammalian UV response by Myc through association with Miz-1. *Mol Cell*. 10:509-521.

Herzig, R.P., S. Scacco, and R.C. Scarpulla. 2000. Sequential serum-dependent activation of CREB and NRF-1 leads to enhanced mitochondrial respiration through the induction of cytochrome c. *The Journal of biological chemistry*. 275:13134-13141.

Hoaglin, D.C., F. Mosteller, and J.W. Tukey. 2000. Understanding robust and Exploratory Data Analysis. John Wiley & Sons, New York [etc.].

Hojberg, P.V., T. Vilsboll, R. Rabol, F.K. Knop, M. Bache, T. Krarup, J.J. Holst, and S. Madsbad. 2009. Four weeks of near-normalisation of blood glucose improves the insulin response to glucagon-like peptide-1 and glucose-dependent insulinotropic polypeptide in patients with type 2 diabetes. *Diabetologia*. 52:199-207.

Holmes, M.H. 1995. Introduction to perturbation methods. Springer-Verlag, New York.

Holst, J.J. 1999. Glucagon-like Peptide 1 (GLP-1): An Intestinal Hormone, Signalling Nutritional Abundance, with an Unusual Therapeutic Potential. *Trends Endocrinol Metab*. 10:229-235.

Honda, R., H. Tanaka, and H. Yasuda. 1997. Oncoprotein MDM2 is a ubiquitin ligase E3 for tumor suppressor p53. *FEBS Lett*. 420:25-27.

Hu, S., A. Balakrishnan, R.A. Bok, B. Anderton, P.E. Larson, S.J. Nelson, J. Kurhanewicz, D.B. Vigneron, and A. Goga. 2011. 13C-pyruvate imaging reveals alterations in glycolysis that precede c-Myc-induced tumor formation and regression. *Cell Metabolism*. 14:131-142.

Hubbell, E., W.M. Liu, and R. Mei. 2002. Robust estimators for expression analysis. *Bioinformatics*. 18:1585-1592.

Hui, H., A. Nourparvar, X. Zhao, and R. Perfetti. 2003. Glucagon-like peptide-1 inhibits apoptosis of insulin-secreting cells via a cyclic 5'-adenosine monophosphate-dependent protein kinase A- and a phosphatidylinositol 3-kinase-dependent pathway. *Endocrinology*. 144:1444-1455.

Hurlin, P.J., C. Queva, and R.N. Eisenman. 1997. Mnt, a novel Max-interacting protein is coexpressed with Myc in proliferating cells and mediates repression at Myc binding sites. *Genes Dev*. 11:44-58.

Hurlin, P.J., C. Queva, P.J. Koskinen, E. Steingrimsson, D.E. Ayer, N.G. Copeland, N.A. Jenkins, and R.N. Eisenman. 1996. Mad3 and Mad4: novel Max-interacting transcriptional repressors that suppress c-myc dependent transformation and are expressed during neural and epidermal differentiation. *Embo J*. 15:2030.

Imagawa, A., T. Hanafusa, J. Miyagawa, and Y. Matsuzawa. 2000. A novel subtype of type 1 diabetes mellitus characterized by a rapid onset and an absence of diabetes-related antibodies. Osaka IDDM Study Group. *N Engl J Med*. 342:301-307.

Irizarry, R.A., B. Hobbs, F. Collin, Y.D. Beazer-Barclay, K.J. Antonellis, U. Scherf, and T.P. Speed. 2003. Exploration, normalization, and summaries of high density oligonucleotide array probe level data. *Biostatistics*. 4:249-264.

Ishihara, K., K. Yasuda, and T. Hatayama. 1999. Molecular cloning, expression and localization of human 105 kDa heat shock protein, hsp105. *Biochim Biophys Acta*. 1444:138-142.

Ismail, I.H., S. Nystrom, J. Nygren, and O. Hammarsten. 2005. Activation of ataxia telangiectasia mutated by DNA strand break-inducing agents correlates closely with the number of DNA double strand breaks. *The Journal of biological chemistry*. 280:4649-4655.

Jackman, M., C. Lindon, E.A. Nigg, and J. Pines. 2003. Active cyclin B1-Cdk1 first appears on centrosomes in prophase. *Nat Cell Biol*. 5:143-148.

Jacobson, A.M., G. Musen, C.M. Ryan, N. Silvers, P. Cleary, B. Waberski, A. Burwood, K. Weinger, M. Bayless, W. Dahms, and J. Harth. 2007. Long-term effect of diabetes and its treatment on cognitive function. *N Engl J Med*. 356:1842-1852.

Jin, P., S. Hardy, and D.O. Morgan. 1998. Nuclear localization of cyclin B1 controls mitotic entry after DNA damage. *J Cell Biol*. 141:875-885.

Johnson, J.D., N.T. Ahmed, D.S. Luciani, Z. Han, H. Tran, J. Fujita, S. Misler, H. Edlund, and K.S. Polonsky. 2003. Increased islet apoptosis in Pdx1+/- mice. *The Journal of clinical investigation*. 111:1147-1160.

Johnson, J.D., and E.U. Alejandro. 2008. Control of pancreatic beta-cell fate by insulin signaling: The sweet spot hypothesis. *Cell Cycle*. 7:1343-1347.

Johnson, J.D., E. Bernal-Mizrachi, E.U. Alejandro, Z. Han, T.B. Kalynyak, H. Li, J.L. Beith, J. Gross, G.L. Warnock, R.R. Townsend, M.A. Permutt, and K.S. Polonsky. 2006. Insulin protects islets from apoptosis via Pdx1 and specific changes in the human islet proteome. *Proceedings of the National Academy of Sciences of the United States of America*. 103:19575-19580.

Jonas, J.-C., A. Sharma, W. Hasenkamp, H. Ilkova, G. Patane, R. Laybutt, S. Bonner-Weir, and G.C. Weir. 1999. Chronic Hyperglycemia Triggers Loss of Pancreatic beta-cell Differentiation in an Animal Model of Diabetes. *J. Biol. Chem.* 274:14112-14121.

Jonas, J.C., D.R. Laybutt, G.M. Steil, N. Trivedi, J.G. Pertusa, M. Van de Casteele, G.C. Weir, and J.C. Henquin. 2001. High glucose stimulates early response gene c-Myc expression in rat pancreatic beta cells. *The Journal of biological chemistry*. 276:35375-35381.

Joshi, A.K.1991. Natural language processing. *Science*. 253(5025):1242-1249.
Juin, P., A.O. Hueber, T. Littlewood, and G. Evan. 1999. c-Myc-induced sensitization to apoptosis is mediated through cytochrome c release. *Genes Dev*. 13:1367-1381.
Juin, P., A. Hunt, T. Littlewood, B. Griffiths, L.B. Swigart, S. Korsmeyer, and G. Evan. 2002. c-Myc functionally cooperates with Bax to induce apoptosis. *Molecular and cellular biology*. 22:6158-6169.
Kahn, S.E., S.M. Haffner, M.A. Heise, W.H. Herman, R.R. Holman, N.P. Jones, B.G. Kravitz, J.M. Lachin, M.C. O'Neill, B. Zinman, and G. Viberti. 2006. Glycemic durability of rosiglitazone, metformin, or glyburide monotherapy. *N Engl J Med*. 355:2427-2443.
Kamijo, T., J.D. Weber, G. Zambetti, F. Zindy, M.F. Roussel, and C.J. Sherr. 1998. Functional and physical interactions of the ARF tumor suppressor with p53 and Mdm2. *Proceedings of the National Academy of Sciences of the United States of America*. 95:8292-8297.
Kaneto, H., A. Sharma, K. Suzuma, D.R. Laybutt, G. Xu, S. Bonner-Weir, and G.C. Weir. 2002. Induction of c-Myc expression suppresses insulin gene transcription by inhibiting NeuroD/BETA2-mediated transcriptional activation. *J Biol Chem*. 277:12998-13006.
Kang, Y., C.R. Chen, and J. Massague. 2003. A self-enabling TGFbeta response coupled to stress signaling: Smad engages stress response factor ATF3 for Id1 repression in epithelial cells. *Mol Cell*. 11:915-926.
Kassem, S.A., I. Ariel, P.S. Thornton, I. Scheimberg, and B. Glaser. 2000. Beta-cell proliferation and apoptosis in the developing normal human pancreas and in hyperinsulinism of infancy. *Diabetes*. 49:1325-1333.
Kauth, T., and J. Metz. 1987. Immunohistochemical localization of glucagon-like peptide 1. Use of poly- and monoclonal antibodies. *Histochemistry*. 86:509-515.
Keener, J.P., and J. Sneyd. 1998. Mathematical physiology. Springer, New York.
Kerr, J.F., A.H. Wyllie, and A.R. Currie. 1972. Apoptosis: a basic biological phenomenon with wide-ranging implications in tissue kinetics. *Br J Cancer*. 26:239-257.
Khanna, K.K., K.E. Keating, S. Kozlov, S. Scott, M. Gatei, K. Hobson, Y. Taya, B. Gabrielli, D. Chan, S.P. Lees-Miller, and M.F. Lavin. 1998. ATM associates with and phosphorylates p53: mapping the region of interaction. *Nat Genet*. 20:398-400.
Khatri, P., and S. Draghici. 2005. Ontological analysis of gene expression data: current tools, limitations, and open problems. *Bioinformatics*. 21:3587-3595.
Khosravi, R., R. Maya, T. Gottlieb, M. Oren, Y. Shiloh, and D. Shkedy. 1999. Rapid ATM-dependent phosphorylation of MDM2 precedes p53 accumulation in response to DNA damage. *Proceedings of the National Academy of Sciences of the United States of America*. 96:14973-14977.
Kiyokawa, H., R.D. Kineman, K.O. Manova-Todorova, V.C. Soares, E.S. Hoffman, M. Ono, D. Khanam, A.C. Hayday, L.A. Frohman, and A. Koff. 1996. Enhanced growth of mice lacking the cyclin-dependent kinase inhibitor function of p27(Kip1). *Cell*. 85:721-732.
Knoepfler, P.S. 2007. Myc goes global: new tricks for an old oncogene. *Cancer research*. 67:5061-5063.

Kohl, N.E., N. Kanda, R.R. Schreck, G. Bruns, S.A. Latt, F. Gilbert, and F.W. Alt. 1983. Transposition and amplification of oncogene-related sequences in human neuroblastomas. *Cell*. 35:359-367.

Kolb, H. 1987. Mouse models of insulin dependent diabetes: low-dose streptozocin-induced diabetes and nonobese diabetic (NOD) mice. *Diabetes Metab Rev*. 3:751-778.

Kotian, S., S. Liyanarachchi, A. Zelent, and J.D. Parvin. 2011. Histone deacetylases 9 and 10 are required for homologous recombination. *The Journal of biological chemistry*. 286:7722-7726.

Krolewski, A.S., and J.H. Warram. 2005. Epidemiology of late complications of diabetes: A basis for the development and evaluation of preventive program. *In* Joslin's diabetes mellitus. Lippincott Williams & Willkins, Philadelphia, Pa.

Kubbutat, M.H., S.N. Jones, and K.H. Vousden. 1997. Regulation of p53 stability by Mdm2. *Nature*. 387:299-303.

Kulkarni, R.N., J.C. Bruning, J.N. Winnay, C. Postic, M.A. Magnuson, and C.R. Kahn. 1999. Tissue-specific knockout of the insulin receptor in pancreatic beta cells creates an insulin secretory defect similar to that in type 2 diabetes. *Cell*. 96:329-339.

Kussie, P.H., S. Gorina, V. Marechal, B. Elenbaas, J. Moreau, A.J. Levine, and N.P. Pavletich. 1996. Structure of the MDM2 oncoprotein bound to the p53 tumor suppressor transactivation domain. *Science*. 274:948-953.

La Rocca, S.A., D.H. Crouch, and D.A. Gillespie. 1994. c-Myc inhibits myogenic differentiation and myoD expression by a mechanism which can be dissociated from cell transformation. *Oncogene*. 9:3499-3508.

Labib, K., and J.F. Diffley. 2001. Is the MCM2-7 complex the eukaryotic DNA replication fork helicase? *Current Opinion in Genetics & Development*. 11:64-70.

Lammert, E., O. Cleaver, and D. Melton. 2001. Induction of pancreatic differentiation by signals from blood vessels. *Science*. 294:564-567.

Lammert, E., G. Gu, M. McLaughlin, D. Brown, R. Brekken, L.C. Murtaugh, H.P. Gerber, N. Ferrara, and D.A. Melton. 2003. Role of VEGF-A in vascularization of pancreatic islets. *Curr Biol*. 13:1070-1074.

Lander, E.S., L.M. Linton, B. Birren, C. Nusbaum, M.C. Zody, J. Baldwin, K. Devon, K. Dewar, M. Doyle, W. FitzHugh, R. Funke, D. Gage, K. Harris, A. Heaford, J. Howland, L. Kann, J. Lehoczky, R. LeVine, P. McEwan, K. McKernan, J. Meldrim, J.P. Mesirov, C. Miranda, W. Morris, J. Naylor, C. Raymond, M. Rosetti, R. Santos, A. Sheridan, C. Sougnez, N. Stange-Thomann, N. Stojanovic, A. Subramanian, D. Wyman, J. Rogers, J. Sulston, R. Ainscough, S. Beck, D. Bentley, J. Burton, C. Clee, N. Carter, A. Coulson, R. Deadman, P. Deloukas, A. Dunham, I. Dunham, R. Durbin, L. French, D. Grafham, S. Gregory, T. Hubbard, S. Humphray, A. Hunt, M. Jones, C. Lloyd, A. McMurray, L. Matthews, S. Mercer, S. Milne, J.C. Mullikin, A. Mungall, R. Plumb, M. Ross, R. Shownkeen, S. Sims, R.H. Waterston, R.K. Wilson, L.W. Hillier, J.D. McPherson, M.A. Marra, E.R. Mardis, L.A. Fulton, A.T. Chinwalla, K.H. Pepin, W.R. Gish, S.L. Chissoe, M.C. Wendl, K.D. Delehaunty, T.L. Miner, A. Delehaunty, J.B. Kramer, L.L. Cook, R.S. Fulton, D.L. Johnson, P.J. Minx, S.W. Clifton, T. Hawkins, E. Branscomb, P. Predki, P. Richardson, S. Wenning, T. Slezak, N. Doggett, J.F. Cheng, A. Olsen, S.

Lucas, C. Elkin, E. Uberbacher, M. Frazier, *et al*. 2001. Initial sequencing and analysis of the human genome. *Nature*. 409:860-921.
Lane, D.P. 1992. Cancer. p53, guardian of the genome. *Nature*. 358:15-16.
Lane, D.P., and L.V. Crawford. 1979. T antigen is bound to a host protein in SV40-transformed cells. *Nature*. 278:261-263.
Lang, D.A., D.R. Matthews, J. Peto, and R.C. Turner. 1979. Cyclic oscillations of basal plasma glucose and insulin concentrations in human beings. *N Engl J Med*. 301:1023-1027.
Lawlor, E.R., L. Soucek, L. Brown-Swigart, K. Shchors, C.U. Bialucha, and G.I. Evan. 2006. Reversible kinetic analysis of Myc targets in vivo provides novel insights into Myc-mediated tumorigenesis. *Cancer research*. 66:4591-4601.
Laybutt, D.R., G.C. Weir, H. Kaneto, J. Lebet, R.D. Palmiter, A. Sharma, and S. Bonner-Weir. 2002. Overexpression of c-Myc in beta-cells of transgenic mice causes proliferation and apoptosis, downregulation of insulin gene expression, and diabetes. *Diabetes*. 51:1793-1804.
Leahy, J.L., S. Bonner-Weir, and G.C. Weir. 1988. Minimal chronic hyperglycemia is a critical determinant of impaired insulin secretion after an incomplete pancreatectomy. *The Journal of clinical investigation*. 81:1407-1414.
Lee, C.S., D.D. De Leon, K.H. Kaestner, and D.A. Stoffers. 2006. Regeneration of pancreatic islets after partial pancreatectomy in mice does not involve the reactivation of neurogenin-3. *Diabetes*. 55:269-272.
Lee, T.I., N.J. Rinaldi, F. Robert, D.T. Odom, Z. Bar-Joseph, G.K. Gerber, N.M. Hannett, C.T. Harbison, C.M. Thompson, I. Simon, J. Zeitlinger, E.G. Jennings, H.L. Murray, D.B. Gordon, B. Ren, J.J. Wyrick, J.B. Tagne, T.L. Volkert, E. Fraenkel, D.K. Gifford, and R.A. Young. 2002. Transcriptional regulatory networks in Saccharomyces cerevisiae. *Science*. 298:799-804.
Lei, M. 2005. The MCM complex: its role in DNA replication and implications for cancer therapy. *Curr Cancer Drug Targets*. 5:365-380.
Leibowitz, G., S. Ferber, A. Apelqvist, H. Edlund, D.J. Gross, E. Cerasi, D. Melloul, and N. Kaiser. 2001. IPF1/PDX1 deficiency and beta-cell dysfunction in Psammomys obesus, an animal With type 2 diabetes. *Diabetes*. 50:1799-1806.
LeRoith, D., and O. Gavrilova. 2006. Mouse models created to study the pathophysiology of Type 2 diabetes. *Int J Biochem Cell Biol*. 38:904-912.
Lew, D.J., V. Dulic, and S.I. Reed. 1991. Isolation of three novel human cyclins by rescue of G1 cyclin (Cln) function in yeast. *Cell*. 66:1197-1206.
Li, C., and W.H. Wong. 2001. Model-based analysis of oligonucleotide arrays: expression index computation and outlier detection. *Proceedings of the National Academy of Sciences of the United States of America*. 98:31-36.
Li, F., Y. Wang, K.I. Zeller, J.J. Potter, D.R. Wonsey, K.A. O'Donnell, J.W. Kim, J.T. Yustein, L.A. Lee, and C.V. Dang. 2005. Myc stimulates nuclearly encoded mitochondrial genes and mitochondrial biogenesis. *Molecular and cellular biology*. 25:6225-6234.
Li, J., Y. Kuang, and C.C. Mason. 2006. Modeling the glucose-insulin regulatory system and ultradian insulin secretory oscillations with two explicit time delays. *J Theor Biol*. 242:722-735.
Li, Y., T. Hansotia, B. Yusta, F. Ris, P.A. Halban, and D.J. Drucker. 2003. Glucagon-like peptide-1 receptor signaling modulates beta cell apoptosis. *The Journal of biological chemistry*. 278:471-478.

Like, A.A., and A.A. Rossini. 1976. Streptozotocin-induced pancreatic insulitis: new model of diabetes mellitus. *Science*. 193:415-417.
Lingohr, M.K., R. Buettner, and C.J. Rhodes. 2002. Pancreatic beta-cell growth and survival--a role in obesity-linked type 2 diabetes? *Trends Mol Med*. 8:375-384.
Linzer, D.I., and A.J. Levine. 1979. Characterization of a 54K dalton cellular SV40 tumor antigen present in SV40-transformed cells and uninfected embryonal carcinoma cells. *Cell*. 17:43-52.
Lipsett, M., and D.T. Finegood. 2002. beta-cell neogenesis during prolonged hyperglycemia in rats. *Diabetes*. 51:1834-1841.
Lipshutz, R.J., S.P. Fodor, T.R. Gingeras, and D.J. Lockhart. 1999. High density synthetic oligonucleotide arrays. *Nat Genet*. 21:20-24.
Littlewood, T.D., D.C. Hancock, P.S. Danielian, M.G. Parker, and G.I. Evan. 1995. A modified oestrogen receptor ligand-binding domain as an improved switch for the regulation of heterologous proteins. *Nucleic acids research*. 23:1686-1690.
Liu, W., and L.M. Ellis. 1998. Regulation of vascular endothelial growth factor receptor KDR in vitro by a soluble factor in confluent endothelial cells. *Pathobiology*. 66:247-252.
Lockhart, D.J., H. Dong, M.C. Byrne, M.T. Follettie, M.V. Gallo, M.S. Chee, M. Mittmann, C. Wang, M. Kobayashi, H. Horton, and E.L. Brown. 1996. Expression monitoring by hybridization to high-density oligonucleotide arrays. *Nat Biotechnol*. 14:1675-1680.
Lockhart, D.J., and E.A. Winzeler. 2000. Genomics, gene expression and DNA arrays. *Nature*. 405:827-836.
Lotter, E.C., and S.C. Woods. 1977. Injections of insulin and changes of body weight. *Physiol Behav*. 18:293-297.
Lovshin, J.A., and D.J. Drucker. 2009. Incretin-based therapies for type 2 diabetes mellitus. *Nat Rev Endocrinol*. 5:262-269.
Lu, M., M.B. Wheeler, X.H. Leng, and A.E. Boyd, 3rd. 1993. The role of the free cytosolic calcium level in beta-cell signal transduction by gastric inhibitory polypeptide and glucagon-like peptide I(7-37). *Endocrinology*. 132:94-100.
Lukas, J., C. Lukas, and J. Bartek. 2004. Mammalian cell cycle checkpoints: signalling pathways and their organization in space and time. *DNA Repair (Amst)*. 3:997-1007.
Luo, X., L. Ding, J. Xu, and N. Chegini. 2005. Gene expression profiling of leiomyoma and myometrial smooth muscle cells in response to transforming growth factor-beta. *Endocrinology*. 146:1097-1118.
Lutz, M., and P. Knaus. 2002. Integration of the TGF-beta pathway into the cellular signalling network. *Cell Signal*. 14:977-988.
Macdonald, F., Ford, C.H.J. and Casson, A.G. 2004. Molecular biology of cancer. BIOS Scientific, London.
MacDonald, P.E., and M.B. Wheeler. 2003. Voltage-dependent K(+) channels in pancreatic beta cells: role, regulation and potential as therapeutic targets. *Diabetologia*. 46:1046-1062.
Mailand, N., J. Falck, C. Lukas, R.G. Syljuasen, M. Welcker, J. Bartek, and J. Lukas. 2000. Rapid destruction of human Cdc25A in response to DNA damage. *Science*. 288:1425-1429.

Makino, S., K. Kunimoto, Y. Muraoka, Y. Mizushima, K. Katagiri, and Y. Tochino. 1980. Breeding of a non-obese, diabetic strain of mice. *Jikken Dobutsu*. 29:1-13.

Maletti, M., B. Portha, M. Carlquist, M. Kergoat, M. Laburthe, J.C. Marie, and G. Rosselin. 1984. Evidence for and characterization of specific high affinity binding sites for the gastric inhibitory polypeptide in pancreatic beta-cells. *Endocrinology*. 115:1324-1331.

Manesso, E., G.M. Toffolo, Y. Saisho, A.E. Butler, A.V. Matveyenko, C. Cobelli, and P.C. Butler. 2009. Dynamics of beta-cell turnover: evidence for beta-cell turnover and regeneration from sources of beta-cells other than beta-cell replication in the HIP rat. *American journal of physiology. Endocrinology and metabolism*. 297:E323-330.

Martinou, J.C., and D.R. Green. 2001. Breaking the mitochondrial barrier. *Nature reviews. Molecular cell biology*. 2:63-67.

Matschinsky, F.M. 1996. Banting Lecture 1995. A lesson in metabolic regulation inspired by the glucokinase glucose sensor paradigm. *Diabetes*. 45:223-241.

Matsuda, S., J. Rouault, J. Magaud, and C. Berthet. 2001. In search of a function for the TIS21/PC3/BTG1/TOB family. *FEBS Lett*. 497:67-72.

Matthews, E.K., and Y. Sakamoto. 1975. Electrical characteristics of pancreatic islet cells. *J Physiol*. 246:421-437.

McEvoy, R.C. 1981. Changes in the volumes of the A-, B-, and D-cell populations in the pancreatic islets during the postnatal development of the rat. *Diabetes*. 30:813-817.

McMahon, S.B., H.A. Van Buskirk, K.A. Dugan, T.D. Copeland, and M.D. Cole. 1998. The novel ATM-related protein TRRAP is an essential cofactor for the c-Myc and E2F oncoproteins. *Cell*. 94:363-374.

Meares, G.P., A.A. Zmijewska, and R.S. Jope. 2008. HSP105 interacts with GRP78 and GSK3 and promotes ER stress-induced caspase-3 activation. *Cell Signal*. 20:347-358.

Meier, J.J., A. Bhushan, A.E. Butler, R.A. Rizza, and P.C. Butler. 2005. Sustained beta cell apoptosis in patients with long-standing type 1 diabetes: indirect evidence for islet regeneration? *Diabetologia*. 48:2221-2228.

Meier, J.J., A.E. Butler, Y. Saisho, T. Monchamp, R. Galasso, A. Bhushan, R.A. Rizza, and P.C. Butler. 2008. {beta}-Cell Replication Is the Primary Mechanism Subserving the Postnatal Expansion of {beta}-Cell Mass in Humans. *Diabetes*. 57:1584-1594.

Meissner, H.P., and H. Schmelz. 1974. Membrane potential of beta-cells in pancreatic islets. *Pflugers Arch*. 351:195-206.

Menssen, A., and H. Hermeking. 2002. Characterization of the c-MYC-regulated transcriptome by SAGE: identification and analysis of c-MYC target genes. *Proceedings of the National Academy of Sciences of the United States of America*. 99:6274-6279.

Misler, S., L.C. Falke, K. Gillis, and M.L. McDaniel. 1986. A metabolite-regulated potassium channel in rat pancreatic B cells. *Proceedings of the National Academy of Sciences of the United States of America*. 83:7119-7123.

Momand, J., G.P. Zambetti, D.C. Olson, D. George, and A.J. Levine. 1992. The mdm-2 oncogene product forms a complex with the p53 protein and inhibits p53-mediated transactivation. *Cell*. 69:1237-1245.

Montanya, E., V. Nacher, M. Biarnes, and J. Soler. 2000. Linear correlation between beta-cell mass and body weight throughout the lifespan in Lewis rats: role of beta-cell hyperplasia and hypertrophy. *Diabetes*. 49:1341-1346.

Morrish, F., N. Neretti, J.M. Sedivy, and D.M. Hockenbery. 2008. The oncogene c-Myc coordinates regulation of metabolic networks to enable rapid cell cycle entry. *Cell Cycle*. 7:1054-1066.

Mortensen, K., L.L. Christensen, J.J. Holst, and C. Orskov. 2003. GLP-1 and GIP are colocalized in a subset of endocrine cells in the small intestine. *Regul Pept*. 114:189-196.

Moustakas, A., S. Souchelnytskyi, and C.H. Heldin. 2001. Smad regulation in TGF-beta signal transduction. *J Cell Sci*. 114:4359-4369.

Nakane, P.K., and G.B. Pierce, Jr. 1966. Enzyme-labeled antibodies: preparation and application for the localization of antigens. *J Histochem Cytochem*. 14:929-931.

Nau, M.M., B.J. Brooks, J. Battey, E. Sausville, A.F. Gazdar, I.R. Kirsch, O.W. McBride, V. Bertness, G.F. Hollis, and J.D. Minna. 1985. L-myc, a new myc-related gene amplified and expressed in human small cell lung cancer. *Nature*. 318:69-73.

Nauck, M., F. Stockmann, R. Ebert, and W. Creutzfeldt. 1986. Reduced incretin effect in type 2 (non-insulin-dependent) diabetes. *Diabetologia*. 29:46-52.

NC3Rs. 2011. Mouse : Decision tree for blood sampling. http://www.nc3rs.org.uk/bloodsamplingmicrosite/page.asp?id=419. National Centre for the Replacement, Refinement and Reduction of Animals in Research.

Nielsen, J.H., C. Svensson, E.D. Galsgaard, A. Moldrup, and N. Billestrup. 1999. Beta cell proliferation and growth factors. *J Mol Med (Berl)*. 77:62-66.

Nilsson, J.A., and J.L. Cleveland. 2003. Myc pathways provoking cell suicide and cancer. *Oncogene*. 22:9007-9021.

Nir, T., D.A. Melton, and Y. Dor. 2007. Recovery from diabetes in mice by beta cell regeneration. *The Journal of clinical investigation*. 117:2553-2561.

Nishizuka, M., A. Koyanagi, S. Osada, and M. Imagawa. 2008. Wnt4 and Wnt5a promote adipocyte differentiation. *FEBS Lett*. 582:3201-3205.

O'Connor, L., A. Strasser, L.A. O'Reilly, G. Hausmann, J.M. Adams, S. Cory, and D.C. Huang. 1998. Bim: a novel member of the Bcl-2 family that promotes apoptosis. *Embo J*. 17:384-395.

O'Hagan, R.C., M. Ohh, G. David, I.M. de Alboran, F.W. Alt, W.G. Kaelin, Jr., and R.A. DePinho. 2000a. Myc-enhanced expression of Cul1 promotes ubiquitin-dependent proteolysis and cell cycle progression. *Genes Dev*. 14:2185-2191.

O'Hagan, R.C., N. Schreiber-Agus, K. Chen, G. David, J.A. Engelman, R. Schwab, L. Alland, C. Thomson, D.R. Ronning, J.C. Sacchettini, P. Meltzer, and R.A. DePinho. 2000b. Gene-target recognition among members of the myc superfamily and implications for oncogenesis. *Nat Genet*. 24:113-119.

Ohlsson, H., K. Karlsson, and T. Edlund. 1993. IPF1, a homeodomain-containing transactivator of the insulin gene. *Embo J*. 12:4251-4259.

Okada, T., C.W. Liew, J. Hu, C. Hinault, M.D. Michael, J. Krtzfeldt, C. Yin, M. Holzenberger, M. Stoffel, and R.N. Kulkarni. 2007. Insulin receptors in beta-cells are critical for islet compensatory growth response to insulin resistance. *Proceedings of the National Academy of Sciences of the United States of America*. 104:8977-8982.

Orci, L., B. Thorens, M. Ravazzola, and H.F. Lodish. 1989. Localization of the pancreatic beta cell glucose transporter to specific plasma membrane domains. *Science*. 245:295-297.

Orskov, C. 1992. Glucagon-like peptide-1, a new hormone of the entero-insular axis. *Diabetologia*. 35:701-711.

Oster, S.K., C.S. Ho, E.L. Soucie, and L.Z. Penn. 2002. The myc oncogene: MarvelouslY Complex. *Adv Cancer Res*. 84:81-154.

Osthus, R.C., H. Shim, S. Kim, Q. Li, R. Reddy, M. Mukherjee, Y. Xu, D. Wonsey, L.A. Lee, and C.V. Dang. 2000. Deregulation of glucose transporter 1 and glycolytic gene expression by c-Myc. *The Journal of biological chemistry*. 275:21797-21800.

Otani, K., R.N. Kulkarni, A.C. Baldwin, J. Krutzfeldt, K. Ueki, M. Stoffel, C.R. Kahn, and K.S. Polonsky. 2004. Reduced beta-cell mass and altered glucose sensing impair insulin-secretory function in betaIRKO mice. *American journal of physiology. Endocrinology and metabolism*. 286:E41-49.

Ou, Y.H., P.H. Chung, F.F. Hsu, T.P. Sun, W.Y. Chang, and S.Y. Shieh. 2007. The candidate tumor suppressor BTG3 is a transcriptional target of p53 that inhibits E2F1. *Embo J*. 26:3968-3980.

Panunzi, S., P. Palumbo, and A. De Gaetano. 2007. A discrete Single Delay Model for the Intra-Venous Glucose Tolerance Test. *Theor Biol Med Model*. 4:35.

Parsons, J.A., A. Bartke, and R.L. Sorenson. 1995. Number and size of islets of Langerhans in pregnant, human growth hormone-expressing transgenic, and pituitary dwarf mice: effect of lactogenic hormones. *Endocrinology*. 136:2013-2021.

Parsons, J.A., T.C. Brelje, and R.L. Sorenson. 1992. Adaptation of islets of Langerhans to pregnancy: increased islet cell proliferation and insulin secretion correlates with the onset of placental lactogen secretion. *Endocrinology*. 130:1459-1466.

Pascal, S.M., Y. Guiot, S. Pelengaris, M. Khan, and J.C. Jonas. 2008. Effects of c-MYC activation on glucose stimulus-secretion coupling events in mouse pancreatic islets. *American journal of physiology. Endocrinology and metabolism*. 295:E92-102.

Pattaranit, R., and H.A. van den Berg. 2008. Mathematical models of energy homeostasis. *J R Soc Interface*. 5:1119-1135.

Pattaranit, R., H.A. van den Berg, and D. Spanswick. 2008. The development of insulin resistance in Type 2 diabetes: insights from knockout studies. *Sci Prog*. 91:285-316.

Pearson, K.W., D. Scott, and B. Torrance. 1977. Effects of partial surgical pancreatectomy in rats. I. Pancreatic regeneration. *Gastroenterology*. 72:469-473.

Pease, A.C., D. Solas, E.J. Sullivan, M.T. Cronin, C.P. Holmes, and S.P. Fodor. 1994. Light-generated oligonucleotide arrays for rapid DNA sequence analysis. *Proceedings of the National Academy of Sciences of the United States of America*. 91:5022-5026.

Pelengaris, S., S. Abouna, L. Cheung, V. Ifandi, S. Zervou, and M. Khan. 2004. Brief inactivation of c-Myc is not sufficient for sustained regression of c-Myc-induced tumours of pancreatic islets and skin epidermis. *BMC Biol*. 2:26.

Pelengaris, S., and M. Khan. 2001. Oncogenic co-operation in beta-cell tumorigenesis. *Endocr Relat Cancer*. 8:307-314.
Pelengaris, S., M. Khan, and G. Evan. 2002a. c-MYC: more than just a matter of life and death. *Nat Rev Cancer*. 2:764-776.
Pelengaris, S., M. Khan, and G.I. Evan. 2002b. Suppression of Myc-induced apoptosis in beta cells exposes multiple oncogenic properties of Myc and triggers carcinogenic progression. *Cell*. 109:321-334.
Pelengaris, S., T. Littlewood, M. Khan, G. Elia, and G. Evan. 1999. Reversible activation of c-Myc in skin: induction of a complex neoplastic phenotype by a single oncogenic lesion. *Mol Cell*. 3:565-577.
Peng, C.Y., P.R. Graves, R.S. Thoma, Z. Wu, A.S. Shaw, and H. Piwnica-Worms. 1997. Mitotic and G2 checkpoint control: regulation of 14-3-3 protein binding by phosphorylation of Cdc25C on serine-216. *Science*. 277:1501-1505.
Perez-Roger, I., S.H. Kim, B. Griffiths, A. Sewing, and H. Land. 1999. Cyclins D1 and D2 mediate myc-induced proliferation via sequestration of p27(Kip1) and p21(Cip1). *Embo J*. 18:5310-5320.
Pick, A., J. Clark, C. Kubstrup, M. Levisetti, W. Pugh, S. Bonner-Weir, and K.S. Polonsky. 1998. Role of apoptosis in failure of beta-cell mass compensation for insulin resistance and beta-cell defects in the male Zucker diabetic fatty rat. *Diabetes*. 47:358-364.
Pines, J., and T. Hunter. 1991. Human cyclins A and B1 are differentially located in the cell and undergo cell cycle-dependent nuclear transport. *J Cell Biol*. 115:1-17.
Plum, L., Schubert, M., and J.C. Brüning. 2005. The role of insulin receptor signaling in the brain. *Trends Endocrinol Metab*. 16(2):59-65.
Prendergast, G.C. 1999. Myc and Myb: are the veils beginning to lift? *Oncogene*. 18:2914-2915.
Quelle, D.E., F. Zindy, R.A. Ashmun, and C.J. Sherr. 1995. Alternative reading frames of the INK4a tumor suppressor gene encode two unrelated proteins capable of inducing cell cycle arrest. *Cell*. 83:993-1000.
Ray, S., K.R. Atkuri, D. Deb-Basu, A.S. Adler, H.Y. Chang, L.A. Herzenberg, and D.W. Felsher. 2006. MYC can induce DNA breaks in vivo and in vitro independent of reactive oxygen species. *Cancer research*. 66:6598-6605.
Ren, B., F. Robert, J.J. Wyrick, O. Aparicio, E.G. Jennings, I. Simon, J. Zeitlinger, J. Schreiber, N. Hannett, E. Kanin, T.L. Volkert, C.J. Wilson, S.P. Bell, and R.A. Young. 2000. Genome-wide location and function of DNA binding proteins. *Science*. 290:2306-2309.
Ribbing, J., B. Hamren, M.K. Svensson, and M.O. Karlsson. 2010. A model for glucose, insulin, and beta-cell dynamics in subjects with insulin resistance and patients with type 2 diabetes. *J Clin Pharmacol*. 50:861-872.
Robey, I.F., A.D. Lien, S.J. Welsh, B.K. Baggett, and R.J. Gillies. 2005. Hypoxia-inducible factor-1alpha and the glycolytic phenotype in tumors. *Neoplasia*. 7:324-330.
Robinson, G., and I. Dawson. 1975. Immunochemical studies of the endocrine cells of the gastrointestinal tract. II An immunoperoxide technique for the localization of secretin containing cells in human duodenum. *J Clin Pathol*. 28:631-635.

Robson, S.C. 2008. Life or cell death: identifying c-Myc regulated genes in two distinct tissues. Vol. Ph. D. University of Warwick, Coventry.
Robson, S.C., L. Ward, H. Brown, H. Turner, E. Hunter, S. Pelengaris, and M. Khan. 2011. Deciphering c-MYC-regulated genes in two distinct tissues. *BMC Genomics*. in press.
Rooman, I., and L. Bouwens. 2004. Combined gastrin and epidermal growth factor treatment induces islet regeneration and restores normoglycaemia in C57Bl6/J mice treated with alloxan. *Diabetologia*. 47:259-265.
Rooman, I., J. Lardon, and L. Bouwens. 2002. Gastrin stimulates beta-cell neogenesis and increases islet mass from transdifferentiated but not from normal exocrine pancreas tissue. *Diabetes*. 51:686-690.
Rorsman, P., L. Eliasson, E. Renstrom, J. Gromada, S. Barg, and S. Gopel. 2000. The Cell Physiology of Biphasic Insulin Secretion. *News Physiol Sci*. 15:72-77.
Rorsman, P., and E. Renstrom. 2003. Insulin granule dynamics in pancreatic beta cells. *Diabetologia*. 46:1029-1045.
Rothenberg, P.L., L.D. Willison, J. Simon, and B.A. Wolf. 1995. Glucose-induced insulin receptor tyrosine phosphorylation in insulin-secreting beta-cells. *Diabetes*. 44:802-809.
Ryan, K.M., and G.D. Birnie. 1997. Cell-cycle progression is not essential for c-Myc to block differentiation. *Oncogene*. 14:2835-2843.
Salway, J.G. 1999. Metabolism at a glance. Blackwell Science, Oxford [etc.].
Sanchez, Y., C. Wong, R.S. Thoma, R. Richman, Z. Wu, H. Piwnica-Worms, and S.J. Elledge. 1997. Conservation of the Chk1 checkpoint pathway in mammals: linkage of DNA damage to Cdk regulation through Cdc25. *Science*. 277:1497-1501.
Schena, M., D. Shalon, R.W. Davis, and P.O. Brown. 1995. Quantitative monitoring of gene expression patterns with a complementary DNA microarray. *Science*. 270:467-470.
Schiene-Fischer, C., and C. Yu. 2001. Receptor accessory folding helper enzymes: the functional role of peptidyl prolyl cis/trans isomerases. *FEBS Lett*. 495:1-6.
Schmidt, R.F., and G. Thews. 1989. Human physiology. Springer, Berlin.
Schreiber-Agus, N., L. Chin, K. Chen, R. Torres, G. Rao, P. Guida, A.I. Skoultchi, and R.A. DePinho. 1995. An amino-terminal domain of Mxi1 mediates anti-Myc oncogenic activity and interacts with a homolog of the yeast transcriptional repressor SIN3. *Cell*. 80:777-786.
Schroeder, A., O. Mueller, S. Stocker, R. Salowsky, M. Leiber, M. Gassmann, S. Lightfoot, W. Menzel, M. Granzow, and T. Ragg. 2006. The RIN: an RNA integrity number for assigning integrity values to RNA measurements. *BMC Mol Biol*. 7:3.
Schuhmacher, M., F. Kohlhuber, M. Holzel, C. Kaiser, H. Burtscher, M. Jarsch, G.W. Bornkamm, G. Laux, A. Polack, U.H. Weidle, and D. Eick. 2001. The transcriptional program of a human B cell line in response to Myc. *Nucleic acids research*. 29:397-406.
Schwab, M., H.E. Varmus, J.M. Bishop, K.H. Grzeschik, S.L. Naylor, A.Y. Sakaguchi, G. Brodeur, and J. Trent. 1984. Chromosome localization in normal human cells and neuroblastomas of a gene related to c-myc. *Nature*. 308:288-291.

Schwartz, N.S., W.E. Clutter, S.D. Shah, and P.E. Cryer. 1987. Glycemic thresholds for activation of glucose counterregulatory systems are higher than the threshold for symptoms. *The Journal of clinical investigation*. 79:777-781.

Schwitzgebel, V.M., A. Mamin, T. Brun, B. Ritz-Laser, M. Zaiko, A. Maret, F.R. Jornayvaz, G.E. Theintz, O. Michielin, D. Melloul, and J. Philippe. 2003. Agenesis of human pancreas due to decreased half-life of insulin promoter factor 1. *J Clin Endocrinol Metab*. 88:4398-4406.

Seoane, J., H.V. Le, and J. Massague. 2002. Myc suppression of the p21(Cip1) Cdk inhibitor influences the outcome of the p53 response to DNA damage. *Nature*. 419:729-734.

Seoane, J., C. Pouponnot, P. Staller, M. Schader, M. Eilers, and J. Massague. 2001. TGFbeta influences Myc, Miz-1 and Smad to control the CDK inhibitor p15INK4b. *Nat Cell Biol*. 3:400-408.

Seufert, J., G.C. Weir, and J.F. Habener. 1998. Differential expression of the insulin gene transcriptional repressor CCAAT/enhancer-binding protein beta and transactivator islet duodenum homeobox-1 in rat pancreatic beta cells during the development of diabetes mellitus. *The Journal of clinical investigation*. 101:2528-2539.

Shapiro, A.M., J.R. Lakey, E.A. Ryan, G.S. Korbutt, E. Toth, G.L. Warnock, N.M. Kneteman, and R.V. Rajotte. 2000. Islet transplantation in seven patients with type 1 diabetes mellitus using a glucocorticoid-free immunosuppressive regimen. *N Engl J Med*. 343:230-238.

Sheiness, D., L. Fanshier, and J.M. Bishop. 1978. Identification of nucleotide sequences which may encode the oncogenic capacity of avian retrovirus MC29. *J Virol*. 28:600-610.

Sherr, C.J. 2004. Principles of tumor suppression. *Cell*. 116:235-246.

Sherr, C.J., D. Bertwistle, D.E.N.B. W, M.L. Kuo, M. Sugimoto, K. Tago, R.T. Williams, F. Zindy, and M.F. Roussel. 2005. p53-Dependent and -independent functions of the Arf tumor suppressor. *Cold Spring Harb Symp Quant Biol*. 70:129-137.

Sherr, C.J., and J.M. Roberts. 1995. Inhibitors of mammalian G1 cyclin-dependent kinases. *Genes Dev*. 9:1149-1163.

Shi, Y., and J. Massague. 2003. Mechanisms of TGF-beta signaling from cell membrane to the nucleus. *Cell*. 113:685-700.

Shiloh, Y. 2003. ATM and related protein kinases: safeguarding genome integrity. *Nature reviews. Cancer*. 3:155-168.

Shim, H., C. Dolde, B.C. Lewis, C.S. Wu, G. Dang, R.A. Jungmann, R. Dalla-Favera, and C.V. Dang. 1997. c-Myc transactivation of LDH-A: implications for tumor metabolism and growth. *Proceedings of the National Academy of Sciences of the United States of America*. 94:6658-6663.

Shioda, T., M.H. Fenner, and K.J. Isselbacher. 1997. MSG1 and its related protein MRG1 share a transcription activating domain. *Gene*. 204:235-241.

Skrivarhaug, T., H.J. Bangstad, L.C. Stene, L. Sandvik, K.F. Hanssen, and G. Joner. 2006. Long-term mortality in a nationwide cohort of childhood-onset type 1 diabetic patients in Norway. *Diabetologia*. 49:298-305.

Sofroniou, M., and G. Spaletta. 2004. Construction of explicit runge-kutta pairs with stiffness detection. *Mathematical and Computer Modelling*. 40:1157-1169.

Soucie, E.L., M.G. Annis, J. Sedivy, J. Filmus, B. Leber, D.W. Andrews, and L.Z. Penn. 2001. Myc potentiates apoptosis by stimulating Bax activity at the mitochondria. *Molecular and cellular biology*. 21:4725-4736.

Southern, E.M., U. Maskos, and J.K. Elder. 1992. Analyzing and comparing nucleic acid sequences by hybridization to arrays of oligonucleotides: evaluation using experimental models. *Genomics*. 13:1008-1017.

Spencer, C.A., and M. Groudine. 1991. Control of c-myc regulation in normal and neoplastic cells. *Adv Cancer Res*. 56:1-48.

Srivastava, S., and H.J. Goren. 2003. Insulin constitutively secreted by beta-cells is necessary for glucose-stimulated insulin secretion. *Diabetes*. 52:2049-2056.

Staller, P., K. Peukert, A. Kiermaier, J. Seoane, J. Lukas, H. Karsunky, T. Moroy, J. Bartek, J. Massague, F. Hanel, and M. Eilers. 2001. Repression of p15INK4b expression by Myc through association with Miz-1. *Nat Cell Biol*. 3:392-399.

Stark, J.M., P. Hu, A.J. Pierce, M.E. Moynahan, N. Ellis, and M. Jasin. 2002. ATP hydrolysis by mammalian RAD51 has a key role during homology-directed DNA repair. *The Journal of biological chemistry*. 277:20185-20194.

Steil, G.M., N. Trivedi, J.C. Jonas, W.M. Hasenkamp, A. Sharma, S. Bonner-Weir, and G.C. Weir. 2001. Adaptation of beta-cell mass to substrate oversupply: enhanced function with normal gene expression. *American journal of physiology. Endocrinology and metabolism*. 280:E788-796.

Stoffers, D.A., N.T. Zinkin, V. Stanojevic, W.L. Clarke, and J.F. Habener. 1997. Pancreatic agenesis attributable to a single nucleotide deletion in the human IPF1 gene coding sequence. *Nat Genet*. 15:106-110.

Stone, J., T. de Lange, G. Ramsay, E. Jakobovits, J.M. Bishop, H. Varmus, and W. Lee. 1987. Definition of regions in human c-myc that are involved in transformation and nuclear localization. *Molecular and cellular biology*. 7:1697-1709.

Stott, F.J., S. Bates, M.C. James, B.B. McConnell, M. Starborg, S. Brookes, I. Palmero, K. Ryan, E. Hara, K.H. Vousden, and G. Peters. 1998. The alternative product from the human CDKN2A locus, p14(ARF), participates in a regulatory feedback loop with p53 and MDM2. *Embo J*. 17:5001-5014.

Street, C.N., J.R. Lakey, A.M. Shapiro, S. Imes, R.V. Rajotte, E.A. Ryan, J.G. Lyon, T. Kin, J. Avila, T. Tsujimura, and G.S. Korbutt. 2004. Islet graft assessment in the Edmonton Protocol: implications for predicting long-term clinical outcome. *Diabetes*. 53:3107-3114.

Sturis, J., K.S. Polonsky, E. Mosekilde, and E. Van Cauter. 1991. Computer model for mechanisms underlying ultradian oscillations of insulin and glucose. *Am J Physiol*. 260:E801-809.

Sun, H.B., Y.X. Zhu, T. Yin, G. Sledge, and Y.C. Yang. 1998. MRG1, the product of a melanocyte-specific gene related gene, is a cytokine-inducible transcription factor with transformation activity. *Proceedings of the National Academy of Sciences of the United States of America*. 95:13555-13560.

Sun, Y. 2003. Targeting E3 ubiquitin ligases for cancer therapy. *Cancer Biol Ther*. 2:623-629.

Sweet, S., and G. Singh. 1995. Accumulation of human promyelocytic leukemic (HL-60) cells at two energetic cell cycle checkpoints. *Cancer research*. 55:5164-5167.

Swenne, I. 1982. The role of glucose in the in vitro regulation of cell cycle kinetics and proliferation of fetal pancreatic B-cells. *Diabetes*. 31:754-760.

Tavazoie, S., J.D. Hughes, M.J. Campbell, R.J. Cho, and G.M. Church. 1999. Systematic determination of genetic network architecture. *Nat Genet*. 22:281-285.

Teta, M., M.M. Rankin, S.Y. Long, G.M. Stein, and J.A. Kushner. 2007. Growth and regeneration of adult beta cells does not involve specialized progenitors. *Dev Cell*. 12:817-826.

Thorens, B., H.K. Sarkar, H.R. Kaback, and H.F. Lodish. 1988. Cloning and functional expression in bacteria of a novel glucose transporter present in liver, intestine, kidney, and beta-pancreatic islet cells. *Cell*. 55:281-290.

Thyssen, S., E. Arany, and D.J. Hill. 2006. Ontogeny of regeneration of beta-cells in the neonatal rat after treatment with streptozotocin. *Endocrinology*. 147:2346-2356.

Tolic, I.M., E. Mosekilde, and J. Sturis. 2000. Modeling the insulin-glucose feedback system: the significance of pulsatile insulin secretion. *J Theor Biol*. 207:361-375.

Topp, B., K. Promislow, G. deVries, R.M. Miura, and D.T. Finegood. 2000. A model of beta-cell mass, insulin, and glucose kinetics: pathways to diabetes. *J Theor Biol*. 206:605-619.

Tortora, G., R. Caputo, V. Damiano, R. Bianco, J. Chen, S. Agrawal, A.R. Bianco, and F. Ciardiello. 2000. A novel MDM2 anti-sense oligonucleotide has anti-tumor activity and potentiates cytotoxic drugs acting by different mechanisms in human colon cancer. *Int J Cancer*. 88:804-809.

Tycko, B. 2000. Epigenetic gene silencing in cancer. *The Journal of clinical investigation*. 105:401-407.

Vafa, O., M. Wade, S. Kern, M. Beeche, T.K. Pandita, G.M. Hampton, and G.M. Wahl. 2002. c-Myc can induce DNA damage, increase reactive oxygen species, and mitigate p53 function: a mechanism for oncogene-induced genetic instability. *Mol Cell*. 9:1031-1044.

Van de Casteele, M., B.A. Kefas, Y. Cai, H. Heimberg, D.K. Scott, J.C. Henquin, D. Pipeleers, and J.C. Jonas. 2003. Prolonged culture in low glucose induces apoptosis of rat pancreatic beta-cells through induction of c-myc. *Biochem Biophys Res Commun*. 312:937-944.

Velculescu, V.E., L. Zhang, B. Vogelstein, and K.W. Kinzler. 1995. Serial analysis of gene expression. *Science*. 270:484-487.

Venkitaraman, A.R. 2005. Medicine: aborting the birth of cancer. *Nature*. 434:829-830.

Venter, J.C., M.D. Adams, E.W. Myers, P.W. Li, R.J. Mural, G.G. Sutton, H.O. Smith, M. Yandell, C.A. Evans, R.A. Holt, J.D. Gocayne, P. Amanatides, R.M. Ballew, D.H. Huson, J.R. Wortman, Q. Zhang, C.D. Kodira, X.H. Zheng, L. Chen, M. Skupski, G. Subramanian, P.D. Thomas, J. Zhang, G.L. Gabor Miklos, C. Nelson, S. Broder, A.G. Clark, J. Nadeau, V.A. McKusick, N. Zinder, A.J. Levine, R.J. Roberts, M. Simon, C. Slayman, M. Hunkapiller, R. Bolanos, A. Delcher, I. Dew, D. Fasulo, M. Flanigan, L. Florea, A. Halpern, S. Hannenhalli, S. Kravitz, S. Levy, C. Mobarry, K. Reinert, K. Remington, J. Abu-Threideh, E. Beasley, K. Biddick, V. Bonazzi, R. Brandon, M. Cargill, I. Chandramouliswaran, R. Charlab, K. Chaturvedi, Z. Deng, V. Di Francesco, P. Dunn, K. Eilbeck, C. Evangelista, A.E. Gabrielian, W. Gan, W. Ge, F. Gong, Z. Gu, P. Guan, T.J. Heiman, M.E. Higgins, R.R. Ji, Z. Ke, K.A. Ketchum, Z. Lai, Y. Lei, Z. Li, J. Li, Y. Liang, X. Lin, F. Lu,

G.V. Merkulov, N. Milshina, H.M. Moore, A.K. Naik, V.A. Narayan, B. Neelam, D. Nusskern, D.B. Rusch, S. Salzberg, W. Shao, B. Shue, J. Sun, Z. Wang, A. Wang, X. Wang, J. Wang, M. Wei, R. Wides, C. Xiao, C. Yan, *et al*. 2001. The sequence of the human genome. *Science*. 291:1304-1351.

Verspohl, E.J., and H.P. Ammon. 1980. Evidence for presence of insulin receptors in rat islets of Langerhans. *The Journal of clinical investigation*. 65:1230-1237.

Vita, M., and M. Henriksson. 2006. The Myc oncoprotein as a therapeutic target for human cancer. *Semin Cancer Biol*. 16:318-330.

Vogelstein, B., D. Lane, and A.J. Levine. 2000. Surfing the p53 network. *Nature*. 408:307-310.

Waguri, M., K. Yamamoto, J.I. Miyagawa, Y. Tochino, K. Yamamori, Y. Kajimoto, H. Nakajima, H. Watada, I. Yoshiuchi, N. Itoh, A. Imagawa, M. Namba, M. Kuwajima, Y. Yamasaki, T. Hanafusa, and Y. Matsuzawa. 1997. Demonstration of two different processes of beta-cell regeneration in a new diabetic mouse model induced by selective perfusion of alloxan. *Diabetes*. 46:1281-1290.

Wang, Q., and P.L. Brubaker. 2002. Glucagon-like peptide-1 treatment delays the onset of diabetes in 8 week-old db/db mice. *Diabetologia*. 45:1263-1273.

Warburg, O. 1956. On the origin of cancer cells. *Science*. 123:309-314.

Warburg, O.H., and F. Dickens. 1930. The metabolism of tumours. Constable, London.

Wechsler, D.S., C.A. Shelly, and C.V. Dang. 1996. Genomic organization of human MXI1, a putative tumor suppressor gene. *Genomics*. 32:466-470.

Weintraub, S.J., K.N. Chow, R.X. Luo, S.H. Zhang, S. He, and D.C. Dean. 1995. Mechanism of active transcriptional repression by the retinoblastoma protein. *Nature*. 375:812-815.

Weintraub, S.J., C.A. Prater, and D.C. Dean. 1992. Retinoblastoma protein switches the E2F site from positive to negative element. *Nature*. 358:259-261.

Weir, G.C., D.R. Laybutt, H. Kaneto, S. Bonner-Weir, and A. Sharma. 2001. Beta-cell adaptation and decompensation during the progression of diabetes. *Diabetes*. 50 Suppl 1:S154-159.

Winter, W., J. DeJongh, T. Post, B. Ploeger, R. Urquhart, I. Moules, D. Eckland, and M. Danhof. 2006. A Mechanism-based Disease Progression Model for Comparison of Long-term Effects of Pioglitazone, Metformin and Gliclazide on Disease Processes Underlying Type 2 Diabetes Mellitus. *Journal of Pharmacokinetics and Pharmacodynamics*. 33:313-343.

Woods, S.C., R.J. Seeley, D. Porte, Jr., and M.W. Schwartz. 1998. Signals that regulate food intake and energy homeostasis. *Science*. 280:1378-1383.

Woods, S.C., Lotter, E.C., McKay, L.D., and D.Jr. Porte . 1979. Chronic intracerebroventricular infusion of insulin reduces food intake and body weight of baboons. *Nature*. 282(5738):503-505.

Wu, Z., R.A. Irizarry, R. Gentleman, F. Martinez-Murillo, and F. Spencer. 2004. A Model-Based Background Adjustment for Oligonucleotide Expression Arrays. *Journal of the American Statistical Association*. 99:909-917.

Xia, S.J., M.A. Shammas, and R.J. Shmookler Reis. 1997. Elevated recombination in immortal human cells is mediated by HsRAD51 recombinase. *Molecular and cellular biology*. 17:7151-7158.

Xu, G., C.A. Marshall, T.A. Lin, G. Kwon, R.B. Munivenkatappa, J.R. Hill, J.C. Lawrence, Jr., and M.L. McDaniel. 1998. Insulin mediates glucose-

stimulated phosphorylation of PHAS-I by pancreatic beta cells. An insulin-receptor mechanism for autoregulation of protein synthesis by translation. *The Journal of biological chemistry*. 273:4485-4491.

Yamagishi, N., Y. Saito, K. Ishihara, and T. Hatayama. 2002. Enhancement of oxidative stress-induced apoptosis by Hsp105alpha in mouse embryonal F9 cells. *Eur J Biochem*. 269:4143-4151.

Yamamoto, A., T. Taki, H. Yagi, T. Habu, K. Yoshida, Y. Yoshimura, K. Yamamoto, A. Matsushiro, Y. Nishimune, and T. Morita. 1996. Cell cycle-dependent expression of the mouse Rad51 gene in proliferating cells. *Mol Gen Genet*. 251:1-12.

Yin, Z., J. Haynie, X. Yang, B. Han, S. Kiatchoosakun, J. Restivo, S. Yuan, N.R. Prabhakar, K. Herrup, R.A. Conlon, B.D. Hoit, M. Watanabe, and Y.C. Yang. 2002. The essential role of Cited2, a negative regulator for HIF-1alpha, in heart development and neurulation. *Proceedings of the National Academy of Sciences of the United States of America*. 99:10488-10493.

Yki-Jarvinen, H. 1992. Glucose toxicity. *Endocr Rev*. 13:415-431.

Zariwala, M., J. Liu, and Y. Xiong. 1998. Cyclin E2, a novel human G1 cyclin and activating partner of CDK2 and CDK3, is induced by viral oncoproteins. *Oncogene*. 17:2787-2798.

Zeller, K.I., A.G. Jegga, B.J. Aronow, K.A. O'Donnell, and C.V. Dang. 2003. An integrated database of genes responsive to the Myc oncogenic transcription factor: identification of direct genomic targets. *Genome biology*. 4:R69.

Zervos, A.S., J. Gyuris, and R. Brent. 1993. Mxi1, a protein that specifically interacts with Max to bind Myc-Max recognition sites. *Cell*. 72:223-232.

Zhang, H., P. Gao, R. Fukuda, G. Kumar, B. Krishnamachary, K.I. Zeller, C.V. Dang, and G.L. Semenza. 2007. HIF-1 inhibits mitochondrial biogenesis and cellular respiration in VHL-deficient renal cell carcinoma by repression of C-MYC activity. *Cancer Cell*. 11:407-420.

Zhang, Y., Y. Xiong, and W.G. Yarbrough. 1998. ARF promotes MDM2 degradation and stabilizes p53: ARF-INK4a locus deletion impairs both the Rb and p53 tumor suppression pathways. *Cell*. 92:725-734.

Zhong, H., A.M. De Marzo, E. Laughner, M. Lim, D.A. Hilton, D. Zagzag, P. Buechler, W.B. Isaacs, G.L. Semenza, and J.W. Simons. 1999. Overexpression of hypoxia-inducible factor 1alpha in common human cancers and their metastases. *Cancer research*. 59:5830-5835.

Zindy, F., C.M. Eischen, D.H. Randle, T. Kamijo, J.L. Cleveland, C.J. Sherr, and M.F. Roussel. 1998. Myc signaling via the ARF tumor suppressor regulates p53-dependent apoptosis and immortalization. *Genes Dev*. 12:2424-2433.

Zindy, F., R.T. Williams, T.A. Baudino, J.E. Rehg, S.X. Skapek, J.L. Cleveland, M.F. Roussel, and C.J. Sherr. 2003. Arf tumor suppressor promoter monitors latent oncogenic signals in vivo. *Proceedings of the National Academy of Sciences of the United States of America*. 100:15930-15935.

Appendix A. Principles of the microarray experiments and microarray data analysis

After the completion of genome sequencing of key model organisms and humans (Lander *et al*., 2001; Venter *et al*., 2001), the application of genomics has brought researchers from a single cellular function study to a molecular level. However, functional genomics is as important as it ever was, because sequences of DNA, hundreds of millions of bases long do not give information about what the genes do until further investigation. Many tools can be used for this purpose and microarray analysis is one of these high-throughput methods (Lockhart and Winzeler, 2000). Researchers can observe the change of gene expression of a group of cells or a specific tissue on a small chip, which contains thousands of mRNA transcripts (also called the transcriptome), in a single experiment at a given time (Hayashizaki and Kawai, 2004). This section will describe the principles of microarray experiments (Section A.1) and microarray analysis procedure (Section A.2).

A.1. Microarray experiments

The first microarray platform was designed about 20 years ago (Pease *et al*., 1994; Southern *et al*., 1992). More complicated array systems were developed with known or unknown transcripts that can be synthesized on a single chip and the gene expression levels can be analysed. cDNA (two-colour) microarray (Duggan *et al*., 1999; Schena *et al*., 1995) and oligonuclotide (one-colour) microarray (Lipshutz *et al*., 1999; Lockhart *et al*., 1996) are two popular array chips of parallel hybridization assays. The main idea of these microarrays is to use the designed DNA probes on a

chip to measure, through hybridisation, the abundance of mRNA transcriptions from an experiment or a sample. Thousands of genes can be studied in parallel. The principles of these two assays are presented in Figure A.1. In Figure A.1 (A), the basic idea of the two-colour microarray is presented, whereas an outline of the one-colour microarray is shown in Figure A.1 (B). The first step of both assays is extracting poly A mRNA from samples obtained from control (healthy) or treatment (disease) groups. The complementary DNA (cDNA) or cRNA will be generated subsequently in two-colour or one-colour microarray and labelled with fluorescent molecules, i.e. Cy3 (green) and Cy5 (red), or biotin nucleotides. The result interpretation for two-colour microarray is using the hybridization ratio of Cy3/Cy5 to show the relative measurement, for example, if control is labelled by Cy3 and treatment is labelled by Cy5, a red fluorescence scanning result of a specific transcript indicates that the transcript of interest is up-regulated because of the treatment, whereas a green signal suggests the opposite. A yellow signal shows that the amounts of mRNA from two samples are the same. In one-colour microarray, the scanning result relates to the abundance of corresponding mRNA transcripts.

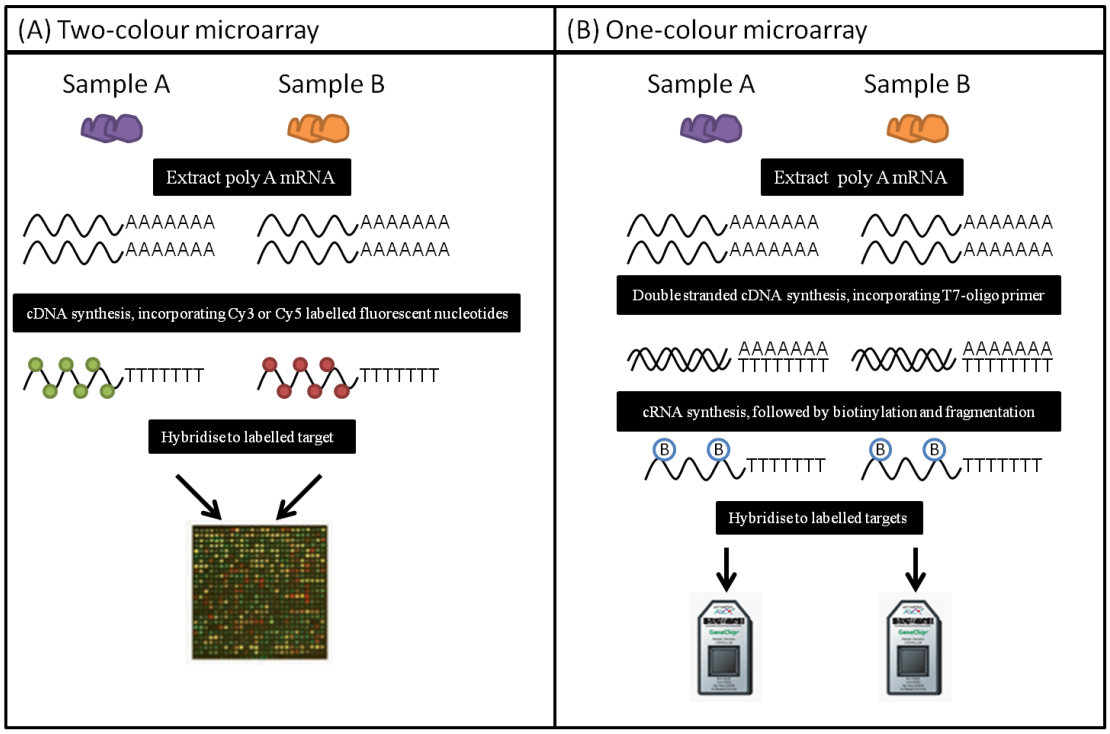

Figure A.1. Principle of DNA microarrays.

(A) Outline of two-colour microarray. In the two-colour microarray assay, mRNA is extracted from two different samples, e.g. sample A stands for control/healthy whereas sample B stands for treatment/disease. This mRNA is subsequently annealed into single-strand of complementary DNA (cDNA), and labelled with one of the suitable fluorescent molecules, e.g. Cy3 (green) and Cy5 (red). The relative transcript abundance is estimated from the Cy5/Cy3 ratio using confocal fluorescence scanning and image processing after this fluorescent-labelled cDNA from two different samples are hybridized to a single array. If the amounts of mRNA from two samples are the same, the scanning result is yellow. A red scanning result indicates that the amount of mRNA in the Cy5 labelled sample is higher than that of the Cy3 labelled one whereas a green scanning result suggests the opposite. (B) Outline of one-colour microarray. The principles of one-colour microarray assay are similar to those of the two-colour assay but the former measures the absolute intensity after hybridization. Therefore, two separate chips are required for a single experiment to represent two different samples, e.g. control/healthy and treatment/disease. The one-colour microarray procedure starts with extracting mRNA from the sample and subsequently synthesizing double stranded cDNA from this mRNA. After the biotin-labelled nucleotides are incorporated, this complementary RNA (cRNA) is fragmented and hybridized to a chip. A staining step is followed by a wash step, and the cRNA

fragments are conjugated with streptavidin fluorescent dye. An absolute intensity is obtained after the scanning step. Comparison between different samples, e.g. treated vs untreated or disease vs healthy, is measured by assaying the intensity of probes across chips.

Affymetrix (Santa Clara, CA) is a company that manufactures oligonucleotide microarrays, also called GeneChips. This high-density oligonucleotide expression array uses the length of 25 base pairs oligonucleotides to form a 'probe'. Because only a short region of target transcript will be formed by a probe, in order to ensure the gene specificity, around 11-20 probe pairs compose a 'probe set', which is used to present a transcript. In each probe pair, not only the interested mRNA, but also a perfect match (PM) and a mismatch probe (MM), which is designed to measure the non-specific binding by replacing the 13^{th} base of the PM probe, will be presented (Lipshutz *et al*., 1999; Lockhart *et al*., 1996). This thesis uses the Affymetrix GeneChip to analyse gene expression because it can assay the absolute gene expression value, instead of the relative value, which is obtained from a two-colour array assay.

A.2. Microarray data analysis

The intensity of scanning result is obtained from the fluorescent molecule after hybridisation onto Affymetrix GeneChips. It is assumed that the intensity of fluorescence is in proportion to the amount of cRNA that has bound to the corresponding probes on the array. Therefore, subtraction of fluorescence signals from the scanned image, which is stored in a file with suffix DAT by Affymetrix platform, is the first step to analyze microarray data by evaluating the pixels in each single probe, and this information will be stored in another file with suffix CEL (Arteaga-Salas *et al*., 2008).

After the image processing step, the intensities of PM and MM are recorded in the CEL file. In order to remove the background from non-specific bindings, the probe-level summarisation is processed. The summarisation step produces a single value to represent a probe set after summarising the probe level values. A normalisation step is followed to remove the systematic errors across different array experiments to ensure different probe sets and arrays are comparable. Some of the common algorithms for data summarisation and normalisation are: Microarray Suite (MAS) 4.0 (Affymetrix, 1999), MAS 5.0 (Affymetrix, 2003), the model-based expression index (MBEI; Li and Wong, 2001), the robust multi-array analysis (RMA; Irizarry *et al*., 2003), and the GeneChip robust multi-array analysis (GC-RMA; Wu *et al*., 2004). MAS 4.0 and MAS 5.0 assume the average difference (AD) intensity value of a probe pair between PM and MM is linear with its corresponding RNA amount. In a given probe set, arrays $i=1,\ldots,I$ and probe pairs $j=1,\ldots,J$, MAS 4.0 models the AD by using $PM_{ij} - MM_{ij} = \theta_i + \varepsilon_{ij}$, $j = 1,\ldots, J$. The expression θ_i

denotes the mean expression of the target probe set on array *i* with an probe-level error ε_{ij}, which is assumed to have equal variance. MAS 5.0 further adjusts this model by using Tukey biweight (Hoaglin *et al*., 2000) and log transformation (Hubbell *et al*., 2002) to reduce the noise from the subtraction of PM, such as the negative numbers that might result after subtraction MM from PM. These data summarisation still may not be able to remove the noise, especially at low intensity (Irizarry *et al*., 2003); Li and Wong (2001) took the probe-specific affinity into account and introduced MBEI.

Apart from those MM subtractive models, Irizarry *et al*. (2003) suggested a model, RMA, using the PM only to do the estimation. Non-specific binding is adjusted by introducing an additive background model. However, this global background adjustment model has a problem of a large false negative rate (Wu *et al*., 2004), especially at low expression level probes. GC-RMA is proposed by Wu *et al*. (2004), and considers the probe-specific GC content to weigh the MM and adjust the background.

To ensure the hybridisation of cRNA to the arrays has been sufficient. Several quality control steps can be carried out, e.g. rRNA ratio (28S/18S) and RNA integrity numbers (RIN) are used for RNA intactness assessment (Schroeder *et al*., 2006). RNA is degraded by ubiquitous RNase enzymes, and the RIN, which is scored from 1 to 10 where 10 refers to an intact RNA whereas 1 refers to the opposite, is used as a criterion to judge mRNA quality.

Gene curation is the next step in selecting differentially expressed genes. After a list of genes has been selected, the next step is to interpret these differentially regulated genes in terms of biological phenomena. Gene Ontology (GO) was proposed to annotate biological data, such as sequences, genes or gene products, with controlled

and structured vocabularies (Harris *et al*., 2004). Several tools have been proposed to use an automatic ontological analysis to help the functional analysis of high throughput experiments, such as Onto-Express, GoMiner, DAVID, EASEonline, GeneMerge, FuncAssociate, GOTM, FatiGO, CLENCH, GOstat, GOToolBOX, GoSurfer, Ontology Traverser, and eGOn (Khatri and Draghici, 2005). The ontological analysis can be performed by various statistical models, such as the hypergeometric (Cho *et al*., 2001b), the binomial, the χ^2 (chi-square), and the Fisher's exact test (Khatri and Draghici, 2005). Using a standard hypergeometric distribution, the probability of a random subset of x genes drawn from the total set of N genes will have y or more entities containing a given GO term can be estimated. However, if the threshold for statistical significance in a given experiment is α=0.05, we can expect to find a false positive for every 1 out of 20 tests. Thus thousands of genes may incur hundreds of false positive results. In order to correct the false positive rate, multiple testing corrections can be applied to adjust p-values derived from multiple statistical tests (Dudoit *et al*., 2003).

Appendix B. Method to analyze time scale physiological interactions in endocrine regulation systems

The dynamics of a physiologically endocrine regulation system can be presented in the following equation:

$$\frac{d}{dt}\mathbf{x} = \mathbf{f}(\mathbf{x}, \mathbf{u}), \tag{A1}$$

where **x** is the output of the system, **u** is the external input, and **f** is the system's dynamics. Output variables in **x** and input variables **u** are assumed to be non-dimensionalised, so the time t is the only unit bearing quantity in this system. The input $\mathbf{u}(t)$ is assumed to be a period function of time with period T. In this thesis, the system was decomposed into two distinct systems of lower dynamic dimension and these two systems may be studied independently of one another. The idea is to construct the slow dynamic that is specific to the fast-scale regime as a map, so that the characters of the dynamic affect the dynamics at the slow time scale can be kept.

In a physiological system, it is natural to have constrains on the rate of changes. Therefore, for each of the n state variables, the dynamics of x_i satisfies a finite positive number ξ_i

$$\left| f_i(\mathbf{x}, \mathbf{u}) \right| < \xi_i < +\infty, \tag{A2}$$

as **x** and **u** are the presentation of physiological associating values. Without loss of generality, the state variables can be ordered so that

$$\xi_1 \geq \xi_2 \geq \cdots \geq \xi_n > 0. \tag{A3}$$

Scaling of the f_i with respect to the corresponding ξ results in

$$\frac{d}{dt}\mathbf{x} = \boldsymbol{\xi} \cdot \mathbf{f}^*(\mathbf{x}, \mathbf{u}), \tag{A4}$$

where $\boldsymbol{\xi}$ is a diagonal matrix with the ξ_i on its main diagonal and f_i^* is a dimensionless quantity which satisfies $\left| f^* \right| \leq 1$. This thesis is going to discuss some of the variables are "rapid", i.e. oscillate on a time scale of order *T*, and others are "slow". So it is considered that $\xi_1 \geq T^{-1} >> \xi_n$ and assumed that there exists an $\nu \leq n$ such that $\xi_i T$ is a small parameter for $\nu \leq i \leq n$. Eqn (A5) represents the separation of time scales.

$$\mathbf{x}(t) = \mathbf{x}^{[0]}(\varphi(t), \tau(t)) + \mathbf{x}^{[1]}(\tau(t)), \tag{A5}$$

where $\mathbf{x}^{[0]}$ refers to the fast component depending on a fast time φ and a slow time τ, whereas $\mathbf{x}^{[1]}$ refers to the slow component depending on the slow time τ only. Eqn (A6) and (A7) define these two times.

$$\varphi = \frac{t}{T} + \left\lfloor \frac{t}{T} \right\rfloor, \tag{A6}$$

$$\tau = \xi_\nu T \left\lfloor \frac{t}{T} \right\rfloor, \tag{A7}$$

where $\lfloor x \rfloor$ denotes the largest integer smaller than or equal to *x*. The input is decomposed into Eqn (A8).

$$\mathbf{u}(t) = \mathbf{u}^{[0]}(\varphi(t), \tau(t)) + \mathbf{u}^{[1]}(\tau(t)). \tag{A8}$$

Eqn (A9) follows the fast dynamics so that the integration of this equation is from φ=0 to φ=1$^-$ subject to initial condition $\mathbf{x}^{[0]}$=**0** at φ=0.

$$\frac{\partial}{\partial \varphi}\mathbf{x}^{[0]} = T\, \boldsymbol{\xi} \cdot \mathbf{f}^*(\mathbf{x}^{[0]}, \mathbf{u}^{[0]}; \mathbf{x}^{[1]}, \mathbf{u}^{[1]}). \tag{A9}$$

Then define the following differential for $\eta \leq \xi_\nu T$ and $i = \nu, \ldots, n$:

$$dx_i^{[1]}(\tau,\eta) = T\xi_i \int_0^{\eta/(\xi_\nu T)} f^*(x^{[0]},u^{[0]};x^{[1]},u^{[1]})d\varphi. \qquad \text{(A10)}$$

Dividing Eqn (A10) by η and specifying for $\eta = \xi_\nu T$, this becomes:

$$\frac{dx_i^{[1]}(\tau,\eta)}{\xi_\nu T} = \frac{\xi_i}{\xi_\nu}\int_0^1 f^*(x^{[0]},u^{[0]};x^{[1]},u^{[1]})d\varphi, \qquad \text{(A11)}$$

for $i = 1,\ldots,\ n$. In the limit $\xi_\nu T \to 0$, the following expressions are exact:

$$\frac{d}{d\varphi}x_i^{[0]} = T\xi_i f^*(\mathbf{x}^{[0]},\mathbf{u}^{[0]};\mathbf{x}^{[1]},\mathbf{u}^{[1]}) \quad \text{for } i = 1,\ldots,\nu\text{-}1, \qquad \text{(A12)}$$

$$\frac{d}{d\tau}x_i^{[1]} = \frac{\xi_i}{\xi_\nu}\int_0^1(\mathbf{x}^{[0]},\mathbf{u}^{[0]};\mathbf{x}^{[1]},\mathbf{u}^{[1]})d\varphi \quad \text{for } i = \nu,\ldots,n, \qquad \text{(A13)}$$

where for $i \geq \nu$, it has $x_i^{[0]} \equiv 0$ and the operator $\partial/(\partial\varphi)$ has been replaced by without impunity since φ is restricted to the interval [0, 1]. If $x_{\nu+}^{[1]} = (x_\nu^{[1]},\ldots,x_n^{[1]})$ then for $i < \nu$, it follows that $x_i^{[1]} = X_i(x_{\nu+}^{[1]})$, where $(X_1(x_{\nu+}^{[1]}),\ldots,X_{\nu-1}(x_{\nu+}^{[1]}))$ is a parametrical representation of the slow manifold of the dynamics of the system. This slow manifold satisfies the condition that $x_i^{[0]}(0,\tau) = x_i^{[0]}(1,\tau)$ for all $i \in \{1,\nu-1\}$, which means that the fast variables move through a forced limit cycle of period *T*. The slow manifold can be varying in slow time τ.

Appendix C. Differentially expressed transcripts in M^+/E^- vs M^-/E^-

The full differentially expressed transcripts list of M^+/E^- vs M^-/E^- is given in this appendix.

Probe Set ID	Gene Symbol	Corrected p-value	Fold change ratio (Treatment/Control) at different time points				Ref_seq_id
			4	8	16	32	
1419238_at	Abca7	3.81E-03	-1.61	-2.71	-1.25	-2.80	NM_013850
1450721_at	Acp1	3.43E-03	1.27	1.39	2.05	1.31	NM_001110239 /// NM_021330
1435605_at	Actr3b	2.29E-03	3.44	2.70	1.71	2.93	NM_001004365
1435923_at	Ado	8.22E-03	1.91	1.61	1.64	2.05	NM_001005419
1418372_at	Adsl	6.36E-03	1.88	2.79	1.64	2.24	NM_009634
1434287_at	Agpat5	1.64E-03	3.27	2.41	2.67	2.05	NM_026792
1424712_at	Ahctf1	7.59E-03	2.80	1.37	1.10	2.95	NM_026375
1451459_at	Ahctf1	8.00E-03	3.51	1.45	1.95	2.98	NM_026375
1441320_a_at	AI413194	4.52E-03	-1.15	-2.39	-1.92	-2.75	
1434266_at	AI847670	3.20E-03	2.18	2.67	2.18	2.09	NM_177869
1448450_at	Ak2 /// LOC100047005	1.28E-03	2.74	2.98	1.17	1.81	NM_001033966 /// NM_016895 /// XM_001477790
1450387_s_at	Ak3l1 /// LOC100047616	1.76E-03	4.00	4.81	-1.11	4.98	NM_009647 /// XM_001478522
1433669_at	Akap8	8.65E-03	2.76	2.04	-1.15	1.50	NM_019774
1437133_x_at	Akr1b3	2.40E-03	2.50	2.50	-1.07	2.11	NM_009658
1456590_x_at	Akr1b3	7.09E-04	2.41	1.96	1.38	2.62	NM_009658
1434721_at	Ankle2	1.95E-03	-1.82	-2.20	-2.34	-2.38	NM_027922
1437217_at	Ankrd6	2.13E-03	9.13	2.55	1.39	8.49	NM_001012450 /// NM_001012451 /// NM_080471
1434555_at	Anp32a	4.79E-03	2.21	1.59	1.01	1.57	NM_009672
1451703_s_at	Aprt	4.63E-03	1.62	1.74	2.23	2.18	NM_009698
1425914_a_at	Armcx1	1.49E-03	-2.93	-4.29	-1.44	-3.65	NM_030066
1422609_at	Arpp19	4.60E-03	1.96	2.89	1.94	2.44	NM_001142655 /// NM_021548
1422461_at	Atad3a	7.46E-04	3.29	2.38	1.93	2.69	NM_179203
1437343_x_at	Atad3a	6.05E-04	4.70	3.90	1.57	2.23	NM_179203
1438178_x_at	Atad3a	3.87E-04	3.97	4.07	1.24	2.35	NM_179203
1427197_at	Atr	6.05E-04	2.57	4.41	1.58	2.96	NM_019864
1433663_s_at	AU014645	6.74E-03	2.52	1.34	1.40	1.64	NM_001033201
1424546_at	BC003965	8.70E-03	3.18	1.27	1.25	1.46	XM_128528 /// XM_914663
1451541_at	Bcs1l	8.55E-03	1.98	2.00	3.68	2.03	NM_025784
1438961_s_at	Blmh	6.64E-03	2.27	3.85	-1.00	1.47	NM_178645
1447679_s_at	Bms1	6.69E-04	1.89	2.05	1.08	1.37	NM_194339
1434543_a_at	Bola2	1.53E-03	1.70	2.97	2.01	1.33	NM_175103
1434545_x_at	Bola2	2.64E-03	1.57	2.42	2.71	1.71	NM_175103
1423264_at	Bop1	7.70E-03	2.86	3.94	2.50	4.55	NM_013481
1419046_at	Brp16	3.68E-03	2.87	3.13	1.59	2.55	NM_021555
1456738_s_at	Brp16	1.52E-03	3.17	3.67	-1.01	2.34	NM_021555
1450742_at	Bysl	5.04E-03	2.17	2.94	1.58	1.81	NM_016859
1423456_at	Bzw2	7.56E-04	6.42	2.83	3.88	6.86	NM_025840
1439027_at	C330023M02Rik	2.64E-03	2.26	2.45	-1.07	1.65	NM_172722
1440910_at	C77370	5.87E-03	3.97	3.37	1.29	2.50	NM_001077354
1424533_a_at	Ccdc137	1.38E-03	4.77	2.21	-1.13	3.01	NM_152807
1459840_s_at	Ccdc28b	1.62E-03	-2.76	-2.25	-2.25	-3.47	NM_025455
1417910_at	Ccna2	9.67E-04	-1.08	4.82	11.07	3.21	NM_009828

1448205_at	Ccnb1	2.37E-03	1.09	3.82	9.56	3.63	NM_172301
1416492_at	Ccne1	1.76E-03	2.10	4.16	5.80	1.28	NM_007633
1441910_x_at	Ccne1	2.08E-03	1.93	8.88	1.74	1.60	NM_007633
1422535_at	Ccne2	4.52E-03	2.17	8.20	6.32	5.70	NM_001037134 /// NM_009830
1417131_at	Cdc25a	4.22E-03	2.55	2.19	1.49	3.07	NM_007658
1417132_at	Cdc25a	7.24E-03	2.29	2.07	1.24	1.76	NM_007658
1452040_a_at	Cdca3	5.88E-03	-1.08	1.05	5.51	1.10	NM_013538
1416802_a_at	Cdca5	5.65E-03	-1.42	22.18	21.74	8.58	NM_026410
1449152_at	Cdkn2b	1.34E-04	-2.39	-2.21	-1.56	-2.39	NM_007670
1424143_a_at	Cdt1	6.36E-03	5.79	24.94	11.12	6.83	NM_026014
1418264_at	Cenpk	5.88E-03	1.14	7.33	15.96	3.49	NM_021790 /// NM_181061
1436034_at	Cep68	3.62E-03	2.73	2.38	-1.22	2.49	NM_172260
1456325_at	Cep68	7.28E-03	1.75	1.81	-1.14	2.30	NM_172260
1417233_at	Chchd4	5.35E-03	1.81	2.04	1.50	2.29	NM_133928
1449708_s_at	Chek1	5.87E-03	2.69	6.39	4.48	4.69	NM_007691
1423884_at	Cirh1a	7.56E-04	2.95	1.98	1.69	4.26	NM_011574
1416698_a_at	Cks1b	9.27E-04	1.52	3.58	3.15	2.45	NM_016904
1417457_at	Cks2	7.14E-03	-1.24	3.77	8.09	6.65	NM_025415
1434866_x_at	Cpt1a	3.38E-03	-1.60	-2.59	-2.42	-1.45	NM_013495
1415948_at	Creg1	3.87E-03	2.13	2.39	1.48	1.79	NM_011804
1435800_a_at	Csda	1.04E-03	2.51	2.14	1.37	2.72	NM_011733 /// NM_139117
1451012_a_at	Csda	3.59E-03	4.95	2.28	2.39	5.30	NM_011733 /// NM_139117
1448809_at	Cse1l	2.72E-03	1.98	2.93	2.48	2.24	NM_023565
1419645_at	Cstf2	3.85E-03	2.09	1.94	1.54	2.45	NM_133196
1416563_at	Ctps	2.89E-04	2.66	3.35	1.97	2.17	NM_016748
1422484_at	Cycs	5.16E-03	1.29	2.15	1.54	2.02	NM_007808
1417071_s_at	Cyp4v3	6.30E-04	-1.12	-3.00	-2.28	-2.50	NM_133969
1454659_at	Dctd	5.58E-05	4.60	3.06	2.33	4.08	NM_178788
1448271_a_at	Ddx21	7.73E-03	1.91	1.83	-1.03	2.00	NM_019553
1448619_at	Dhcr7	5.69E-03	2.57	3.10	1.13	1.51	NM_007856
1428267_at	Dhx40	6.36E-03	-2.04	-2.19	1.64	-2.12	NM_026191
1426609_at	Dis3	4.06E-03	3.54	2.58	1.90	4.32	NM_028315
1426265_x_at	Dlat	8.21E-03	1.03	2.28	1.69	2.60	NM_145614
1417182_at	Dnaja2	8.55E-03	2.10	2.02	1.50	1.44	NM_019794
1433880_at	Dnajc11	2.94E-03	3.00	2.17	1.34	2.54	NM_172704
1428087_at	Dnm1l	5.35E-03	1.82	1.75	1.21	3.76	NM_001025947 /// NM_152816
1459973_x_at	Dpp4	6.36E-03	-1.21	-1.98	-2.71	-4.33	NM_001159543 /// NM_010074
1423767_at	Dpy30	8.15E-03	1.17	1.94	2.18	2.00	NM_001146222 /// NM_001146223 /// NM_001146224 /// NM_024428
1436301_at	Dstyk	6.89E-03	-1.50	-3.23	-1.04	-3.14	NM_172516
1424697_at	Dtwd1	2.29E-03	3.51	1.62	1.74	2.57	NM_026981
1435734_x_at	Dus1l	2.64E-03	3.03	2.54	-1.08	1.25	NM_026824
1424229_at	Dyrk3	1.62E-03	1.80	1.21	4.53	2.77	NM_145508
1454963_at	E430028B21Rik	7.70E-03	2.85	3.28	1.30	3.07	NM_178668
1440338_at	E430028B21Rik	9.02E-03	1.97	1.38	1.11	2.02	NM_178668
1449044_at	Eef1e1	7.46E-04	3.26	2.75	5.25	8.83	NM_025380
1437829_s_at	Eef2k	2.13E-03	3.26	3.26	-1.52	2.42	NM_007908
1456107_x_at	Eftud2	1.20E-03	2.24	3.14	1.02	1.96	NM_001109995 /// NM_011431
1416021_a_at	EG620603 /// Fabp5	5.04E-03	3.64	2.87	1.81	4.34	NM_010634 /// XR_031387
1424343_a_at	Eif1a	7.91E-03	1.28	1.63	2.21	1.51	NM_010120
1424344_s_at	Eif1a	7.09E-04	1.92	3.30	1.35	1.84	NM_010120
1426394_at	Eif3j	5.78E-03	1.93	1.85	1.74	2.69	NM_144545
1426395_s_at	Eif3j	2.73E-03	1.58	1.85	1.56	2.85	NM_144545
1423220_at	Eif4e	4.57E-04	2.86	2.75	1.54	2.11	NM_007917 /// XM_001004193
1450908_at	Eif4e	2.73E-03	1.95	2.84	2.07	4.23	NM_007917 /// XM_001004193
1435803_a_at	Eif4e2	8.87E-03	1.50	2.15	1.40	1.62	NM_001039169 /// NM_001039170 /// NM_023314
1434976_x_at	Eif4ebp1	1.65E-03	3.47	3.78	1.25	2.12	NM_007918
1428477_at	Elac2	5.54E-03	3.18	1.32	1.12	2.14	NM_023479
1417403_at	Elovl6	6.94E-05	3.10	4.60	2.47	5.50	NM_130450
1417404_at	Elovl6	5.41E-05	3.49	3.28	2.74	2.99	NM_130450

1421097_at	Endog	1.07E-03	2.79	3.90	1.74	2.44	NM_007931
1438317_a_at	Endog	1.03E-03	2.79	3.74	1.27	1.68	NM_007931
1450380_at	Epdr1	3.87E-04	2.47	2.35	2.89	5.04	NM_134065
1420024_s_at	Etf1	3.06E-03	2.16	2.73	1.16	1.66	NM_144866
1452012_a_at	Exosc1	1.62E-03	2.72	2.68	1.18	2.60	NM_025644
1435544_at	Exosc6	2.81E-03	3.18	5.31	1.36	3.43	NM_028274
1435076_at	Fam57a	5.60E-05	2.91	2.42	1.66	2.80	NM_027773
1423828_at	Fasn	4.63E-03	2.62	3.52	1.98	2.28	NM_007988
1435369_at	Fastkd5	5.07E-03	2.16	3.19	1.73	2.37	NM_001146084 /// NM_198176
1419577_at	Fig4	6.60E-05	4.28	3.52	1.35	6.03	NM_133999
1438953_at	Figf /// LOC100047108	2.64E-03	-1.01	-2.51	-1.01	-1.01	NM_010216 /// XM_001477393
1438167_x_at	Flcn	4.66E-03	-2.11	-2.58	-1.08	-2.06	NM_146018
1422801_at	G3bp1	2.70E-03	1.62	2.00	1.30	1.78	NM_013716
1441911_x_at	Gart	5.42E-03	1.97	2.37	1.29	2.31	NM_010256
1432164_a_at	Gcsh	1.51E-03	2.24	1.65	1.43	1.57	NM_026572
1424300_at	Gemin6	1.62E-03	1.78	2.20	5.22	2.23	NM_026053
1451400_at	Gemin8	5.69E-03	2.02	1.95	1.78	2.04	NM_146238
1435245_at	Gls2	1.87E-05	9.89	6.97	5.23	5.61	NM_001033264
1428784_at	Gmip	9.02E-03	9.99	5.18	-1.47	10.74	NM_198101
1439489_at	Gpr120	6.95E-04	4.97	2.28	2.11	3.21	NM_181748
1455841_s_at	Grwd1	3.75E-03	3.56	2.42	-1.15	2.12	NM_153419
1448704_s_at	H47	7.54E-03	-1.74	-1.29	1.01	-2.29	NM_024439
1438510_a_at	Hars	6.89E-03	1.53	2.02	1.16	1.48	NM_008214
1428823_at	Hddc2	2.23E-03	1.94	2.01	1.54	1.53	NM_027168
1419964_s_at	Hdgf	2.48E-03	1.66	1.82	2.07	2.08	NM_008231
1436050_x_at	Hes6	8.87E-03	3.11	2.26	-1.02	3.01	NM_019479
1416101_a_at	Hist1h1c	5.63E-03	-1.78	-3.16	-1.17	-1.80	NM_015786
1434736_at	Hlf	1.51E-03	3.37	3.66	-1.15	3.49	NM_172563
1416184_s_at	Hmga1	5.16E-03	2.73	3.09	1.99	3.98	NM_001025427 /// NM_001039356 /// NM_016660
1450156_a_at	Hmmr	3.39E-05	-1.11	1.02	8.41	-1.06	NM_013552
1438988_x_at	Hn1	2.89E-04	4.29	3.72	1.13	2.77	NM_008258
1448180_a_at	Hn1	3.42E-03	5.35	5.96	2.57	4.82	NM_008258
1431349_at	Hnrnpab	4.26E-03	2.10	1.89	1.93	1.34	NM_001048061 /// NM_010448
1455120_at	Hpdl	1.84E-03	2.86	2.23	1.04	4.30	NM_146256
1450047_at	Hs6st2	7.82E-03	1.20	1.54	2.44	3.25	NM_001077202 /// NM_015819
1434642_at	Hsd17b11	6.95E-04	-1.83	-2.09	-1.54	-2.02	NM_053262
1416968_a_at	Hsd3b7	1.62E-03	2.57	3.12	1.19	2.93	NM_001040684 /// NM_133943
1426351_at	Hspd1	7.32E-03	1.31	1.84	2.45	2.63	NM_010477
1426705_s_at	Iars	6.21E-03	1.62	1.28	2.01	1.42	NM_172015
1435140_at	Ide	5.16E-04	2.21	2.09	1.83	1.80	NM_031156
1422501_s_at	Idh3a	8.09E-03	1.54	1.66	1.87	2.22	NM_029573
1432016_a_at	Idh3a	2.73E-03	1.38	1.66	2.11	2.96	NM_029573
1451775_s_at	Il13ra1	8.35E-03	1.96	-1.03	1.38	2.66	NM_133990
1453784_at	Ilkap	7.09E-04	1.15	1.13	2.20	1.27	NM_023343
1426213_at	Imp4	2.37E-03	2.77	2.90	2.16	2.94	NM_178601
1426858_at	Inhbb /// LOC100046802	7.70E-03	-1.01	-1.01	4.05	-1.06	NM_008381 /// XM_001476835
1456200_at	Ipmk	2.29E-03	3.31	1.16	1.66	1.53	NM_027184
1426946_at	Ipo5	6.33E-03	2.68	2.61	2.78	4.82	NM_023579
1450084_s_at	Ivns1abp	6.16E-03	2.06	1.98	1.47	1.42	NM_001039511 /// NM_001039512 /// NM_054102
1460676_at	Josd1	1.31E-04	3.70	2.97	1.66	3.08	NM_028792
1457587_at	Kcnq5	3.85E-03	4.60	4.82	-1.05	7.23	NM_001160139 /// NM_023872
1434154_at	Kctd13	5.42E-03	1.39	1.26	1.10	2.56	NM_172747
1449379_at	Kdr	7.70E-03	-2.26	-1.82	-2.72	-2.20	NM_010612
1450386_at	Kpna3	5.28E-03	1.35	3.25	2.04	1.80	NM_008466
1448526_at	Kpnb1	8.89E-03	1.36	2.41	1.84	1.25	NM_008379
1455434_a_at	Ktn1	1.94E-03	3.37	1.51	2.11	3.28	NM_008477
1438633_x_at	Lasp1	1.41E-03	-2.71	-2.55	-1.34	-1.53	NM_010688
1438634_x_at	Lasp1	1.41E-03	-2.83	-2.38	-1.56	-2.14	NM_010688
1455470_x_at	Lasp1	8.22E-03	-3.22	-2.40	-1.37	-1.48	NM_010688
1456309_x_at	Lasp1	9.21E-03	-2.52	-1.41	-1.32	-1.49	NM_010688
1438977_x_at	LOC100045999 /// Ran	4.91E-03	1.50	1.34	1.51	2.07	NM_009391 /// XM_001475422

1452226_at	LOC100047340 /// Rcc2	5.88E-03	2.87	2.62	-1.02	8.23	NM_173867 /// XM_001477942
1433842_at	Lrrfip1	2.73E-03	4.45	4.11	1.01	4.45	NM_001111311 /// NM_001111312 /// NM_008515
1432431_s_at	Macrod2	7.18E-03	1.33	1.70	2.15	2.30	NM_001013802 /// NM_028387
1415928_a_at	Map1lc3b	3.31E-04	-1.72	-2.15	-1.16	-1.36	NM_026160
1452798_s_at	Mapk1ip1	8.57E-03	-1.74	-2.06	-1.25	-1.24	NM_001045483 /// NM_027115
1433576_at	Mat2a	5.42E-03	3.21	2.98	-1.44	2.05	NM_145569
1438386_x_at	Mat2a	2.93E-03	2.17	1.81	-1.24	1.79	NM_145569
1438630_x_at	Mat2a	6.95E-04	2.49	2.50	-1.22	1.87	NM_145569
1438976_x_at	Mat2a	5.16E-04	2.58	2.64	-1.25	1.85	NM_145569
1456702_x_at	Mat2a	1.62E-03	2.57	2.07	-1.19	1.93	NM_145569
1434079_s_at	Mcm2	1.66E-03	1.84	4.18	2.56	3.05	NM_008564
1436708_x_at	Mcm4	4.85E-03	2.10	8.25	1.43	2.69	NM_008565
1436808_x_at	Mcm5	7.63E-03	4.34	28.35	2.00	9.02	NM_008566
1438320_s_at	Mcm7	1.62E-03	2.81	5.93	3.11	3.61	NM_008568
1439269_x_at	Mcm7	1.45E-03	2.40	7.40	2.73	3.72	NM_008568
1429911_at	Mcph1	8.65E-03	2.71	2.60	1.67	2.24	NM_173189
1460050_x_at	Mettl13	3.87E-04	3.17	1.97	-1.02	2.38	NM_144877
1455529_at	Mex3a	7.39E-03	1.51	2.64	1.02	1.45	NM_001029890
1424001_at	Mki67ip	3.52E-03	2.23	1.80	1.72	2.80	NM_026472
1416313_at	Mllt11	5.14E-03	2.32	3.06	2.46	3.38	NM_019914
1435232_x_at	Mrpl15	2.31E-03	2.20	1.97	1.67	2.90	NM_025300
1416349_at	Mrpl34	2.73E-03	2.39	2.00	1.99	3.07	NM_053162
1449194_at	Mrps25	1.84E-03	1.77	2.56	1.26	1.55	NM_025578
1433878_at	Mrps26	1.76E-03	1.97	2.01	2.54	1.81	NM_207207
1427158_at	Mrps30	7.09E-04	2.13	1.91	1.25	2.80	NM_021556
1424425_a_at	Mtap	1.04E-04	3.17	3.38	1.26	2.74	NM_024433
1424426_at	Mtap	1.10E-03	6.30	5.80	1.24	3.51	NM_024433
1451346_at	Mtap	1.62E-03	3.05	2.91	1.33	3.78	NM_024433
1456653_a_at	Mthfd1l	2.47E-03	3.16	1.45	1.62	4.59	NM_172308
1434278_at	Mtm1	3.83E-04	5.67	9.10	3.98	8.94	NM_019926
1452110_at	Mtrr	8.02E-04	4.28	5.67	1.77	2.59	NM_172480
1450376_at	Mxi1	2.93E-03	2.36	1.42	2.52	4.78	NM_001008542 /// NM_001008543 /// NM_010847
1449072_a_at	N6amt2	1.15E-03	1.28	2.13	1.98	1.74	NM_026526
1452192_at	Naf1	5.58E-05	5.70	4.67	1.65	4.73	XR_032374 /// XR_032626
1420477_at	Nap1l1	4.44E-03	1.90	1.68	2.20	1.68	NM_001146707 /// NM_015781
1436707_x_at	Ncaph	6.21E-03	-2.35	7.60	20.88	3.76	NM_144818
1415772_at	Ncl	1.86E-04	2.70	3.47	1.38	1.76	NM_010880
1433205_at	Ndfip2	6.96E-03	1.09	-2.50	-1.03	-1.03	NM_029561
1427997_at	Ndufaf4	3.69E-04	2.33	2.26	1.12	2.39	NM_026742
1416972_at	Nhp2l1	7.56E-04	2.31	2.37	1.70	1.88	NM_011482
1416973_at	Nhp2l1	2.91E-03	1.91	2.11	2.05	1.76	NM_011482
1437238_x_at	Nmd3	1.41E-04	2.24	1.84	2.06	3.77	NM_133787
1430530_s_at	Nmral1	4.04E-03	2.36	4.58	4.56	3.57	NM_026393
1438095_x_at	Noc4l	9.67E-03	2.86	3.35	1.25	2.49	NM_153570
1443794_x_at	Noc4l	7.54E-03	2.76	2.38	1.20	2.38	NM_153570
1428870_at	Nolc1	2.12E-03	4.89	3.42	2.01	4.16	NM_001039351 /// NM_001039352 /// NM_001039353 /// NM_053086
1424620_at	Nop16	8.86E-04	3.20	2.31	1.95	6.32	NM_178605
1424019_at	Nop2	3.46E-03	1.90	2.39	1.27	2.52	NM_138747
1426533_at	Nop56	3.88E-03	2.06	4.74	1.66	3.90	NM_024193
1455035_s_at	Nop56	1.34E-04	3.19	3.14	2.89	2.52	NM_024193
1423850_at	Nsun2	5.88E-03	3.12	1.72	5.57	3.32	NM_145354
1434216_a_at	Nudt19	1.18E-03	3.20	2.58	1.42	3.00	NM_033080
1448651_at	Nudt5	5.88E-03	1.55	1.88	2.37	3.16	NM_016918
1450111_a_at	Nudt8	7.18E-03	1.75	1.95	2.13	2.47	NM_025529
1438951_x_at	Nup54	1.62E-03	1.87	3.51	1.27	1.65	NM_183392
1416073_a_at	Nup85	7.09E-04	3.33	6.81	4.49	5.34	NM_001002929
1437520_a_at	Nup85	1.11E-04	3.13	6.64	1.61	2.42	NM_001002929
1449017_at	Nutf2	4.31E-03	1.51	1.50	2.04	1.30	NM_026532
1427364_a_at	Odc1	1.27E-03	1.99	2.93	1.29	1.78	NM_013614
1418225_at	Orc2l	3.06E-03	2.28	2.01	1.33	2.31	NM_001025378 /// NM_008765

1417037_at	Orc6l	9.78E-03	2.17	2.22	1.98	2.66	NM_019716
1420142_s_at	Pa2g4	4.79E-03	2.30	6.21	1.33	1.57	NM_011119
1450854_at	Pa2g4	1.66E-03	2.34	4.59	2.06	1.97	NM_011119
1423564_a_at	Paics	5.16E-03	1.57	1.38	2.40	2.45	NM_025939
1423766_at	Pak1ip1	2.18E-03	2.40	1.45	1.35	2.02	NM_026550
1421989_s_at	Papss2	3.47E-03	-2.29	-5.58	-1.02	-4.27	NM_011864
1434510_at	Papss2	8.17E-03	-1.85	-9.15	1.17	-3.70	NM_011864
1448627_s_at	Pbk	2.40E-03	-1.30	4.18	18.83	3.28	NM_023209
1424081_at	Pcgf6	8.02E-05	2.35	2.28	2.40	2.42	NM_027654
1426981_at	Pcsk6	6.62E-04	2.59	1.94	5.45	4.84	XM_355911 /// XM_886136 /// XM_905687 /// XM_919493
1423747_a_at	Pdk1	8.82E-06	4.74	4.40	2.45	5.13	NM_172665
1423748_at	Pdk1	7.09E-04	5.64	6.35	4.16	6.23	NM_172665
1435836_at	Pdk1	7.08E-04	3.28	2.66	1.76	3.01	NM_172665
1428309_s_at	Pdrg1	6.72E-03	2.15	3.12	1.37	1.82	NM_178939
1427929_a_at	Pdxk	2.59E-03	2.38	1.89	1.05	1.43	NM_172134
1435440_at	Pdzd8	7.09E-04	3.28	1.94	1.12	2.45	NM_001033222
1435562_at	Pdzd8	7.09E-04	4.33	5.99	1.71	2.21	NM_001033222
1439088_at	Pdzd8	2.91E-03	2.34	2.27	1.22	2.81	NM_001033222
1425042_s_at	Pelp1	6.36E-03	1.74	2.36	1.20	1.79	NM_029231
1455496_at	Pfas	3.80E-03	4.32	3.65	2.65	7.32	NM_001159519 /// XM_111232 /// XM_908501
1426554_a_at	Pgam1	5.16E-04	1.77	1.83	1.72	2.16	NM_023418
1428080_at	Pgam5	8.12E-04	2.43	2.68	2.01	3.78	NM_028273
1452919_a_at	Pgp	3.31E-03	1.90	2.37	1.63	1.79	NM_025954
1416202_at	Phb2	2.09E-03	3.12	2.51	2.62	2.94	NM_007531
1438938_x_at	Phb2	5.96E-07	2.94	2.89	1.43	2.52	NM_007531
1455713_x_at	Phb2	5.58E-05	3.12	4.18	2.01	2.10	NM_007531
1454862_at	Phldb2	5.63E-03	-1.65	-1.75	-1.44	-2.63	NM_153412
1452676_a_at	Pnpt1	1.91E-03	2.27	2.88	1.53	2.71	NM_027869
1448277_at	Pold2	8.55E-03	3.10	4.32	3.17	3.41	NM_008894
1416126_at	Polr1b	3.30E-03	4.49	1.78	1.60	3.95	NM_009086
1435057_x_at	Polr1e	8.77E-04	2.74	2.00	-1.02	2.58	NM_022811
1449155_at	Polr3g	1.11E-04	4.71	3.09	1.76	5.99	NM_001081176
1424227_at	Polr3h	6.69E-04	2.84	3.86	2.00	2.77	NM_030229
1439266_a_at	Polr3k	1.65E-03	1.57	2.42	1.86	1.56	NM_025901
1452831_s_at	Ppat	5.87E-03	2.65	3.69	1.49	1.55	XM_001002879 /// XM_001002886 /// XM_896000 /// XM_924520 /// XM_973937 /// XM_973973
1418369_at	Prim1	4.37E-03	1.37	4.55	6.60	3.36	NM_008921
1449061_a_at	Prim1	1.11E-04	1.50	4.82	4.72	3.25	NM_008921
1428783_at	Prkar2a	3.87E-04	3.29	3.24	1.31	2.76	NM_008924
1452915_at	Prkar2a	2.98E-03	2.85	3.11	1.47	2.36	NM_008924
1417425_at	Prkrip1	6.69E-04	1.88	2.67	1.31	1.78	NM_025774
1416844_at	Prmt2	6.02E-04	-1.94	-2.95	-1.06	-1.72	NM_001077638 /// NM_133182
1437234_x_at	Prmt2	1.28E-03	-3.13	-4.03	-1.51	-2.69	NM_001077638 /// NM_133182
1454789_x_at	Prpf6	3.66E-03	-1.24	-1.45	-1.69	-2.60	NM_133701
1451064_a_at	Psat1	1.03E-03	5.57	11.92	4.08	8.53	NM_177420
1454607_s_at	Psat1	8.33E-04	3.53	4.98	3.91	6.60	NM_177420
1428853_at	Ptch1	8.35E-03	2.18	1.56	1.24	1.65	NM_008957
1450344_a_at	Ptger3	6.21E-03	10.97	5.48	-1.36	10.49	NM_011196
1451845_a_at	Ptrh2	6.36E-03	1.70	1.20	2.24	3.97	NM_001098810 /// NM_175004
1428800_a_at	Pus7l	8.46E-04	3.41	3.84	-1.10	3.54	NM_172437
1460447_at	Pus7l	4.72E-04	2.73	5.25	1.29	2.75	NM_172437
1424193_at	Pwp2	5.14E-03	2.68	3.03	-1.33	2.31	NM_029546
1433947_at	Rab37	7.56E-04	-2.49	-6.53	-1.33	-7.12	NM_021411
1418281_at	Rad51	8.22E-03	1.09	4.62	9.60	1.58	NM_011234
1417938_at	Rad51ap1	3.22E-03	1.29	7.28	6.77	7.52	NM_009013
1460551_at	Ran	1.80E-03	2.00	2.13	2.21	2.83	NM_009391
1423749_s_at	Rangap1	8.09E-03	1.80	1.75	2.34	2.04	NM_001146174 /// NM_011241
1448740_at	Rangrf	2.80E-03	2.13	1.69	1.77	2.04	NM_021329
1427344_s_at	Rasd2	8.35E-03	7.09	5.34	1.72	5.75	NM_029182 /// XM_204287 /// XM_905295
1439622_at	Rassf4	7.70E-03	-2.18	-3.70	-1.85	-1.88	NM_178045

1444009_at	Rassf4	7.62E-03	-2.02	-1.31	-1.75	-2.42	NM_178045
1452091_a_at	Rbm28	1.38E-03	2.88	2.27	1.28	4.10	NM_026650 /// NM_133925
1438161_s_at	Rfc4	4.47E-03	1.16	10.82	3.13	4.65	NM_145480
1451516_at	Rhebl1	3.06E-03	4.53	2.87	1.94	2.79	NM_026967
1447818_x_at	Rhebl1	1.33E-04	3.43	4.73	1.24	1.83	NM_026967
1419460_at	Rpp14	2.17E-04	2.94	3.09	2.00	2.42	NM_025938 /// XM_001471720
1419461_at	Rpp14	8.33E-04	2.72	3.61	2.10	3.68	NM_025938 /// XM_001471720
1424792_at	Rpp40	4.32E-03	3.19	2.43	1.12	3.05	NM_145938
1455174_at	Rps19bp1	3.75E-03	1.80	2.50	1.44	2.43	NM_175109
1423254_x_at	Rps27l	3.39E-03	1.27	1.78	2.58	2.41	NM_026467
1450925_a_at	Rps27l	5.35E-03	1.27	1.74	2.12	2.29	NM_026467
1415878_at	Rrm1	2.81E-03	1.09	6.36	6.77	2.32	NM_009103
1456117_at	Rrp1b	2.12E-03	3.71	5.12	-1.19	4.06	NM_028244
1456383_at	Rsl1d1	3.98E-03	2.50	2.38	1.17	3.56	NM_025546
1452649_at	Rtn4	2.81E-03	-1.83	-2.23	1.12	-1.67	NM_024226 /// NM_194051 /// NM_194052 /// NM_194053 /// NM_194054
1437991_x_at	Rusc1	6.44E-04	-2.03	-1.94	-2.46	-5.23	NM_001083807 /// NM_001083808 /// NM_028188
1437279_x_at	Sdc1	4.60E-03	1.69	6.31	-1.12	5.00	NM_011519
1426853_at	Set	1.33E-04	2.37	3.52	-1.02	1.46	NM_023871
1428797_at	Setd6	1.78E-03	1.89	2.27	2.94	2.52	NM_001035123
1424619_at	Sf3b4	7.62E-03	1.44	1.40	-1.20	2.06	NM_153053
1428100_at	Sfrs1	7.56E-04	3.47	2.65	-1.25	2.85	NM_001078167 /// NM_173374
1416151_at	Sfrs3	7.56E-04	2.34	2.21	1.81	1.81	NM_013663
1437370_at	Sgol2	1.20E-03	1.02	1.11	3.87	1.14	NM_199007
1425178_s_at	Shmt1	6.60E-03	1.16	3.00	1.03	1.52	NM_009171
1415802_at	Slc16a1	2.12E-03	10.37	9.98	1.60	6.76	NM_009196
1420138_at	Slc19a1	4.26E-03	4.38	4.25	1.53	3.02	NM_031196
1448132_at	Slc19a1	7.56E-04	4.97	2.86	2.00	6.22	NM_031196
1424211_at	Slc25a33	9.45E-03	2.82	2.26	-1.22	1.98	NM_027460
1447748_x_at	Slc29a2	4.72E-03	2.62	1.51	-1.06	1.32	NM_007854
1434015_at	Slc2a6	5.16E-04	3.55	6.09	2.11	2.66	NM_172659
1436164_at	Slc30a1	7.09E-04	2.06	1.35	3.12	2.23	NM_009579
1417042_at	Slc37a4	7.45E-03	2.71	2.00	3.72	2.41	NM_008063
1433751_at	Slc39a10	1.84E-03	2.65	3.37	-1.13	8.51	NM_172653
1426712_at	Slc6a15	3.06E-03	6.94	3.06	1.44	7.96	NM_175328 /// XR_035425 /// XR_035434
1454991_at	Slc7a1	3.82E-03	3.93	2.12	1.94	3.05	NM_007513
1448321_at	Smoc1	4.31E-03	3.63	3.58	3.09	3.63	NM_001146217 /// NM_022316
1417300_at	Smpdl3b	5.96E-07	5.08	8.81	5.39	15.15	NM_133888
1451722_s_at	Smyd5	2.06E-03	4.46	2.41	1.22	4.93	NM_144918
1455552_at	Snapc4	3.17E-03	3.44	2.17	1.18	3.95	NM_172339
1452680_at	Snrpd2	8.55E-03	1.30	1.26	2.02	1.55	NM_026943
1438844_x_at	Spata5	3.46E-03	1.69	2.00	1.09	2.00	NM_021343
1431087_at	Spc24	7.45E-03	-1.42	2.99	14.46	1.42	NM_026282
1454962_at	Spire1	6.61E-03	2.56	2.01	1.98	8.95	NM_176832 /// NM_194355
1454042_a_at	Srpk1	5.88E-03	1.96	2.22	1.30	1.71	NM_016795
1417725_a_at	Sssca1	6.60E-05	6.78	5.85	1.52	4.73	NM_020491
1420928_at	St6gal1	9.27E-04	-1.76	-1.90	-1.41	-2.70	NM_145933
1418074_at	St6galnac4	1.34E-04	4.77	5.72	1.02	4.16	NM_011373
1418075_at	St6galnac4	5.97E-03	4.39	4.14	2.36	5.06	NM_011373
1415849_s_at	Stmn1	7.45E-03	-1.57	3.11	4.91	1.87	NM_019641
1419912_s_at	Strap	2.41E-03	2.28	1.93	1.74	1.94	NM_011499
1418089_at	Stx8	9.27E-04	2.41	2.28	2.02	2.43	NM_018768
1429711_at	Styx	7.87E-04	3.95	4.27	1.02	2.34	NM_019637
1428546_at	Syncrip	2.37E-03	2.96	1.62	1.65	1.97	NM_019666 /// NM_019796
1423483_s_at	Taf1c	6.05E-04	4.02	2.78	-1.22	1.76	NM_021441
1435302_at	Taf4b	1.45E-03	4.07	2.74	1.20	4.97	NM_001100449 /// XM_128905 /// XM_911701
1451509_at	Taf9	2.31E-03	1.68	1.86	2.11	1.32	NM_001015889 /// NM_027139 /// NM_027592
1436856_x_at	Tars2	5.16E-03	2.02	3.52	1.13	1.33	NM_027931

1423809_at	Tcf19	8.55E-03	-1.52	9.76	14.09	3.90	NM_025674
1423989_at	Tecpr1	3.80E-03	-1.53	-1.85	-1.36	-2.90	NM_027410
1460378_a_at	Tes	8.13E-04	-2.47	-2.01	-1.37	-2.21	NM_011570 /// NM_207176
1423441_at	Tfb2m	6.99E-03	2.05	1.20	2.25	2.13	NM_008249
1423241_a_at	Tfdp1	3.80E-03	3.48	1.93	3.10	3.13	NM_009361
1448907_at	Thop1	7.91E-03	2.79	2.98	6.56	10.90	NM_022653
1438769_a_at	Thyn1	7.09E-04	2.78	4.00	2.79	3.59	NM_144543
1416485_at	Timm23	4.13E-03	1.89	1.88	1.55	2.10	NM_016897
1416345_at	Timm8a1	2.13E-04	4.30	5.75	2.03	4.26	NM_013898
1430084_at	Tlcd1	6.36E-03	2.13	4.48	1.58	2.37	NM_026708
1419655_at	Tle3	9.24E-03	-1.20	-1.58	-1.69	-2.76	NM_001083927 /// NM_001083928 /// NM_009389
1433895_at	Tmem127	2.40E-03	-2.21	-1.88	-1.91	-2.06	NM_175145
1428074_at	Tmem158	1.24E-05	6.46	7.47	1.48	8.08	NM_001002267
1424191_a_at	Tmem41a	4.32E-03	2.50	1.48	1.49	2.53	NM_025693
1433735_a_at	Tmem64	1.20E-03	3.07	4.11	-1.54	4.60	NM_181401
1454709_at	Tmem64	2.89E-04	2.67	3.37	-1.29	3.59	NM_181401
1416376_at	Tmem97	7.70E-03	1.96	1.27	1.69	2.82	NM_133706
1426302_at	Tmprss4	5.28E-03	-1.62	-6.11	-1.47	-2.97	NM_145403
1423081_a_at	Tomm20	5.88E-03	1.65	2.67	2.35	1.99	NM_024214
1415733_a_at	Tomm5	1.65E-04	2.92	3.40	2.12	3.30	NM_001099675 /// NM_001134646 /// XM_001474120 /// XM_898905 /// XM_906738 /// XM_920041
1460370_at	Top1mt	6.60E-05	5.54	3.97	2.24	6.53	NM_028404
1454694_a_at	Top2a	6.36E-03	-1.65	3.58	13.89	3.46	NM_011623
1421998_at	Tor3a	4.77E-03	-1.63	-2.50	-1.35	-2.87	NM_023141
1448276_at	Tspan4	7.08E-04	6.09	14.25	1.96	12.06	NM_053082
1451351_at	Ttc13	5.88E-03	2.22	3.30	1.16	2.18	NM_145607
1436833_x_at	Ttll1	6.36E-03	-2.56	-2.09	1.05	-4.49	NM_178869
1417373_a_at	Tuba4a	8.31E-03	1.61	2.21	1.82	1.13	NM_009447
1427347_s_at	Tubb2a	7.44E-03	-2.10	-2.04	-1.04	-1.44	NM_009450
1447780_x_at	Tufm	1.62E-03	1.59	2.28	1.54	1.81	NM_172745
1433698_a_at	Txnl4a	4.63E-03	2.24	1.65	1.58	2.75	NM_001038608 /// NM_001042408 /// NM_025299 /// NM_178604
1428689_at	Tysnd1	7.56E-04	3.45	1.74	1.96	2.79	XM_125636 /// XM_905996
1441856_x_at	Tysnd1	8.96E-05	2.99	1.99	1.40	2.00	XM_125636 /// XM_905996
1424281_at	Ubap2	6.71E-03	2.00	1.61	1.43	2.21	NM_026872
1417188_s_at	Ube2k	3.20E-03	1.76	3.55	3.41	2.78	NM_016786
1425753_a_at	Ung	3.87E-04	10.07	21.53	-2.41	3.55	NM_001040691 /// NM_011677
1455829_at	Usp14	2.57E-03	2.50	3.26	1.10	1.90	NM_001038589 /// NM_021522
1437007_x_at	Usp39	3.31E-03	2.48	2.65	-1.08	2.16	NM_138592
1434125_at	Utp15	5.68E-03	2.03	1.51	1.40	2.20	NM_178918
1454846_at	Utp15	7.52E-03	1.81	1.73	-1.22	2.18	NM_178918
1435114_at	Wdhd1	6.60E-03	5.61	4.97	4.95	5.08	NM_172598
1433746_at	Wdr3	7.87E-04	2.30	2.24	-1.16	1.92	NM_175552
1423735_a_at	Wdr36	8.35E-03	2.62	1.67	1.37	2.42	NM_001110015 /// NM_001110016 /// NM_144863
1426496_at	Wdr55	1.48E-03	2.03	3.91	2.37	2.65	NM_026464
1428677_at	Wdr73	6.69E-04	2.64	2.42	1.28	2.11	XM_001479473 /// XM_001479496
1451649_a_at	Wdr75	1.28E-03	1.79	1.55	1.02	2.35	NM_028599
1453433_at	Wdr89	4.70E-03	2.90	1.86	1.30	1.38	NM_028203 /// XM_001001795 /// XM_001476702 /// XM_001476717 /// XM_001479426
1418442_at	Xpo1	4.02E-04	2.14	3.02	1.92	2.40	NM_001035226 /// NM_134014
1418443_at	Xpo1	2.57E-03	2.08	2.48	2.27	2.63	NM_001035226 /// NM_134014
1439442_x_at	Yars2	7.66E-04	3.32	2.15	1.47	3.11	NM_198246
1434501_at	Ypel4	2.79E-03	-1.63	-1.60	-1.18	-4.43	NM_001005342
1451196_at	Ypel5	3.74E-04	-2.37	-2.73	-1.86	-3.22	NM_027166
1428779_at	Zbtb41	1.10E-03	2.75	2.45	2.64	2.57	NM_172643
1418495_at	Zc3h8	6.51E-04	2.91	3.24	1.09	2.32	NM_020594
1439057_x_at	Zdhhc6	9.27E-04	1.79	2.27	1.49	2.12	NM_001033573 ///

							NM_025883
1454787_at	Zdhhc9	3.87E-04	3.33	1.69	1.00	3.93	NM_172465
1447403_a_at	Zmynd19	8.08E-03	3.32	2.31	-1.08	3.67	NM_026021
1454967_at		9.77E-03	-2.46	-2.25	-1.28	-1.68	
1433813_at		1.05E-03	1.93	8.95	3.29	1.71	
1440205_at		6.94E-05	8.80	5.96	1.52	4.23	
1456396_at		1.46E-03	2.02	1.54	1.63	1.65	
1457132_at		9.46E-03	-2.50	-3.09	-1.16	-5.25	

Appendix D. Significant gene ontology (GO) terms in c-MYC early activation

In this appendix, the significant gene ontology (GO) terms in c-MYC early activation are presented. Significant GO terms of cluster 1 were found to be 167 and were split into three categories according to their functions, i.e. cellular process, metabolic process and cellular component organization or biogenesis, which are shown in Table C.1, Table C.2, and Table C.3.

Table D.1. Significant GO terms relating to cellular process.

GO ACCESSION	GO Term	p-value	corrected p-value	Count in Selection	% Count in Selection	Count in Total	% Count in Total
GO:0006564	L-serine biosynthetic process	6.20E-24	9.84E-20	14	5.51	15	0.09
GO:0006563	L-serine metabolic process	2.70E-23	1.43E-19	15	5.91	19	0.11
GO:0006566	threonine metabolic process	2.40E-21	9.52E-18	13	5.12	15	0.09
GO:0006544	glycine metabolic process	3.19E-21	1.01E-17	14	5.51	23	0.13
GO:0006541	glutamine metabolic process	1.51E-20	3.00E-17	16	6.30	30	0.17
GO:0009070	serine family amino acid biosynthetic process	1.47E-20	3.00E-17	14	5.51	20	0.12
GO:0009448	gamma-aminobutyric acid metabolic process	1.26E-20	3.00E-17	13	5.12	16	0.09
GO:0019530	taurine metabolic process	1.86E-19	3.29E-16	13	5.12	18	0.10
GO:0009069	serine family amino acid metabolic process	2.15E-19	3.41E-16	15	5.91	34	0.20
GO:0034641	cellular nitrogen compound metabolic process	3.97E-19	5.73E-16	110	43.31	3658	21.24
GO:0016070	RNA metabolic process	3.45E-17	4.21E-14	45	17.72	754	4.38
GO:0006396|GO:0006394	RNA processing	1.13E-15	1.28E-12	39	15.35	477	2.77
GO:0009064	glutamine family amino acid metabolic process	2.04E-15	2.16E-12	16	6.30	55	0.32
GO:0009066	aspartate family amino acid metabolic process	5.98E-15	5.94E-12	13	5.12	32	0.19
GO:0021782	glial cell development	2.42E-14	2.26E-11	13	5.12	35	0.20
GO:0008652	cellular amino acid biosynthetic process	1.08E-13	9.53E-11	14	5.51	58	0.34
GO:0034660	ncRNA metabolic process	2.93E-13	2.45E-10	22	8.66	236	1.37
GO:0006520	cellular amino acid metabolic process	3.81E-13	3.02E-10	18	7.09	219	1.27
GO:0022613	ribonucleoprotein complex biogenesis	1.40E-12	1.01E-09	18	7.09	157	0.91
GO:0044106	cellular amine metabolic process	1.54E-12	1.06E-09	18	7.09	296	1.72
GO:0034470	ncRNA processing	2.05E-12	1.36E-09	22	8.66	178	1.03

GO:0071843	cellular component biogenesis at cellular level	2.30E-12	1.46E-09	18	7.09	161	0.93
GO:0006139|GO:0055134	nucleobase, nucleoside, nucleotide and nucleic acid metabolic process	2.53E-12	1.54E-09	93	36.61	3405	19.77
GO:0042254|GO:0007046	ribosome biogenesis	3.86E-12	2.27E-09	18	7.09	131	0.76
GO:0009309	amine biosynthetic process	1.38E-11	7.57E-09	14	5.51	93	0.54
GO:0006519	cellular amino acid and derivative metabolic process	1.93E-11	1.02E-08	18	7.09	261	1.52
GO:0006575	cellular amino acid derivative metabolic process	2.60E-11	1.33E-08	13	5.12	69	0.40
GO:0044237	cellular metabolic process	4.46E-11	2.21E-08	122	48.03	6993	40.60
GO:0010001|GO:0007404| GO:0043360	glial cell differentiation	6.98E-11	3.17E-08	13	5.12	61	0.35
GO:0022402	cell cycle process	7.65E-11	3.37E-08	13	5.12	450	2.61
GO:0042063	gliogenesis	2.97E-10	1.21E-07	13	5.12	68	0.39
GO:0044271	cellular nitrogen compound biosynthetic process	6.90E-10	2.67E-07	20	7.87	333	1.93
GO:0006260|GO:0055133	DNA replication	9.24E-10	3.41E-07	17	6.69	140	0.81
GO:0090304	nucleic acid metabolic process	1.60E-09	5.77E-07	81	31.89	2791	16.20
GO:0006364|GO:0006365	rRNA processing	2.56E-09	8.66E-07	14	5.51	96	0.56
GO:0016072	rRNA metabolic process	2.95E-09	9.75E-07	14	5.51	97	0.56
GO:0007049	cell cycle	3.17E-09	1.03E-06	35	13.78	734	4.26
GO:0016053	organic acid biosynthetic process	3.32E-09	1.03E-06	14	5.51	152	0.88
GO:0046394	carboxylic acid biosynthetic process	3.32E-09	1.03E-06	14	5.51	152	0.88
GO:0006261|GO:0006262| GO:0006263	DNA-dependent DNA replication	1.39E-08	3.94E-06	8	3.15	36	0.21
GO:0006790	sulfur compound metabolic process	2.78E-08	7.48E-06	13	5.12	115	0.67
GO:0006259|GO:0055132	DNA metabolic process	3.66E-08	9.36E-06	18	7.09	403	2.34
GO:0019752	carboxylic acid metabolic process	3.61E-08	9.36E-06	18	7.09	518	3.01
GO:0043436	oxoacid metabolic process	3.61E-08	9.36E-06	18	7.09	518	3.01
GO:0006082	organic acid metabolic process	4.10E-08	1.03E-05	18	7.09	521	3.02
GO:0042180	cellular ketone metabolic process	5.74E-08	1.42E-05	18	7.09	529	3.07
GO:0006270|GO:0042024	DNA-dependent DNA replication initiation	5.92E-08	1.45E-05	6	2.36	13	0.08
GO:0004017	adenylate kinase activity	8.90E-07	1.86E-04	5	1.97	11	0.06
GO:0006268	DNA unwinding involved in replication	2.41E-06	4.77E-04	5	1.97	13	0.08
GO:0006399	tRNA metabolic process	3.60E-06	7.05E-04	8	3.15	125	0.73
GO:0032508	DNA duplex unwinding	5.44E-06	0.001041	5	1.97	15	0.09
GO:0006189	'de novo' IMP biosynthetic process	6.29E-06	1.19E-03	3	1.18	3	0.02
GO:0051301	cell division	8.28E-06	0.001528	17	6.69	290	1.68
GO:0006913|GO:0000063	nucleocytoplasmic transport	1.12E-05	2.04E-03	10	3.94	117	0.68
GO:0051169	nuclear transport	1.32E-05	0.002286	10	3.94	119	0.69
GO:0019201	nucleotide kinase activity	1.48E-05	0.002505	5	1.97	18	0.10
GO:0044249	cellular biosynthetic process	1.63E-05	0.00273	62	24.41	3487	20.24
GO:0006188	IMP biosynthetic process	2.48E-05	3.79E-03	3	1.18	4	0.02
GO:0046040	IMP metabolic process	2.48E-05	0.003788	3	1.18	4	0.02
GO:0071841	cellular component organization or biogenesis at cellular level	3.65E-05	0.005412	22	8.66	1548	8.99
GO:0006606	protein import into nucleus	3.97E-05	5.84E-03	8	3.15	69	0.40
GO:0008033	tRNA processing	5.42E-05	0.007677	8	3.15	72	0.42

GO:0051170	nuclear import	5.99E-05	0.00841	8	3.15	73	0.42
GO:0009113	purine base biosynthetic process	6.12E-05	0.008522	2	0.79	5	0.03
GO:0008380|GO:0006395	RNA splicing	6.73E-05	0.009045	14	5.51	221	1.28
GO:0006397	mRNA processing	7.10E-05	9.47E-03	15	5.91	280	1.63
GO:0034504	protein localization to nucleus	7.28E-05	0.009559	8	3.15	75	0.44
GO:0016071	mRNA metabolic process	8.58E-05	0.010986	15	5.91	315	1.83
GO:0009127	purine nucleoside monophosphate biosynthetic process	9.98E-05	0.012372	3	1.18	14	0.08
GO:0009168	purine ribonucleoside monophosphate biosynthetic process	9.98E-05	0.012372	3	1.18	14	0.08
GO:0031175	neuron projection development	1.24E-04	0.015215	13	5.12	234	1.36
GO:0000059	protein import into nucleus, docking	1.34E-04	1.62E-02	4	1.57	15	0.09
GO:0006605	protein targeting	1.68E-04	1.97E-02	10	3.94	157	0.91
GO:0009126	purine nucleoside monophosphate metabolic process	1.76E-04	0.020409	3	1.18	16	0.09
GO:0009167	purine ribonucleoside monophosphate metabolic process	1.76E-04	0.020409	3	1.18	16	0.09
GO:0046939	nucleotide phosphorylation	2.06E-04	0.023312	5	1.97	30	0.17
GO:0033365	protein localization to organelle	3.28E-04	0.035466	8	3.15	117	0.68
GO:0071103	DNA conformation change	3.70E-04	0.03792	5	1.97	172	1.00
GO:0003899|GO:0000129	DNA-directed RNA polymerase activity	4.34E-04	4.36E-02	5	1.97	35	0.20
GO:0044260|GO:0034960	cellular macromolecule metabolic process	4.75E-04	0.047455	81	31.89	5089	29.54
GO:0046112	nucleobase biosynthetic process	4.87E-04	0.04826	2	0.79	9	0.05
GO:0009156	ribonucleoside monophosphate biosynthetic process	5.39E-04	0.053084	3	1.18	21	0.12
GO:0000278	mitotic cell cycle	6.40E-04	6.27E-02	1	0.39	275	1.60
GO:0006144	purine base metabolic process	6.86E-04	6.67E-02	2	0.79	10	0.06
GO:0048666	neuron development	7.01E-04	0.067812	14	5.51	310	1.80
GO:0009161	ribonucleoside monophosphate metabolic process	7.74E-04	0.073541	3	1.18	23	0.13
GO:0055086	nucleobase, nucleoside and nucleotide metabolic process	7.71E-04	0.073541	11	4.33	672	3.90
GO:0019205	nucleobase, nucleoside, nucleotide kinase activity	8.16E-04	0.076653	5	1.97	40	0.23
GO:0032392	DNA geometric change	8.16E-04	0.076653	5	1.97	40	0.23

Table D.2. metabolic process

GO ACCESSION	GO Term	p-value	corrected p-value	Count in Selection	% Count in selection	Count in Total	% Count in Total
GO:0006564	L-serine biosynthetic process	6.20E-24	9.84E-20	14	5.51	15	0.09
GO:0004617	phosphoglycerate dehydrogenase activity	2.36E-23	1.43E-19	13	5.12	13	0.08
GO:0006563	L-serine metabolic process	2.70E-23	1.43E-19	15	5.91	19	0.11
GO:0006566	threonine metabolic process	2.40E-21	9.52E-18	13	5.12	15	0.09
GO:0006544	glycine metabolic process	3.19E-21	1.01E-17	14	5.51	23	0.13

GO:0006541	glutamine metabolic process	1.51E-20	3.00E-17	16	6.30	30	0.17
GO:0009070	serine family amino acid biosynthetic process	1.47E-20	3.00E-17	14	5.51	20	0.12
GO:0009448	gamma-aminobutyric acid metabolic process	1.26E-20	3.00E-17	13	5.12	16	0.09
GO:0009069	serine family amino acid metabolic process	2.15E-19	3.41E-16	15	5.91	34	0.20
GO:0034641	cellular nitrogen compound metabolic process	3.97E-19	5.73E-16	110	43.31	3658	21.24
GO:0006807	nitrogen compound metabolic process	3.49E-18	4.62E-15	110	43.31	3746	21.75
GO:0016070	RNA metabolic process	3.45E-17	4.21E-14	45	17.72	754	4.38
GO:0006396|GO:0006394	RNA processing	1.13E-15	1.28E-12	39	15.35	477	2.77
GO:0009064	glutamine family amino acid metabolic process	2.04E-15	2.16E-12	16	6.30	55	0.32
GO:0009066	aspartate family amino acid metabolic process	5.98E-15	5.94E-12	13	5.12	32	0.19
GO:0008652	cellular amino acid biosynthetic process	1.08E-13	9.53E-11	14	5.51	58	0.34
GO:0034660	ncRNA metabolic process	2.93E-13	2.45E-10	22	8.66	236	1.37
GO:0006520	cellular amino acid metabolic process	3.81E-13	3.02E-10	18	7.09	219	1.27
GO:0044106	cellular amine metabolic process	1.54E-12	1.06E-09	18	7.09	296	1.72
GO:0034470	ncRNA processing	2.05E-12	1.36E-09	22	8.66	178	1.03
GO:0006139|GO:0055134	nucleobase, nucleoside, nucleotide and nucleic acid metabolic process	2.53E-12	1.54E-09	93	36.61	3405	19.77
GO:0009309	amine biosynthetic process	1.38E-11	7.57E-09	14	5.51	93	0.54
GO:0016616	oxidoreductase activity, acting on the CH-OH group of donors, NAD or NADP as acceptor	5.98E-11	2.88E-08	14	5.51	118	0.69
GO:0016614	oxidoreductase activity, acting on CH-OH group of donors	2.86E-10	1.19E-07	14	5.51	130	0.75
GO:0009308	amine metabolic process	3.44E-10	1.36E-07	18	7.09	372	2.16
GO:0006260|GO:0055133	DNA replication	9.24E-10	3.41E-07	17	6.69	140	0.81
GO:0090304	nucleic acid metabolic process	1.60E-09	5.77E-07	81	31.89	2791	16.20
GO:0006364|GO:0006365	rRNA processing	2.56E-09	8.66E-07	14	5.51	96	0.56
GO:0016072	rRNA metabolic process	2.95E-09	9.75E-07	14	5.51	97	0.56
GO:0008152	metabolic process	1.14E-08	3.34E-06	149	58.66	8720	50.62
GO:0006261|GO:0006262|GO:0006263	DNA-dependent DNA replication	1.39E-08	3.94E-06	8	3.15	36	0.21
GO:0006259|GO:0055132	DNA metabolic process	3.66E-08	9.36E-06	18	7.09	403	2.34
GO:0006270|GO:0042024	DNA-dependent DNA replication initiation	5.92E-08	1.45E-05	6	2.36	13	0.08
GO:0004017	adenylate kinase activity	8.90E-07	1.86E-04	5	1.97	11	0.06
GO:0003824	catalytic activity	1.58E-06	3.16E-04	79	31.10	5311	30.83
GO:0006268	DNA unwinding involved in replication	2.41E-06	4.77E-04	5	1.97	13	0.08
GO:0006399	tRNA metabolic process	3.60E-06	7.05E-04	8	3.15	125	0.73
GO:0006189	'de novo' IMP	6.29E-06	1.19E-03	3	1.18	3	0.02

	biosynthetic process						
GO:0019201	nucleotide kinase activity	1.48E-05	0.002505	5	1.97	18	0.10
GO:0006188	IMP biosynthetic process	2.48E-05	3.79E-03	3	1.18	4	0.02
GO:0046040	IMP metabolic process	2.48E-05	0.003788	3	1.18	4	0.02
GO:0008033	tRNA processing	5.42E-05	0.007677	8	3.15	72	0.42
GO:0009113	purine base biosynthetic process	6.12E-05	0.008522	2	0.79	5	0.03
GO:0008380|GO:0006395	RNA splicing	6.73E-05	0.009045	14	5.51	221	1.28
GO:0006397	mRNA processing	7.10E-05	9.47E-03	15	5.91	280	1.63
GO:0016071	mRNA metabolic process	8.58E-05	0.010986	15	5.91	315	1.83
GO:0009127	purine nucleoside monophosphate biosynthetic process	9.98E-05	0.012372	3	1.18	14	0.08
GO:0009168	purine ribonucleoside monophosphate biosynthetic process	9.98E-05	0.012372	3	1.18	14	0.08
GO:0009126	purine nucleoside monophosphate metabolic process	1.76E-04	0.020409	3	1.18	16	0.09
GO:0009167	purine ribonucleoside monophosphate metabolic process	1.76E-04	0.020409	3	1.18	16	0.09
GO:0016740	transferase activity	2.06E-04	0.023312	48	18.90	1744	10.12
GO:0046939	nucleotide phosphorylation	2.06E-04	0.023312	5	1.97	30	0.17
GO:0016776	phosphotransferase activity, phosphate group as acceptor	2.82E-04	0.031508	5	1.97	32	0.19
GO:0003899|GO:0000129	DNA-directed RNA polymerase activity	4.34E-04	4.36E-02	5	1.97	35	0.20
GO:0034062	RNA polymerase activity	4.34E-04	0.043624	5	1.97	35	0.20
GO:0046112	nucleobase biosynthetic process	4.87E-04	0.04826	2	0.79	9	0.05
GO:0009156	ribonucleoside monophosphate biosynthetic process	5.39E-04	0.053084	3	1.18	21	0.12
GO:0006144	purine base metabolic process	6.86E-04	6.67E-02	2	0.79	10	0.06
GO:0009161	ribonucleoside monophosphate metabolic process	7.74E-04	0.073541	3	1.18	23	0.13
GO:0055086	nucleobase, nucleoside and nucleotide metabolic process	7.71E-04	0.073541	11	4.33	672	3.90
GO:0019205	nucleobase, nucleoside, nucleotide kinase activity	8.16E-04	0.076653	5	1.97	40	0.23

Table D.3. Significant GO terms relating to cellular component organization or biogenesis.

GO ACCESSION	GO Term	p-value	corrected p-value	Count in Selection	% Count in Selection	Count in Total	% Count in Total
GO:0022613	ribonucleoprotein complex biogenesis	1.40E-12	1.01E-09	18	7.09	157	0.91
GO:0071843	cellular component biogenesis at	2.30E-12	1.46E-09	18	7.09	161	0.93

	cellular level						
GO:0042254|GO:0007046	ribosome biogenesis	3.86E-12	2.27E-09	18	7.09	131	0.76
GO:0006364|GO:0006365	rRNA processing	2.56E-09	8.66E-07	14	5.51	96	0.56
GO:0044085	cellular component biogenesis	2.51E-07	5.53E-05	22	8.66	695	4.03
GO:0071840	cellular component organization or biogenesis	4.61E-06	8.93E-04	35	13.78	2224	12.91
GO:0071841	cellular component organization or biogenesis at cellular level	3.65E-05	5.41E-03	22	8.66	1548	8.99
GO:0031175	neuron projection development	1.24E-04	1.52E-02	13	5.12	234	1.36
GO:0000059	protein import into nucleus, docking	1.34E-04	1.62E-02	4	1.57	15	0.09

Appendix E. Significant biological processes in cluster 1

I. Cellular process

Genes relating to cell cycle, cell cycle process, cell division and DNA conformation change

Probe Set ID	Gene Symbol	Fold change ratio (Treatment/Control) at different time points				Ref_seq_id
		4	8	16	32	
1433669_at	*Akap8*	2.76	2.04	-1.15	1.5	NM_019774
1417910_at	*Ccna2*	-1.08	4.82	11.07	3.21	NM_009828
1448205_at	*Ccnb1*	1.09	3.82	9.56	3.63	NM_172301
1416492_at	*Ccne1*	2.10	4.16	5.80	1.28	NM_007633
1441910_x_at	*Ccne1*	1.93	8.88	1.74	1.6	NM_007633
1422535_at	*Ccne2*	2.17	8.20	6.32	5.7	NM_001037134 /// NM_009830
1417131_at	*Cdc25a*	2.55	2.19	1.49	3.07	NM_007658
1417132_at	*Cdc25a*	2.29	2.07	1.24	1.76	NM_007658
1452040_a_at	*Cdca3*	-1.08	1.05	5.51	1.1	NM_013538
1416802_a_at	*Cdca5*	-1.42	22.18	21.74	8.58	NM_026410
1424143_a_at	*Cdt1*	5.79	24.94	11.12	6.83	NM_026014
1449708_s_at	*Chek1*	2.69	6.39	4.48	4.69	NM_007691
1416698_a_at	*Cks1b*	1.52	3.58	3.15	2.45	NM_016904
1417457_at	*Cks2*	-1.24	3.77	8.09	6.65	NM_025415
1434079_s_at	*Mcm2*	1.84	4.18	2.56	3.05	NM_008564
1436708_x_at	*Mcm4*	2.10	8.25	1.43	2.69	NM_008565
1436808_x_at	*Mcm5*	4.34	28.35	2.00	9.02	NM_008566
1438320_s_at	*Mcm7*	2.81	5.93	3.11	3.61	NM_008568
1439269_x_at	*Mcm7*	2.40	7.40	2.73	3.72	NM_008568
1420477_at	*Nap1l1*	1.90	1.68	2.20	1.68	NM_001146707 /// NM_015781
1436707_x_at	*Ncaph*	-2.35	7.60	20.88	3.76	NM_144818
1416073_a_at	*Nup85*	3.33	6.81	4.49	5.34	NM_001002929
1437520_a_at	*Nup85*	3.13	6.64	1.61	2.42	NM_001002929
1418281_at	*Rad51*	1.09	4.62	9.60	1.58	NM_011234
1426853_at	*Set*	2.37	3.52	-1.02	1.46	NM_023871
1437370_at	*Sgol2*	1.02	1.11	3.87	1.14	NM_199007
1431087_at	*Spc24*	-1.42	2.99	14.46	1.42	NM_026282
1415849_s_at	*Stmn1*	-1.57	3.11	4.91	1.87	NM_019641
1423241_a_at	*Tfdp1*	3.48	1.93	3.1	3.13	NM_009361
1460370_at	*Top1mt*	5.54	3.97	2.24	6.53	NM_028404
1454694_a_at	*Top2a*	-1.65	3.58	13.89	3.46	NM_011623
1433698_a_at	*Txnl4a*	2.24	1.65	1.58	2.75	NM_001038608 /// NM_001042408 /// NM_025299 /// NM_178604

II. Metabolic process

Genes relating to cellular metabolic process

Probe Set ID	Gene Symbol	Fold change ratio (Treatment/Control) at different time points				Ref_seq_id
		4	8	16	32	
1450721_at	*Acp1*	1.27	1.39	2.05	1.31	NM_001110239 /// NM_021330
1418372_at	*Adsl*	1.88	2.79	1.64	2.24	NM_009634
1434287_at	*Agpat5*	3.27	2.41	2.67	2.05	NM_026792
1424712_at	*Ahctf1*	2.80	1.37	1.10	2.95	NM_026375
1451459_at	*Ahctf1*	3.51	1.45	1.95	2.98	NM_026375

1448450_at	*Ak2 /// LOC100047005*	2.74	2.98	1.17	1.81	NM_001033966 /// NM_016895 /// XM_001477790
1450387_s_at	*Ak3l1 /// LOC100047616*	4.00	4.81	-1.11	4.98	NM_009647 /// XM_001478522
1433669_at	*Akap8*	2.76	2.04	-1.15	1.50	NM_019774
1434555_at	*Anp32a*	2.21	1.59	1.01	1.57	NM_009672
1451703_s_at	*Aprt*	1.62	1.74	2.23	2.18	NM_009698
1427197_at	*Atr*	2.57	4.41	1.58	2.96	NM_019864
1433663_s_at	*AU014645*	2.52	1.34	1.40	1.64	NM_001033201
1423264_at	*Bop1*	2.86	3.94	2.50	4.55	NM_013481
1440910_at	*C77370*	3.97	3.37	1.29	2.50	NM_001077354
1448205_at	*Ccnb1*	1.09	3.82	9.56	3.63	NM_172301
1416492_at	*Ccne1*	2.10	4.16	5.80	1.28	NM_007633
1441910_x_at	*Ccne1*	1.93	8.88	1.74	1.60	NM_007633
1422535_at	*Ccne2*	2.17	8.20	6.32	5.70	NM_001037134 /// NM_009830
1417131_at	*Cdc25a*	2.55	2.19	1.49	3.07	NM_007658
1417132_at	*Cdc25a*	2.29	2.07	1.24	1.76	NM_007658
1452040_a_at	*Cdca3*	-1.08	1.05	5.51	1.10	NM_013538
1424143_a_at	*Cdt1*	5.79	24.94	11.12	6.83	NM_026014
1449708_s_at	*Chek1*	2.69	6.39	4.48	4.69	NM_007691
1417457_at	*Cks2*	-1.24	3.77	8.09	6.65	NM_025415
1435800_a_at	*Csda*	2.51	2.14	1.37	2.72	NM_011733 /// NM_139117
1451012_a_at	*Csda*	4.95	2.28	2.39	5.30	NM_011733 /// NM_139117
1419645_at	*Cstf2*	2.09	1.94	1.54	2.45	NM_133196
1416563_at	*Ctps*	2.66	3.35	1.97	2.17	NM_016748
1422484_at	*Cycs*	1.29	2.15	1.54	2.02	NM_007808
1454659_at	*Dctd*	4.60	3.06	2.33	4.08	NM_178788
1448271_a_at	*Ddx21*	1.91	1.83	-1.03	2.00	NM_019553
1426609_at	*Dis3*	3.54	2.58	1.90	4.32	NM_028315
1426265_x_at	*Dlat*	1.03	2.28	1.69	2.60	NM_145614
1417182_at	*Dnaja2*	2.10	2.02	1.50	1.44	NM_019794
1428087_at	*Dnm1l*	1.82	1.75	1.21	3.76	NM_001025947 /// NM_152816
1435734_x_at	*Dus1l*	3.03	2.54	-1.08	1.25	NM_026824
1424229_at	*Dyrk3*	1.80	1.21	4.53	2.77	NM_145508
1449044_at	*Eef1e1*	3.26	2.75	5.25	8.83	NM_025380
1437829_s_at	*Eef2k*	3.26	3.26	-1.52	2.42	NM_007908
1456107_x_at	*Eftud2*	2.24	3.14	1.02	1.96	NM_001109995 /// NM_011431
1424343_a_at	*Eif1a*	1.28	1.63	2.21	1.51	NM_010120
1424344_s_at	*Eif1a*	1.92	3.30	1.35	1.84	NM_010120
1426394_at	*Eif3j*	1.93	1.85	1.74	2.69	NM_144545
1426395_s_at	*Eif3j*	1.58	1.85	1.56	2.85	NM_144545
1423220_at	*Eif4e*	2.86	2.75	1.54	2.11	NM_007917 /// XM_001004193
1450908_at	*Eif4e*	1.95	2.84	2.07	4.23	NM_007917 /// XM_001004193
1435803_a_at	*Eif4e2*	1.50	2.15	1.40	1.62	NM_001039169 /// NM_001039170 /// NM_023314
1428477_at	*Elac2*	3.18	1.32	1.12	2.14	NM_023479
1417403_at	*Elovl6*	3.10	4.60	2.47	5.50	NM_130450
1417404_at	*Elovl6*	3.49	3.28	2.74	2.99	NM_130450
1421097_at	*Endog*	2.79	3.90	1.74	2.44	NM_007931
1438317_a_at	*Endog*	2.79	3.74	1.27	1.68	NM_007931
1420024_s_at	*Etf1*	2.16	2.73	1.16	1.66	NM_144866
1452012_a_at	*Exosc1*	2.72	2.68	1.18	2.60	NM_025644
1435544_at	*Exosc6*	3.18	5.31	1.36	3.43	NM_028274
1423828_at	*Fasn*	2.62	3.52	1.98	2.28	NM_007988
1435369_at	*Fastkd5*	2.16	3.19	1.73	2.37	NM_001146084 /// NM_198176
1419577_at	*Fig4*	4.28	3.52	1.35	6.03	NM_133999
1441911_x_at	*Gart*	1.97	2.37	1.29	2.31	NM_010256
1432164_a_at	*Gcsh*	2.24	1.65	1.43	1.57	NM_026572
1424300_at	*Gemin6*	1.78	2.20	5.22	2.23	NM_026053
1451400_at	*Gemin8*	2.02	1.95	1.78	2.04	NM_146238
1435245_at	*Gls2*	9.89	6.97	5.23	5.61	NM_001033264
1438510_a_at	*Hars*	1.53	2.02	1.16	1.48	NM_008214
1419964_s_at	*Hdgf*	1.66	1.82	2.07	2.08	NM_008231
1436050_x_at	*Hes6*	3.11	2.26	-1.02	3.01	NM_019479

1434736_at	*Hlf*	3.37	3.66	-1.15	3.49	NM_172563
1416184_s_at	*Hmga1*	2.73	3.09	1.99	3.98	NM_001025427 /// NM_001039356 /// NM_016660
1431349_at	*Hnrnpab*	2.10	1.89	1.93	1.34	NM_001048061 /// NM_010448
1455120_at	*Hpdl*	2.86	2.23	1.04	4.30	NM_146256
1416968_a_at	*Hsd3b7*	2.57	3.12	1.19	2.93	NM_001040684 /// NM_133943
1426351_at	*Hspd1*	1.31	1.84	2.45	2.63	NM_010477
1426705_s_at	*Iars*	1.62	1.28	2.01	1.42	NM_172015
1422501_s_at	*Idh3a*	1.54	1.66	1.87	2.22	NM_029573
1432016_a_at	*Idh3a*	1.38	1.66	2.11	2.96	NM_029573
1453784_at	*Ilkap*	1.15	1.13	2.20	1.27	NM_023343
1426213_at	*Imp4*	2.77	2.90	2.16	2.94	NM_178601
1456200_at	*Ipmk*	3.31	1.16	1.66	1.53	NM_027184
1434154_at	*Kctd13*	1.39	1.26	1.10	2.56	NM_172747
1433842_at	*Lrrfip1*	4.45	4.11	1.01	4.45	NM_001111311 /// NM_001111312 /// NM_008515
1433576_at	*Mat2a*	3.21	2.98	-1.44	2.05	NM_145569
1438386_x_at	*Mat2a*	2.17	1.81	-1.24	1.79	NM_145569
1438630_x_at	*Mat2a*	2.49	2.50	-1.22	1.87	NM_145569
1438976_x_at	*Mat2a*	2.58	2.64	-1.25	1.85	NM_145569
1456702_x_at	*Mat2a*	2.57	2.07	-1.19	1.93	NM_145569
1434079_s_at	*Mcm2*	1.84	4.18	2.56	3.05	NM_008564
1436708_x_at	*Mcm4*	2.10	8.25	1.43	2.69	NM_008565
1436808_x_at	*Mcm5*	4.34	28.35	2.00	9.02	NM_008566
1438320_s_at	*Mcm7*	2.81	5.93	3.11	3.61	NM_008568
1439269_x_at	*Mcm7*	2.40	7.40	2.73	3.72	NM_008568
1460050_x_at	*Mettl13*	3.17	1.97	-1.02	2.38	NM_144877
1435232_x_at	*Mrpl15*	2.20	1.97	1.67	2.90	NM_025300
1416349_at	*Mrpl34*	2.39	2.00	1.99	3.07	NM_053162
1427158_at	*Mrps30*	2.13	1.91	1.25	2.80	NM_021556
1424425_a_at	*Mtap*	3.17	3.38	1.26	2.74	NM_024433
1424426_at	*Mtap*	6.30	5.80	1.24	3.51	NM_024433
1451346_at	*Mtap*	3.05	2.91	1.33	3.78	NM_024433
1456653_a_at	*Mthfd1l*	3.16	1.45	1.62	4.59	NM_172308
1434278_at	*Mtm1*	5.67	9.10	3.98	8.94	NM_019926
1452110_at	*Mtrr*	4.28	5.67	1.77	2.59	NM_172480
1450376_at	*Mxi1*	2.36	1.42	2.52	4.78	NM_001008542 /// NM_001008543 /// NM_010847
1449072_a_at	*N6amt2*	1.28	2.13	1.98	1.74	NM_026526
1452192_at	*Naf1*	5.70	4.67	1.65	4.73	XR_032374 /// XR_032626
1416972_at	*Nhp2l1*	2.31	2.37	1.70	1.88	NM_011482
1416973_at	*Nhp2l1*	1.91	2.11	2.05	1.76	NM_011482
1424019_at	*Nop2*	1.90	2.39	1.27	2.52	NM_138747
1423850_at	*Nsun2*	3.12	1.72	5.57	3.32	NM_145354
1448651_at	*Nudt5*	1.55	1.88	2.37	3.16	NM_016918
1427364_a_at	*Odc1*	1.99	2.93	1.29	1.78	NM_013614
1418225_at	*Orc2l*	2.28	2.01	1.33	2.31	NM_001025378 /// NM_008765
1417037_at	*Orc6l*	2.17	2.22	1.98	2.66	NM_019716
1420142_s_at	*Pa2g4*	2.30	6.21	1.33	1.57	NM_011119
1450854_at	*Pa2g4*	2.34	4.59	2.06	1.97	NM_011119
1423564_a_at	*Paics*	1.57	1.38	2.40	2.45	NM_025939
1448627_s_at	*Pbk*	-1.30	4.18	18.83	3.28	NM_023209
1424081_at	*Pcgf6*	2.35	2.28	2.40	2.42	NM_027654
1423747_a_at	*Pdk1*	4.74	4.40	2.45	5.13	NM_172665
1423748_at	*Pdk1*	5.64	6.35	4.16	6.23	NM_172665
1435836_at	*Pdk1*	3.28	2.66	1.76	3.01	NM_172665
1428309_s_at	*Pdrg1*	2.15	3.12	1.37	1.82	NM_178939
1427929_a_at	*Pdxk*	2.38	1.89	1.05	1.43	NM_172134
1425042_s_at	*Pelp1*	1.74	2.36	1.20	1.79	NM_029231
1455496_at	*Pfas*	4.32	3.65	2.65	7.32	NM_001159519 /// XM_111232 /// XM_908501
1426554_a_at	*Pgam1*	1.77	1.83	1.72	2.16	NM_023418
1452919_a_at	*Pgp*	1.90	2.37	1.63	1.79	NM_025954
1416202_at	*Phb2*	3.12	2.51	2.62	2.94	NM_007531
1438938_x_at	*Phb2*	2.94	2.89	1.43	2.52	NM_007531

1455713_x_at	*Phb2*	3.12	4.18	2.01	2.10	NM_007531
1452676_a_at	*Pnpt1*	2.27	2.88	1.53	2.71	NM_027869
1448277_at	*Pold2*	3.10	4.32	3.17	3.41	NM_008894
1416126_at	*Polr1b*	4.49	1.78	1.60	3.95	NM_009086
1435057_x_at	*Polr1e*	2.74	2.00	-1.02	2.58	NM_022811
1449155_at	*Polr3g*	4.71	3.09	1.76	5.99	NM_001081176
1424227_at	*Polr3h*	2.84	3.86	2.00	2.77	NM_030229
1439266_a_at	*Polr3k*	1.57	2.42	1.86	1.56	NM_025901
1452831_s_at	*Ppat*	2.65	3.69	1.49	1.55	XM_001002879 /// XM_001002886 /// XM_896000 /// XM_924520 /// XM_973937 /// XM_973973
1418369_at	*Prim1*	1.37	4.55	6.60	3.36	NM_008921
1449061_a_at	*Prim1*	1.50	4.82	4.72	3.25	NM_008921
1428783_at	*Prkar2a*	3.29	3.24	1.31	2.76	NM_008924
1452915_at	*Prkar2a*	2.85	3.11	1.47	2.36	NM_008924
1451064_a_at	*Psat1*	5.57	11.92	4.08	8.53	NM_177420
1454607_s_at	*Psat1*	3.53	4.98	3.91	6.60	NM_177420
1451845_a_at	*Ptrh2*	1.70	1.20	2.24	3.97	NM_001098810 /// NM_175004
1428800_a_at	*Pus7l*	3.41	3.84	-1.10	3.54	NM_172437
1460447_at	*Pus7l*	2.73	5.25	1.29	2.75	NM_172437
1418281_at	*Rad51*	1.09	4.62	9.60	1.58	NM_011234
1417938_at	*Rad51ap1*	1.29	7.28	6.77	7.52	NM_009013
1460551_at	*Ran*	2.00	2.13	2.21	2.83	NM_009391
1452091_a_at	*Rbm28*	2.88	2.27	1.28	4.10	NM_026650 /// NM_133925
1438161_s_at	*Rfc4*	1.16	10.82	3.13	4.65	NM_145480
1419460_at	*Rpp14*	2.94	3.09	2.00	2.42	NM_025938 /// XM_001471720
1419461_at	*Rpp14*	2.72	3.61	2.10	3.68	NM_025938 /// XM_001471720
1424792_at	*Rpp40*	3.19	2.43	1.12	3.05	NM_145938
1423254_x_at	*Rps27l*	1.27	1.78	2.58	2.41	NM_026467
1450925_a_at	*Rps27l*	1.27	1.74	2.12	2.29	NM_026467
1415878_at	*Rrm1*	1.09	6.36	6.77	2.32	NM_009103
1456117_at	*Rrp1b*	3.71	5.12	-1.19	4.06	NM_028244
1456383_at	*Rsl1d1*	2.50	2.38	1.17	3.56	NM_025546
1424619_at	*Sf3b4*	1.44	1.40	-1.20	2.06	NM_153053
1428100_at	*Sfrs1*	3.47	2.65	-1.25	2.85	NM_001078167 /// NM_173374
1416151_at	*Sfrs3*	2.34	2.21	1.81	1.81	NM_013663
1425178_s_at	*Shmt1*	1.16	3.00	1.03	1.52	NM_009171
1417042_at	*Slc37a4*	2.71	2.00	3.72	2.41	NM_008063
1417300_at	*Smpdl3b*	5.08	8.81	5.39	15.15	NM_133888
1455552_at	*Snapc4*	3.44	2.17	1.18	3.95	NM_172339
1452680_at	*Snrpd2*	1.30	1.26	2.02	1.55	NM_026943
1454042_a_at	*Srpk1*	1.96	2.22	1.30	1.71	NM_016795
1418074_at	*St6galnac4*	4.77	5.72	1.02	4.16	NM_011373
1418075_at	*St6galnac4*	4.39	4.14	2.36	5.06	NM_011373
1419912_s_at	*Strap*	2.28	1.93	1.74	1.94	NM_011499
1429711_at	*Styx*	3.95	4.27	1.02	2.34	NM_019637
1428546_at	*Syncrip*	2.96	1.62	1.65	1.97	NM_019666 /// NM_019796
1423483_s_at	*Taf1c*	4.02	2.78	-1.22	1.76	NM_021441
1435302_at	*Taf4b*	4.07	2.74	1.20	4.97	NM_001100449 /// XM_128905 /// XM_911701
1451509_at	*Taf9*	1.68	1.86	2.11	1.32	NM_001015889 /// NM_027139 /// NM_027592
1436856_x_at	*Tars2*	2.02	3.52	1.13	1.33	NM_027931
1423441_at	*Tfb2m*	2.05	1.20	2.25	2.13	NM_008249
1423241_a_at	*Tfdp1*	3.48	1.93	3.10	3.13	NM_009361
1448907_at	*Thop1*	2.79	2.98	6.56	10.90	NM_022653
1460370_at	*Top1mt*	5.54	3.97	2.24	6.53	NM_028404
1454694_a_at	*Top2a*	-1.65	3.58	13.89	3.46	NM_011623
1417373_a_at	*Tuba4a*	1.61	2.21	1.82	1.13	NM_009447
1447780_x_at	*Tufm*	1.59	2.28	1.54	1.81	NM_172745
1433698_a_at	*Txnl4a*	2.24	1.65	1.58	2.75	NM_001038608 /// NM_001042408 /// NM_025299 /// NM_178604
1417188_s_at	*Ube2k*	1.76	3.55	3.41	2.78	NM_016786

1425753_a_at	*Ung*	10.07	21.53	-2.41	3.55	NM_001040691 /// NM_011677
1455829_at	*Usp14*	2.50	3.26	1.10	1.90	NM_001038589 /// NM_021522
1437007_x_at	*Usp39*	2.48	2.65	-1.08	2.16	NM_138592
1434125_at	*Utp15*	2.03	1.51	1.40	2.20	NM_178918
1454846_at	*Utp15*	1.81	1.73	-1.22	2.18	NM_178918
1433746_at	*Wdr3*	2.30	2.24	-1.16	1.92	NM_175552
1423735_a_at	*Wdr36*	2.62	1.67	1.37	2.42	NM_001110015 /// NM_001110016 /// NM_144863
1426496_at	*Wdr55*	2.03	3.91	2.37	2.65	NM_026464
1439442_x_at	*Yars2*	3.32	2.15	1.47	3.11	NM_198246
1428779_at	*Zbtb41*	2.75	2.45	2.64	2.57	NM_172643

III. Cellular component organization or biogenesis

Genes relating to cellular component organization or biogenesis

Probe Set ID	Gene Symbol	Fold change ratio (Treatment/Control) at different time points				Ref_seq_id
		4	8	16	32	
1433669_at	*Akap8*	2.76	2.04	-1.15	1.5	NM_019774
1447679_s_at	*Bms1*	1.89	2.05	1.08	1.37	NM_194339
1423264_at	*Bop1*	2.86	3.94	2.5	4.55	NM_013481
1450742_at	*Bysl*	2.17	2.94	1.58	1.81	NM_016859
1417910_at	*Ccna2*	-1.08	4.82	11.07	3.21	NM_009828
1448205_at	*Ccnb1*	1.09	3.82	9.56	3.63	NM_172301
1417131_at	*Cdc25a*	2.55	2.19	1.49	3.07	NM_007658
1417132_at	*Cdc25a*	2.29	2.07	1.24	1.76	NM_007658
1452040_a_at	*Cdca3*	-1.08	1.05	5.51	1.1	NM_013538
1416802_a_at	*Cdca5*	-1.42	22.18	21.74	8.58	NM_026410
1448809_at	*Cse1l*	1.98	2.93	2.48	2.24	NM_023565
1426609_at	*Dis3*	3.54	2.58	1.9	4.32	NM_028315
1421097_at	*Endog*	2.79	3.9	1.74	2.44	NM_007931
1438317_a_at	*Endog*	2.79	3.74	1.27	1.68	NM_007931
1420024_s_at	*Etf1*	2.16	2.73	1.16	1.66	NM_144866
1452012_a_at	*Exosc1*	2.72	2.68	1.18	2.6	NM_025644
1435544_at	*Exosc6*	3.18	5.31	1.36	3.43	NM_028274
1419577_at	*Fig4*	4.28	3.52	1.35	6.03	NM_133999
1424300_at	*Gemin6*	1.78	2.2	5.22	2.23	NM_026053
1451400_at	*Gemin8*	2.02	1.95	1.78	2.04	NM_146238
1426213_at	*Imp4*	2.77	2.9	2.16	2.94	NM_178601
1426946_at	*Ipo5*	2.68	2.61	2.78	4.82	NM_023579
1448526_at	*Kpnb1*	1.36	2.41	1.84	1.25	NM_008379
1434079_s_at	*Mcm2*	1.84	4.18	2.56	3.05	NM_008564
1435232_x_at	*Mrpl15*	2.2	1.97	1.67	2.9	NM_025300
1452192_at	*Naf1*	5.7	4.67	1.65	4.73	XR_032374 /// XR_032626
1420477_at	*Nap1l1*	1.9	1.68	2.2	1.68	NM_001146707 /// NM_015781
1436707_x_at	*Ncaph*	-2.35	7.6	20.88	3.76	NM_144818
1416972_at	*Nhp2l1*	2.31	2.37	1.7	1.88	NM_011482
1416973_at	*Nhp2l1*	1.91	2.11	2.05	1.76	NM_011482
1437238_x_at	*Nmd3*	2.24	1.84	2.06	3.77	NM_133787
1428870_at	*Nolc1*	4.89	3.42	2.01	4.16	NM_001039351 /// NM_001039352 /// NM_001039353 /// NM_053086
1424019_at	*Nop2*	1.9	2.39	1.27	2.52	NM_138747
1426533_at	*Nop56*	2.06	4.74	1.66	3.9	NM_024193
1455035_s_at	*Nop56*	3.19	3.14	2.89	2.52	NM_024193
1416073_a_at	*Nup85*	3.33	6.81	4.49	5.34	NM_001002929
1437520_a_at	*Nup85*	3.13	6.64	1.61	2.42	NM_001002929
1420142_s_at	*Pa2g4*	2.3	6.21	1.33	1.57	NM_011119
1450854_at	*Pa2g4*	2.34	4.59	2.06	1.97	NM_011119
1456117_at	*Rrp1b*	3.71	5.12	-1.19	4.06	NM_028244
1426853_at	*Set*	2.37	3.52	-1.02	1.46	NM_023871

1437370_at	*Sgol2*	1.02	1.11	3.87	1.14	NM_199007
1448321_at	*Smoc1*	3.63	3.58	3.09	3.63	NM_001146217 /// NM_022316
1431087_at	*Spc24*	-1.42	2.99	14.46	1.42	NM_026282
1415849_s_at	*Stmn1*	-1.57	3.11	4.91	1.87	NM_019641
1423441_at	*Tfb2m*	2.05	1.2	2.25	2.13	NM_008249
1416345_at	*Timm8a1*	4.3	5.75	2.03	4.26	NM_013898
1454694_a_at	*Top2a*	-1.65	3.58	13.89	3.46	NM_011623
1417373_a_at	*Tuba4a*	1.61	2.21	1.82	1.13	NM_009447
1433698_a_at	*Txnl4a*	2.24	1.65	1.58	2.75	NM_001038608 /// NM_001042408 /// NM_025299 /// NM_178604
1434125_at	*Utp15*	2.03	1.51	1.4	2.2	NM_178918
1454846_at	*Utp15*	1.81	1.73	-1.22	2.18	NM_178918
1433746_at	*Wdr3*	2.3	2.24	-1.16	1.92	NM_175552
1423735_a_at	*Wdr36*	2.62	1.67	1.37	2.42	NM_001110015 /// NM_001110016 /// NM_144863
1426496_at	*Wdr55*	2.03	3.91	2.37	2.65	NM_026464
1418442_at	*Xpo1*	2.14	3.02	1.92	2.4	NM_001035226 /// NM_134014
1418443_at	*Xpo1*	2.08	2.48	2.27	2.63	NM_001035226 /// NM_134014

Appendix F. Differentially expressed transcripts in condition 1 and condition 2

In this appendix, the full statistically significant differential expressed genes lists will be provided, in which condition 1 (M^+/E^+ vs M^+/E^-): the effect of exenatide under c-MYC activation, and condition 2 (M^-/E^+ vs M^-/E^-): the effects of exenatide without c-MYC activation.

Table F.1. Differentially expressed transcripts in condition 1.

Probe Set ID	Gene Symbol	Corrected p-value	Fold change ratio (Treatment/Control) at different time points				Ref_seq_id
			4	8	16	32	
1417612_at	Ier5	2.97E-02	-2.41	-1.28	-2.26	-1.69	NM_010500
1418057_at	Tiam1	3.06E-02	-1.17	-1.20	-3.34	-1.86	NM_001145886 /// NM_001145887 /// NM_009384
1420909_at	Vegfa	4.06E-02	-2.40	-1.52	-1.49	-1.61	NM_001025250 /// NM_001025257 /// NM_001110266 /// NM_001110267 /// NM_001110268 /// NM_009505
1422629_s_at	Shroom3	4.87E-02	-1.61	1.10	-2.25	-1.24	NM_001077595 /// NM_001077596 /// NM_015756
1423099_a_at	Mettl3	4.28E-02	-1.32	-1.57	-1.81	-2.04	NM_019721
1425993_a_at	Hsph1	4.28E-02	-1.77	-1.39	-2.11	-1.37	NM_013559
1426406_at	Setd8	2.97E-02	-2.61	-1.64	-2.15	-2.16	NM_030241
1426965_at	Rap2a	4.68E-02	-2.31	1.04	-2.08	-2.20	NM_029519
1432431_s_at	Macrod2	4.28E-02	-1.78	-1.84	-2.50	-1.07	NM_001013802 /// NM_028387
1435030_at	Upf2	4.63E-02	-3.21	1.02	-1.90	-1.16	NM_001081132
1435551_at	Fhod3	2.97E-02	-1.78	-1.48	-2.62	-2.88	NM_175276
1428800_a_at	Pus7l	4.68E-02	-1.33	-2.12	-1.84	-1.54	NM_172437
1428945_at	Uba6	3.23E-02	-1.99	-1.16	-4.63	-1.56	NM_172712
1429073_at	2210015D19Rik	2.97E-02	-2.30	1.08	-1.02	-1.57	XM_001475228 /// XM_893272
1429118_a_at	Zh2c2	2.97E-02	1.03	1.01	-2.16	1.04	NM_026250
1429682_at	Fam46c	4.06E-02	-3.18	1.01	-3.21	-1.63	NM_001142952 /// XR_001536 /// XR_002338 /// XR_005163
1433641_at	LOC100046891 /// Smad5	2.97E-02	-2.62	-1.61	-1.37	-1.49	NM_008541 /// XR_033104
1434083_a_at	Elmod1	4.28E-02	-1.25	-1.08	-2.06	1.01	NM_177769
1434572_at	Hdac9	3.49E-02	-3.10	-3.55	-1.59	-3.91	NM_024124
1435074_at	Tmem106b	3.98E-02	-2.17	-1.41	-1.56	-1.51	NM_027992
1435717_at	4833428C12Rik	2.97E-02	-2.98	1.02	-2.88	-1.36	
1436650_at	Filip1	2.97E-02	-3.85	-4.05	-6.58	-2.51	NM_001081243
1440435_at	Ky	4.28E-02	-2.38	-1.82	-1.62	-1.18	NM_024291
1441578_at	Ccdc86	3.16E-02	-1.85	-1.03	-1.22	-2.21	NM_023731
1455970_at		2.97E-02	-4.76	-1.61	-2.12	-3.08	
1456092_at	Kctd7	4.63E-02	-1.01	-1.09	-2.03	-1.03	NM_172509
1458341_x_at		3.45E-02	-2.89	-2.93	-1.07	-1.91	
1459723_at	Zdhhc22	2.97E-02	-3.19	-4.16	-3.50	-1.56	NM_001080943
1419105_at	Nr1h4	3.66E-02	1.30	1.09	2.59	-1.03	NM_009108
1419874_x_at	Zbtb16	2.97E-02	3.18	2.05	1.60	2.04	NM_001033324
1424250_a_at	Arhgef3	2.97E-02	2.44	4.21	1.89	7.71	NM_027871
1425144_at	Klk1b11	3.06E-02	2.24	-1.10	1.00	-1.00	NM_010640
1425837_a_at	Ccrn4l /// LOC100047134	2.97E-02	1.95	5.47	1.95	3.00	NM_009834 /// XM_001477322
1435949_at	Zc3h3	2.97E-02	2.78	1.86	1.15	1.62	NM_172121
1439060_s_at	Wipi1	4.98E-02	2.29	1.31	1.58	1.41	NM_145940

1442025_a_at		2.97E-02	3.97	3.65	2.22	4.08	
1450779_at	Fabp7	4.91E-02	1.20	-1.09	5.23	1.02	NM_021272
1437989_at	Pde8b	2.97E-02	1.16	-1.14	2.93	1.28	NM_172263
1445709_at	Mdm1	2.97E-02	1.18	9.29	-1.29	10.12	NM_010785 /// NM_148922
1456321_at	Nipal1	4.63E-02	1.39	2.33	1.03	2.20	NM_001081205
1456518_at	4930422I07Rik	4.06E-02	1.03	-1.07	2.04	-1.02	NM_001142943 /// XM_150216 /// XM_918228
1457132_at		4.06E-02	2.57	3.04	1.70	3.26	
1459957_at		9.47E-03	-1.10	-1.07	4.91	1.05	

Table F.2. Differentially expressed transcripts in condition 2

Probe Set ID	Gene Symbol	Corrected p-value	Fold change ratio (Treatment/Control) at different time points				Ref_seq_id
			4	8	16	32	
1418176_at	Vdr	4.61E-02	-1.25	-2.61	-1.80	-1.90	NM_009504
1421147_at	Terf2	2.64E-02	-1.96	-1.95	-2.58	-1.56	NM_001083118 /// NM_009353
1422556_at	Gna13	1.32E-02	-1.44	-1.28	-3.40	-1.12	NM_010303
1422629_s_at	Shroom3	9.54E-03	-2.53	-1.67	-1.81	-1.29	NM_001077595 /// NM_001077596 /// NM_015756
1425274_at	Asph	6.19E-03	1.05	1.02	-3.29	-1.10	NM_023066 /// NM_133723
1451419_at	Spsb4	2.83E-02	-3.31	-3.08	-2.73	-1.11	NM_145134
1452207_at	Cited2	3.37E-03	-5.01	-6.71	-3.78	-3.22	NM_010828
1428637_at	Dyrk2 /// LOC100044376	2.25E-03	-2.25	-3.36	-2.11	-1.49	NM_001014390 /// XR_030576
1433205_at	Ndfip2	2.25E-03	1.08	-2.68	-1.03	-1.00	NM_029561
1434572_at	Hdac9	1.00E-04	-5.22	-3.45	-13.81	-4.84	NM_024124
1436368_at	Slc16a10	3.37E-03	-2.08	-1.49	-2.19	-1.56	NM_001114332 /// NM_028247
1436650_at	Filip1	4.01E-02	-6.31	-3.12	1.03	-2.64	NM_001081243
1439753_x_at	Six4	4.73E-03	-2.93	-3.08	-2.65	-1.75	NM_011382
1439836_at	Asb15	2.44E-02	-2.88	-5.39	-2.12	-1.06	NM_080847
1440435_at	Ky	3.19E-02	-1.83	-2.38	-1.39	-1.71	NM_024291
1441881_x_at	Fam101a	2.60E-02	-2.16	-1.73	-2.28	-1.42	NM_028443
1442077_at	2310076G05Rik	1.08E-02	1.01	1.01	-3.44	-1.00	
1455970_at		3.82E-02	-2.62	-2.34	-1.87	-2.38	
1456862_at	Six4	3.37E-03	-2.31	-3.05	-2.69	-1.60	
1458081_at		2.50E-02	-2.01	-1.54	-1.89	-1.11	
1458341_x_at		3.36E-02	-1.99	-1.73	-2.34	-2.30	
1416125_at	Fkbp5	4.25E-02	2.04	2.04	3.97	1.84	NM_010220
1416129_at	Errfi1	4.83E-03	2.79	5.07	4.35	2.21	NM_133753
1418183_a_at	Cyth1	4.73E-03	2.27	2.19	2.27	1.75	NM_001112699 /// NM_001112700 /// NM_011180
1419100_at	Serpina3n	2.44E-02	1.23	1.01	2.15	1.10	NM_009252
1424250_a_at	Arhgef3	8.06E-03	3.33	2.48	8.16	5.70	NM_027871
1425837_a_at	Ccrn4l /// LOC100047134	2.25E-03	5.05	6.97	2.55	2.69	NM_009834 /// XM_001477322
1429379_at	Lyve1	1.94E-02	1.76	2.42	9.76	2.08	NM_053247
1433575_at	Sox4	2.60E-02	4.57	2.85	2.98	3.58	NM_009238
1434465_x_at	Vldlr	3.82E-02	3.02	1.99	3.05	3.25	NM_013703
1434496_at	Plk3	8.06E-03	1.68	2.74	2.57	2.72	NM_013807
1449007_at	Btg3 /// EG654432	2.65E-02	1.47	1.80	2.75	1.54	NM_009770 /// NR_002700
1451053_a_at	Mdm1	1.04E-02	4.61	7.18	5.06	4.68	NM_010785 /// NM_148922
1433762_at	C630043F03Rik	2.65E-02	1.59	2.20	1.70	1.26	
1435893_at	Vldlr	3.53E-03	2.28	1.76	4.91	2.93	NM_013703
1441687_at	Wnt4	4.91E-02	2.29	3.38	5.06	2.10	NM_009523
1457132_at		1.03E-02	2.57	6.69	2.96	2.14	

Publication

Mathematical Biosciences 235 (2012) 8–18

Contents lists available at SciVerse ScienceDirect

Mathematical Biosciences

journal homepage: www.elsevier.com/locate/mbs

Interaction of fast and slow dynamics in endocrine control systems with an application to β-cell dynamics

Yi-Fang Wang [a], Michael Khan [a], Hugo A. van den Berg [b,*]

[a] Biological Sciences, University of Warwick, Coventry CV4 7AL, UK
[b] Mathematics Institute, University of Warwick, Coventry CV4 7AL, UK

ARTICLE INFO

Article history:
Received 20 May 2011
Received in revised form 4 October 2011
Accepted 7 October 2011
Available online 25 October 2011

Keywords:
Glucose
Insulin
β-Cell
Diabetes
Endocrine control system

ABSTRACT

Endocrine dynamics spans a wide range of time scales, from rapid responses to physiological challenges to with slow responses that adapt the system to the demands placed on it. We outline a non-linear averaging procedure to extract the slower dynamics in a way that accounts properly for the non-linear dynamics of the faster time scale and is applicable to a hierarchy of more than two time scales, although we restrict our discussion to two scales for the sake of clarity. The procedure is exact if the slow time scale is infinitely slow (the dimensionless ε-quantity is the period of the fast time scale fluctuation times an upper bound to the slow time scale rate of change). However, even for an imperfect separation of time scales we find that this construction provides an excellent approximation for the slow-time dynamics at considerably reduced computational cost. Besides the computation advantage, the averaged equation provided a qualitative insight into the interaction of the time scales. We demonstrate the procedure and its advantages by applying the theory to the model described by Tolić et al. [I.M. Tolić, E. Mosekilde, J. Sturis, Modeling the insulin–glucose feedback system: the significance of pulsatile insulin secretion, J. Theor. Biol. 207 (2000) 361–375.] for ultradian dynamics of the glucose–insulin homeostasis feedback system, extended to include β-cell dynamics. We find that the dynamics of the β-cell mass are dependent not only on the glycemic load (amount of glucose administered to the system), but also on the way this load is applied (i.e. three meals daily versus constant infusion), effects that are lost in the inappropriate methods used by the earlier authors. Furthermore, we find that the loss of the protection against apoptosis conferred by insulin that occurs at elevated levels of insulin has a functional role in keeping the β-cell mass in check without compromising regulatory function. We also find that replenishment of β-cells from a rapidly proliferating pool of cells, as opposed to the slow turn-over which characterises fully differentiated β-cells, is essential to the prevention of type 1 diabetes.

1. Introduction

Neuroendocrine control systems respond rapidly to physiological challenges while concurrently undergoing adaptation on much slower time scales (e.g [11,36]). Moreover, an interplay prevails between processes at disparate scales: the slow adaptation is dependent on the fast events. Such an interplay is a pervasive characteristic of many biological systems.

As is well known, the dynamics of such systems can be analysed by considering separate and distinct dynamical systems that correspond to the biological system as it operates on two or more time scales. In such procedures, the approximation usually is exact if the slower component is "infinitely slower" than the faster component (see e.g. [19], for examples and applications). On a given time scale, the slower variables are "frozen" and figure as constant parameters, whereas the faster ones can often be treated using a quasi-steady state approximation (up to boundary or transition layers) in which the fast variable is essentially replaced by a function which relates its (fast-time system) equilibrium value to the prevailing values of the slower variables. Similarly, in those cases where the fast-time system does not equilibrate but tends to a periodic solution (e.g., a limit cycle or the stationary response to periodic forcing), intuition would suggest that the fast variables might be replaced by a long-term average. However, this intuition need not be correct. We outline a homogenisation method to tackle such problems on two time scales (see [28] for an introduction to homogenisation techniques). The type of system we have in mind describes the dynamics of an organism's physiology (or the relevant part thereof) together with the dynamics of the (neuro)endocrine system that regulates this physiology. We apply the method to a well-established model of the regulation of glucose concentration in the blood plasma, which we extend with a slow component, viz. the dynamics of the mass of endocrine cells. A diagrammatic representation of this system is given in Fig. 1.

* Corresponding author.
E-mail address: hugo@maths.warwick.ac.uk (H.A. van den Berg).

0025-5564/$ - see front matter © 2011 Elsevier Inc. All rights reserved.
doi:10.1016/j.mbs.2011.10.003

1.1. Introduction to the biological application

Glucose in the blood plasma provides an essential supply of immediately available energy substrate to all tissues of the body [35]. Adverse effects ensue when the concentration of glucose in the blood plasma becomes either very low or very high; avoidance of these effects defines a "euglycemic" range of values and, moreover, endocrine control loops operate so as to keep the blood glucose concentration in this range [43]. Whenever the supply of glucose derived from dietary carbohydrate exceeds demand from the tissues, the blood glucose level rises, stimulating the secretion of the hormone insulin, which in turn stimulates the disposition of glucose, either to be taken up as energy substrate rather than fatty acids, or to be stored away as a storage polymer, which is glycogen in liver, muscle, and kidneys, and lipid in adipose tissue [11]. When energy demand outstrips supply, the blood glucose level drops and insulin is not secreted. The resulting drop in the insulin concentration leads to a decrease of insulin-dependent uptake of glucose from the bloodstream as well as an increase of the release of storage-derived glucose from the liver, both of which have the effect of restoring glucose levels. At low levels of glucose, the hormone glucagon is released, which promotes the breakdown of glycogen and fatty acids [6]. A paracrine interaction between insulin and glucagon secretion has been proposed [14]. However, inasmuch as glucagon plays a prominent role in humans only when glucose falls significantly below the euglycemic range [32], the focus here is on the glucose–insulin feedback loop.

Insulin is a peptide hormone, consisting of two peptide chains linked by disulphide bonds, and produced by the β-cells in the so-called Islets of Langerhans, which are clusters of endocrine cells found scattered throughout the predominantly exocrine pancreas [6]. The total mass of β-cells changes over time: it continues to do so during adult life and it has become apparent during the past decade that the pathogenesis of both type 1 and type 2 diabetes involves failure to maintain an appropriate β-cell mass [4,7,20,38]. The total mass is the combined result of three processes: proliferation (cell division), apoptosis (programmed cell death), and neogenesis (regeneration from a pool of rapidly dividing cells, which themselves derive from pluripotent stem cells, or possibly de-differentiated β-cells, or alternatively trans-differentiated pancreatic cells); these processes are influenced by the levels of both glucose and insulin [3,5,9,10,16,22,34,45]. As a result, there is an interplay between the fast, ultradian fluctuations of glucose and insulin and the slower (>days) changes in β-cell mass. This means that we need to consider a fairly realistic, high-dimensional mathematical model on the fast time scale in order to abstract the slow-time dynamics; we choose the model developed by the Lyngby group (see [27] for a review of several comparable models).

2. Theory: time-scale homogenisation

The dynamics of a system comprising both the regulated physiology and the associated (neuro)endocrine system can, in many cases, be represented as a dynamical system of the following form:

$$\frac{d}{dt}\mathbf{x} = \mathbf{f}(\mathbf{x}, \mathbf{u}) \tag{1}$$

where $\mathbf{x}$ is the state of the system, $\mathbf{u}$ represents an external input, and $\mathbf{f}$ is the system's dynamics. We assume that the state variables in $\mathbf{x}$ and the input variables in $\mathbf{u}$ have been non-dimensionalised, so that time t is the only unit-bearing quantity remaining. The input $\mathbf{u}(t)$ is assumed to be a periodic function of time with period T. We now outline a construction that decomposes the original dynamics into two uncoupled systems of lower dynamical dimension. These two systems may be studied independently of one another. The idea is to preserve the way in which features of the dynamics affect the dynamics at the slow time scale, by constructing the slow dynamics as a map that is specific for the fast-scale regime. If this formulation seems obscure: the application in Section 3 provides examples.

For physiological systems it may naturally be assumed that the rates of change are bounded, that is, for each of the n state variables, there is a finite number ξ_i such that the dynamics of x_i satisfies

$$|f_i(\mathbf{x}, \mathbf{u})| < \xi_i < +\infty \tag{2}$$

as $\mathbf{x}$ and $\mathbf{u}$ range over all physiologically attainable values. Without loss of generality, the state variables can be ordered so that

$$\xi_1 \geqslant \xi_2 \geqslant \cdots \geqslant \xi_n > 0$$

(i.e., fastest first). Scaling of the f_i with respect to the corresponding ξ leads to

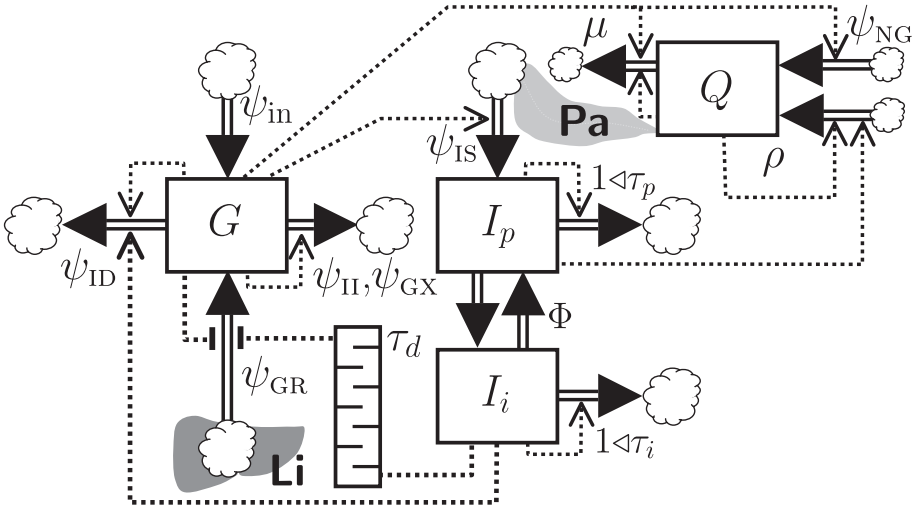

Fig. 1. Diagram of the extended Sturis–Tolić model. Squares are state variables, clouds are sources/sinks. Dotted lines indicate functional dependence (arrowheads: positive; blunt ends: negative). A delay line marked τ_d intervenes between I_i and ψ_{GR}. The state variable Q is the relative β-cell mass; with Q fixed at 1, the original Sturis–Tolić model is recovered. **Li**: liver, source of glucose derived from glycogen breakdown. **Pa**: pancreas, site of β-cells which are a source of insulin. See Table 1 for an explanation of the symbols.

$$\frac{d}{dt}\mathbf{x} = \boldsymbol{\xi}\cdot\mathbf{f}^*(\mathbf{x},\mathbf{u}) \tag{3}$$

where $\boldsymbol{\xi}$ is a diagonal matrix with the ξ_i on its main diagonal and f_i^* is a dimensionless quantity satisfying $|f^*| \leqslant 1$. We are interested in the case where some variables are "rapid" (i.e. oscillate on a time scale of order T) and others are "slow". That is to say, we consider the case where $\xi_1 \geqslant T^{-1} \gg \xi_n$ and we assume that there exists an $v \leqslant n$ such that $\xi_i T$ is a small parameter (i.e., $\xi_i T \ll 1$) for $v \leqslant i \leqslant n$. Anticipating the separation of time scales, we write

$$\mathbf{x}(t) = \mathbf{x}^{[0]}(\varphi(t),\tau(t)) + \mathbf{x}^{[1]}(\tau(t)) \tag{4}$$

where the fast component $\mathbf{x}^{[0]}$ depends on a fast time φ and a slow time τ, whereas the slow component $\mathbf{x}^{[1]}$ depends on slow time τ only. These two times are defined as follows:

$$\varphi = \frac{t}{T} - \left\lfloor \frac{t}{T} \right\rfloor \tag{5}$$

$$\tau = \xi_v T \left\lfloor \frac{t}{T} \right\rfloor \tag{6}$$

where $\lfloor x \rfloor$ denotes the largest integer smaller than or equal to x. The input is similarly decomposed;

$$\mathbf{u}(t) = \mathbf{u}^{[0]}(\varphi(t),\tau(t)) + \mathbf{u}^{[1]}(\tau(t)). \tag{7}$$

Let us write

$$\frac{\partial}{\partial\varphi}\mathbf{x}^{[0]} = T\boldsymbol{\xi}\cdot\mathbf{f}^*(\mathbf{x}^{[0]},\mathbf{u}^{[0]};\mathbf{x}^{[1]},\mathbf{u}^{[1]}) \tag{8}$$

for $\varphi \in [0,1)$. To follow the fast dynamics, Eq. (8) is integrated from $\varphi = 0$ to $\varphi = 1^-$ subject to initial condition $\mathbf{x}^{[0]} = \mathbf{0}$ at $\varphi = 0$. Now define the following variation: for $\eta \leqslant \xi_v T$ and $i = v,\ldots,n$:

$$\delta x_i^{[1]}(\tau,\eta) = T\xi_i \int_0^{\eta/(\xi_v T)} f_i^*(\mathbf{x}^{[0]},\mathbf{u}^{[0]};\mathbf{x}^{[1]},\mathbf{u}^{[1]})\,d\varphi \tag{9}$$

(this variation may be regarded as a total differential *sensu* [31, p. 724]). Dividing Eq. (9) by η and specifying for $\eta = \xi_v T$, this becomes:

$$\frac{\delta x_i^{[1]}(\tau,\eta)}{\xi_v T} = \frac{\xi_i}{\xi_v}\int_0^1 f_i^*(\mathbf{x}^{[0]},\mathbf{u}^{[0]};\mathbf{x}^{[1]},\mathbf{u}^{[1]})\,d\varphi \tag{10}$$

for $i = 1,\ldots,n$. In the limit $\xi_v T \to 0$, the following expressions are exact:

$$\frac{d}{d\varphi}x_i^{[0]} = T\xi_i f_i^*(\mathbf{x}^{[0]},\mathbf{u}^{[0]};\mathbf{x}^{[1]},\mathbf{u}^{[1]}) \quad \text{for } i = 1,\ldots v-1 \tag{11}$$

$$\frac{d}{d\tau}x_i^{[1]} = \frac{\xi_i}{\xi_v}\int_0^1 f_i^*(\mathbf{x}^{[0]},\mathbf{u}^{[0]};\mathbf{x}^{[1]},\mathbf{u}^{[1]})\,d\varphi \quad \text{for } i = v,\ldots n \tag{12}$$

where for $i \geqslant v$ we have $x_i^{[0]} \equiv 0$, τ now denotes the argument of the $\mathbb{R} \mapsto \mathbb{R}$ function $x_i^{[1]}(\cdot)$, and the operator $\partial/\partial\varphi$ has been replaced by $d/d\varphi$ without impunity since φ is restricted to the interval $[0,1)$. If we let $\mathbf{x}_{v+}^{[1]} = \left(x_v^{[1]},\ldots,x_n^{[1]}\right)$ then for $i < v$ we have $x_i^{[1]} = X_i\left(\mathbf{x}_{v+}^{[1]}\right)$, where $\left(X_1\left(\mathbf{x}_{v+}^{[1]}\right),\ldots,X_{v-1}\left(\mathbf{x}_{v+}^{[1]}\right)\right)$ is a parametrical representation of the slow manifold of the dynamics of the system (or a branch of this manifold). The fast variables $x_1,\ldots,x_{v-1}$ move close to through a forced limit cycle of period T (and exactly so in the limit $\xi_v T \to 0$). The slow manifold can and generally will be varying in slow time τ. It may be desirable to have the slow variable represent a cycle average, rather than the start-of-cycle value which depends on the arbitrary assignment of phase value 0; this is not problematic but would render the notation somewhat more cumbersome and less perspicacious.

3. Calculation: application to the regulation of the glucose concentration in the blood plasma

We apply time-scale homogenisation to glycemic homeostasis, which is representative of a well-studied and important physiological system in which fast (regulatory) and slow (adaptive) responses interact in a way that is essential to the system's operation, both in health and disease.

3.1. The extended Sturis–Tolić model

The model for glucose dynamics as originally proposed by [39] and subsequently further developed by Tolić et al. [40] is depicted diagrammatically in Fig. 1 and is described by the following system of ordinary differential equations:

$$\frac{dG}{dt} = \psi_{\text{in}}(t) - \psi_{\text{II}}(G) - \psi_{\text{ID}}(G,I_i) + \psi_{\text{GR}}(G,w_3) - \psi_{\text{GX}}(G) \tag{13}$$

$$\frac{dI_p}{dt} = Q\psi_{\text{IS}}(G) - \Phi\left(\frac{I_p}{V_p} - \frac{I_i}{V_i}\right) - \frac{I_p}{\tau_p} \tag{14}$$

$$\frac{dI_i}{dt} = \Phi\left(\frac{I_p}{V_p} - \frac{I_i}{V_i}\right) - \frac{I_i}{\tau_i} \tag{15}$$

$$\frac{dw_1}{dt} = \frac{3(I_p - w_1)}{\tau_d} \tag{16}$$

$$\frac{dw_2}{dt} = \frac{3(w_1 - w_2)}{\tau_d} \tag{17}$$

$$\frac{dw_3}{dt} = \frac{3(w_2 - w_3)}{\tau_d} \tag{18}$$

$$\frac{dQ}{dt} = (\rho(I_p) - \mu(G))Q(t) + \psi_{\text{NG}}(G) \tag{19}$$

where we have adapted the notation slightly to facilitate cross-referencing. In the model, the state variable $G(t)$ denotes the blood plasma content of glucose whereas $I_p(t)$ denotes the blood plasma content of insulin (so that G/V_g and I_p/V_p are plasma concentrations) and $I_i(t)$ is the amount of insulin in the interstitial spaces of the body tissues. Furthermore, $w_1(t)$, $w_2(t)$, and $w_3(t)$ are auxiliary state variables that mimic a delay of duration τ_d in the release of glucose from hepatic glycogen stores, in response to I_p (see [27], for a more detailed explanation); and $Q(t)$ is the β-cell mass, which is a slow state variable presently added to the original model. The input is the forcing function $\psi_{\text{in}}(t)$, which represents the flux of glucose into the blood stream from external sources. The parameter Φ represents the diffusive exchange of insulin between blood and interstitial space; V_p and V_i are the distribution volumes of blood plasma and interstitial space, respectively, for insulin. The parameter τ_p represents the mean life time of an insulin molecule in the blood plasma, whereas τ_i represents the mean life time of an insulin molecule in the interstitial space. These dependencies are modelled in the Sturis–Tolić model by means of plausible, empirical functional relationships, which are listed in Appendix A.

As indicated in Fig. 1, there are a number of rates and fluxes that depend in various different ways on the state variables. Glucose-uptake by the tissue depends on the plasma glucose level only in the case of insulin-independent uptake (ψ_{II}), but also on the plasma insulin level in the case of insulin-dependent glucose uptake (ψ_{id}). When glucose levels become very high, the kidneys begin to excrete glucose; this flux is indicated as ψ_{GX}. Two fluxes contribute to increases of plasma glucose: these are the input from the food (or glucose administered by an injection or infusion), denoted as ψ_{in}, which is treated as a forcing function in the present model. The second flux is glucose secreted by the liver; this glucose release flux ψ_{GR} is also dependent on both plasma glucose and plasma insulin. Glucose stimulates the secretion of insulin, and thus the insulin secretion ψ_{IS} is glucose-dependent.

The model has been extended here with the dynamics of the β-cell mass, which involves three processes: β-cell proliferation, whose specific rate ρ is assumed to depend on plasma insulin; β-cell death, occurring at a specific rate μ that depends on both plasma glucose and insulin, and a neogenesis flux ψ_{NG} which also depends on both plasma glucose and insulin. Empirical formulas for these dependencies, as well as a justification, are given in Appendices A and B. Inasmuch as the contribution of neogenesis remains to be fully elucidated and may be considered controversial, we shall analyse the model first on the assumption that this term is absent.

The glucose input $\psi_{in}(t)$ can assume various forms. It may be set to a constant value, as can be arranged under experimental conditions where glucose is administered by means of an infusion, or it may be time-varying. If ψ_{in} is set to a constant value, ultradian oscillations may become prominent feature of the dynamics, as shown by Tolić et al. [40]. Here we choose as standard reference a periodic function with a period of 24 h and three "meal peaks" in every day, as shown in the top panel of Fig. 2. Under this particular input, the system settles on a stationary forced cycle within a few days, also shown in Fig. 2.

3.2. Analysis without neogenesis of β-cells

To analyse the dynamics in the absence of neogenesis, we set $\hat{\psi}_{NG} = 0$. It will emerge that the resulting β-cell dynamics is very slow on this assumption, which can be taken as indirect evidence that neogenesis is an important factor in rapid (i.e., hours/days rather than months or years) adaptation, provided we accept the parameter values taken from the literature.

Following the method outlined in Section 2, the steps are to render the system dimensionless, except for time, determine the maximum absolute rates (the ξs), and to rank the scaled variables according to these rates. Choosing 10 g as the reference value for glucose and 44 mU as the reference value for insulin, we find the following ranking (ξs all in min^{-1}; Q is already dimensionless):

$x_1 = I_p/I_{ref}$	$x_2 = G/G_{ref}$	$x_3 = I_i/I_{ref}$	$x_4 = w_1/I_{ref}$	$x_5 = w_2/I_{ref}$	$x_6 = w_3/I_{ref}$	$x_7 = Q$
$\xi_1 = 4.8$	$\xi_2 = 0.11$	$\xi_3 = 0.066$	$\xi_4 = 0.028$	$\xi_5 = 0.028$	$\xi_6 = 0.028$	$\xi_7 = 8.7 \times 10^{-7}$

A time-scale separation at $v = 7$ is apparent, with small parameter $\xi_v T = 8.7 \times 10^{-7}\,\text{min}^{-1} \times (24 \times 60\,\text{min}) = 0.00125$; a unit of slow time τ thus corresponding to 800 days.

The theory of Section 2 now prescribes that the dynamics in slow time for $x_7^{[1]}$ is derived using Eq. (12), whereas the variables $x_1^{[1]}, \ldots x_6^{[1]}$ are to be obtained as functions of $x_7^{[1]}$ on the basis of the slow-manifold condition, which corresponds to the stationary forced cycle in fast time when $x_7^{[1]}$ is held at a fixed value. These relations can be obtained numerically without trouble: results are shown in Fig. 3. Since the reference cycle corresponds to a fairly high glycemic load, higher loads may be regarded as hyperglycemic. At such loads, the dynamics of the β-cell mass has two fixed points: a lower unstable one and a higher stable point. The existence of the unstable fixed point, referred to as a "pathological fixed point" by [41], indicates that catastrophic involution of β-cell mass will occur when x_7 becomes lower than this equilibrium value. It will then decay to zero: the loss of β-cells leads to further hyperglycemia and lower insulinemia, which leads to further β-cell losses [41]. Such a process may underlie non-autoimmune diabetes mellitus, as described by [15].

As the glycemic load increases, these two fixed points move together and collide. At even higher glycemic loads, the globally attracting point is the trivial equilibrium $Q = 0$, that is, zero β-cell mass. The decrease in the stable equilibrium value with increasing glycemic load is due to an increased β-cell death rate at such high

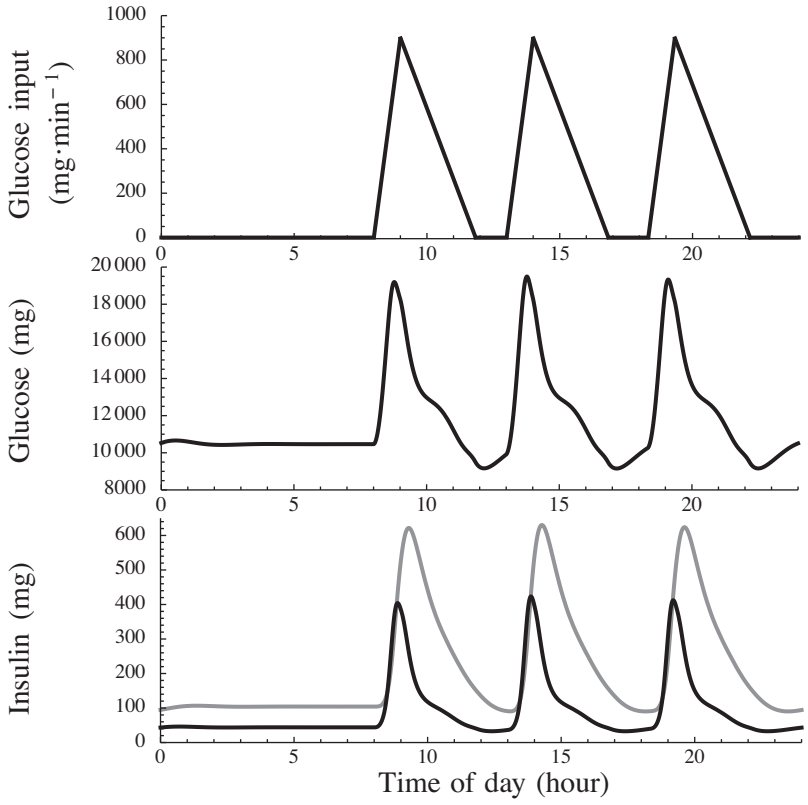

Fig. 2. Reference cycle. Top: glucose input; middle: plasma glucose content; bottom: plasma (black line) and interstitial space (grey line) insulin content.

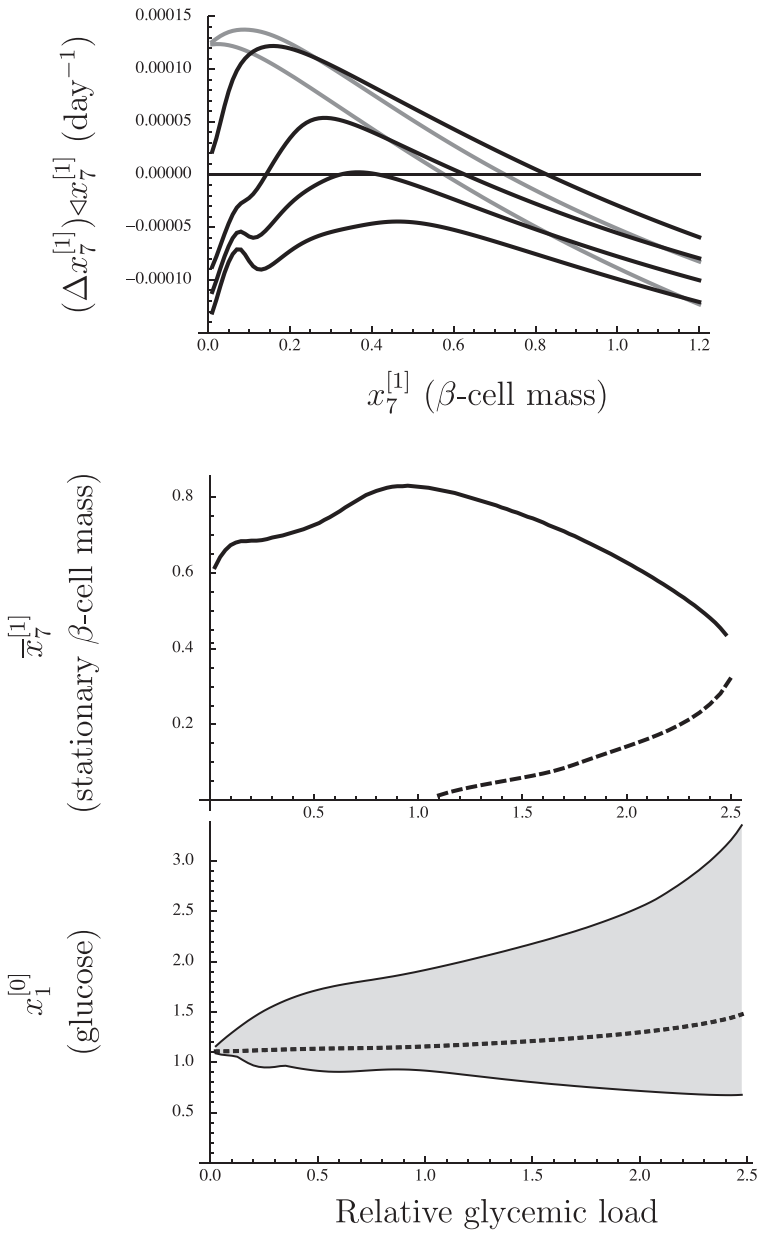

Fig. 3. Dynamics of β-cell mass on the slow time scale. Top: relative daily change of β-cell mass, for various glycemic loads (black curves, from top to bottom: 1, 2, 2.5, and 3 times the reference input; grey curves, from top to bottom: 0.5 and 0 times the reference input). Middle: fixed point of the β-cell dynamics as a function of the relative glycemic load (solid line: stable branch; dashed line: unstable branch). Bottom: fast-time scale glucose stationary cycle characteristics (dotted line: average value; bottom and top of filled region: minimum and maximum values).

loads, both as a result of higher glucose toxicity [10], and of increased susceptibility to apoptosis at higher insulin levels [16]; the latter authors describe this situation as a "sweet spot" for insulin in the high pico-molar range, which corresponds to order 1 levels in the scaled system.

As might be expected from the strong separation of time scales, the approximation for the slow-time scale dynamics is excellent. Fig. 4 compares the dynamics according to the approximation (which is simple and 1-dimensional) to the dynamics of the original, 7-dimensional, system, in an overfeeding and an underfeeding simulation. The results are indistinguishable: thus, the long-term dynamics is well-captured by the approximation. The full system was numerically integrated in fast time using an explicit Runge–Kutta method of order 2(1), which is the *Mathematica* default method [37]. The slow system was evaluated using Euler-forward with a step size of one day, giving virtually the same result at less than a thousandth of the computational cost (run time; excluding the one-time cost of establishing the dynamics of x_7, which costs about 1% of the full-system's run time).

In formulating a mathematical model for the long-term dynamics of the β-cell mass, it is tempting, although incorrect, to represent the glycemic load as a constant that represents the average of the daily cycle (e.g., [8,41]; Ribbing et al., [33]). However, the dynamics of $x_7^{[1]}$ in slow time τ does in fact depend critically on the "temporal fine structure" of glucose uptake on the fast time scale t, through the integration in Eq. (12). Such dependence is neglected by an approach that replaces glucose uptake by its short-term average. This becomes readily apparent when we consider the case where the glycemic load is assimilated as a constant infusion (set to zero for the first 30 minutes after midnight, to enforce a 24-hour cycle) instead of a daily 3-meal cycle. It is found that the long-term dynamics of the β-cell mass is strikingly different: the

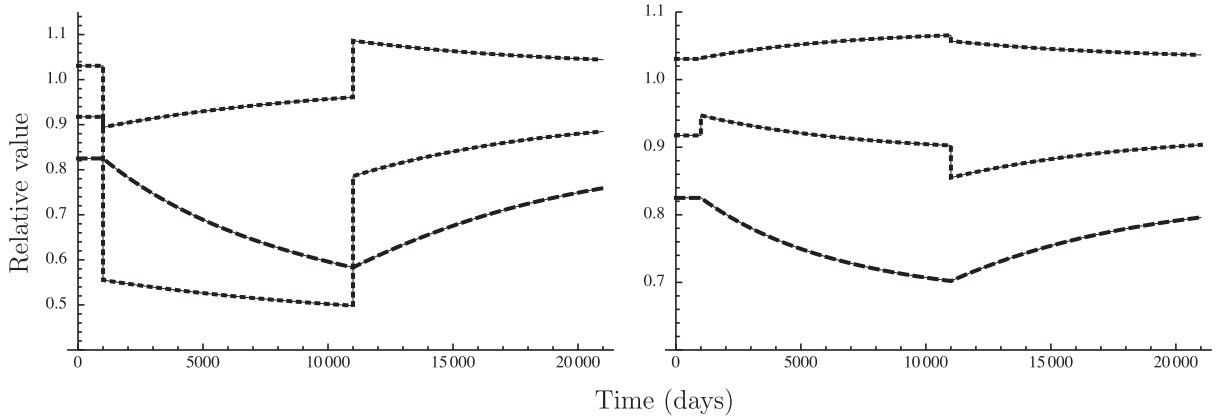

Fig. 4. Simulations of overfeeding (left) and (underfeeding) right. On day 1000, the glycemic load is changed to 2.5 (left) or 0.1 (right) normal; on day 11,000 the load is restored to the normal value. Dotted line: slow glucose; dot-dashed line: slow plasma insulin; dashed line: slow β-cell mass. Thin lines show the results of a direct simulation of the 7-dimensional system. ("Relative value" refers to scaling by G_{ref} and I_{ref}, as explained in the text; $Q = x_7 = 1$ corresponds to the stationary value of β-cell mass if the standard-cycle glycemic load were administered at a constant rate; stationary values can be read off from Fig. 3).

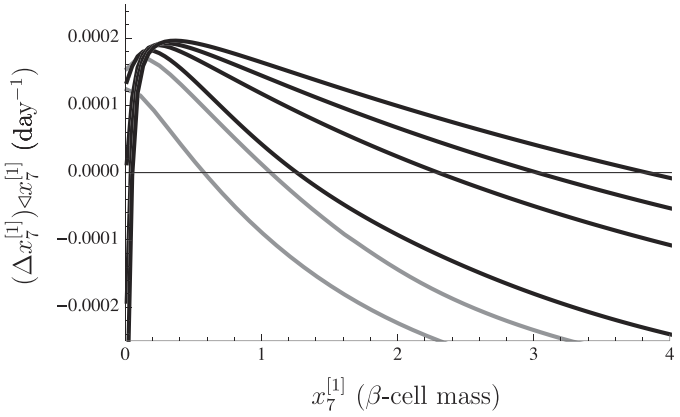

Fig. 5. Dynamics of β-cell mass on the slow time scale: relative daily change of β-cell mass, for various glycemic loads, administered as a constant infusion (black curves, from left to right: 1, 2, 2.5, and 3 times the reference input; grey curves, from left to right: 0 and 0.5 times the reference input).

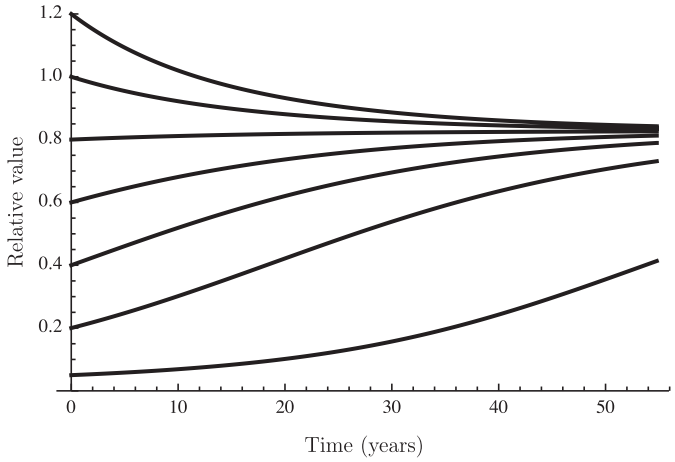

Fig. 6. Dynamics of β-cell mass on the slow time scale: recovery to normal values after addition or destruction of β-cells at time $t = 0$. ("Relative value" has the meaning explained in the caption for Fig. 4).

"pathological fixed point" remains very close to zero and the system achieves near-perfect regulation of the average glucose level even at a hyperglycemic load that is 4 times higher than normal, as shown in Fig. 5. Comparison with the case $\iota_{\mathrm{AI}} \to \infty$ (not shown) shows that decrease of insulin's potency in inhibiting apoptosis at high levels is responsible for keeping the β-mass in check without compromising the ability to regulate: for $\iota_{\mathrm{AI}} \to \infty$, the fixed point of x_7 increases sharply with load, even though normalisation of glucose levels is already achieved at x_7-values comparable to those indicated in Fig. 5.

3.3. Extended model with neogenesis of β-cells

The response dynamics shown in Fig. 4 is very slow. An example of such sluggish dynamics is shown in Fig. 6: if 80% of the β-cell mass is destroyed, it takes about 50 years to recover. This means that the subject will be effectively diabetic for much of his or her lifetime; the baseline turn-over dynamics of β-cells is too sluggish to respond adequately to such challenges. However, in reality, recovery from such damage is accomplished within a few weeks' time [5]. It has been proposed that the slowly proliferating β-cell pool may, under certain conditions, be replenished by differentiation of cells from a more quickly proliferating pool of progenitor cells [7,34] that is phenotypically distinct from the differentiated β-cells themselves [1]. A competing hypothesis is that β-cells themselves are capable of rapid proliferation [9,20,25]. The two hypotheses may be reconciled if the rapidly proliferating pool of cells is derived (by a process akin to dedifferentiation) from adult β-cells, since such cells are readily driven back into cell cycle by activation of the proto-oncogene c-myc [30]. Here, the pool of proliferators will be treated as a source term, an approach compatible with either point of view. We shall refer, for the sake of clarity, to the proliferator pool as "progenitors", with the caveat noted above.

We propose to describe the neogenesis of β-cells from progenitor cells by the following equation:

$$\psi_{\mathrm{NG}}(G) = \hat{\psi}_{\mathrm{NG}} \left(1 + \exp\left\{\alpha_{\mathrm{NG,g}}\left(1 - \frac{G/V_g}{\gamma_{\mathrm{NG}}}\right)\right\}\right)^{-1} \left(1 + \exp\left\{\alpha_{\mathrm{NG,i}}\left(1 - \frac{I_i/V_g}{\iota_{\mathrm{NG}}}\right)\right\}\right)^{-1} \tag{20}$$

with positive parameters $\hat{\psi}_{\mathrm{NG}}, \alpha_{\mathrm{NG,g}}, \alpha_{\mathrm{NG,i}}, \iota_{\mathrm{NG}}$, and γ_{NG}. This equation is built from the same generic sigmoid building blocks used in the original model, to represent graded responses to the relevant stimuli. The key assumption is that neogenesis is driven by prolonged hyperglycemia [22] in conjunction with elevated insulin levels [12]. It may be observed that the right-hand side of Eq. (20) behaves like a soft AND-gate: the flux ψ_{NG} is large when both glucose and

insulin levels are elevated. Prolonged concurrence of high glucose and insulin levels may be associated with insufficiency, so it would make sense to control β-cell mass compensation in this manner. From a mechanistic point of view, it is known that the pathway regulating rapid β-cell proliferation can act like an AND-gate. Specifically, the proto-oncogene gene c-myc, which encodes the transcription factor c-Myc, which stimulates proliferation as well as susceptibility to apoptosis [29] such that the net effect is loss of β-cells unless an anti-apoptotic co-signal is present [30]. Expression of c-Myc is induced by glucose [18] whereas insulin induces an anti-apoptotic signal [17]. Thus, whereas glucose alone induces a net loss of β-cells [42], the simultaneous presence of glucose and insulin would stimulate rapid proliferation, possibly via rapid (partial) dedifferentiation of existing adult β-cells to the proliferative phenotype. It has been suggested that this dual proliferation/apoptosis pathway acting via c-myc acts as a fail-safe that defaults to β-cell loss unless both glucose and insulin are elevated [29].

The action of glucose is indirect and thought to be via glucagon-like peptide 1 (GLP-1; [7]), an incretin and cytokine which is secreted by enteroendocrine L-cells. Since the half-life of GLP-1 is extremely short [23], an instantaneous functional dependence on G/V_p appears warranted. In principle, ψ_{NG} should also depend on, and be limited by, the amount of progenitor cells present in the pancreas; in the present model, this pool is assumed to be non-limiting and is thought of as an unlimited source.

When neogenesis is included in the model, recovery from partial ablation of β-cell mass is much more rapid and in keeping with the various values quoted in the literature (recovery in a 1 to 5 week period; see [5], for a review of the experimental data), as shown in Fig. 7. The slow-time approximation is still excellent, despite the fact that time-scale separation is now up to two orders of magnitude worse due to the rapid β-cell expansion that occurs when the β-cell mass is too low. The relationship between $\frac{d}{d\tau}x_7$ and x_7 remains qualitatively the same, except that the lower, unstable fixed point (the pathological fixed point) is now very low and the positive rate of change that prevails when x_7 lies in between the fixed points is now several orders of magnitude larger.

If too much of the β-cell mass is destroyed, recovery takes disproportionally longer, as shown in the bottom panel of Fig. 7: when more than ~80% of the β-cells are destroyed, recovery takes the best part of a year, which implies the subject is diabetic for a number of months until recovery occurs.

Type 1 diabetes is an illness due to autoimmunity directed against β-cells [43]. The simulations in Fig. 7 suggest that there is a critical level of ablation at which recovery becomes very much slower. If the progenitor cells do not express the insulin-derived antigen, or do so in sufficiently low levels to escape immune attack, the progression to type 1 diabetes is a matter of ψ_{NG} being unable to compensate for the losses, leading to a net diminishment of β-cell mass until the critical depletion level is reached. If the progenitor cells are also susceptible to immune attack, the rate of recovery will be further compromised and the rate at which the β-cell mass descends to the critical level may be accelerated.

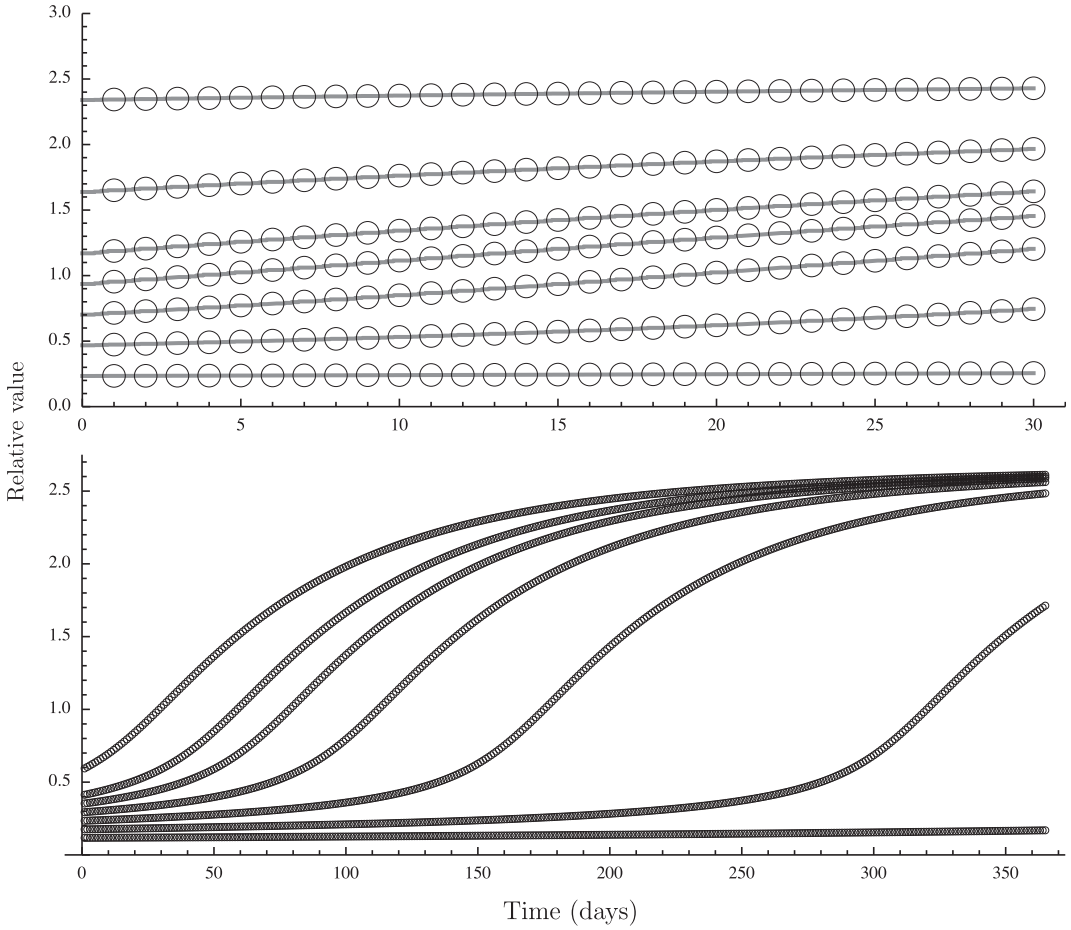

Fig. 7. Model with neogenesis: recovery to normal values after addition or destruction of β-cells at time $t = 0$. Gray curves: direct simulation; circles: approximation according to slow-time approximation. Top panel: recovery over a month; bottom panel: recovery over a year. ("Relative value" has the meaning explained in the caption for Fig. 4, but the normal stationary value is now different since the dynamics includes neogenesis).

4. Discussion

The interplay between the glycemic homeostasis feedback loop, which operates on the ultradian time scale, and the adaptive changes in β-cell mass, which happen on a days-to-months time scale, is a typical feature of endocrinological and neuroendocrinological regulation, where a slower adaptive feedback loop is superimposed on a more rapid feedback loop, the latter directly involved with a physiological system, with the former regulating the level of activity in some manner, e.g. by controlling rates of transcription, translation, electrical activity (secretion), or, as in the present example, number of endocrine cells [6]. Moreover, the dynamics of such systems usually exhibits a strongly non-linear character [19], which means that small variations in the precise time courses of the fast processes (the temporal fine structure) can have a profound effect on the rates of change of the slow processes. Time-scale separation can be a powerful tool to abstract a low-dimensional dynamical system modeling the slow adaptation process, which is considerably more easy to analyse and visualise. In the present case, a 7-dimensional dynamics is reduced to 1-dimensional dynamics, which is straightforward to analyse; indeed, as Fig. 3 shows, in qualitative terms the system is much like logistic growth with an Allee effect.

When Eq. (12) is evaluated (in most cases this needs to be done numerically), the causal relationships may be obscured somewhat. For instance, in the present model, the rate of change of the β-mass is dependent, in the direct, mechanistic sense of the word, on glucose and insulin, as the model's equations make explicit. However, the time courses of glucose and insulin depend on the prevailing β-cell mass, together with the input ψ_{in}, and as a result, in slow time, the rate of change of the β-cell mass depends on the β-cell mass itself in conjunction with the input waveform, i.e., the rate of change in slow time is a *functional* of the input $\psi_{\text{in}}(t)$, as is clear from the integration over the fast-time scale cycle in Eq. (12). In this way, the temporal fine structure is taken into account, in analogy to similar spatial homogenisation procedures (see [13,19]).

The assumption in this paper has been that rapid compensation in β-cell mass is driven by proliferation, based on the observation that β-cells can be driven back into cell cycle by activation of c-myc [30] and data on recovery from partial pancreatomy and hyperglycemic challenge ([5]). However, it is also possible that β-cells respond by adjusting the amount of hormone-producing machinery per cell (and, concomitantly, cell volume) and that data concerning short-term changes in numbers of β-cells are distorted by the fact that temporarily depleted cells (degranulated cells) are spuriously not counted as β-cells [2]. The relative importance of such non-proliferative adaptation, which possibly depends on the time scales and extend of challenge at hand, remains to be elucidated in detail; whereas hypertrophy was held to be the main mechanism for increases in β-cell mass in man until the last decade [24,44], recent years have seen a change in emphasis towards proliferation and neogenesis [5,21,30].

In the model considered here, all but one of the state variables was fast. The Sturis–Tolić model can be extended with further slow variables. One such variable might be the insulin sensitivity of the body's tissues, which plays a major role in the etiology of type 2 diabetes [35]. However, a more precise characterisation of the process we have referred to as neogenesis is essential to make progress: in particular, the maximum rate at which this pool can proliferate, as well as the rates at which it is replenished (which may depend on the sources: β-cells are transdifferentiated pancreatic cells) are likely to be critical to the ability of neogenesis to furnish the amount of new β-cells required. The present paper has shown that the pathological fixed point, first noted and so termed by [41], becomes a prominent factor only when neogenesis is impaired, and, moreover, that this pathological fixed point has a value that is dependent on the diel time course of the rate at which glucose is administered to the system. Whereas mathematical modelling can never replace the experiments that elucidate these processes, it can help to characterise the functional consequences of these findings along the lines outlined in the present paper.

Acknowledgements

Y-FW is grateful the University of Warwick and the EPSRC for financial support.

Appendix A. Functional relationships for rates and fluxes

The ψs are fluxes and rates modelled by empirical functions: ψ_{II} represents insulin-independent glucose uptake by body cells:

$$\psi_{\text{II}}(G) = \hat{\psi}_{\text{II}}\left[\delta\left(1-\exp\left\{-\frac{G/V_g}{\gamma_{\text{II,lo}}}\right\}\right)+\frac{1-\delta}{1+\exp\left\{\alpha_{\text{II}}\left(1-\frac{G/V_g}{\gamma_{\text{II,hi}}}\right)\right\}}\right] \tag{A.1}$$

where $\hat{\psi}_{\text{II}}, \gamma_{\text{II,lo}}, \gamma_{\text{II,hi}}, \delta$, and V_g are positive parameters (see Table 1 for values). Insulin-dependent glucose uptake is represented by ψ_{ID}:

$$\psi_{\text{ID}}(G) = \frac{G/V_g}{\gamma_{\text{ID}}}\left[\psi_0+\frac{\hat{\psi}_{\text{ID}}-\psi_0}{1+\exp\left\{-\alpha_{\text{ID}}\ln\left\{(I_i/\iota_{\text{ID}})(V_i^{-1}+(\Phi\tau_i)^{-1})\right\}\right\}}\right] \tag{A.2}$$

with positive parameters $\psi_0, \hat{\psi}_{\text{ID}}, \alpha_{\text{ID}}\gamma_{\text{ID}}$, and ι_{ID}. Endogenous release of glucose is represented by ψ_{GR}:

$$\psi_{\text{GR}}(G,w_3) = \hat{\psi}_{\text{GR}}\left(1+\exp\left\{-\alpha_{\text{GR,g}}\left(1-\frac{G/V_g}{\gamma_{\text{GR}}}\right)\right\}\right)^{-1}\left(1+\exp\left\{-\alpha_{\text{GR,i}}\left(1-\frac{w_3/V_p}{\iota_{\text{GR}}}\right)\right\}\right)^{-1} \tag{A.3}$$

with positive parameters $\hat{\psi}_{\text{GR}}, \alpha_{\text{GR,i}}, \alpha_{\text{GR,g}}, \iota_{\text{GR}}$, and γ_{GR}. Insulin secretion from pancreatic β-cells is represented by ψ_{IS}:

$$\psi_{\text{IS}}(G) = \hat{\psi}_{\text{IS}}\left(1+\exp\left\{\alpha_{\text{IS}}\left(1-\frac{G/V_g}{\gamma_{\text{IS}}}\right)\right\}\right)^{-1} \tag{A.4}$$

with positive parameters $\hat{\psi}_{\text{IS}}, \alpha_{\text{IS}}$, and γ_{IS}. Renal excretion of glucose, which becomes important at elevated glucose levels, is represented by ψ_{GX}:

$$\psi_{\text{GX}} = \psi^*_{\text{GX}}\ln\left\{1+\alpha_{\text{GX}}\exp\left\{\frac{G/V_g}{\gamma_{\text{GX}}}\right\}\right\} \tag{A.5}$$

with positive parameters $\psi^*_{\text{GX}}, \alpha_{\text{GX}}$, and γ_{GX}. The proliferation rate of the β-cells is assumed to be dependent on the insulin concentration:

$$\rho(I_p) = \rho_0\left(1+\delta_0\frac{I_p}{\iota_0 V_p + I_p}\right) \tag{A.6}$$

with positive parameters ρ_0, α_0, and ι_0. The death rate of the β-cells is assumed to be dependent on the glucose concentration and the interstitial insulin concentration:

$$\mu(G,I_i) = \hat{\mu}\left(1+\frac{I_i/V_i}{\iota_{\text{AI}}}\right)\left(1+\exp\left\{\alpha_1-\frac{G/V_g}{\gamma_1}-\alpha_2\left(1-\frac{G/V_g}{\gamma_2}\right)^4\right\}\right)^{-1} \tag{A.7}$$

with positive parameters $\hat{\mu}, \alpha_1, \alpha_2, \gamma_1$, and γ_2. The above formulas and the values listed in Table 1 have been taken from [40], with the addition of two novel elements: glucose excretion (ψ_{GX}), which is necessary to represent hyperglycaemic challenges, and the β-cell mass dynamics. Glucose excretion is based on the graph given in

Table 1
Notation and parameter values.

Parameter	Value	Units	Interpretation
Φ	0.2	l min^{-1}	Blood/interstitial space permeability
V_p	3	l	Insulin distribution volume
V_i	11	l	Interstitial space volume
V_g	10	l	Glucose distribution volume
τ_g	6	min	Mean lifetime of insulin in plasma
τ_i	100	min	Mean lifetime of insulin in interstitial space
τ_d	36	min	Response delay of glucose release
α_1	1.86	–	First sensitivity of β-cell death
α_2	14.5	–	Second sensitivity of β-cell death
α_{II}	4.8	–	Sensitivity of insulin-independent glucose uptake
α_{ID}	1.77	–	Sensitivity of insulin-dependent glucose uptake
$\alpha_{\mathrm{GR,i}}$	7.54	–	Insulin sensitivity of hepatic glucose release
$\alpha_{\mathrm{GR,g}}$	10	–	Glucose sensitivity of hepatic glucose uptake
α_{IS}	6.67	–	Sensitivity of insulin secretion
α_{GX}	0.00065	–	Renal excretion parameter
$\alpha_{\mathrm{NG,i}}$	0.5	–	Sensitivity of neogenesis to insulin
$\alpha_{\mathrm{NG,g}}$	0.5	–	Sensitivity of neogenesis to glucose
γ'_1	1.6	g l^{-1}	First pivot point of β-cell death rate
γ'_2	2.6	g l^{-1}	Second pivot point of β-cell death rate
$\gamma'_{\mathrm{II,lo}}$	144	mg l^{-1}	Pivot point of non-splanchnic insulin-independent glucose uptake
$\gamma'_{\mathrm{II,hi}}$	2	g l^{-1}	Pivot point of splanchnic insulin-independent glucose uptake
γ'_{ID}	1	g l^{-1}	Pivot point of insulin-dependent glucose uptake
γ'_{GR}	2	g l^{-1}	Pivot point of glucose release
γ'_{IS}	2	g l^{-1}	Pivot point of insulin secretion
γ'_{GX}	0.3	g l^{-1}	Renal excretion parameter
γ'_{NG}	1.3	g l^{-1}	Pivot point of neogenesis for glucose dependence
δ	0.34	–	Contribution of non-splanchnic insulin-independent glucose uptake
δ_0	0.64	–	Insulin-sensitive portion of β-cell proliferation
$\imath_0$	115	mU l^{-1}	Pivot point of β-cell proliferation rate
$\imath_{\mathrm{ID}}$	80	mU l^{-1}	Pivot point of insulin-dependent glucose uptake
$\imath_{\mathrm{GR}}$	26	mU l^{-1}	Pivot point of hepatic glucose release
$\imath_{\mathrm{AI}}$	0.3	U l^{-1}	Pivot point for apoptosis inhibition
$\imath_{\mathrm{NG}}$	30	mU l^{-1}	Pivot point for neogenesis for insulin dependence
ψ_0	40	mg min^{-1}	Baseline of insulin-dependent glucose uptake
$\hat{\psi}_{\mathrm{II}}$	0.21	g min^{-1}	Maximum flux: insulin-independent glucose uptake
$\hat{\psi}_{\mathrm{ID}}$	0.94	g min^{-1}	Maximum flux: insulin-dependent glucose uptake
$\hat{\psi}_{\mathrm{GR}}$	0.18	g min^{-1}	Maximum flux: hepatic glucose release
$\hat{\psi}_{\mathrm{IS}}$	0.21	U min^{-1}	Maximum flux: insulin secretion
$\hat{\psi}_{\mathrm{NG}}$	0.001	min^{-1}	Maximum flux: neogenesis of β-cell mass
ψ^*_{GX}	29	mg min^{-1}	Renal excretion parameter
ρ_0	0.166	yr^{-1}	Baseline β-cell proliferation rate
$\hat{\mu}$	0.311	yr^{-1}	Maximum β-cell death rate

The term "pivot point" refers to midrange values, saturation constants etc. of saturating responses.
Insulin units: 1 U $\doteq$ 6.67 nmol.

[36], whereas β-cell mass dynamics is based on various data from the literature, as detailed in Appendix B.

Appendix B. Parameter estimation for β-cell dynamics

Whereas the fast time-scale parameters could be adopted from [40], the rates of proliferation, death, and neogenesis of β-cells had to be estimated from the experimental literature. Although the model describes the human system, the parameter values here are taken from experiments on rodents, which is a limitation. However, the parameters represent cellular characteristics which may to a first approximation be assumed to be transferrable from the rodent to the human setting. An exception is the parameter $\hat{\psi}_{\mathrm{NG}}$, but our method of estimating this parameter implicitly contains the required scaling.

B.1. Death

Efanova et al. [10] reported fractions of surviving β-cells after 40 hours and exposure to varying levels of glucose. The average death rate per hour over this interval can be estimated using the formula $-\ln\{f\}/(40\,\mathrm{h})$ where f is the fraction of cells alive after 40 h of exposure. Death rates thus obtained are plotted as a function of the ambient glucose concentration in Fig. B.8. Eq. (A.7), which is not intended as a mechanistic explanation but merely to capture

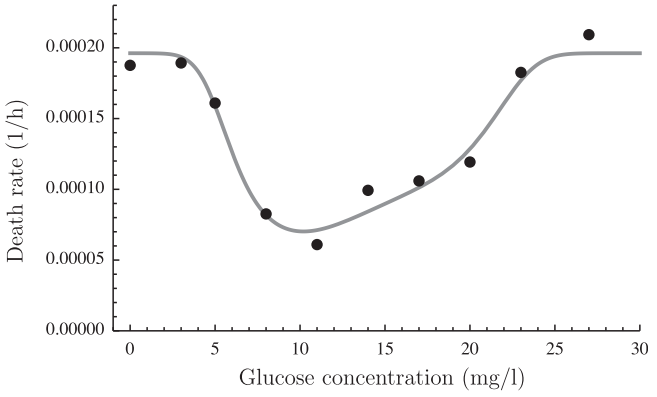

Fig. B.8. Pancreatic β-cell death rate data and least-squares fit of the formula used in the model.

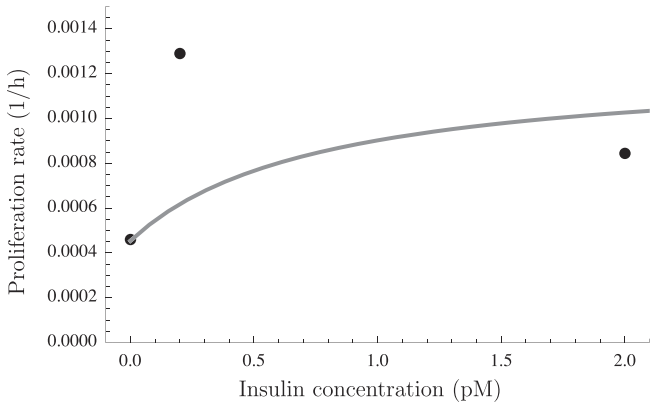

Fig. B.9. Pancreatic β-cell proliferation rate data and least-squares fit of the hyperbolic formula used in the model.

the phenomenology, was fitted to these data by non-linear least-squares. However, it was found that these rates were several orders of magnitude larger than the accepted β-cell turn-over rate quoted in the literature [9,41], which may be attributed to the unfavourable *ex vivo* conditions under which these data were obtained. For this reason, the parameter was scaled $\hat{\mu}$ in such a way that the standard cycle described in the main text would be characterised by a balance of β-cell birth and death.

Johnson et al. [17] documented a direct anti-apoptotic effect of insulin, quantified by various measures which showed broadly similar trends in dependence upon insulin concentration, the effect being most pronounced at low insulin levels and diminishing hyperbolically as insulin is increased to hyper-physiological levels. Johnson and Alejandro [16] synthesised these trends in a single graph, which shows that the relative potency of the anti-apoptotic effect drops off more or less hyperbolically with insulin concentration I, i.e. as follows:

$$\text{relative effect} = \frac{1}{\iota_{\text{AI}} + I} \tag{B.1}$$

where ι_{AI} is approximately $0.3\,\text{U}\,\text{l}^{-1}$. The reciprocal of this protective effect appears as a prefactor of the death rate in Eq. (A.7).

B.2. Proliferation

Okada et al. [26] and Beith et al. [3] demonstrated that insulin stimulates β-cell proliferation. Data taken from the latter paper were used to fit a simple hyperbolic model, Eq. (A.6), shown in Fig. B.9.

B.3. Neogenesis

Neogenesis of β-cells remains to be fully characterised in quantitative terms. The formula used in this paper to represent the rate at which β-cells are replenished is therefore speculative. To obtain reasonable values for the relevant parameters (those with subscript NG), simulations were performed that mimicked an experiment described by Steil et al. [38] in which rats were given infusions of glucose that initially doubled the plasma glucose levels. Within a day, euglycemia was re-established and the β-cell mass had doubled. The simulations are shown in Fig. B.10.

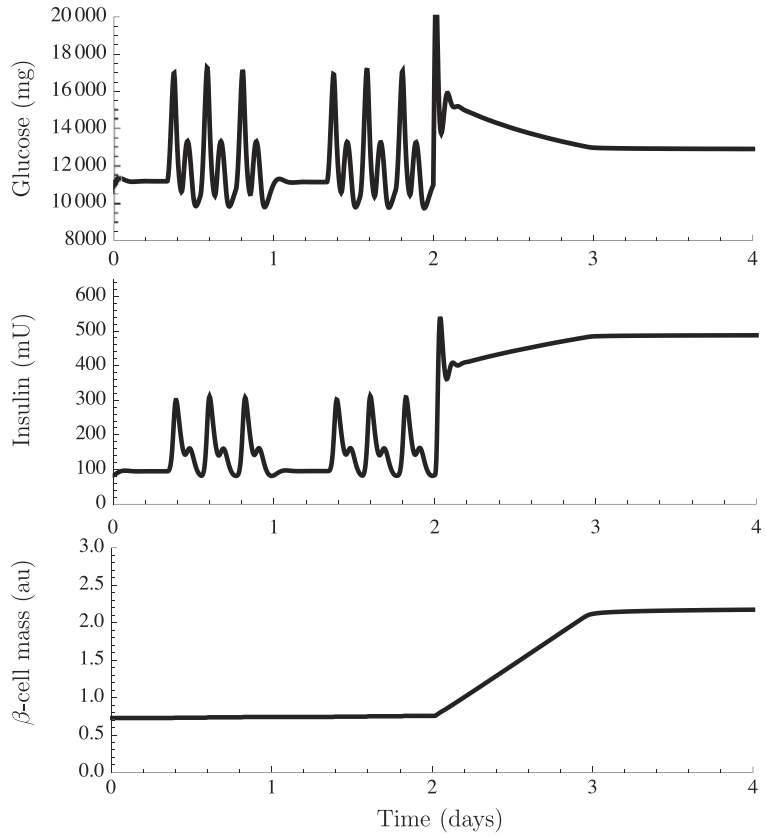

Fig. B.10. The Steil et al. experiment as simulated by the present model. After two control days, glucose is switched to an infusion. Top: plasma glucose content; middle: interstitial space insulin content; bottom: β-cell mass.

References

[1] A. Ackermann Misfeldt, R.H. Costa, M. Gannon, β-cell proliferation, but not neogenesis, following 60% partial pancreatomy is impaired in the absence of FoxM1, Diabetes 57 (2008) 3069.
[2] E. Akirav, J.A. Kushner, K.C. Herold, β-Cell mass and Type 1 diabetes, Diabetes 57 (2008) 2883.
[3] J.L. Beith, E.U. Alejandro, J.D. Johnson, Insulin stimulates primary β-cell proliferation via Raf-1 kinase, Endocrinology 149 (1998) 2251.
[4] S. Bonner-Weir, Perspective: postnatal pancreatic β cell growth, Endocrinology 141 (2000) 1926.
[5] L. Bouwens, I. Rooman, Regulation of pancreatic beta-cell mass, Physiol. Rev. 85 (2005) 1255.
[6] C.G.D. Brook, N.J. Marshall, Essential Endocrinology, Blackwell Science, 2001.
[7] D.D. De León, S. Deng, R. Madani, R.S. Ahima, D.J. Drucker, D.A. Stoffers, Role of endogenous glucagon-like peptide-1 in islet regeneration after partial pancreatectomy, Diabetes 52 (2003) 365.
[8] W. De Winter, J. DeJongh, T. Post, B. Ploeger, R. Urquhart, I. Moules, D. Eckland, M. Danhof, A mechanism-based disease progression model for comparison of long-term effects of prioglitazone, metformin and gliclazide on disease processes underlying type 2 diabetes mellitus, J. Pharmacokinet. Pharmacodyn. 33 (3) (2006) 313.
[9] Y. Dor, J. Brown, O.I. Martinez, D.A. Melton, Adult pancreatic β-cells are formed by self-duplication rather than stem-cell differentiation, Nature 429 (2004) 41.
[10] I. Efanova, S. Zaitsev, B. Zhivotoysky, M. Köhler, S. Efendić, S. Orrenius, P.O. Berggren, Glucose and tolbutamide induce apoptosis in pancreatic β-cells. A process dependent on intracellular Ca^{2+} concentration, J. Biol. Chem. 273 (1998) 33501.
[11] K.N. Frayn, Metabolic Regulation: A Human Perspective, W.B. Saunders, 2003.
[12] E.J. Grossman, D.D. Lee, J. Tao, R.A. Wilson, S.-Y. Park, G.I. Bell, A.S. Chong, Glycemic control promotes pancreatic beta-cell regeneration in streptozotocin-induced diabetic mice, PLoS ONE 5 (2010) e8749, doi:10.1371/journal.pone.0008749.
[13] M.H. Holmes, Introduction to Perturbation Methods, Springer, 1995.
[14] K.M. Hope, P.O.T. Tran, H. Zhou, E. Oseid, E. Leroy, R.P. Robertson, Regulation of α-cell function by the β-cell in isolated human and rat islets deprived of glucose: the "switch-of" hypothesis, Diabetes 53 (2004) 1488.
[15] A. Imagawa, T. Hanafusa, J.-I. Miyagawa, Y. Matsuzawa, A novel subtype of type 1 diabetes mellitus characterized by a rapid onset and an absence of diabetes-related antibodies, N. Engl. J. Med. 342 (2000) 301.
[16] J.D. Johnson, E.U. Alejandro, Control of pancreatic β-cell fate by insulin signaling: the sweet spot hypothesis, Cell Cycle 7 (2008) 1343.
[17] J.D. Johnson, E. Bernal-Mizrachi, E.U. Alejandro, Z. Han, T.B. Kalynyak, H. Li, J.L. Beith, J. Gross, G.L. Warnock, R.R. Townsend, M.A. Permutt, K.S. Polonsky, Insulin protects islets from apoptosis via Pdx1 and specific changes in the human islet proteome, Proc. Natl. Acad. Sci. USA 103 (2006) 19575.
[18] J.-C. Jonas, D.R. Laybutt, G.M. Steil, N. Trivedi, J.G. Pertusa, M. Van de Casteele, G.C. Weir, J.-C. Henquin, High glucose stimulates early response gene c-Myc expression in rat pancreatic cells, J. Biol. Chem. 276 (2001) 35375.
[19] J. Keener, J. Sneyd, Mathematical Physiology, Springer, 1998.
[20] C.S. Lee, D.D.D. León, K.H. Kaestner, D.A. Stoffers, Regeneration of pancreatic islets after partial pancreatectomy in mice does not involve the reactivation of neurogenin-3, Diabetes 55 (2006) 269.
[21] M.K. Lingohr, R. Buettner, C.J. Rhodes, Pancreatic β-cell growth and survival—a role in obesity-linked type 2 diabetes?, Trends Mol Med. (2002) 375.
[22] M. Lipsett, D.T. Finegood, β-cell neogenesis during prolonged hyperglycemia in rats, Diabetes 51 (2002) 1834.
[23] R. Mentlein, B. Gallwitz, W.E. Schmidt, Dipeptidyl peptidase IV hydrolyses gastric inhibitory polypeptide, glucagon-like peptide-1(7–36)amide, peptide histidine methionine and is responsible for their degradation in human serum, Eur. J. Biochem. 214 (1993) 829.
[24] J.H. Nielsen, C. Svensson, E.D. Galsgaard, A. Møldrup, N. Billestrup, Beta cell proliferation and growth factors, J. Mol. Med. 77 (1999) 62.
[25] T. Nir, D.A. Melton, Y. Dor, Recovery from diabetes in mice by β cell regeneration, J. Clin. Invest. 117 (2007) 2553.
[26] T. Okada, C.W. Liew, J. Hu, C. Hinault, M.D. Michael, J. Krützfeldt, C. Yin, M.H. abd Markus Stoffel, R.N. Kulkarni, Insulin receptors in β-cells are critical for islet compensatory growth response to insulin resistance, Proc. Natl. Acad. Sci. USA 104 (2007) 8892.
[27] R. Pattaranit, H.A. van den Berg, Mathematical models of energy homeostasis, J. R. Soc. Interf. 5 (2008) 1119.
[28] G. Pavliotis, A. Stuart, Multiscale Methods: Averaging and Homogenization, Springer, 2008.
[29] S. Pelengaris, M. Khan, The many faces of c-Myc, Arch. Biochem. Biophys. 416 (2003) 129.
[30] S. Pelengaris, M. Khan, G.I. Evan, Suppression of Myc-induced apoptosis in β cells exposes multiple oncogenic properties of Myc and triggers carcinogenic progression, Cell 109 (2002) 321.
[31] M.H. Protter, C.B. Morrey, College Calculus with Analytic Geometry, Addison-Wesley, 1970.
[32] B. Raju, P.E. Cryer, Maintenance of the postabsorptive plasma glucose concentration: Insulin or insulin plus glucagon? Am, J. Physiol. Endocrinol. Metab. 289 (2005) E181.
[33] J. Ribbing, B. Hamrén, M.K. Svensson, M.O. Karlsson, A model for glucose, insulin, and beta-cell dynamics in subjects with insulin resistance and patients with Type 2 diabetes, J. Clin. Pharmacol. 50 (2010) 861.
[34] I. Rooman, J. Lardon, L. Bouwens, Gastrin stimulates β-cell neogenesis and increases islet mass from transdifferentiated but not from normal exocrine pancreas tissue, Diabetes 51 (2002) 686.
[35] J.G. Salway, Metabolism at a Glance, Blackwell Science, 1999.
[36] R.F. Schmidt, G. Thews (Eds.), Human Physiology, second ed., Springer, 1989.
[37] M. Sofroniou, G. Spaletta, Construction of explicit Runge–Kutta pairs with stiffness detection, Math. Computer Model. 40 (2004) 1157.
[38] G.M. Steil, N. Trivedi, J.-C. Jonas, W.M. Hasenkamp, A. Sharma, S. Bonner-Weir, G.C. Weir, Adaptation of β-cell mass to substrate oversupply: Enhanced function with normal gene expression, Am. J. Physiol. Endocrinol. Metab. 280 (2001) E788.
[39] J. Sturis, K.S. Polonsky, E. Mosekilde, E.V. Cauter, Computer model for mechanisms underlying ultradian oscillations of insulin and glucose, Am. J. Physiol. Endocrinol. Metab. 260 (1991) E801.
[40] I.M. Tolić, E. Mosekilde, J. Sturis, Modeling the insulin–glucose feedback system: the significance of pulsatile insulin secretion, J. Theor. Biol. 207 (2000) 361.
[41] B. Topp, K. Promislow, G.D. Vries, R.M. Miura, D.T. Finegood, A model of β-cell mass, insulin, and glucose kinetics: Pathways to diabetes, J. Theor. Biol 206 (2000) 605.
[42] M. Van de Casteele, B.A. Kefas, Y. Cai, H. Heimberg, D.K. Scott, J.C. Henquin, D. Pipeleers, J.C. Jonas, Prolonged culture in low glucose induces apoptosis of rat pancreatic β-cells through induction of c-myc, Biochem. Biophys. Res. Commun. 312 (2003) 937.
[43] P.J. Watkins, ABC of Diabetes, BMJ Books, 2003.
[44] G.C. Weir, D.R. Laybutt, H. Kaneto, S. Bonner-Weir, A. Sharma, β-Cell adaptation and decompensation during the progression of diabetes, Diabetes (2001) S154.
[45] J. Young, S. Pelengaris, A. Chipperfield, W.P. Heath, M. Khan, Engineering beta cell mass regulation in diabetes, Curr. Topics Biochem. Res. 10 (2008) 47.